AUTONOMA UNIVERSITY OF MADRID

MOLECULAR BIOLOGY DEPARTMENT

Genetic characterization of Cdk1 in mouse development and homeostasis: a novel dichotomy between stem and committed mitotic cell cycles

DOCTORAL THESIS

Catherine Evangeline Symonds

Madrid, 2015

Molecular Biology Department

Faculty of Science

AUTONOMA UNIVERSITY OF MADRID

Genetic characterization of Cdk1
in mouse development and homeostasis: a novel dichotomy
between stem and committed mitotic cell cycles

Catherine Evangeline Symonds
Microbiology, B.S., M.S.; Italian Studies, B.S.

Directors:
Dr. Mariano Barbacid Montalbán
Dr. David Santamaría Villella

Spanish National Cancer Center (CNIO)

Madrid, 2015

Acknowledgements

I would first and foremost like to thank Mariano Barbacid and David Santamaría, who welcomed me into the Experimental Oncology Group and provided me with the opportunity to carry-out this research. I would like to thank them for their support and guidance over these past five years. I would also like to thank my CNIO Ph.D. Thesis Committee members, Marcos Malumbres, Sergio Moreno and Juan Mendéz for following the progress of my work from the beginning and offering helpful advice. I would like to thank all the members of the Experimental Oncology Group, past and present, for their support, both scientific and emotional. You have taken me in as part of the family and I will forever be grateful. Thank you to our animal facility technicians, especially Conchi, Gema, Vicky, Alejandra, Alba for all of the work that you have done for me over the years without ever the slightest complaint. Thank you to the heads and technicians of the CNIO technical units, especially Lola Martinez, Diego Megias, Paqui Mulero, Sagrario Ortega, Orlando Dominguez and Isabel Blanco for the training and support you have offered in helping me with experimental protocols and technique, I will forever be appreciative of your time and dedication. Thank you to Rebeca Sanchez and Jose Carlos Segovia for your collaboration for the HSC analysis. Thank you to all the students and scientists at the CNIO, I have been blessed to be part of such a wonderful and collaborative research institute, which has been my home and my family these past five years. I would like to thank all of my friends from the CNIO, swimming, here and abroad for your support over these past five years, helping me realize my potential and being there during the good times and the bad. Last but not least, I would like to thank my loving family, whom I owe so much to, I love you!

Finally, this work would not have been possible without the financial support from the La Caixa International Ph.D. Fellowship, which I am grateful to for the opportunity to pursue my Ph.D.

Summary/Resumen

Summary

Cellular division is the basis for the continuation of life and is regulated by the careful progression of events known as the cell cycle. The primary drivers behind the cell cycle are the Cyclins and their Cyclin-dependent kinases, however many regulatory mechanisms act to balance their activity in order to avoid unscheduled cell division. Cdk1 has been identified as the essential Cdk for mammalian cell cycle progression and is capable of compensating for the lack of other cell cycle Cdks. In order to better understand the role of Cdk1 in early embryonic development and adult homeostasis, we have developed a germ-line and conditional knockout mouse for Cdk1. In addition we investigated the role of Cdk1 in a tissue and cell type-specific manner. This work provides novel insight on the regulation of the mammalian cell cycle as well as the potential therapeutic advantages of targeting Cdk1 in hyperproliferative diseases, such as cancer.

Resumen

La división celular es la base para la continuación de la vida y está regulada mediante una cuidadosa progresión de eventos conocidos como ciclo celular. Las impulsoras primarias del ciclo celular son las ciclinas y sus quinasas dependientes de ciclinas (Cdks), sin embargo son muchos los mecanismos que actúan para equilibrar su actividad con el objetivo de evitar divisiones celulares no programadas. Cdk1 ha sido identificada como la Cdk esencial en la progresión del ciclo celular en mamíferos y es capaz de compensar la ausencia de las demás Cdks implicadas en el ciclo celular. Para mejorar la comprensión de las funciones de Cdk1 en el desarrollo embrionario temprano y en la homeostasis en adultos, hemos desarrollado un ratón knock-out en línea germinal y condicional de Cdk1. Asimismo hemos investigado el papel de Cdk1 a nivel específico de tejido y célula. Este trabajo proporciona nuevos conocimientos en la regulación del ciclo celular en mamíferos así como de las potenciales ventajas de utilizar Cdk1 como diana terapéutica en enfermedades hiperproliferativas, tales como el cáncer.

Index

Abbreviations

#h	hours
#min	minutes
#n	DNA Content/Ploidy
4-OHT	4-hydroxytamoxifen
7AAD	7-amino-actinomycin D
Ad-x	Adenovirus
APC	Anaphase Promoting Complex
Arpp19	cAMP regulated phosphoprotein
ATP	adenosine tri-phosphate
B-gal	Beta-galactosidase
B-geo	Beta-galactosidase and Neomycin Resistance Fusion
BrdU	5-bromo-2'-deoxyrudine
BSA	Bovine Serum Albumin
CAK	Cdk Activating Kinase
Casp	Caspase
CD##	Cluste of Differentiation
Cdc	Cell Division Control Protein
Cdh	Major Cadherin Family
Cdk	Cyclin Dependent Kinase
cDNA	Complementary DNA
Cdx	Caudal Type Homeobox Transcription Factor
Chk	Checkpoint Kinase
CK	Casein Kinase
CKI	Cdk-inhibitor
CMV	Cytomegalovirus
CO2	Carbon Dioxide
Cre	Cre Recombinase
CSC	Cancer Stem Cell
CT	Computerized Tomography
Ct	Cycle Threshold
D#	Day
DAPI	4',6-diamidino-2-phenylindole
DDR	DNA Damage Response
DEG	Differentially Expressed Genes
DKO	Double Knock Out
DMEM	Dulbecco's Modified Eagle's Medium
DMSO	Dimethyl Sulfoxide
DNA	Deoxyribonucleic Acid
DNase	Deoxyribonuclease
dNTP	Deoxynucleotide
DTT	Dithiothrietol
E#.#	Embryonic Day #.#
E2F	E2 Factor Family of Transcription Factors
ECL	Enhanced Chemiluminescence
ENSA	Endosulfine
ERT2	Human Estrogen Receptor Ligand Binding Domain

ES	Embryonic Stem
FACS	Flourescence Associated Cell Sorting
FBS	Fetal Bovince Serum
FCS	Fetal Calf Serum
FDR	False Discovery Rate
Flox	Flanked by loxP sequences
FVB	Friend Leukemia Virus B Mouse Strain
G0	Quiescence
G1	Gap Phase 1 of Cell Cycle
G2	Gap Phase 2 of Cell Cycle
GAP	GTPase-Activating Protein
GAPDH	Glyceraldehyde 3-phosphate dehydrogenase
Gata	Globin Transcription Factor
GDP	Guanosine Diphosphate
GEF	Guanine Nucleotide Exchange Factor
GFP	Green Fluorescent Protein
GMP	Granulocyte Monocyte Progenitor Cells
GO	Gene Ontology
GSEA	Gene Set Enrichment Analysis
Gt	Gene Trap
GTP	Guanosine Triphosphate
GTPase	Guanosinetriphosphatase
Gwl	Greatwall
H&E	Hematoxylin and Eosin
H2B	Histone H2B
H3	Histone H3
hCG	Human Chorionic Gonadotropin
Het	Heterozygous
HPC	Hematopoietic Precursor Cell
HRP	Horseradish Peroxidase
HSC	Hematopoietic Stem Cell
HU	Hydroxyurea
hUBC	Human Ubiquitin C
ICM	Inner Cell Mass
IF	Immunofluorescence
IHC	Immunohistochemistry
IP	Intraperitoneal
iPS	Induced Pluripotent Stem Cell
Kap1	Krüppel-associated box associated protein
KI	Knock In
Klf-4	Kruppel Like Factor
KO	Knock Out
KSOM	Potassium (K+) Simplex Optimized Media
KSR	Knockout Serum Replacement
KT	Keratinocyte
LIF	Leukemia Inhibitory Factor

LSK	Lineage negative, c-Kit and Sca1 positive hematopoietic stem cells
M	Mitosis
M2	Modified Krebs-Ringer Bicarbonate Solution with HEPES
MAPK	Mitogen Activated Protein Kinase
MAPKK	Mitogen Activated Protein Kinase Kinase
MCC	Mitotic Checkpoint Complex
Mcm	Minichromosome Maintenance Complex
MEF	Mouse Embryonic Fibroblast
MEM	Minimal Essential Media
MES	2-[N-morpholino]ethanesulfonic acid containing Running Buffer
MMTV	Mouse Mammary Tumor Virus
MOI	Multiplicity of Infection
MPF	Maturation Promoting Factor
MPM2	Mitotic Protein Monoclonal
Myt	Myelin Transcription Factor
n#	Number of Samples/Mice
NCBI	National Center for Biotechnology Information
ND	Not Detected
Neo	Neomycin
NFR	Nuclear Fast Red
o.n.	Overnight
OA	Okadaic Acid
OCT	Optimum Cutting Temperature Formulation
Oct3/4	Octamer Binding Transcription Factor
ORC	Origin Recognition Complex
P##	Postnatal Day ##
PBS	Phosphate Buffered Saline
PCP	Purkinje Cell Protein
PCR	Polymerase Chain Reaction
PGK	Mouse Phosphoglycerate Kinase 1 Promoter
pH3	Phosphorylated Histone H3
PI	Propidium Iodide
Plk	Polo-like Kinase
PMSG	Pregnant Mare's Serum Gonadotropin
PP	Protein Phosphatase
PyMT	Polyoma Virus Middle T Antigen
qRT-PCR	Quantitative Reverse Transcription Polymerase Chain Reaction
R point	Restriction Point
Rb	Retinoblastoma
RERT	RNA Polymerase II fused with Cre-ERT2
RNA	Ribonucleic Acid
RNase	Ribonuclease
RPA	Replication Protein A
RT	Room Temperature
RT-PCR	Reverse Transcription Polymerase Chain Reaction
RTK	Receptor Tyrosine Kinase

S	Synthesis
SAC	Spindle Assembly Checkpoint
Sca	Spinocerebellar Ataxia Type
SCF	Skp, Cullin, F-box Containing Complex
SDS	Sodium Dodecyl Sulfate
shRNA	Small Hairpin Ribonucleic Acid
siRNA	Small Interfering Ribonucleic Acid
Smc	Structural Maintenance of Chromosomes
Sox	Sex-determing region Y box
SSC	Saline Sodium Citrate
TAM	Tamoxifen
Taq	*Thermus aquaticus* DNA Polymerase
TBS-T	Tris-Buffered Saline with Tween
TE	Tris-EDTA Buffer
Tg	Transgenic
TKO	Triple Knock Out
TMA	Tissue Microarray
Tpx	Targeting Protein For Xklp2, Microtubule Associated
VEGFR	Vascular Endothelial Growth Factor Receptor
VWF	Von Willebrand Factor
WT	Wild Type
X-Gal	5-bromo-4-chloro-3-indolyl-β-D-galactopyranoside
yH2AX	Histone H2A.X phosphorylated at Ser139
yIR	Gamma-Irradiation

1. Introduction

1.1 The Eukaryotic cell cycle

Cellular division is the basis for the continuation of life. For single-cell prokaryotic organisms, cell division represents reproduction and is simply a replication of genetic material equally divided between two daughter cells by binary fission with very limited molecular regulation. In eukaryotes there are two forms of cellular division, mitotic cell division and meiosis. Mitotic cell division is the process by which a cell will faithfully replicate its genetic material and divide it between two daughter cells; this can be done either in a symmetric or asymmetric fashion determining the fate of the daughter cells. Whereas meiosis is the specialized process by which a diploid cell will replicate its genetic material and divide into haploid gametes for sexual reproduction. The intricacy of cellular division varies among organisms; in mammals the process is carried out in four active phases (G1, S, G2 and M)(Sisken & Morasca 1965) that are tightly regulated by the cyclins and their respective cyclin-dependent kinases (Cdks). This regulation ensures proper replication of genetic material and safeguards against mutations and damage that could harm the fitness of the organism. The ordered molecular mechanisms underlying the proper progression of mitotic cell division are generally described as the cell cycle.

1.1.1 Exit from quiescence (G0) and entry into the cell cycle (G1)

Mammalian mitotic cell division begins from fertilization and continues throughout adulthood. However, upon terminal differentiation, specialized cells become post-mitotic and irreversibly lose their proliferative capability, such as neurons and muscle cells. Rather, mitotic cells constitute renewable tissues and organs, including epithelial, stromal and hematopoietic cells, and will maintain their proliferative capabilities. Mitotic cells can also enter a reversible non-proliferative state, termed quiescence, where they maintain transcriptional activity, downregulate cell cycle genes, inhibit terminal differentiation to ensure their re-entry into the cell cycle. Quiescence (also termed G0) is an essential process in tissue homeostasis and many factors can induce quiescence, including mitogen starvation, stress, and contact inhibition. Many essential cell cycle regulators are significantly downregulated or completely inhibited during quiescence. Cyclin dependent kinases (Cdks), a family of up to 21 protein kinases and five Cdk-like kinases (Malumbres et al. 2009), first identified as the primary kinetic regulators of the cell cycle are completely inactive during quiescence. As such, the Retinoblastoma (Rb) family of pocket proteins, direct substrates of Cdks, remain

hypophosphorylated and bound to the E2F family of transcription factors, inhibiting transcriptional activation of genes necessary for the progression of the cell cycle.

Re-entry into the cell cycle requires the activation of the mitogen-activated protein kinase (MAPK) and the extracellular-signal-regulated kinase (ERK) pathway. The presence of extracellular mitogens or growth factor, cytokine and hormone ligands results in binding and activation of their respective transmembrane receptor tyrosine kinases (RTKs)(Jones & Kazlauskas 2001). RTKs can induce multiple downstream pathways, but for cell cycle entry the activation of Ras (H-Ras, N-Ras, or K-Ras) family member G proteins (guanosine-nucleotide-binding proteins) is essential (Pulciani et al. 1982; Shih & Weinberg 1982; Goldfarb et al. 1982; Robinson & Cobb 1997). Ras proteins are GTPases bound to the inner cell membrane and can hydrolyze guanosine triphosphate (GTP) into guanosine diphosphate (GDP)(Scolnick et al. 1979). Under physiological conditions the transfer of the phosphate group is aided by guanine nucleotide exchange factors (GEFs)(Panniers & Henshaw 1983) during the activation of Ras (to the GTP-bound state) and GTPase activating proteins (GAPs) in the inactivation of Ras (to the GDP-bound state)(Gibbs et al. 1988). GTP-bound Ras proteins can bind and activate Raf proteins (a-Raf, b-Raf and c-Raf) subsequently activating the MAPK/ERK signal transduction pathway. Raf is a serine/threonine protein kinase which, when active, phosphorylates members of the mitogen activated protein kinase kinase (MAPKK) family, or mitogen/extracellular signal-regulated kinase proteins (Mek1 and Mek2)(Rapp et al. 1983; Anderson et al. 1991). Phosphorylated Mek proteins will then phosphorylate the downstream Erk or MAPK family of proteins (Erk1 and Erk2). Erk serine/threonine kinases are responsible for activating a milieu of downstream cytoplasmic, membranous and nuclear protein cascades that are crucial in cell fate decisions including cell cycle entry. Specifically, Erk can act in various ways to promote Cyclin D1 transcription via activation of the Elk and Myc transcription factors (Gille et al. 1995; Murphy et al. 2004; Murphy et al. 2002; Volmat et al. 2001; Seth et al. 1991; Daksis et al. 1994) as well as aid in Cdk activation (Keenan et al. 2001; Lents et al. 2002). Furthermore, Erk can transcriptionally repress anti-proliferative genes throughout the G1 phase of the cell cycle (Yamamoto et al. 2006).

The initial observation that resting cells could be stimulated by serum to enter into the cell cycle and divide by Todaro et al. in 1965, piqued the interest to understand the molecular regulatory mechanisms governing G0 arrest and exit. Tobey and Ley (1970) demonstrated the ability to synchronously stimulate a population of arrested cells

to enter into the cell cycle. From these studies the restriction point (R point) was suggested as a shifting point from a state of low metabolic activity to that of active proliferation (Pardee 1974). The R point was mapped to 2-3 hours prior to S phase (Tobey & Ley 1970; Pardee 1974; Campisi et al. 1982). These studies made clear that when cells are exposed to unfavorable conditions for proliferation (e.g. high cell density, nutrient or serum insufficiency, and high levels of cAMP) they would become quiescent, however when sufficient stimulation with serum or growth factors was provided, cells would exit quiescence and if the cell passed the R point, it was committed to completing the cell cycle.

Quiescence is a long-term resting phase of the cell and is characterized by no Cdk activity and hypophosphorylated Rb inhibition of E2F factors. However, in cellular populations cell cycling is not homogeneous and not all cells immediately enter the cell cycle after division. The decision on whether to continue proliferating or to enter quiescence seems to be due to signaling during the prior cell cycle. Cells can actually incorporate mitogenic information during a "restriction window" at the end of the previous cell cycle in order to decide between continued proliferation and entrance into quiescence (Spencer et al. 2013). This bifurcation upon mitotic exit is dependent upon levels of Cdk2 and its inhibitor p21/Cip1 (cyclin dependent kinase inhibitor 1, *Cdkn1a*), where no active Cdk2 results in quiescence and measurable levels of Cdk2 activity result in the re-entry of the cell into the cell cycle.

Cdks work in heterodimeric complexes with their Cyclin family counterparts, initially named for their cyclic expression during the cell cycle but now identified for their conserved 100 amino acid cyclin box domain (Noble et al. 1997). Commitment to the cell cycle is based on the sequential activation of Cdks4/6 and Cyclin D, phosphorylation of Rb family proteins, release of E2F transcription factors, further transcriptional induction of Cyclin D, ubiquitination and degradation of the Cdk-inhibitor p21 and eventual expression of Cyclin E and Cdk2/3, which allow for S phase entry (Dou et al. 1993; Chen et al. 1995). Without sufficient activation of Cdks, cells will be unable to counteract inhibitory anti-proliferative signals. Therefore, in either scenario, exit from quiescence or progression from a previous cell cycle, the cell requires enough signaling to commit to the energy- and resource-demanding process of cellular division.

1.1.2 Interphase - G1

Interphase is the growth phase of the cell cycle leading up to mitosis and is comprised of gap phase 1 (G1), the DNA synthesis phase (S), and gap phase 2 (G2).

During G1, mitogens signal to induce Ras/Mek/Erk signaling and downstream cell cycle initiation. Expression of Cyclin D, encoded as three genes in vertebrates (Cyclins D1, D2 and D3), increases along with its associated Cdk4 and Cdk6 activity. Under highly mitogenic conditions several Cdk-inhibitors from the *Cdkn2a* or *Ink4a/Arf* tumor suppressor locus can act as a break mechanism towards cell cycle progression (Quelle et al. 1995; Serrano et al. 1993; Hiebert et al. 1992). In fact many tumor types are associated with mutations in the *Ink4a/Arf* locus. The increased Cdk activity during G1 is also essential for the phosphorylation and inactivation of the Rb family of tumor suppressor proteins.

The Rb family of tumor suppressors contains three members, Rb/p105, p107 and Rb2/p130, which are collectively referred to as pocket proteins for the conserved pocket region where they bind viral oncoproteins that possess an LXCXE motif (Lee et al. 1998), E2F transcription factors (Hiebert et al. 1992; Nevins 1992), the D-type cyclins (Ewen et al. 1993) and other cellular factors. Initially identified as a biallelic driver mutation in Retinoblastoma, *RB* mutations have also been identified in osteosarcoma, melanoma, lung and breast cancers (Dunn et al. 1988). When wild-type Rb proteins are overexpressed in cells they can induce growth arrest (Harrington et al. 1998). Therefore, Rb proteins are critical guardians of cell cycle induction and must be regulated accordingly. Rb proteins are believed to be inactivated in two stages, primarily by phosphorylation of the C-terminal domain by Cdk4 and Cdk6 bound by Cyclin D, followed by phosphorylation of the pocket domain by Cyclin E/Cdk2. Only when Rb is hyperphosphorylated will it fully release the E2F transcription factor allowing for progression of the cell cycle.

The family of E2F transcription factors is made up of three activators, E2F1, E2F2, and E2F3a, as well as six repressors E2F3b, E2F4, E2F5, E2F6, E2F7 and E2F8. All are involved in cell cycle regulation binding a TTTCCCGC consensus sequence (or similar) in the promoters of genes involved in cell cycle regulation, nucleotide synthesis, DNA replication and repair. The activators, in particular E2F1 dimerizes with transcription factor Dp-1 and promotes transcription of cell cycle genes (Helin et al. 1993), whereas the repressors are active in cells during quiescence. The function of the E2F activators is somewhat redundant as mouse embryos develop normally when lacking E2F1, E2F2, and one of the E2F3 isoforms (Tsai et al. 2008). E2F activators are most active during the G1/S phase of the cell cycle, whereas the repressors remain expressed at constant levels and actively repress once the activators are displaced.

Multiple positive feedback loops are in place for the E2F activators, including the inhibition of the tumor suppressor p53 and activation of Cyclin E, demonstrating that the Rb-E2F axis acts as a bistable switch to ensure commitment of cells to the cell cycle (Wong et al. 2011).

Both the exit of mitosis as well as G0 represent states of little to no Cdk activity, allowing for Rb hypophosphorylation and E2F transcription factor repression. For the cell to ensure proper exit from mitosis and inhibit premature entry into a new cell cycle the phosphorylation levels of Rb proteins are further regulated by serine/threonine protein phosphatases PP1 and PP2A. These phosphatases acquire cell cycle specific functions upon holoenzyme assembly with their various catalytic subunits (PP1a, PP1b/d, PP1c1 and PP1c2 for PP1 and the Ca and Cb isoforms of PP2A). PP1 has been noted to form complexes with as many as 650 mammalian proteins (Hendrickx et al. 2009) and PP2A represents a family of four dimeric and over 90 heterotrimeric holoenzymes (Bollen et al. 2010). PP2A is believed to be functionally regulated by the B-type subunit that is present within the complex (Shi 2009; Slupe et al. 2011), however the complexity of the activation and regulation of the protein phosphatases has yet to be fully elucidated. During mitotic exit and G1, PP1 is the primary inhibitor of Rb family member phosphorylation and can directly bind to Rb. Upon mitogen activation and induced Cdk activity, PP1 will become phosphorylated by Cdks allowing for Rb hyperphosphorylation and cell cycle entry. However, this negative feedback mechanism allows for cells to require a threshold of Cdk activation in order to completely inhibit PP1 and induce hyperphosphorylation of Rb family member proteins, adding yet another level of regulation for entry into the cell cycle (Kolupaeva & Janssens 2012; Novak et al. 2010).

The anaphase promoting complex (APC) and the Skp, Cullin, F-box containing complex (SCF), are both multimeric E3 ubiquitin ligases that provide an extra layer of regulation to the cell cycle, by targeting cell cycle proteins for degradation by the 26S proteasome. APC and its cofactor Cdh1 are mainly active during mitotic exit and early G1 to degrade mitotic and S phase cyclins. APC-Cdh1 also targets the APC co-factor Cdc20, which is active during mitosis, for degradation during the exit of mitosis in order to further promote G1. As G1 cyclin and cdk activity increases Cdh1 is phosphorylated and inactivated allowing for entry into S phase where the Cdc20 co-factor will once again bind to the APC. The SCF ubiquitin ligase when bound with its cofactors S-phase kinase-associated protein 2 (Skp2) and Cyclin-dependent kinase regulatory subunit 1

(Cks1) will ubiquitinate and degrade cyclin dependent kinase inhibitors, such as p21 and p27. During G1 the APC-Cdh1 complex will target Skp2 for degradation and maintain Cdk2-specific CKI levels until necessary kinase activity is present for Cdh1 to be inactivated (Bashir et al. 2004). Upon Cdh1 inactivation, Skp2 can then activate the SCF inducing degradation of CKIs and allowing Cdk2 and Cyclins A and E to promote S phase progression.

1.1.3 Interphase – S Phase

The G1 phase of the cell cycle is critical in ensuring proper preparation and energy requirements for S phase progression. Mitogenic signaling and sufficient activity of protein phosphatases, protein degradation and CKIs all cooperate in maintaining low Cdk activity allowing for pre-replication complex formation for DNA synthesis to occur. The synthesis, or S phase of the cell cycle is where genetic DNA is accurately replicated with a host of regulatory mechanisms in order to avoid mutations, which could result in disease or death. The human diploid genome is composed of 46 chromosomes, approximately $6x10^9$ base pairs of DNA, requiring around 50,000 origins of replication. In simple eukaryotes, each replication origin has a consensus sequence where the origin recognition complex (ORC) can bind and recruit pre-replication complexes (pre-RCs) during late M phase and early G1, while Cdk activity is low, increased Cdk activity allows for the initiation of DNA synthesis at the proper time. In higher eukaryotes the replication origins are not well defined, but are believed to be topologically regulated by epigenetic chromatin modifications. In order to ensure one round of DNA replication per cell cycle the origins are licensed by the loading of the pre-RCs. ORC1-6 bind to origins during M phase and are bound and inhibited by Cyclin B1/Cdk1 to prevent re-replication until mitosis is complete (Wuarin et al. 2002). The degredation of Cyclin B1 and inactivation of Cdk1 allows for ORC1-6 to recruit cell division cycle 6 (Cdc6), an ATP binding protein which then recruits DNA replication factor Cdt1 and helps load the minichromosome maintenance complex Mcm2-7. The MCM proteins form a hexamer around the DNA and act as DNA helicases initiating the unwinding of the DNA for synthesis and elongation. Cdc6 is essential for the initiation of DNA replication. Mammalian Cdc6 protein levels peak in late G1 and are destabilized during G2-M by SCF-Skp2 (Williams et al. 1997; Méndez & Stillman 2000). In order to prevent re-replication of the DNA during S phase and G2, SCF-Skp2 polyubiquitinates Orc1 and the DNA replication inhibitor Geminin is induced during S phase to inhibit the replication factor Cdt1 until mitosis. During late mitosis and G1 the APC complex

ubiquitinates Geminin allowing for pre-RC formation. These regulatory mechanisms and feedback loops ensure only one round of replication per cell cycle.

Once DNA replication has been initiated the pre-RC is no longer needed and thus inactivated. However the hexameric Mmc2-7 remains and forms a functional helicase, the CMG complex, with cell division cycle protein 45 (Cdc45) and GINS (Go, Ichi, Ni and San; Japanese for "five, one, two and three" which refers to the annotation of the genes that encode the complex)(Moyer et al. 2006). The CMG complex interacts with DNA polymerase alpha/primase, DNA polymerase delta and epsilon, topoisomerases 1 and 2, Mcm10, chromosome transmission fidelity protein 4 (Ctf4), proliferating cell nuclear antigen (PCNA), single stranded binding proteins (SSB), and the many other factors required to faithfully execute DNA replication at the replication forks (Zhu et al. 2007; Solomon et al. 1992; Merchant et al. 1997; Yeeles et al. 2015). Replication terminates when two replication forks meet and the nascent DNA strands are ligated together.

Progression of the S phase is associated with an increase in both Cdk2 and Cdk1 activity, which act congruently with both Cyclin A2 and B1 to inhibit re-replication of the DNA (Nguyen et al. 2001). During S phase, Cdk1 will interact with both Cyclin A2 as well as Cyclin B1, inherent mechanisms control Cdk-cyclin binding in terms of specificity and timing (Merrick et al. 2008). The activation of Cdk1 in late S phase allows for inhibitory phosphorylation of PCNA co-regulators and the termination of DNA replication. However, negative regulators of Cdk1 kinase activity including Wee1 protein kinase and myelin transcription factor 1 (Myt1) remain present during S phase to ensure that cells do not prematurely enter into mitosis.

1.1.4 Interphase – G2

The second gap phase of the cell cycle, G2, is the most robust checkpoint of the cell cycle, where cells ensure that DNA replication has been properly completed to allow for mitosis. The primary regulator of the G2/M transition is the Cyclin B1 - Cdk1 complex, also referred to as maturation promoting factor (MPF). Unlike all other cyclins, Cyclin B1 has a significant peak in expression at the G2/M transition, reaching very high levels, allowing sufficient Cdk1 kinase activity to induce mitosis. If mitosis is initiated and cells have not fully resolved the replication complexes or DNA is damaged, mitotic defects or cell death can occur. Therefore, the G2/M transition maintains the necessary control via the requirement for high levels of Cdk1 activity along with numerous feedback regulatory mechanisms.

Cdk1 is a highly conserved serine/threonine kinase, with the human CDK1 sharing 63% amino acid identity with its yeast homologue. Cdk1 is a small protein, primarily made-up of the protein kinase domain. It has an ATP cleft in the active site close to where its substrates bind allowing for the catalysis of the gamma-phosphate of ATP to the oxygen of the hydroxyl serine/threonine residue of the substrate. Cdk1 also contains a PSTAIRE alpha helix motif, which is shared among major Cdks and is responsible for interacting with Cyclin binding. When the Cyclin binds to the Cdk, the PSTAIRE helix is reoriented, resulting in a conformational change in the active site. Cdk1 also has a Cdk-activation loop or T-loop, which is shared among several Cdks. The T-loop blocks the active site on the Cdk until it is phosphorylated by the Cdk-activating kinase (CAK), a trimeric protein complex made up of Cdk7, Cyclin H and Mat1. When the CAK phosphorylates the T-loop at the threonine residue (Thr161 in Cdk1), the T-loop is re-oriented allowing for substrates to access the active site. Thus Cdk1 must undergo substantial conformational reorganization for it to be activated at the G2/M transition.

In order for Cdk1 to induce mitotic entry it must be bound to Cyclin B1 as well as be phosphorylated on a residue of its T-loop (Threonine 161, $Cdk1^{Thr161}$). During G2 Cdk1 is maintained in an inactive state by phosphorylation of the Tyrosine 15 ($Cdk1^{Tyr15}$) residue by Wee1 and the Threonine 14 ($Cdk1^{Thr14}$) residue by Myt1. Cdk1 in turn will phosphorylate Wee1, as well as polo-like kinase 1 (Plk1) and casein kinase 1(CK1), this phosphodegron targets Wee1 to degradation by $SCF^{B\text{-}TrCP}$. Plk1 is activated at the G2/M transition by Aurora A kinase and Bora, which accumulate during G2 forming an activation complex. Plk1 will then further activate Cdk1 by phosphorylating the cell division cycle protein 25 (Cdc25), a dual-specificity phosphatase, which then activates Cdk1 by removing the inhibitory phosphorylations. Moreover, Cdk1 will activate Cdc25 itself creating a positive-feedback loop. Myt1 activity is also inhibited during mitosis by phosphorylation by both Plk1 and Cdk1. These feedback loops represent a bistable switch system (Lindqvist et al. 2009), which will become autocatalytic once threshold activation has been reached.

Mitosis requires the phosphorylation of numerous Cdk1 substrates and in order to prevent aberrant mitotic entry the PP2A phosphatase along with its B55 subunit is primarily responsible for dephosphorylating Cdk1 substrates at the end of mitosis and during interphase. In order to bypass this inhibition at the G2/M transition Cdk1-dependent activation of the kinase greatwall (Gwl, also known as MastL in mammals)

activates Arpp-19 or ENSA, which is a specific PP2A-B55 inhibitor, resulting in decreased PP2A-B55 levels and an increase in Cdk1 activity and phosphorylated mitotic substrates (Gharbi-Ayachi et al. 2010; Mochida et al. 2010). This represents yet another regulatory mechanism of the Cdk1 bistable switch at the G2/M transition.

Lastly, the active Cyclin B1-Cdk1 complex must be translocated into the nucleus in order to fully induce mitosis. While Cyclin B1 can shuttle between the nucleus and cytoplasm during interphase, mitotic onset requires the phosphorylation of Cyclin B1 in its cytoplasmic retention sequence (CRS) along with an inhibition of its nuclear export signal (NES). Initial studies in Xenopus have suggested that Erk and Plk1 phosphorylate Cyclin B1 in the CRS (Walsh et al. 2003), however, further studies in mammalian cells demonstrated that initial phosphorylation of Cyclin B1 by Plk1 occurs on the centrosomes during prophase but phosphorylation was not specific to the nuclear export sequence (NES) and did not result in nuclear translocation (Jackman et al. 2003). Recent reports demonstrates that self phosphorylation of Cdk1-Cyclin B1 at the centrosome promotes its nuclear translocation and that nuclear translocation further activates Cdk1-Cyclin B1 complexes in a autoregulatory positive-feedback mechanism (Gavet & Pines 2010b; Gavet & Pines 2010a). This mechanism ensures that once Cdk1-Cyclin B1 complexes are activated, cells are committed to enter into mitosis.

1.1.5 Mitosis

Mitosis is the process by which the cell divides its chromosomes into two daughter cells. Mitosis is characterized by six phases including prophase, prometaphase, metaphase, anaphase, telophase and cytokinesis.

During prophase the loosely organized heterochromatin organizes itself and condenses into the sister chromatids that are attached at the centromere. The multisubunit Cohesin complex regulates this process. Namely multimeric protein complex formed between Scc1/RAD21, Scc3/STAG1 (stromal antigen 1, SA1), Smc1 and Smc3 (structural maintenance of chromosomes). SMC proteins are a family of ATPases that catalyze higher order chromosome structure and dynamics. Smc-1 and Smc3 dimerize forming the hinge domain and are connected to the ATP-binding cassette-like head domain via long anti-parallel coiled-coils. Scc1 and Scc3 bind to the head domain of the Smc proteins forming a closed loop structure when ATP is bound. ATP hydrolysis can control the opening and closing of the cohesin structure. Scc1 or RAD21 is a nuclear phosphoprotein binding to the head regions of Smc-1 and Smc-3 stabilizing their interaction and recruiting the remaining SA-1, Pds5, and Wap1

interacting proteins. Cohesin acts to hold the sister chromatids together during mitosis until anaphase and sister chromatid separation. It also facilitates spindle attachment onto chromosomes. During prophase the centrosomes, which were duplicated during G1 and S phase, are separated to opposite poles of the cell forming a bridge of spindle fibers. Finally the nucleolus dissolves.

Prometaphase is marked by nuclear membrane dissolution, the formation of the kinetochore and attachment of microtubules to the kinetochores. Kinetochores are highly specialized structures that form around the centromere of the chromosome and allow for microtubule attachment. The kinetochore is formed by an inner plate chromatin structure containing nucleosomes, specialized histones, auxiliary proteins and DNA. Outside of the inner plate is the outer plate composed primarily of protein (Cooke et al. 1993). The kinetochore forms at the time of nuclear envelope breakdown. Once the microtubules from the centrosomes have attached to all the chromosomes' kinetochores the mitotic spindle is formed and the cell will enter into metaphase.

Metaphase is characterized by the polar orientation of the centrosomes and the alignment of the chromosomes at the equatorial axis. Until all chromosomes are properly aligned and attached to the centrosomes, the Spindle Assembly Checkpoint (SAC) is active. The SAC will be active even if one unattached chromosome is present in the cell and improper regulation of chromosome segregation during mitosis can cause aneuploidy leading to serious health defects such as cancer. The SAC is primarily regulated by the protein complex Cohesin. Cohesin forms a ring like structure around sister chromatids and protects them from separation until the SAC has been deactivated. The SAC inhibits primarily the Anaphase Promoting Complex/Cyclosome (APC/C) ubiquitin ligase by catalyzing the association of its coactivator, Cdc20, into the mitotic checkpoint complex (MCC). Moreover, active Cdk1 will phosphorylate Securin inducing binding to and inactivation of Separase, the kinase responsible for dissolving the Cohesin rings to allow separation of sister chromatids. These forces act congruently to inhibit anaphase from progressing until all sister chromatids are properly aligned.

Anaphase progression occurs upon proper chromosome alignment. The induced activation of the APC/C-Cdc20 ubiquitin ligase is responsible for the degradation of Cyclin B and securin. This in turn deactivates Cdk1 and releases separase, which will hydrolyze the cohesin rings allowing for chromatid separation. The centromeres are split and the daughter chromosomes are pulled towards opposite poles by the microtubules attached to the kinetochore. Non-kinetochore microtubules are also active during

anaphase in elongating the cell. Once the daughter chromosomes reach the poles the cell undergoes a reversal of the prophase and prometaphase events, termed telophase. The microtubules attached to the chromosomes will release and a new nuclear envelope will form around the two sets of daughter chromosomes. The chromosomes will then relax or decondense. At this stage mitosis is complete and the cell will most likely continue into the final stage of cellular division, cytokinesis, or the separation of the cell into two equal daughter cells.

1.2 Genetically modified mouse models targeting Cdk alleles

Initial cell cycle studies performed in *S. pombe* identified *cdc2* (Cdk1 yeast mue) as the key regulator of the mitotic cell cycle (Nurse 1990; Gould & Nurse 1989). *Cdc2* is the only Cdk family member in yeast and together with the nine encoded cyclins, it is capable of performing all necessary kinase functions throughout the cell cycle. Recent studies have demonstrated the capability to manipulate the progression of the cell cycle in yeast by varying the levels of cdc2 kinase activity, lending to the kinase activity threshold model of cell cycle progression (Coudreuse & Nurse 2010). Under this theory it is believed that the stage and cyclin-specific expression, concentration and localization act to engage cdc2 activity at the proper threshold necessary to progress through the cell cycle. A steady increase in cdc2 activity is required for initial entry and G1 and S phase progression. For the cell to enter into Mitosis, a high-energy and consequential stage of the cell cycle, cdc2 activity must significantly increase in order to overcome inhibitory signals from Cdk inhibitors and phosphatases. Once the cell has fully entered into mitosis all Cdk activity must be eliminated for proper completion of mitosis and cytokinesis.

In higher eukaryotes, however, there is more than just one Cdk. In humans there are up to 21 CDK family proteins and at least 5 CDK-like family proteins. Traditionally the Cdks responsible for mammalian cell cycle progression have been Cdk2, Cdk3, Cdk4, Cdk6 and Cdk1. While there has been significant research on the roles of Cdk1, Cdk2, Cdk4 and Cdk6, the role of Cdk3 has yet to be fully elucidated. Cdk3 is a homologue of Cdk2 and cdc2 and ectopic expression of human Cdk3 suggests a role in G1/S transition. Studies have been difficult due to low levels of endogenous protein. Moreover, in commonly utilized laboratory *Mus musculus* strains a point mutation was found to generate a stop codon, functionally acting as a *Cdk3-null* allele (Ye et al. 2001). Therefore, all genetic analysis performed in laboratory mouse strains has been done in the absence of Cdk3. Given that these laboratory strains are viable and present with no

identified phenotypic change, Cdk3 is not required for normal cell cycle or mouse homeostasis and its absence can be compensated for by the remaining Cdks. To further analyze the functional characteristics of these Cdks in homeostasis and the cell cycle, genetically modified knockout mice have been generated.

1.2.1 Cdk2

A conditional *Cdk2* knockout mouse was generated using the Cre-loxP strategy. When the investigators generated a full germline knockout, they observed no effect on mitotic cell cycle progression or vitality of the mice. However, mice lacking Cdk2 were sterile and the authors reported a defect in Prophase I of the meiotic cell cycle(Ortega et al. 2003). Previous to this study, general belief was that Cdk2 was the major regulator for the mammalian cell cycle. In fact many anticancer drugs were being developed to target Cdk2 activity in tumors. However, these findings established, that when absent, Cdk2 mitotic cell cycle activity can be fully compensated for by the remaining Cdks. Moreover, further research demonstrated this to be true in tumors lacking the Cdk inhibitors p21 and/or p27 (Martín et al. 2005).

1.2.2 Cdk4

A conditional *Cdk4* knockout mouse was generated using the Cre-loxP strategy. Mice devoid of *Cdk4* were found to be viable but small in size (Rane et al. 1999). Similar to the mice lacking *Cdk2*, *Cdk4*-null mice were also sterile. Furthermore, it was reported that the lack of *Cdk4* resulted in insulin-deficient diabetes due to a reduction of β-islet pancreatic cells (Rane et al. 1999). When looking specifically at mitotic cell cycle progression, mouse embryonic fibroblasts could proliferate normally in the absence of Cdk4 but portrayed a delayed entry into S phase upon re-entry into the cell cycle (Rane et al. 1999).

1.2.3 Cdk6

Cdk6 knockout mice were generated by targeting the first coding exon with a *PGK-neo* cassette by homologous recombination in ES cells. Similar to other interphase Cdk knockout mice, *Cdk6* knockout mice were viable showing a slight anemia and defective proliferation of some hematopoietic cell types. However, the majority of mitotic cell types proliferated normally without Cdk6 (Malumbres et al. 2004).

1.2.4 Combined knockout models

Given that mice are viable in the absence of individual interphase Cdks, it can be concluded that cell cycle functions are compensated for by the remaining interphase Cdks. In order to understand this compensation better, combined knockout models were generated of the interphase Cdks.

Double knockout *Cdk2, Cdk4* mice complete embryonic development successfully but die shortly after birth presumably due to heart failure (Barrière et al. 2007). However, when Cdk2 was conditionally ablated from adult mice lacking Cdk4 there were no obvious phenotypes and mice could recover from partial hepatectomy. Double knockout embryonic fibroblasts could be immortalized, showed robust phosphorylation of Rb and had normal cell cycle kinetics (Barrière et al. 2007).

Double knockout *Cdk4, Cdk6* mice are unable to fully complete embryonic development, dying at late stages due to severe anemia and improper hematopoiesis. However, embryonic fibroblasts lacking Cdk4 and Cdk6 proliferate normally, can be immortalized, and can re-enter the cell cycle with normal kinetics but a lower efficiency (Malumbres et al. 2004).

In light of the double knockout mouse models, it was clear that interphase Cdks were capable of compensating for each other. Thus to determine the necessity of interphase Cdks a triple knockout mouse was generated. Mice lacking *Cdk2, Cdk4 and Cdk6* were found to develop and undergo organogenesis until midgestation (Santamaría et al. 2007). Mice show similar phenotypes as the double and single knockout models, including anemia and hematopoietic defects. Cells lacking interphase Cdks proliferate albeit with an elongated cell cycle due to delayed phosphorylation of Rb and compensation for the lack of interphase Cdks is carried out by Cdk1, which is capable of binding to all cyclin counterparts and phosphorylating Rb (Santamaría et al. 2007). These findings demonstrate the similarities between simple eukaryotic cell cycles and mammalian mitotic cell cycles in that a single cell cycle Cdk, namely Cdk1 is capable of maintaining essential cell cycle progression.

1.2.5 Cdk1

Further evidence demonstrating that Cdk1 is the only essential Cdk1 was generated using mice lacking all Cdk1 expression, by the insertion of a β-geo cassette (a proviral β-galactosidase and neomycin resistance fusion gene) into the *Cdc2a* locus upstream of exon 3 (Santamaría et al. 2007). These mice were not viable, being unable to

develop to even the morula stage of embryonic development (Santamaría et al. 2007). Therefore, Cdk1 is capable of compensating for all interphase Cdk activity, whereas interphase Cdks are not able to compensate for the loss of Cdk1. This could result from an inability to reach threshold kinase levels necessary, or simply an inability to phosphorylate mitotic substrates.

In an effort to further clarify the role of Cdk1 both *in* vivo and in cell cycle regulation, a conditional knockout mouse was generated (Diril et al. 2012). Mice lacking Cdk1 did not develop past the blastocyst stage. Moreover, cells depleted of Cdk1 were unable to progress through the cell cycle, completing S phase but undergoing multiple rounds of endoreplication. Liver-specific depletion of Cdk1 was well tolerated and mice were able to fully regenerate their livers after partial hepatectomy through cell growth without cell division (Diril et al. 2012). Moreover, the findings show that in the absence of Cdk1, the liver is completely refractory to tumorigenesis by loss of p53 or activation of Ras (Diril et al. 2012). These findings taken together with those of the interphase Cdks demonstrate the essential role of Cdk1 in the mammalian cell cycle. However, there are clearly Cdk-specific functions that have been associated to interphase Cdks, and the role of Cdk1 in the adult cell cycle as well as cell-type specific cell cycles has yet to be addressed. Importantly it is still unclear why Cdk1 cannot be functionally replaced by interphase Cdks, especially Cdk2 which is expressed during S and G2 phases and has been found to both bind Cyclin B1 as well as phosphorylate mitotic targets (Brown et al. 2007). Thus further investigation is required to address the specific role of Cdk1 in regulating the essential mammalian cell cycle.

1.3 Cell cycle and development

The cell cycle has long been studied in model cell lines such as 3T3 fibroblasts and human cancer cell lines (e.g. HeLa). However, the mechanisms regulating the cell cycle of these cell types may not hold true across all mammalian cells. In fact, the findings from the interphase knockout mouse models demonstrate just that, with the specific roles for interphase Cdks in hematopoiesis and heart development. Moreover, there is increasing evidence for substantial regulatory differences in early embryonic or stem cell cycles and those of differentiated cell types.

During early embryonic development the mammalian cell cycle has distinct progression and regulatory mechanisms. As cells differentiate the cell cycle becomes longer and thus more complex (Figure 1). For pluripotent stem cells (ES cells) that will go on to form all somatic tissues, the first differentiation occurs at peri-implantation or

approximately embryonic day 5 in mice (E5), when the cells differentiate into the endodermal, mesodermal and ectodermal lineages (Lawson et al. 1991; O'Farrell et al. 2004). This differentiation restricts cells to the respective germ layer thus losing pluripotent capabilities. Within each organ system, a subset of cells will retain stem cell properties (multipotent stem cells) and be capable of maintaining tissue homeostasis and regeneration. During organogenesis, multipotent stem cells will give rise to two major subsets of cells, progenitor cells that will be more restrictive in their proliferative potential and capacity to generate different cell types as well as post-mitotic cells that will provide the structural and physiological requirements necessary for the tissue. During organogenesis multipotent stem cells are actively proliferating, however once organogenesis is complete and throughout adulthood, multipotent stem cells will exit the cell cycle and remain quiescent.

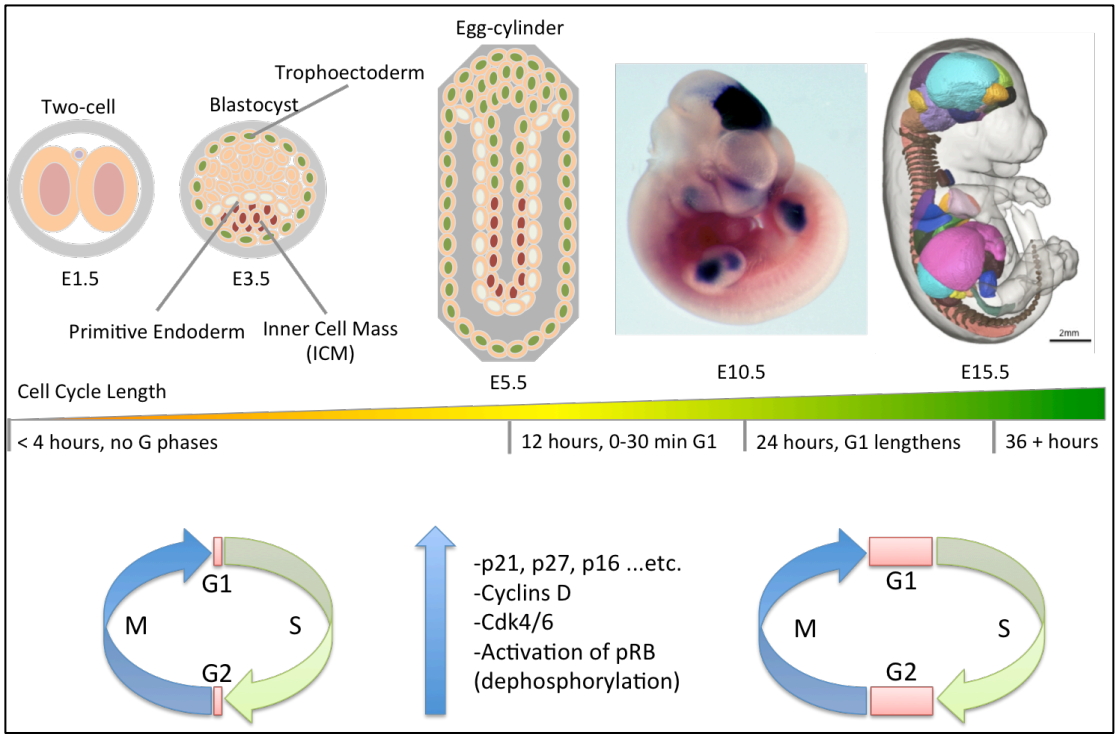

Figure 1: Cell cycle complexity through mouse development. Initial cell cycles are rapid lasting less than 4 hours and are composed primarily of synthesis and mitotic phases. As the embryo develops and cells differentiate into specific cellular lineages the regulatory mechanisms increase and the cell cycle lengthens, gap phases are introduced and cells will take up to 24 hours or longer to progress through the cell cycle.

Mouse ES cells are generated from the inner cell mass of the developing blastocyst (E3.5) and express the transcription factors Nanog, Oct-4 and Sox-2, which are essential in maintaining self-renewal and pluripotency. When cultured under proper conditions ES cells are capable of differentiating into any of the three germ layers. Throughout differentiation there is a progressive lengthening of the cell cycle and many

reports have linked cell cycle length to differentiation (Singh & Dalton 2009; Salomoni & Calegari 2010; Orford & Scadden 2008). The cell cycle phase that varies the most throughout development is G1. Pluripotent ES cells have little to no G1 phase and have been shown to have constitutively high levels of cyclin E and cyclin A associated Cdk activity (Stead et al. 2002). The Cdk inhibitors p16, p21 and p27 are silenced in pluripotent ES cells, allowing for uninhibited interphase Cdk activity (Faast et al. 2004). Moreover, due to continuous Cdk2 activity, Rb is maintained in its hyperphosphorylated form, rendering the cells independent of Rb cell cycle regulation and the R point (Savatier et al. 1994). As cells differentiate the G1 phase of the cell cycle lengthens (White & Dalton 2005; Bryja et al. 2008). Inhibition of Cdk2 in ES cells was found to lengthen G1 and induce differentiation and cells with elevated levels of Cdk2 show impaired differentiation (Koledova et al. 2010; Kim et al. 2009). These findings illustrate significant differences between cell cycle regulation in stem versus differentiated cell types. Given the increasing use of embryonic stem cells in research and potential therapeutic applications, the understanding of the basic molecular pathways regulating the cell cycle and differentiation will be needed and may shed light on key biological and evolutionary roles of cell cycle proteins.

2. Objectives

The kinase threshold model of cell cycle progression argues that a single Cdk is capable of interacting with all Cyclins and Cdk-substrates necessary to progress the cell through the mitotic cell cycle. Previous studies genetically targeting interphase Cdks, have identified Cdk1 as the essential Cdk for mammalian cell cycle progression and its ability to compensate for the loss of other cell cycle Cdks. However, if the threshold model holds true, other Cdks should be able to compensate for the loss of Cdk1, unless Cdk1 holds a specific function that has yet to be elucidated. While research has focused on the role of Cdk1 in the mitotic cell cycle, much remains to be understood about the role of Cdk1 in development and homeostasis.

Hence the objectives of this thesis are the following:

1. Generate a conditional *Cdk1lox* allele for the study and characterization of the role of Cdk1 in mouse embryonic development and adult homeostasis.

2. Utilizing the *Cdk1lox* conditional allele, identify cell specific or novel functions of Cdk1 *in vivo*.

3. Characterize the effect of genetic disruption of Cdk1 on mitotic cell cycle progression both *in vitro* and *in vivo*.

4. Identify the potential for interphase Cdks to compensate for loss of Cdk1 in the progression of the mitotic cell cycle.

5. Analyze the effect of genetic disruption of Cdk1 on cell cycle progression of embryonic and adult stem cell populations.

6. Identify the therapeutic potential for targeting Cdk1 in tumoral cell populations.

3. Materials and Methods

3.1 Mouse Generation and Maintenance

3.1.1 Generation of Cdk1lox allele

For the generation of the murine *Cdk1lox* allele, the genomic region encoding m*Cdk1* was cloned from the BAC clone RP23-178K6. The BAC-encoded fragments of interest were then subcloned by recombineering into a minimal vector pMV with a ColE1 origin of replication and an ap^R resistance marker. The insertion of FRT-PGK-gb2-neo/km-FRT-loxP cassette and the distal loxP site into the *mCdk1*-locus of the corresponding subclone was performed by one Red/ET step ("triple recombination"). Finally, the functional regions (FRT and loxP sites, restriction sites and resistance cassette) were verified by sequencing. These steps were carried out by Gene Bridges (P238.03.11.09). The linearized targeting vector was electroporated into mouse embryonic stem (ES) cells by the Transgenic Mice Unit of the CNIO. ES cell clones having undergone proper homozygous recombination with both arms of the targeting vector were identified by Southern Blot as described below. Single cell suspensions of two independent and positive ES cell clones (ESSD12.188 and ESSD12.193) were microinjected into FVB donor blastocysts which were then implanted into hormonally induced pregnant C57Bl/6J females. Two male founder chimera pups (with 100% penetrance of coat color) were utilized to generate germline transmission and were backcrossed to C57Bl/6J mice to establish pure genetic background.

3.1.2 Previously generated mouse strains

Other lines utilized in this thesis include: The *Tg.Flpe* line (Rodríguez et al. 2000), which was generated in Susan M. Dymecki's laboratory (Harvard Medical School, Boston, MA, USA); The *EIIa-Cre* line (Clausen et al. 1999), which was generated in Irmgard Foster's laboratory (Institute for Genetics, University of Cologne, Germany); The $Rosa26^{lslLacZ}$ line (Mao et al. 1999), which was generated in Stuart H. Orkins' laboratory (Dana Farber Cancer Institute, Boston, MA, USA); The *RERT* line (Guerra et al.2003), which was generated in Mariano Barbacid's laboratory (Spanish National Cancer Research Centre, Madrid, Spain); The *Tg.hUBC-CreERT2* line (Ruzankina et al. 2007), which was generated in Eric J. Brown's laboratory (University of Pennsylvania School of Medicine, Philadelphia, PA, USA); The *Tie2-CreERT2* line (Rodrigo Dieguez-Hurtado unpublished data), which was generated in Sagrario Ortega's laboratory (Spanish National Cancer Research Centre, Madrid, Spain); The *Tg.Pcp-2-Cre* line (Barski et al. 2000), which was generated in Michael Meyer's laboratory (Max-Plank Institute of

Neurobiology, Martinsried, Germany); Wild-type C57Bl-6J and Hsd:Athymic Nude-Foxn1nu provided by the Animal Facility at CNIO.

3.1.3 Mouse maintenance

All mice used were housed in the animal facility of the CNIO (Spanish National Cancer Centre, Madrid, Spain), where mice are submitted to 12 hour light/dark cycles. All mouse work and maintenance was performed in accordance with the Federation of European Laboratory Animal Science Association's recommendations and following the European Union legislation. All experiments described in this thesis were previously approved by the Bioethics and Animal Welfare Committee of the Health Institute Carlos III (CBA PA 04_2013-v2). Mice were fed *ad libidum* the Harlan diet except in cases where the Tamoxifen inducible *Cre* recombinase was induced, then animals were fed a high-fat transition diet for 10 days (Harlan) followed by a Tamoxifen-containing diet (Harlan).

3.1.4 Standard Necropsy

Animals were sacrificed in a CO2 chamber and samples of interest were collected in tissue sample blocks and fixed in formalin. Samples were processed in paraffin, cut and stained as needed by the Comparative Pathology Unit at CNIO. Some organs were frozen in OCT (Sakura) and stored at -80 °C for later cryostat sectioning. Partial tissue samples were collected for biochemical analysis in eppendorf tubes, flash frozen in dry ice powder and stored at -80 °C for later processing.

3.1.5 Wound Healing Assay

Mice were fed a high-fat transition diet (Harlan) for 10 days followed by a Tamoxifen-containing diet (Harlan) for indicated time period up-to and during the wound healing assay. Mice were housed individually for the duration of the assay. To induce wound healing mice were first anesthetized using isofluorane while maintaining 5% oxygen. The backs of the mice were shaved, treated with hair-removal cream for 30 seconds and skin was sterilized with iodine. A circular 4 mm or 6 mm skin hole punch was utilized to make a circular incision (as indicated below) in the epidermis and dermis of the back skin. Hair was routinely removed either by shaving or hair-removal cream to avoid possible interference with wound healing process. Wound was measured at the time of incision and daily to monitor healing process. Mice were sacrificed in a CO2 chamber at the indicated day of interest and wound was collected including 0.5-1 cm of surrounding back skin and placed on an index card to maintain tissue architecture.

Peritoneum and diaphragm samples were collected on glass slides and dried for several hours. They were then fixed in formalin and processed for X-gal staining (described below).

3.1.6 Genotyping

Mice were routinely genotyped by extracting DNA from tail samples.

1. 490 µl of lysis buffer (20mM Tris/HCl pH 8.0, 100 mM NaCl, 0.5% SDS, 10 mM EDTA pH 8.0) and 10 µl of proteinase K were added to each tail, and left overnight (o.n.) at 55°C.
2. 300 µl of saturated NaCl was added.
3. The solution was mixed and incubated for 10 min on ice.
4. The samples were centrifuged at 13000 rpm for 10 min.
5. The supernatant was transferred to a clean eppendorf.
6. 800 µl of isopropanol was added, then the solution was mixed vigorously.
7. The mixture was incubated for at least 1 hour at -20°C.
8. The samples were centrifuged at 13000 rpm for 10 min.
9. The supernatant was discarded.
10. 400 µl of 70% ethanol (EtOH) was added.
11. The samples were centrifuged at 13000 rpm for 10 min.
12. The supernatant was discarded.
13. The pellets were left to dry.
14. The pellets were resuspended in 200 µl of MilliQ-filtered H_2O.

Once the DNA was isolated we performed polymerase chain reaction (PCR) in a volume of 20 µl with the following sample conditions:

- 1.25 µl $MgCl_2$ (25 mM)
- Taq Polymerase Buffer (1X)
- 0.5 µl dNTPs (10 mM)
- 0.1 µl BSA (10 mg/ml)
- 0.1 µl Taq Polymerase (5 units/µl EcoTaq, Ecogen)
- 1 µl of each of the primers (10 µM, Sigma)
- 1 µl of DNA

The oligonucleotides used for genotyping were:

Cdk1

Cdk1 F: 5' CATAGATAGCTAGGGAATCCGCA 3'

Cdk1 R: 5' AGGCATTGAAGATAACTACGATCT 3'

Cdk1-null

Cdk1-null-F: 5' GAGATGTAGGATGACTCAGTG 3'

Cdk1-null-R: 5' TAGCTTATCTACCTCAGCCTG 3'

Cdk1-Flp

Cdk1Flp F: 5' CAGAGTCACTGGCCAGATAG 3'

Cdk1Flp R: 5' GGTGAGCTAGAGTAATATCCTG 3'

RERT

Polr2aR_10B6: 5' CCTCTCTGAGCCTCAATTAAGCAG 3'

ESRF1f_10B7: 5' TGAGTAACAAAGGCATGGAGCA 3'

Polr2aF_14B5: 5'CCAGATGACAGCGATGAGGA 3'

KI allele: Polr2aR_10B6-ESRF1f_10B7, 390bp.

WT allele: Polr2aR_10B6-Polr2aF_14B5, 480bp.

Rosa26^{LSL1acZ}

oIMR8052: 5' GCGAAGAGTTTGTCCTCAACC 3'

oIMR8545: 5' AAAGTCGCTCTGAGTTGTTAT 3'

oIMR8546: 5' GGAGCGGGAGAAATGGATATG 3'

KI allele: oIMR8052-oIMR8545, 340bp.

WT allele: oIMR8545-oIMR8546, 650bp.

The PCR program used was:

94°C 1 min

94°C 30 sec
60°C 30 sec } x 35 cycles
72°C 1 min

72°C 10 min

The length of the amplified fragments was assessed by 2% agarose gel electrophoresis.

Alternatively, the mice were genotyped by Transnetyx (Cordova, TN, USA).

3.1.7 Southern Blot

1. Sample DNA was prepared to be 30-50 µg in a 50 µl volume.
2. To perform digestion the following was added to sample:
    a. 5 µl of Restriction Enzyme of interest
    b. 1 µl RNase, DNase-free
    c. 5 µl Spermidine
    d. 7 µl of 10x Buffer
    e. 2 µl of 100x BSA
    f. Total = 20 µl
3. The final mix of 70 µl was mixed well and incubated at 37°C o.n.
4. 250 ml of 0.7% agarose gel was prepared
5. 6 µl of 6x loading dye was added to each sample and samples were loaded into gel wells.
6. Gel was run at 100 V until the blue dye front of the loading dye ran off the gel.
7. To ensure proper digestion of DNA samples a picture of the gel was taken using the transilluminator.
8. Gel was washed with dH_2O.
9. Gel was incubated with 0.25 N HCl for 15 min in light agitation.
10. Gel was washed with dH_2O.
11. Gel was incubated with Denaturing Solution (0.5 M NaOH + 1.5 M NaCl) for 20 min with light agitation.
12. Gel was incubated with Neutralizing Solution (0.5 M Tris-HCl pH 8.0; 1.5 M NaCl).
13. Gel was then equilibrated with transfer buffer (10x SSC).
14. The gel was then capillary transferred in 10x SSC placing first 3mm Whatman blotting paper on a face-down plastic gel mold with the edges emerged in the 10x SSC buffer. The following order was followed from bottom up: Gel, nylon Hybond N+ membrane (Amersham), two pieces of Whatman paper (cut to size of gel and membrane), and a pack of paper towels. The entire transfer is wrapped

in plastic wrap to avoid evaporation of buffer. A weight is placed on top and the gel is transferred o.n.

15. The next day top weight and papers are removed, and the membrane is marked with a pencil where the gel's wells were positioned.
16. Membrane was autocrosslinked 2x.
17. Membrane was incubated with 10 ml of Hybridization buffer for at least 4 hours or o.n in glass tube (with the DNA side facing inwards) incubated in a rotisserie oven at 42°C.
18. The DNA probe was prepared as follows:
    a. 2μl of the probe were added to 43 μl of water or TE buffer and boiled for 5 min.
    b. Sample was placed on ice for 2 min.
    c. Sample was spun.
    d. Sample was kept on ice.
    e. The probe sample was added to a tube with glass beads and 50 μCi (5 μl) of α32dCTP was added.
    f. Sample was incubated at 37°C for 5 min for the probe to be radioactively labeled.
    g. The reaction was stopped by adding 5 μl of NaOH.
    h. The sample was filtered on a spin column.
    i. The filtered radioactively labeled probe was then added to the glass tube with the membrane and incubated o.n.
    j. The following day the membrane was washed
        i. 30 min with 2x SSC, 0.1% SDS.
        ii. 30 min with 1x SSC, 0.1% SDS
        iii. 30 min with 0.1% SSC, 0.1% SDS
    k. The membrane was then placed in a plastic sleeve and exposed to a Phosphoimager screen.
    l. The screen was then developed using the Phosphoimager and its software.

3.2 Staining and processing of tissue samples

3.2.1 X-Gal whole mount staining

1. Tissues were fixed at RT for 60-90 min in fixative solution:

- 0.2% glutaraldehyde (Sigma)
- 1.5% formalin solution (Sigma)
- 2 mM $MgCl_2$
- 5 mM EGTA
- 100 mM sodium phosphate pH 7.3

2. The tissues were washed 3 times (20 min each at RT) in washing solution:
   - 0.2% NP-40
   - 0.1% sodium deoxycolate (Sigma)
   - 2 mM $MgCl_2$
   - 100 mM sodium phosphate pH 7.3
3. Following the washes, the tissues were stained for 48 hours at 37°C in the staining solution:
   - 0.2% NP-40
   - 0.1% sodium deoxycolate (Sigma)
   - 2 mM $MgCl_2$
   - 100 mM sodium phosphate pH 7.3
   - 5 mM $K_3Fe(CN)_6$ (ProLab)
   - 5 mM $K_4Fe(CN)_6$ (ProLab)
   - 1 mg/ml X-Gal (dissolved in dimethylformamide)
4. The tissues were washed 3 times and for 10 min with the above mentioned washing solution.
5. The samples were postfixed o.n. in phosphate buffered 10% formaldehyde.
6. The fixed and stained tissues were washed twice with 1X PBS for 5 min.
7. The tissues were washed twice with 50% EtOH and twice with 70% EtOH (1 hour each).
8. At this point tissues were processed by the Comparative Pathology Unit at CNIO, which produced 4 μm sections on a 3-aminopropyltrethoxylan coated slides and counter-stained with Nuclear Fast Red (NFR).

3.2.2 X-Gal staining on cryostat sections

1. Samples were cut in the cryostat at a 10 μm thickness and placed on a slide.
2. The slides were stored at 4°C o.n. or 1 hour at RT.
3. Sections were washed with PBS 1X.
4. Sections were fixed for 10 min at RT in the following solution:

- 0.2% glutaraldehyde (Sigma)
- 5 mM EGTA
- 2 mM $MgCl_2$
- 0.1 M phosphate buffer pH 7.3

5. The sections were washed 3 times with the following washing solution:
   - 2 mM $MgCl_2$
   - 0.1 M phosphate buffer pH 7.3
   - 0.02% NP-40
   - 0.01% sodium deoxycolate (Sigma)
6. After the washes, the sections were stained o.n. at 37°C with:
   - 2 mM $MgCl_2$
   - 0.1 M phosphate buffer pH 7.3
   - 0.02% NP-40
   - 0.01% sodium deoxycolate (Sigma)
   - 1 mg/ml X-Gal
   - 5 mM $K_3Fe(CN)_6$ (ProLab)
   - 5 mM $K_4Fe(CN)_6$ (ProLab)
7. The sections were washed 3 times with washing solution.
8. Sections were counter-stained with NFR

3.2.3 Nuclear Fast Red Staining (NFR)

1. The NFR solution was prepared:
   - 25 g aluminum sulphate (Sigma)
   - 0.5 g NFR (Sigma)
   - 500 ml milli-q H_2O
   - Solution was boiled for 2-3 min and then filtered
2. The samples were washed with H_2O.
3. The sections were stained with NFR for 1 min and 30 sec.
4. The sections were washed with H_2O.
5. The sections were washed twice for 2 min with 70% EtOH.
6. The sections were washed twice for 2 min with 100% EtOH.
7. The sections were rinsed with Xilol (Merck) for 1 min.
8. The sections were mounted with coverslip.

3.2.4 Immunofluorescence

1. Sections were deparaffinized (see 1a). Or cells were seeded on poly-d-lysine coated glass coverslips, glass bottom 96-well plates or human recombinant Lamin and 0.1% gelatin coated Ibidi μ-Slide 8 well chamber.
    a. The deparaffinized sections were treated with sodium citrate 10 mM (pH 6) at 95°C for 20 min (antigen retrival).
2. The samples were permeabilized for 30 min at RT with:
    - 0.4% Triton
    - 0.04% SDS
    - 1X PBS
3. The slides were washed twice with 1X PBS.
4. The slides were blocked for 45 min in 5% BSA at 37°C.
5. The primary antibodies were diluted in 5% BSA (mouse anti-γH2AX 1:500 Millipore 05-636, rabbit anti-Histone H3 Ser10 Phospho 1:500 Upstate 06-570, mouse anti-MPM2 Ser/Thr-Pro Phospho 1:500 Millipore 05-368) and incubated with sample for 1 hour at 37°C or o.n. at 4°C.
6. The slides were washed twice with 1X PBS.
7. The secondary antibodies were diluted in 5% BSA (Alexa Flour 647 chicken anti-mouse 1:200 Invitrogen A21463, Alexa Fluor 488 goat anti-mouse 1:200 Invitrogen A11029, Alexa Fluor 488 chicken anti-rabbit 1:200 Invitrogen A21441) and incubated with the samples 45 min at 37°C.
8. The first wash was done with diluted DAPI or 670 Phalloidin 1:1000 in 1X PBS.
9. Two additional washes were performed with 1X PBS.
10. The slides were mounted with mowiol and the coverslip.
11. The slides were analyzed on the Leica SP5, DeltaVision (Time Lapse) or Opera High Throughput (Perkin Elmer) confocal microscopes.
12. For the Opera a 20x magnification lens was used and pictures were taken at non-saturating conditions. Images were segmented using the DAPI staining to generate masks matching cell nuclei from with the average fluorescence signal was calculated using scripts developed by Diego Megias from CNIO's Microscopy Unit. Statistical analysis was computed with SPSS software. All other confocal images and time-lapse videos were processed using ImageJ/Fiji software.

3.2.5 Extraction of early-stage embryos (E1.5-E3.5)

Female mice between 5 and 8 weeks of age were superovulated by priming with PMSG and hCG (provided by CNIO animal facility) at 14:00 hours two days prior to mating and at 13:00 hours on the day of mating respectively. Female mice were mated with stud males and checked for plugs the following morning. Plug positive females were sacrificed by cervical dislocation on day of interest. The uterus and oviducts were carefully separated by teasing away from mesometrium with closed scissors or forceps. The uterus was cut half-way between oviduct and uterine horn joining. Another cut was made between the oviduct and the ovary. Isolated uterus and oviducts were placed in 50 µl of M2 media. Using a dissection microscope the embryos were flushed from the ampule of the oviduct through the uterus and collected in M2 media. Embryos were micropipetted with a mouth pipette in three drops of M2 media and then either processed for DNA extraction, immunofluorescence staining or continued culture.

3.2.6 Early embryo culture

Embryos extracted as previously described (3.2.5) were washed by micropipette transfer through three drops of KSOM media. Individual embryos were then transferred to 50 µl drops of KSOM media (preheated to 37°C for proper pH adjustment) and partially covered with glycerol. Once transferred, KSOM drops were completely covered with glycerol and maintained at 37°C with 5% CO2. Embryos were maintained in KSOM until blastocyst formation (approximately day 4). Embryos were then transferred to individual wells of 96-well plates with mitomycin C mitotically-inactivated feeder cells and grown with DMEM+LIF (provided from CNIO's Transgenic Mouse Unit).

3.2.7 Genotyping of early embryos

Early embryos were washed and collected in 10 or 20 µl of PCR-K buffer with Proteinase K and incubated at 55°C for 2 hours. Proteinase K was inactivated by incubation at 95°C for 15 min. One microliter of digest was utilized for PCR reaction.
PCR-K buffer was composed of:

- 50 mM KCl
- 1.5 mM $MgCl_2$
- 10 mM Tris-HCl pH 8.5
- 0.01% gelatin
- 0.45% Nonidet P-40

- 0.45% Tween 20
- 100 μg/ml Proteinase K

PCR was performed as previously described and following the previously published protocol (Malumbres et al. 1997).

3.2.8 Immunofluorescence of mouse embryos

1. Preimplantation embryos were isolated as described (3.2.5).
2. Embryos were fixed in methanol at -20°C for 1h or o.n.
3. Embryos were washed in 3 drops of M2 media.
4. Embryos were washed in 3 drops of PBS + 0.1% BSA.
5. To permeabilize, embryos were incubated for 5 min in PBS + 0.1% BSA + 0.1% Triton X-100.
6. Embryos were washed in 3 drops of PBS + 0.1% BSA.
7. To block embryos were incubated in blocking solution (PBS + 0.1% BSA + 10% goat serum) for 1-2 hours.
8. Primary Antibody: Embryos were incubated with 1st antibody for 2-4 hours at RT (mouse anti-γH2AX 1:100 Millipore 05-636, mouse anti-Cdx2 1:100 Biogenix MU392A-UC) diluted in blocking solution.
9. Embryos were washed in 3 drops of PBS + 0.1% BSA.
10. Secondary Antibody: Embryos were incubated with secondary antibody for 2 h at RT (Alexa Fluor 488 chicken anti-rabbit 1:200 Invitrogen A21441) diluted 1:500 in blocking solution.
11. Embryos were washed in 3 drops of PBS + 0.1% BSA.
12. DNA Staining: Embryos were incubated with DAPI (1mg/ml) diluted 1:500 in PBS + 0.1% BSA.
13. Embryos were washed in 3 drops of PBS + 0.1% BSA.
14. Embryos were washed in 2 drops of PBS.
15. Embryos were imaged in drops of PBS in microwells on the confocal microscope Leica SP5.

3.2.9 Histopathology and immunohistochemistry

Tissues including pancreas, spleen, thymus, liver, kidney, lung, heart, skeletal muscle, intestine, stomach, colon, skin, ovary, uterus, prostate, testis, mammary gland, white adipose tissue, brown adipose tissue, brain, eye, and femur were dissected, fixed in 10%-buffered formalin (Sigma) and embedded in paraffin. 4 μm thick sections were cut and

stained with haematoxylin and eosin (H&E). Antibodies used for immunohistochemistry included mouse anti-Cdk1 (BD Biosciences 610038), rabbit anti-CD31 (Abcam ab28364), rat monoclonal anti-β-Galactosidase (produced by the Monoclonal Antibody Unit at CNIO), mouse monoclonal anti-bromo-deoxyuridine (GE Healthcare RPN202), rabbit polyclonal anti-caspase 3 Asp175(Cell Signaling 9661), rat monoclonal anti-Tpx-2 (produced by the Monoclonal Antibody Unit at CNIO), rabbit anti-Ki67 (Master Diagnostica 0003110QD), rabbit anti-FVIII Von Willebrand Factor (Dako A9982).

3.3 Quantitative real time RT-PCR

3.3.1 RNA Extraction

Total RNA was extracted from samples using RNeasy Mini Kit (Qiagen) following manufacturers instructions. Briefly, cells were resuspended in provided lysis buffer and RNA was purified using the provided columns. On-column DNase digestion was performed to eliminate residual genomic DNA. RNA was eluted into 50 µl of elution buffer and quantified using the nano-drop spectrophotometer. RNA quality for sequencing experiments was assessed on the Agilent 2100 Bioanalyzer.

3.3.2 cDNA synthesis

cDNA synthesis was performed using SuperScript II RT kit from Invitrogen following the manufacturer's instructions.

For each sample the following mix was prepared:

- 200 ng random primers
- 40-100 ng total RNA
- 1 µl dNTP mix (10mM each)
- Sterile, distilled H2O

1. The mixture was incubated at 65°C for 5 min.
2. The samples were chilled on ice.
3. For each sample the following mix was added:
    - 4 µl 5X First Strand Buffer
    - 2 µl 0.1 M DTT
    - 1 µl RNaseOUT (40 units/µl)
4. The content of the tubes was gently mixed.
5. Samples were incubated at 25°C for 2 min.

6. 1 µl of SuperScript II RT enzyme was added and samples were mixed by pipetting.
7. Samples were incubated at 25°C for 10 min.
8. Samples were incubated at 42°C for 50 min.
9. The reaction was inactivated by heating at 70°C for 10 min.

3.3.3 Real time PCR

3.3.3.1 Primer design criteria

1. Tm: 58°C to 61°C
2. Primer length: 19-24 bp
3. Guanine cytosine (GC) content: 45-55%
4. PCR amplicon length: 100-200 bp
5. Cover an exon-exon junction (to avoid the problem of possible residual genomic DNA contamination)
6. Order primers with standard desalting purification

3.3.3.2 Primers

mCdk1 5'

mCdk1 5' F: 5' GAGAAGGTACTTACGGTGTG 3'

mCdk1 5' R: 5' GACAGGAACTCAAAGATGAG 3'

mCdk1 3'

mCdk1 3' F: 5' CAGGATCTTCAGAGCTCTG 3'

mCdk1 3' R: 5' GGCAGGATCATAGACTAGCA 3'

PPP2R2D

PPP2R2D RT For: 5' GCGGAAGCCGACATCATC 3'

PPP2R2D RT Rev: 5' CATGACTCTGAAAGGTACTG 3'

PCP2

PCP2 RT For: 5' CAGTTAATTCCCTGCCTG 3'

PCP2 RT Rev: 5' GTTTTCAGGGGCCAGTGG 3'

Myt1

Myt1 RT For: 5' GACATCGAAGCTTACAGAG 3'

Myt1 RT Rev: 5' CCTTCTGATTCATCTGAAACAG 3'

Wee1

Wee1 RT For: 5' CACTCCCAAGAGTTTGCTTTCC 3'

Wee1 RT Rev: 5' CTGAGGAATGGAGCAGTACAGG 3'

PPP2R2A

PPP2R2A RT For: 5' ATTCAGCCATAGCGGTCGTT 3'

PPP2R2A RT Rev: 5' TGACAACACTGTCAGACCCA 3'

Casp2

Casp3 Rt For: 5' GGAGCAGGATTTTGGCAGTGT 3'

Casp3 Rt Rev: 5' GCCTGGGGTCCTCTCTTTG 3'

Akt1

Akt1 Rt For: 5' ATGAACGACGTAGCCATTGTG 3'

Akt Rt Rev: 5' TTGTAGCCAATAAAGGTGCCAT 3'

Bag3

Bag3 Rt For: 5' CTGGGAGATCAAAATCGACCC 3'

Bag3 Rt Rev: 5' GCTGAAGATGCAGTGTCCTTAG 3'

Bak1

Bak1 Rt For: 5' CAACCCCGAGATGGACAACTT 3'

Bak1 Rt Rev: 5' CGTAGCGCCGGTTAATATCAT 3'

Bcl2l1

Bcl2l1 Rt For: 5' GACAAGGAGATGCAGGTATTGG 3'

Bcl2l1 Rt Rev: 5' TCCCGTAGAGATCCACAAAAGT 3'

Birc5

Birc5 Rt For: 5' GAGGCTGGCTTCATCCACTG 3'

Birc5 Rt Rev: 5' CTTTTTGCTTGTTGTTGGTCTCC 3'

Cide-A

Cidea Rt For: 5' TGACATTCATGGGATTGCAGAC 3'

Cidea Rt Rev: 5' GGCCAGTTGTAGATGACTAAGAC 3'

Mcl-1

Mcl1 Rt For: 5' AAAGGCGGCTGCATAAGTC 3'

Mcl1 Rt Rev: 5' TGGCGGTATAGGTCGTCCTC 3'

Klf-4

RT Klf4 Endo. For: 5' GCGAACTCACACAGGCGAGAAACC 3'

RT Klf4 Endo. Rev: 5' TCGCTTCCTCTTCCTCCGACACA 3'

Sox-2

RT Sox2 Endo. For: 5' TAGAGCTAGACTCCGGGCGATAGA 3'

RT Sox2 Endo. Rev: 5' TTGCCTTAAACAAGACCACGAAA 3'

Oct3/4

RT Oct3/4 Endo. For: 5' TCTTTCCACCAGGCCCCCGGCTC 3'

RT Oct3/4 Endo. Rev: 5' TGCGGGCGGACATGGGGAGATCC 3'

Gata-6

RT Gata6 For: 5' ACCTTATGGCGTAGAAATGCTGAGGGTG 3'

RT Gata6 Rev: 5' CTGAATACTTGAGGTCACTGTTCTCGGG 3'

Brachyury

RT Brachyury For: 5' ATGCCAAAGAAAGAAACGAC 3'

RT Brachyury Rev: 5' ACGAGTGGCAGTTTCTTCTTGGGA 3'

Cdx-2

RT Cdx2 For: 5' GGCGAAACCTGTGCGAGTGGATGCGGAA 3'

RT Cdx2 Rev: 5' GATTGCTGTGCCGCCGCCGCTTCAGACC 3'

Nanog

RT Nanog For: 5' AGGGTCTGCTACTGAGATGCTCTG 3'

RT Nanog Rev: 5' CAACCACTGGTTTTTCTGCCACCG 3'

p21

$p21^{Cip1}$-F: 5' TTCCGCACAGGAGCAAAGT 3'

$p21^{Cip1}$-R: 5' CGGCGCAACTGCTCACT 3'

GAPDH

GAPDH forward: 5'TGCACCACCAACTGCTTAG 3'

GAPDH reverse: 5'GGATGCAGGGATGATGTTT 3'

β-actin

β-actin forward: 5'GACGGCCAGGTCATCACTATT 3'

β-actin reverse: 5'AGGAAGGCTGGAAAAGAGCC 3'

3.3.3.3 qRT-PCR

The PCR mix was prepared as follows:

- 10 µl SYBR Green Mix 2X (Roche)
- 0.5 µl primer forward primer (10 µM - Sigma)
- 0.5 µl primer reverse (10 µM – Sigma)
- 1 µl template cDNA
- 8 µl H2O

Samples were prepared in a 96-well plate, sealed with optical adhesive film and processed in the AB 7900HT Fast Real Time PCR System.

The settings were as follows:

- Stage 1: 2 min at 50°C
- Stage 2: 10 min at 95°C
- Stage 3: 15 sec at 95°C then 1 min at 60°C (repeat 40 cycles)

- Dissociation stage: 95°C for 15 seconds, 60°C for 15 seconds, followed by a slow ramp to 95°C

3.3.3.4 Data analysis

The data were analyzed using the SDS software (Applied Biosystems). The relative mRNA expression was calculated using the comparative Ct (cycle threshold) method:

$\Delta\Delta Ct = \Delta Ct,sample - \Delta Ct,reference$

$\Delta CT,sample$ is the Ct value for any sample normalized to the endogenous housekeeping gene and ΔCt, reference is the Ct value for the calibrator also normalized to the endogenous housekeeping gene.

3.4 RNA Sequencing

RNA was isolated from samples as previously described (3.3.2) and 1 μg of RNA with an RNA integrity number (RIN) of 10 was provided to the Genomics Unit at CNIO. The PolyA+ fraction was purified and randomly fragmented, converted to double stranded cDNA and processed through subsequent enzymatic treatments of end-repair, dA-tailing, and ligation to adapters as in Illumina's "TruSeq Stranded mRNA Sample Preparation Part #15031047 Rev. D" (this kit incorporates dUTP during 2nd strand cDNA synthesis, which implies that only the cDNA strand generated during 1st strand synthesis is eventually sequenced). Adapter-ligated library was completed by PCR with Illumina PE primers (8 cycles). The resulting purified cDNA library was applied to an Illumina flow cell for cluster generation (TruSeq cluster generation kit v5) and sequenced on the Genome Analyzer IIx with SBS TruSeq v5 reagents by following manufacturer's protocols. Image analysis and per-cycle basecalling was performed with Illumina Real Time Analysis software (RTA1.13). Conversion to FASTQ read format and sequence alignment with the ELAND algorithm (v2e) was performed with CASAVA-1.8 (Illumina).

3.5 Western Blot

3.5.1 Protein extraction

1. Either tissues or cells were resuspended in lysis buffer: 50 mM Tris-HCl (pH 7.4) solution, containing 150 mM NaCl, NP-40 0.5% and protease (PMSF 100 mM, Roche) and phosphatase inhibitors (100 mM vanadate sodium, Roche and 1 mM NaF, Sigma).
2. For tissue protein extraction we used a homogenizer to mechanically breakdown the tissue samples and maximize the efficiency of lysis.
3. The samples were incubated on ice for a minimum of 15 min.
4. The extracts were centrifuged for 15 min at 13000 rpm to remove the undigested membranes.
5. The supernatant was transferred to a new tube.
6. In order to quantify the amount of protein obtained, we used the Bradford method (1 μl of the protein extract was added to 1 ml of Bradford reagent and the absorbance was read on a spectrophotometer).

3.5.2 Acrylamide Gel

1. The quantity of tissue/cell extracts needed to load the same total amount of protein was estimated (30-50 μg).
2. 4X loading buffer and 20X reducing agent (Biorad) were added.
3. The samples were boiled for 5 min. at 95°C.
4. The samples were placed on ice for 5 min.
5. Criterion XT precast gels were run into with running buffer (MES 1X, Biorad).
6. The samples were loaded into the gel.
7. 10 μl of the molecular weight color marker was loaded as well.
8. The gel was run with a constant voltage of 120 V for approximately 1.5 hours.

3.5.3 Transfer

1. Nitrocellulose transfer membrane and Whatman paper were sized to gel and pre-wet in transfer buffer (1X Tris-Glycine and 20% MeOH).
2. The transfer "sandwich" was assembled in a wet blotter as follows:
   Cathode – 3x Whatman – gel – nitrocellulose membrane – 3x Whatman – Anode
3. The gel was transferred for 1 hour and 10 min at 450 mAmp

4. When the transfer was finished, the amount of protein transferred was checked by staining with Ponceau S solution (Sigma).

3.5.4 Blocking and antibodies

1. The membrane was incubated in the blocking solution (5% BSA in 1X TBS-T) for 1 hour at RT.
2. The membrane was incubated with the primary antibody diluted in the blocking solution o.n. at 4°C. Primary antibodies included: mouse anti-Cdk1 (Santa Cruz sc-54), rabbit anti-Cdk2 (Santa Cruz sc-163), mouse anti-Cyclin A2 (Sigma C4710), mouse anti-Cyclin B1 (Millipore MAB3684), mouse anti-β-actin (Sigma A5441), mouse anti-GAPDH (Sigma G8795), rabbit anti-Caspase 3 (Cell Signaling 9662), rabbit anti-Cleaved Caspase 3 (Cell Signaling 9661), anti-Chk2, rabbit anti-pChk1 (Cell Signaling 2348), mouse anti-Chk1 (Novocastra NCL-ChK1), mouse anti-γH2AX (Millipore 05-636), anti-Smc1, anti-Kap1, rabbit anti-pRPA RPA32 S4/S8 (Bethyl A300-245A), and rabbit anti-Nanog (Novus Biologicals NB100-58842).
3. The membrane was washed twice with 1X TBS-T.
4. The membrane was incubated with the appropriate HRP-conjugated secondary antibody (1:2000, Dako).
5. The membrane was washed twice with 1X TBS-T.
6. Protein visualization was carried out with ECL detection reagent (Amersham) using different exposure times depending on the antibody.

3.6 Stem Cell Protocols

3.6.1 iPS Generation

1. Day 1: Transfection
    a. 5 x 10^6 293T cells were seeded per 10 cm plate in DMEM + 10% FBS + Antibiotics and transfected with 4 μg of pMX plasmid (either Sox2, Oct4, Klf4 or cMyc) + 4 μg of pCL Eco plasmid and 24 μl of Fugene 6.
    b. Same day as transfection primary MEFs (Passage 2 or 3) were thawed.
2. Day 2: Seeding
    a. Media was changed for 293T cells.
    b. MEFs were seeded at 2.5 x 10^5 per 6 well plate.

3. Day 3: Infection
    a. Morning: Viral media was from individual transfections and spun at 1000 rpm for 5 min.
    b. Viral media was filtered through 0.45 mm filters and 8 μl/ml of polybrene was added.
    c. Equal parts of viral media were mixed and 1 ml of each viral media was added to every well of primary MEFs (so each well had 4 ml of media, 1 ml from each viral prep.).
    d. Afternoon: Steps a-c were repeated.
4. Day 4: The infection was repeated both in the morning and in the afternoon for a total of 4 infections.
5. Day 5: Media was changed to DMEM + 15% KSR + 1000 U/ml LIF + Antibiotics (Transgenic Mouse Unit).
6. Following Days: Media was changed daily.
7. 10 days following infection iPS colonies started to appear.
8. 14 days following infection iPS colonies had ES morphology and were individually picked and transferred to 96-well feeder plate (see below 3.6.2).
9. Once the 96-well plate was confluent clones were passed to 24-well feeder plates and then 6-well feeder plates.
10. Cells were frozen down at 6-well feeder passage in 60% ES Cell Media + 30% KSR + 10% DMSO.

3.6.2 Feeder generation

1. Primary MEFs (passage 2 or 3) were thawed in a 15 cm plate with DMEM + 10% FBS + Antibiotics.
2. Once confluent they were passed to 5, 15 cm plates (1:5).
3. Once the 5, 15 cm plates were confluent they were passed 1:5 to generate 25, 15 cm plates.
4. Once confluent plates were treated with 10 μg/ml of Mitomycin C for 2-3 hours.
5. Mitomycin C containing media was removed and cells were washed twice with PBS.
6. Cells were trypsinized and spun at 1250 rpm
7. Cells were frozen at a density of 2 x 10^6 per vial (so 1 vial can be used for 1 6-well plate).

3.6.3 Generation of Embryonic Stem Cells

1. Female mice were superovulated as previously described (3.2.5) and mated with stud males.
2. Embryos were extracted at E2.5 (as previously described 3.2.5.).
3. Embryos were grown in KSOM media *in vitro* for one day to allow blastocyst formation.
4. Outer *zona pelucida* was removed using Tyrode's Solution (acidic pH 2.5).
5. Embryos were plated on 6-well feeder plates (10-20 embryos per well) in DMEM + 100 U/ml LIF + 15% KSR (Transgenic Mouse Unit).
6. We waited 4-6 days for ICM outgrowth, changing media daily.
7. Using a dissecting microscope we picked colonies.
8. Colonies were dissociated using a 1:3 dilution of 0.5% Trypsin in PBS.
9. Clones were then individually plated in 96-well feeder wells.
10. Once confluent they were passed to 24-well feeder plates and then to 6-well feeder plates.
11. At 6-well passage clones were frozen in 60% ES Cell Medium + 30% KSR + 10% DMSO.

3.6.4 Alkaline Phosphatase Assay

1. ES/iPS cells were plated at 1.5 x 10^3 cells per well of a 6-well plate coated with 1% (w/v) porcine gelatin in DMEM + 10% (v/v) FBS and 1000 U/ml LIF and cultured for five days.
2. Cells were washed twice with PBS and fixed with 100% methanol (3-5 ml) for 10 minutes.
3. Methanol was aspirated and fixed cells were allowed to air dry.
4. Colonies were incubated for 15-20 minutes with a solution of 0.1 M Tris-HCl pH 9.2, 200 μg/ml Naphthol AS-MX (Sigma N4875) and 1 mg/ml Fast Red TR Salt (Sigma F2768). To make the solution we dissolved 2 mg of Naphthol AS-MX in 10 ml of 0.1 M Tris-HCl pH 9.2 and this was added to a tube containing 10 mg Fast Red TR Salt and mixed to dissolve. We added 2 ml/well of this solution and incubated for 15-20 minutes.
5. Reaction was stopped by rinsing cells twice with dH2O and allowed to air dry.

3.6.5 Teratoma Assay

1. Early passage ES cells were grown on feeder plates and when 80% confluent clones were trypsinized and counted.
2. 2.0 x 10^6 cells were suspended into 100 µl total volume of PBS and injected subcutaneously into the back hind-side of Hsd:Athymic Nude-Foxn1nu mice.
3. Mice were monitored for tumor growth and upon palpable tumor size mice were placed on a Tamoxifen-containing diet for five days.
4. After five days of Tamoxifen-containing diet, mice were sacrificed and tumors were collected for histopathological analysis.

3.7 Tissue Culture and Cell Maintenance

3.7.1 MEFs

Mouse embryonic fibroblasts were isolated from E13.5 day old embryos. Pregnant females were sacrificed and embryos were isolated into PBS. Heads of embryos were removed for genotyping. Fetal liver and heart were removed from embryos. Embryos were mechanically dissociated and then enzymatically with 0.5% Trypsin. Cellular suspensions were then plated in 15 cm plates with DMEM + 10% FBS. Once confluent MEFs were frozen into four vials.

3.7.2 Immortalization of MEFs

To immortalize primary MEFs we followed the traditional 3T3 protocol. We continuously plated 1.0 x 10^6 cells in a 10 cm tissue culture plate with DMEM + 10% FBS + Antibiotics every 3 days for 12-15 passages. Cells would tend to enter a crisis stage around passage 5-6 ,where they would not actively proliferate between passages. Once crisis stage had passed and cells continuously proliferated to more than double the seeded density they were considered immortal and frozen down. Each clone was tested for active p53 by treating with Doxorubicin and probing for increased p53 and p21 protein levels. Clones that had a defective p53 pathway were noted and not utilized for further analysis.

3.7.3 Keratinocytes

Keratinocytes were isolated from neonate heterozygous or homozygous mutant *Cdk1lox; Tg.hUBC-CreERT2* mice according to previously described protocols (Lichti et

al. 2008). Briefly, tail was isolated from euthanized mice and bone was removed. Tail skin was then incubated in 0.75% trypsin with the dermis down in a petri dish for 1h at 37°C with 5% CO_2. The dermis and epidermis were separated with forceps and the epidermis was then treated with 250 μg/ml DNaseI (Sigma DN25-IG)), 2% Chelated FCS in MEM (Sigma M8167) in a 37°C water bath for 30 minutes with gentle agitation. Solution was then filtered through a 70 μm cell strainer and centrifuged. Cells were resuspended in culture media: MEM, 8% chelated FCS, Pen/Strep/Glu, 0.05 mM CaCl. Cells were plated on tissue culture plates previously coated for 1h at 37°C with coating matrix from Cascade Biologicals kit (R-011-K).

3.7.4 Mammary Tumor Cell Lines

Mammary tumor cell lines were established from *Tg.MMTV-PyMT* tumors by dissecting out tumor. Tumor was mechanically dissociated using a blade and scissors. Dissociated tumors were treated with 0.5% trypsin for 30 minutes. Cell suspensions were then plated in 15 cm plates with DMEM + 10% FBS + Antibiotics. The following day the media was changed and once confluent cells were passaged 1:2. Cells were frozen down at passage two. Not all clones continued proliferating after several passages, we utilized those that maintained proliferative capacity *in vitro*.

3.8 Flow Cytometry

3.8.1 DNA and Cell Cycle Analysis by Flow Cytometry

1. Cells grown in culture were trypsinized and washed to have a single cell suspension resuspended into 300 μl of PBS.
2. Cells were then fixed by adding 700 μl 100% EtOH dropwise to the 300 μl cellular suspension in a 15 ml falcon tube while vortexing and incubated at 4°C o.n.
3. Fixed cells were then centrifuged 5 min at 2000 rpm to remove EtOH.
4. Cells were washed 1x in PBS-Tween 0.05%
5. Cells were incubated with 100 μl of primary antibody diluted 1:500 in PBS-Tween 0.05% for 45 min at RT.
6. Cells were washed with 5 ml of PBS-Tween 0.05%.
7. Cells were then incubated with 100 μl of secondary antibody diluted 1:500 in PBS-Tween 0.05% for 45 minutes at RT in the dark.

8. Cells were washed with 5 ml of PBS-Tween 0.05%.
9. Cells were then resuspended in 300-500 μl of PBS + 10 μg of propidium iodide (PI) and 100 μg of RNase.
10. Samples were incubated at least 1 hour at 4°C before analyzing.
11. Samples were analyzed on a BD FACS Calibur or BD LSR Fortessa.
12. Samples were analyzed using FloJo software.

3.8.2 HSC Analysis

Bone marrow from mice was isolated from the femur and tibia of both hind legs. All cell isolation and processing was performed by R. Sanchez Dominguez at the CIEMAT (Madrid, Spain) following standard protocols. LSK (Lin-, c-Kit-, Sca1-), c-Kit (Lin-, c-Kit+) and GMP (granulocyte and monocyte progenitors) cells were isolated by standardized live cell surface marker fluorescence associated cell sorting (FACS) into 96-well plates with the following media (Stem Spam 7% Hyclone, 100 nm/ml SCF, 100 ng/ml IL-3, and 100 ng/ml Il-11). Two wells were isolated per cell type per mouse. One well was treated with 400 nM 4-OHT for five days. After five days of culture with 4-OHT all samples were processed for cell cycle and apoptosis. Samples analysis was performed with FlowJo software.

3.8.3 MMTV-PyMT Stem Cell Analysis

Cell lines from *Tg.MMTV-PyMT* tumors were infected with 50 MOI of cre-expressing adenovirus (Adeno-cre) and analyzed 3-5 days post infection. Live cells were probed with the following cell surface marker profile: APC-Lin, AF-488 Annexin V, APC-780 anti-CD24, PerCP-Cy5.5 anti-Sca-1, PE anti-CD49f, and PE-Cy7 anti-CD44. DAPI was included as a live cell marker. Cells were processed on the BD LSR Fortessa and analyzed using FlowJo software.

4. Results

4.1 Generation and characterization of *Cdk1lox* allele

In order to analyze the role of Cdk1 in adult tissue proliferation, homeostasis and pathology we generated mice with a conditional *Cdk1* allele. Previous results, obtained by the gene-trap insertion of a β-geo cassette (a proviral β-galactosidase and neomycin resistance fusion gene) into the *Cdc2a* locus upstream of exon 3, demonstrated efficient disruption of the locus and production of a Cdk1-β-geo fusion protein expressing only the 12 amino-terminal residues of Cdk1 (Santamaría et al. 2007). Therefore, we designed a targeting vector (Figure 2a) with a floxed exon 3 and a frt-flanked neomycin resistance

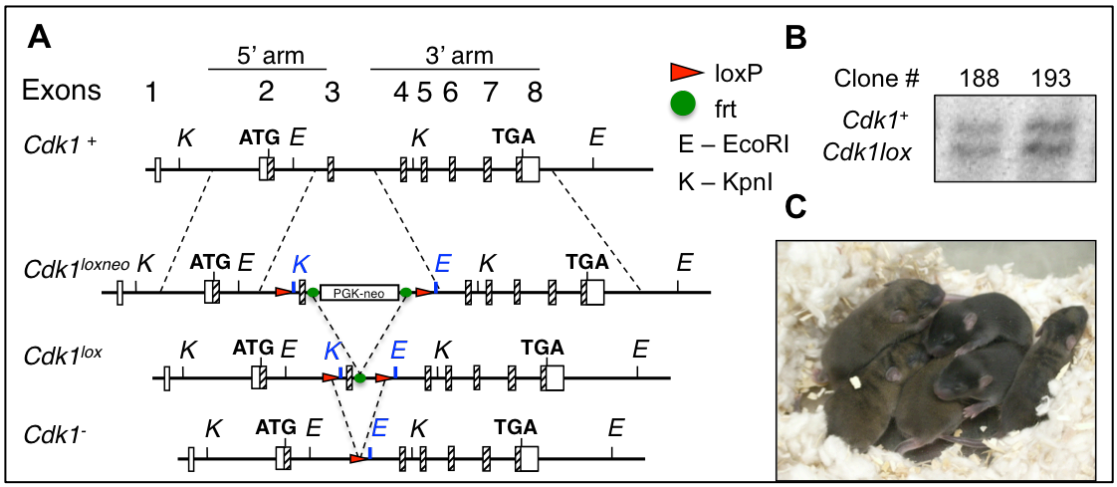

Figure 2: Cdk1 targeted allele and generation of chimera mice. A) Mouse Cdk1 wild-type allele, targeted allele, and targeted allele post cleavage with Flpase (frt) and Cre (loxP). B) Southern blot analysis of ES cell clones positive for homologous recombination with Cdk1 targeting vector. C) Litter of Cdk1 Chimera mice.

cassette in order to select recombined ES cell clones. We identified by southern blot two unique ES cell clones (clones ESSD12.188 and ESSD12.193) which successfully recombined with the targeting vector (Figure 2b). Cells from each clone were microinjected into FVB donor blastocysts (agouti fur color), which were then implanted into hormonally induced pregnant C57Bl/6J females. From clone ESSD12.188, sixty-four microinjected blastocysts were transferred to six pseudo-pregnant female surrogates resulting in eighteen pups and eleven chimeras (with varying penetrance as identified by coat color, see Figure 2c and Table 1). From clone ESSD12.193, fifty-two microinjected blastocysts were transferred to five pseudo pregnant female surrogates resulting in seven pups and one male chimera with 90% penetrance (Table 1). In order to eliminate the frt-flanked neomycin selection cassette, male founder chimeras from each ES cell clone were crossed to transgenic female mice expressing the Flpe recombinase under the control of the

pCAG element (beta-actin promoter-CMV enhancer)(Rodríguez et al. 2000). Excision was assessed by PCR and the F1 generation of mice from these crosses was then backcrossed to C57Bl/6J mice and we observed transmission of the *Cdk1lox* allele at normal Mendelian ratios.

ES Cell Clone	Date of Injection	Number of Donors	DOB	Chimeras/Pups Born	Chimeras % coat color (agouti)
ESSD12.188	1/10/10	10	20/10/10	11/18	5 (M) – 100% 4 (M) – 90% 1 (M) – 70% 1 (M) – 30%
ESSD12.193	29/10/10	10	17/11/10	1/4	1 (M) – 90%

Table 1: ES cell clone number and generation of chimeras. ES cell clones, date of microinjection, number of female donors, date of birth, chimeras/pups born and the number of males (M) from litters with respective percentage of aguti coat color.

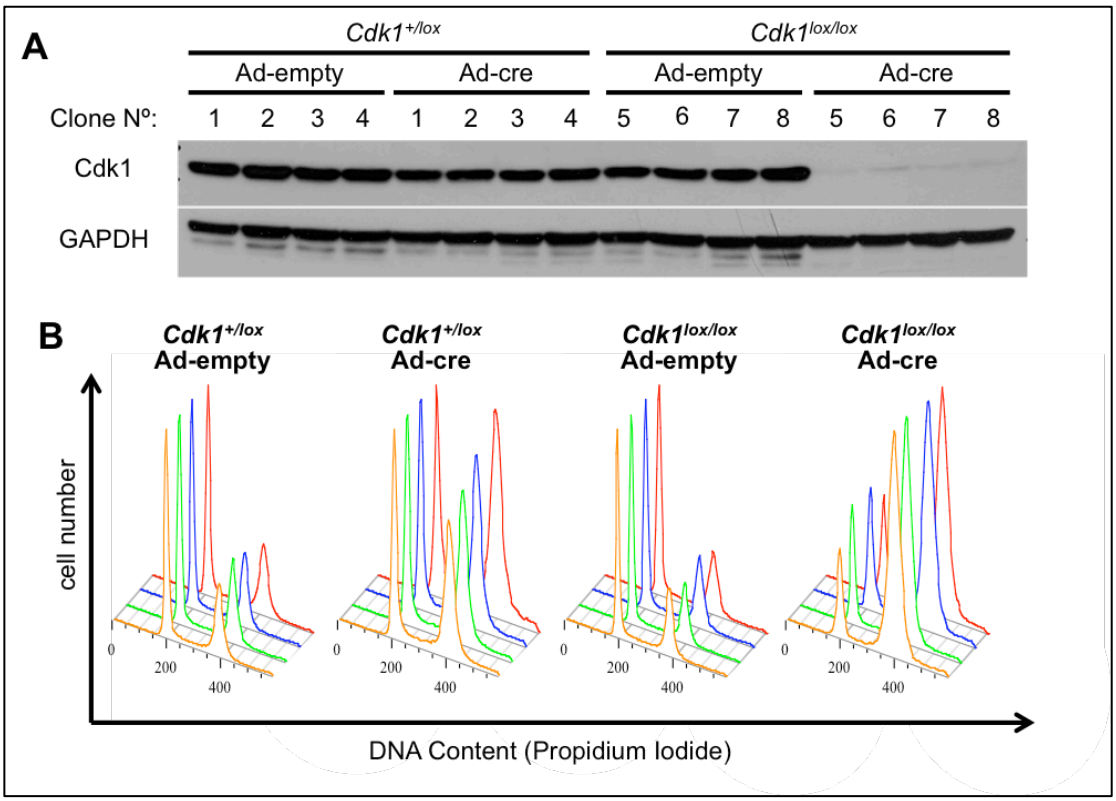

Figure 3: **Validation of *Cdk1lox* allele *in vitro*.** A) Western blot analysis of Cdk1 expression from four unique clones from respective genotypes of primary MEFs, extracted at E13.5 and infected at passage 2 with 100 MOI (multiplicity of infection) of either control Adenovirus (Ad-empty) or Adenovirus-expressing Cre-recombinase (Ad-cre) and analyzed 72 hours post-infection, GAPDH was analyzed as a control for protein loading. B) Cell cycle analysis (DNA content via PI) by flow cytometry of samples analyzed above, the four histograms (orange, green, blue and red) represent each individual clone for the respective genotype/condition.

In order to validate the functionality of the *Cdk1lox* allele, *Cdk1*$^{+/lox}$ animals were crossed and MEFs were extracted at E13.5. *Cdk1*$^{+/lox}$ and *Cdk1*$^{lox/lox}$ clones were seeded at equal densities and at passage 2 were infected with 100 MOI (multiplicity of infection) of Adenovirus (empty or Cre recombinase expressing) in order to analyze the ability of Cre recombinase in cleaving the *Cdk1lox* allele. The cells were then collected 72 hours post-infection to analyze for proper *Cdk1lox* recombination, protein expression of Cdk1 by western blot, and cell cycle distribution as determined by DNA content (incorporation of propidium iodide) by flow cytometry (Figure 3a,b). Our results show that upon Adeno-Cre infection the *Cdk1lox* allele is successfully cleaved resulting in a complete ablation of protein expression and an accumulation of cells with a 4n DNA content.

4.2 Generation and characterization of *Cdk1* knockout mice

The previously characterized *Cdk1* gene-trap mice resulted in early embryonic lethality at E1.5 (Santamaría et al. 2007). Therefore, to determine the effect of cleavage of the *Cdk1lox* allele on mouse homeostasis and viability, we crossed the *Cdk1*$^{+/lox}$ mice to the transgenic mouse strain expressing Cre recombinase under the control of the EIIa promoter. These mice transiently express Cre in the oocyte and fertilized embryos early during embryonic development (Clausen et al. 1999). Indeed the F1 generation of mice demonstrated efficient cleavage of the *Cdk1lox* allele (Figure 4a). We backcrossed *Cdk1*$^{+/\Delta}$ mice to C57Bl/6J and observed germline transmission and normal Mendelian ratios of the *Cdk1null* allele in heterozygosity. Crosses between heterozygous *Cdk1*$^{+/-}$ mice did not yield homozygous *Cdk1*$^{-/-}$ animals. Therefore, we set crosses between heterozygous *Cdk1*$^{+/-}$ superovulated female and stud male mice to extract early embryos. When embryos were extracted at E3.5 we could detect homozygous *Cdk1*$^{-/-}$ embryos by PCR (Figure 4b). However, when embryos were extracted at E1.5 and allowed to grow *in vitro*, the *Cdk1*$^{-/-}$ embryos were unable to progress past the two-cell stage, arresting and undergoing cell death (Figure 4c). This is congruent with the observation by immunofluorescence of an accumulation of phosphorylated γH2AX in the *Cdk1*$^{-/-}$ embryos extracted at E3.5 (Figure 4d,e). Moreover, *Cdk1*$^{-/-}$ E3.5 embryos had fewer and larger nuclei and did not appear to properly undergo compaction nor blastocyst formation. When we stained for Cdx-2 (trophoblast marker) and Oct4 (inner-cell mass marker) we observed no specific lineage pattern in the *Cdk1-null* embryos (Figure 4f). These findings, when taken together demonstrate that germline elimination of *Cdk1 in vivo* results in early embryonic lethality.

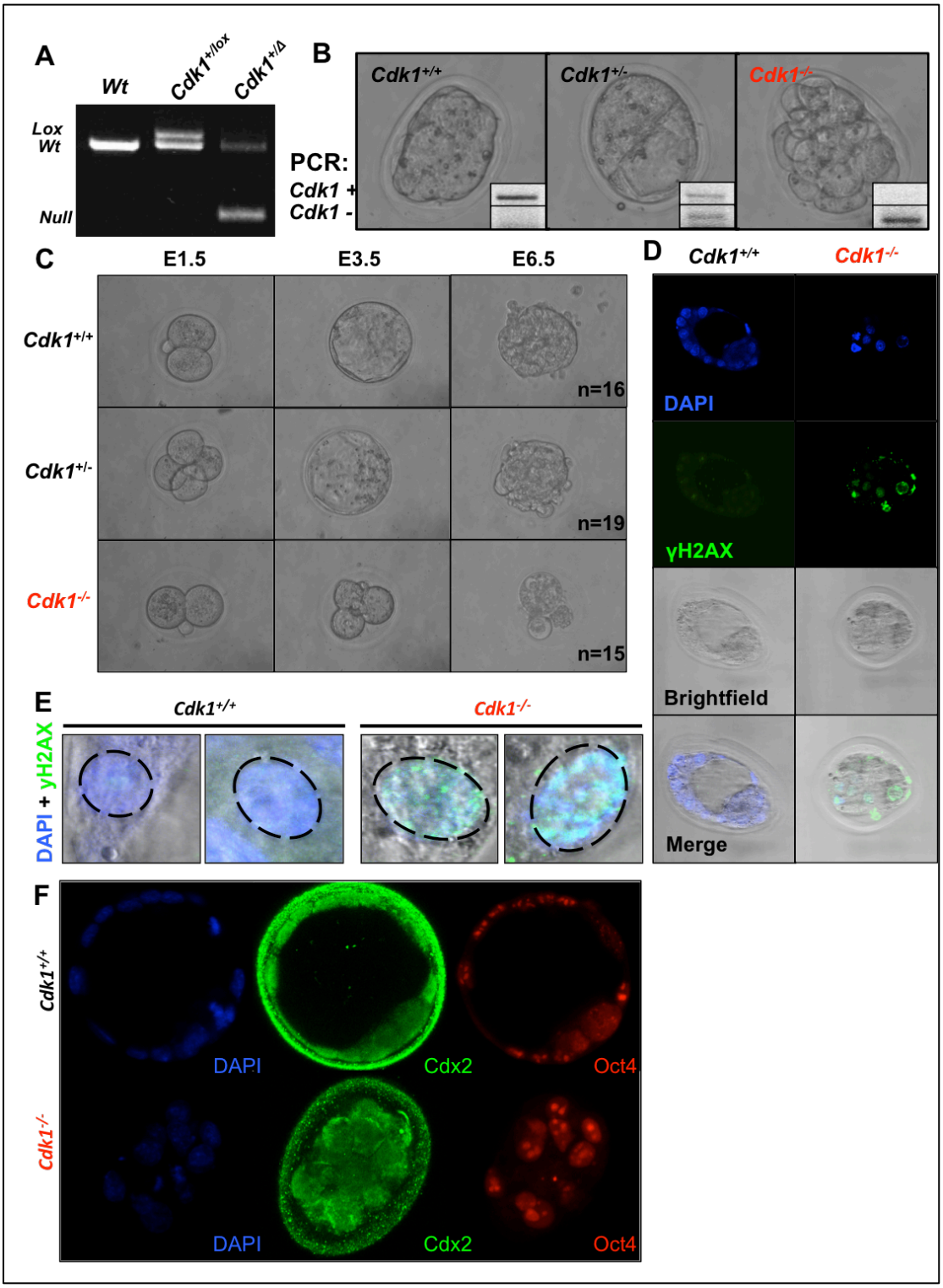

Figure 4: *Cdk1*-null mice are embryonic lethal. A) PCR identifying wild type (wt), *Cdk1lox* and cleaved *Cdk1lox* alleles from wild-type (Wt), *Cdk1*$^{+/lox}$ and *Cdk1*$^{+/lox}$*; EIIa-Cre*$^{+/T}$ mouse tail DNA. B) Representative images of embryos extracted at E3.5 and genotyped by PCR, inset showing *Cdk1* wild-type (Cdk1+), and *Cdk1-null* (Cdk1-) amplicons. C) Images of embryos extracted at E1.5 and grown *in vitro* up to hatching, photos are of E1.5, E3.5 and E6.5 respective to days post-coitum (genotypes as detected by PCR, n=number of embryos detected). D) Representative immunofluorescence of embryos extracted and stained at E3.5 for phosphorylated γH2AX (green) and DAPI (blue). E) High magnification of nuclei from two independent E3.5 embryos from each genotype stained for phosphorylated γH2AX (green) and DAPI (blue). F) Representative images of embryos extracted and stained at E3.5 for DAPI and lineage markers Cdx2 (green) and Oct4 (red).

4.3 Characterization of ubiquitous elimination of Cdk1 in adult mice

Cell division is essential for early embryonic development, therefore, the inability of *Cdk1-null* embryos to progress past several cell divisions was not surprising. However, in adult tissues and general homeostasis the role of Cdk1 had yet to be defined. Utilizing the conditional *Cdk1lox* mouse strain along with a conditionally induced and ubiquitously expressed Cre recombinase, our aim was to address this.

4.3.1 Comparison of Tg.hUBC-CreERT2 and RERT Cre recombinase activity

We first analyzed the efficiency of two commonly utilized Tamoxifen-inducible Cre recombinase strains: a transgenic line expressing the tamoxifen-inducible *Cre-ERT2* recombinase (Brocard et al. 1997) under the control of the human Ubiquitin C promoter (*Tg.hUBC-CreERT2*)(Ruzankina et al. 2007) and a knockin strain expressing the inducible *Cre-ERT2* recombinase under the control of the locus encoding the large subunit of RNA polymerase II (*RERT*)(Guerra et al. 2003). In order to assess the efficiency and expression of Cre recombinase activity, we utilized a β-geo reporter strain (*Gt-Rosa26-LSL-lacZ*)(Mao et al. 1999). This strain has a floxed stop cassette integrated downstream of exon 1 of the *Rosa26* locus and upstream of the β-geo (lacZ) reporter and antibiotic resistance fusion gene. Upon Cre-mediated excision of the stop cassette, transcription of the proviral *geo* gene is initiated from exon 1 of the *Rosa26* allele and is expressed ubiquitously during embryonic development and also in adult tissues (Mao et al. 1999; Zambrowicz et al. 1997).

We compared expression of the reporter allele by performing X-gal staining of tissues from *Gt-Rosa*$^{+/lslacZ}$*; Tg.hUBC-CreERT2*$^{+/T}$ and *Gt-Rosa26*$^{+/lslacZ}$*; RERT*$^{+ert}$ mice fed a Tamoxifen-containing diet *ad libitum* for two, four and eight weeks post weaning. We observed a more rapid and ubiquitous induction of expression in the *Gt-Rosa*$^{+/lslacZ}$*; Tg.hUBC-CreERT2*$^{+/T}$ mice as compared to the *Gt-Rosa26*$^{+/lslacZ}$*; RERT*$^{+/ert}$ mice (Figure 5 and Supplementary Figure 1a-c). Moreover, we found no expression of the *lacZ* reporter gene in the brain of *RERT* mice. Given that the expression and Cre recombinase efficiency of the *Tg.hUBC-CreERT2* was found to be superior to that of the *RERT* mice, we utilize this strain to determine the effect of *Cdk1* elimination in adult tissue homeostasis.

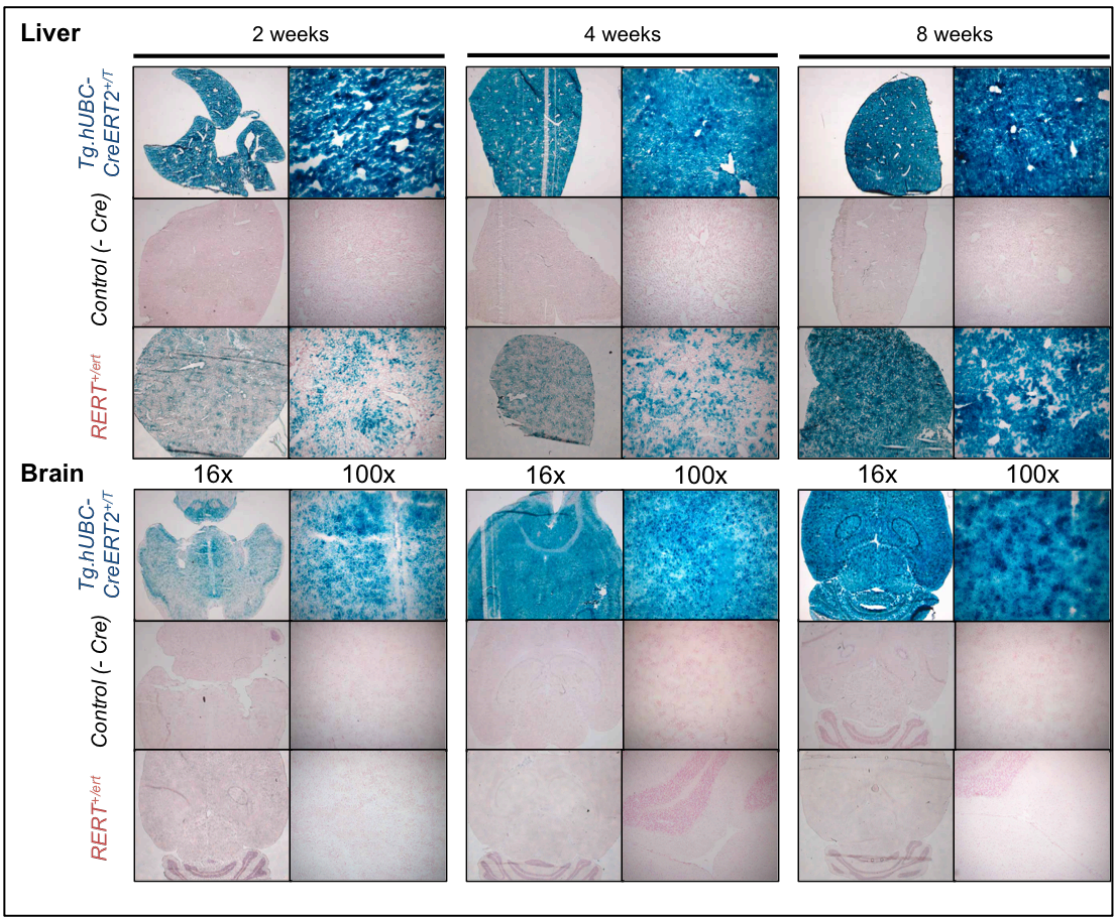

Figure 5: Comparison of *RERT* and *Tg.hUBC-CreERT2* inducible Cre cleavage efficiency. X-gal stained sections from liver and brain of 1) *Rosa26*$^{+/lslLacZ}$, *Tg.hUBC-CreERT2*$^{+/T}$ (*Tg.hUBC-CreERT2*$^{+/T}$), 2) *Rosa26*$^{+/lslLacZ}$, *RERT*$^{+/ert}$ (*RERT*$^{+/ert}$) or 3) *Rosa26*$^{+/lslLacZ}$ (-Cre) control mice at 2, 4 and 8 weeks of Tamoxifen-containing diet *ad libidum*.

4.3.2 Characterization of ubiquitous deletion of Cdk1 in adult mice

Wild-type, heterozygous and homozygous *Cdk1lox* mice were generated with the *Tg.hUBC-CreERT2* allele in heterozygosity. At post-natal day 30 (P30) mice were fed a Tamoxifen-containing diet *ad libitum* and placed under observation. Within two weeks of diet, homozygous *Cdk1*$^{lox/lox}$ mice presented at humane end-point with significant weight loss, hunched back, ruffled fur and decreased motility, whereas both wild-type and heterozygous animals appeared healthy (Figure 6a,b). We found that all homozygous *Cdk1*$^{lox/lox}$ mice would either die in their cage or need to be euthanized at humane end-point between seven and fifteen days in diet (Figure 6c). When histopathological analysis was performed on tissues collected at humane end-point (and respective time point in control animals), we observed significant atrophy and disorganization of all proliferative tissue compartments (Figure 6d). Specifically, in the gastrointestinal tract we observed an absence of crypts and villi in the stomach, intestine and colon, indicative of an inability to absorb nutrients which will lead to malnourishment and weight loss. In the skin we

observed a reduction in the epidermal layer as well as a thinning in the keratinized epithelium (Figure 6d). Bone marrow of mice depleted of Cdk1 presented with a depletion in the majority of cell types and the thymi were significantly reduced in size and showed disorganization of the cortex and medulla cellular compartments (Figure 6d). Isolated tissues processed for DNA extraction and assessed by southern blot showed near to complete *Cdk1lox* cleavage (Figure 6e). These results demonstrate that Cdk1 is essential for adult mouse tissue homeostasis and viability.

When Cdk1 is depleted from MEFs we observed an arrest at the G2-M transition of the cell cycle (Figure 3), thus we attempted to address the cell cycle arrest of cells in a proliferative tissue compartment (colon) of mice lacking Cdk1 by nuclear volume quantification. Samples were stained with DAPI and imaged by confocal microscopy to analyze for nuclear volume. When cells were divided into quartiles by nuclear size, we observe an decrease in the number of nuclei in the first quartile (with smaller nuclear size) as well as a significant increase in quartile 4 (with larger nuclear size)(Figure 7). This demonstrates that cells *in vivo* also acquire higher ploidy upon ablation of Cdk1.

To address the effect of Cdk1 elimination on proliferative cells *in vivo*, we performed immunohistochemical analysis of molecular markers associated with proliferation and cell death in proliferative tissue compartments. In mice depleted of Cdk1, we observed that cells in the intestine and colon were positive for both Ki-67 and Tpx-2 and unlike control heterozygous and wild-type animals, positive cells were distributed throughout the tissue and not restricted to the basal layer of the crypts (Figure 8 a,b). Ki-67 is a proliferative cell antigen and is present during all active phases of the cell cycle (G1, S, G2 and M)(Scholzen & Gerdes 2000). Tpx-2 is a microtubule binding protein and is expressed during S, G2 and M phases of the cell cycle. Given the significant disorganization of tissue structure it is difficult to conclude if there is an increase of positive staining cells or mainly a re-distribution of positive cells through the tissue compartment. We utilized 5-bromo-2'-deoxyrudine (BrdU), a synthetic nucleoside analog of thymidine that when injected into the peritoneum (IP) of mice will spread through the body and incorporate into the DNA of actively replicating cells. In mice lacking Cdk1, we also observed that BrdU positive cells were spread throughout the tissue and delocalized from the basal layer of the intestine and colon (Figure 8 a,b). Proliferation in the colon and intestine has been thoroughly investigated and is known to occur in the basally located crypts. Once the cells have divided they move up the villi towards the lumen where they are eventually shed.

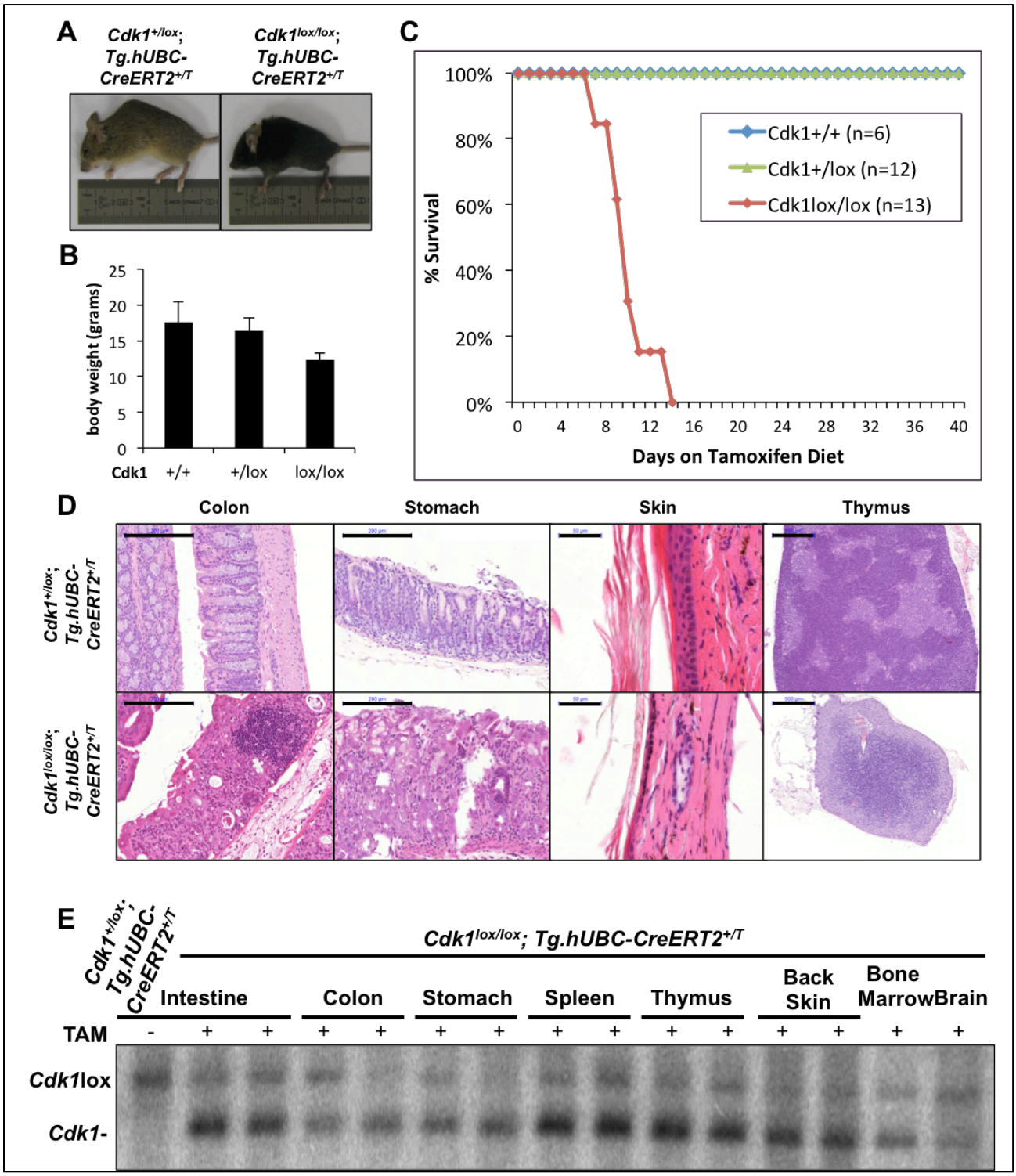

Figure 6: Cdk1 is essential for adult homeostasis and viability. A) Representative images of heterozygous and homozygous mutant *Cdk1lox; Tg.hUBC-CreERT2* mice at sacrifice (2 weeks of Tamoxifen containing diet). B) Average weight at sacrifice of *Cdk1* wild-type, heterozygous and homozygous mutant mice. C) Kaplan-Meier survival curve of *Cdk1lox; Tg.hUBC-CreERT2* mice from start of Tamoxifen-containing diet. D) Hematoxylin and Eosin staining of proliferative tissues. Scale bars are the following lengths: 200μm for colon & stomach, 50μm for skin and 500μm for thymus. E) Southern blot of *Cdk1lox* excision in two respective tissue sample lysates from independent mice after treatment with Tamoxifen-containing diet (TAM) for two weeks.

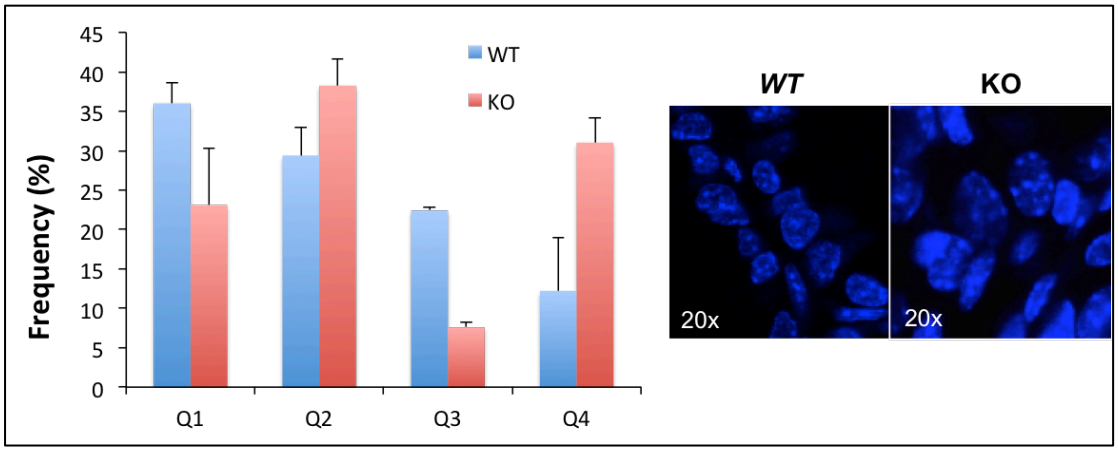

Figure 7: Cdk1 ablation *in vivo* results in an increase in ploidy. DAPI stained colon sections were assessed for nuclear size by confocal microscopy analysis and nuclei were divided into four size quartiles. Graph depicts the percentage of cells in each quartile (Q1-4) for the wild-type and KO respectively. The standard deviation was calculated between 2 WT and 3 KO respective independent samples. Representative images of DAPI-stained nuclei from a WT and KO sample of the same scale.

The delocalization of cells positive for proliferative markers (Ki-67, Tpx-2 and Brd-U) could suggest that cells are arresting in the cell cycle and being displaced from the crypts, although with the significant atrophy that we observe it is difficult to conclude. To determine if elimination of Cdk1 resulted in cell death, we also stained for cleaved Caspase-3 in proliferative tissue compartments. We observed an increase in positive cells in the spleen, thymus and bone marrow of mice depleted of Cdk1 (Figure 8 c,d). When taken together, these data demonstrate that Cdk1 is essential for proliferative tissue compartment homeostasis and that upon depletion of Cdk1 cells will increase in ploidy, stain positive for proliferative cell markers and functionally disrupt the homeostatic tissue architecture. Moreover, we observe an increase in cleaved Caspase-3 a molecular marker for apoptosis.

When analyzing the samples, we also observed a significant depletion of bone marrow, with the exception of megakaryocytes, which appeared to be unaffected by the loss of Cdk1 (Figure 9a,b). Megakaryocytes undergo endomitosis, a process of polypoloidization where cells enter mitosis but exit without segregation. In collaboration with Marianna Trakala and Marcos Malumbres, further genetic analysis of Cdk1 using a megakaryocyte-specific Cre (Pf4-Cre)(Tiedt et al. 2007) demonstrated that megakaryocytes lacking Cdk1 cannot undergo endomitosis but rather undergo endoreplication as an alternative to polyploidization (Trakala et al. 2015, Appendix 2). Endoreplication is a process of polypoloidization where the cell undergoes multiple rounds of replication without entering mitosis and can be a result of Cdk1 inhibition (Zielke et al. 2015).

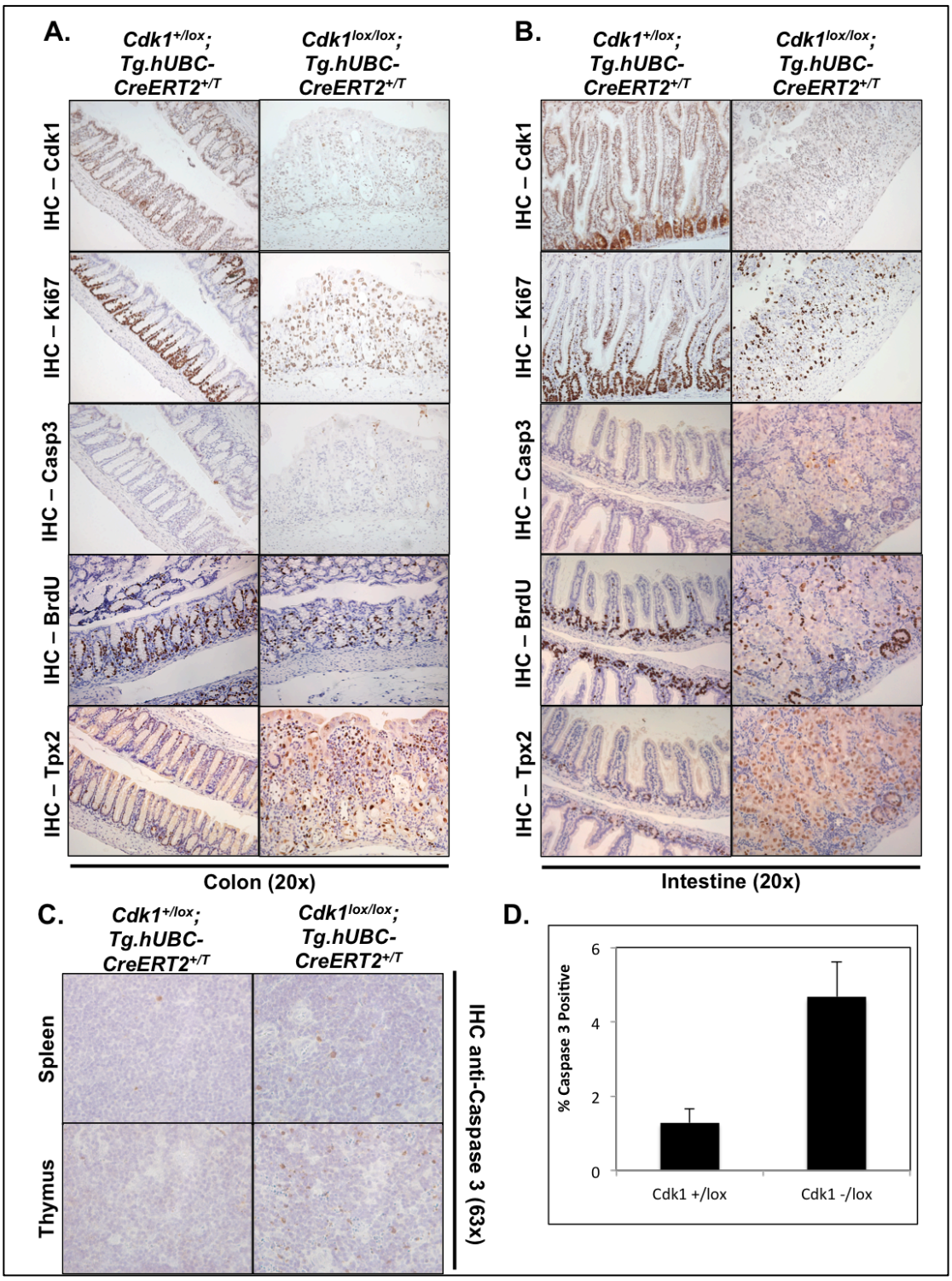

Figure 8: Ablation of Cdk1 *in vivo* results in proliferative tissue atrophy and functional disorganization of tissue architecture along with inducing apoptosis. A) Representative images of colon samples from *Cdk1*$^{+/lox}$ and *Cdk1*$^{lox/lox}$ mice sacrificed at humane end-point and stained for Cdk1, Ki-67, Caspase 3, BrdU, and Tpx2. B) Representative images of intestine samples from *Cdk1*$^{+/lox}$ and *Cdk1*$^{lox/lox}$ mice sacrificed at humane end-point and stained for Cdk1, Ki-67, Caspase 3, BrdU, and Tpx2. C) Representative images of thymus and spleen samples stained for cleaved Caspase 3. D) Quantification of Caspase 3 positive cells in the bone marrow of *Cdk1*$^{+/lox}$ and *Cdk1*$^{-/lox}$ mice (at least 1100 cells were counted per sample, n=2 for each genotype).

These findings are consistent with the observation that *in vivo,* Cdk1 is dispensable for entry into the cell cycle as well as S phase progression and can lead to increased ploidy in proliferative cell types.

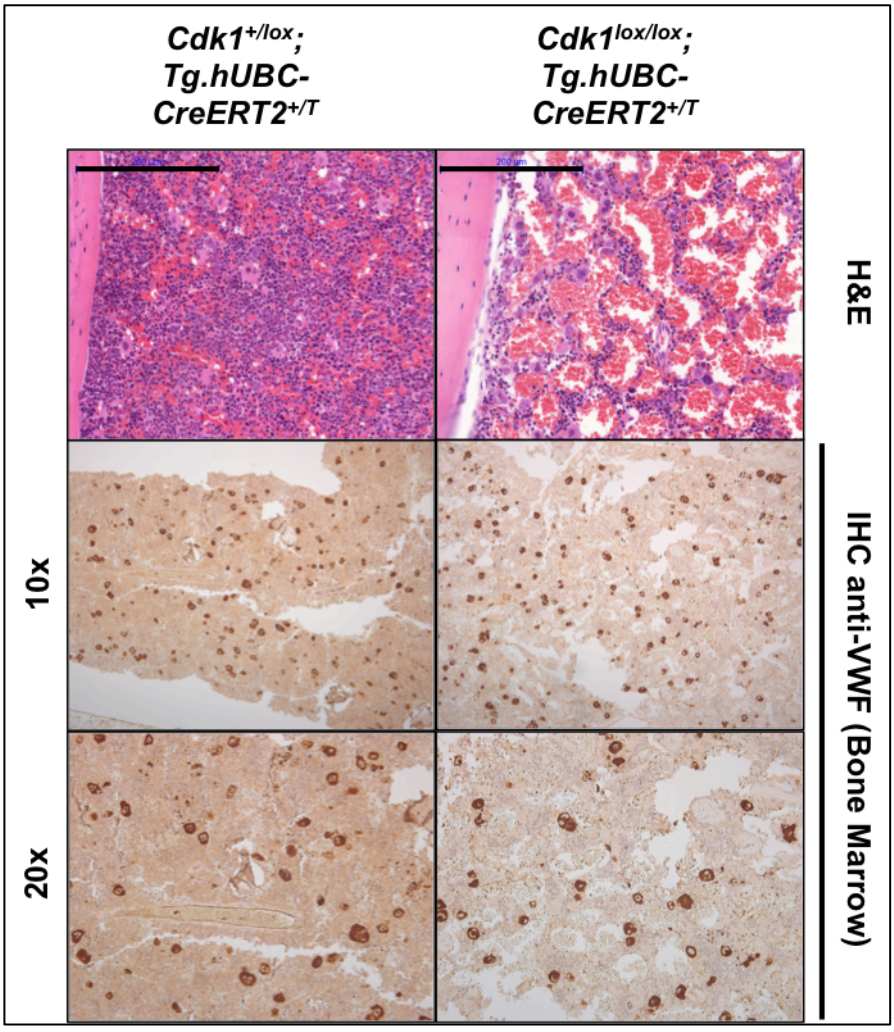

Figure 9: Cdk1 is dispensable for Megakaryocytes. (Top panel) Hematoxylin and Eosin staining of bone marrow samples from *Cdk1*$^{+/lox}$ and *Cdk1*$^{lox/lox}$ mice sacrificed after two weeks of Tamoxifen-containing diet, scale bar 200μm. (Middle and lower panel) Von Willebrand Factor staining in bone marrow of samples from *Cdk1*$^{+/lox}$ and *Cdk1*$^{lox/lox}$ mice after two weeks of Tamoxifen-containing diet.

4.4 Analysis of tissue-specific roles of Cdk1 *in vivo*

4.4.1 Cdk1 expression in the Purkinje cells of the cerebral cortex

Given that Cdk1 was initially identified as a regulator of cellular division, its role in proliferative tissues and the cell cycle was to be expected. With the aim of determining if Cdk1 plays a tissue-specific or physiological role *in vivo* aside from its cell cycle associated kinase activity, we prepared a tissue microarray from three 8 week old females,

three 60 week old females and six males from the respective ages for testis samples. All mice were from a C57Bl6/129 background and samples were collected from the central nervous system (brain and cerebellum), epithelial organs (back and tail skin, stomach, intestine, colon, lung bronchi and alveoli, bladder, kidney and mammary gland), hematopoietic and lymphatic systems (bone marrow, thymus, lymph node from mammary gland and spleen), endocrine system (pituitary, pancreas, suprarenal and thyroid) and others (white adipose tissue, brown adipose tissue, liver, heart, ovary and testis). We then performed immunohistochemical analysis on TMA sections for the colocalization of Cdk1 and Ki-67 or lack thereof (Figure 10a). While almost all tissues showed the expected colocalization of Cdk1 and Ki-67 (Figure 10b), we identified Cdk1 expression to be independent of Ki-67 in Purkinje cells of the cerebellum of both young and old mice (Figure 10b). Purkinje cells are GABAergic neurons located in the cortex of the cerebellum and play a fundamental role in controlling motor movement. To identify if there is active transcription of Cdk1 in the Purkinje cells, we isolated RNA from laser-capture microdissected Purkinje cells. The expression of Cdk1 in Purkinje cells was only identified in one out of nine samples of microdissected Purkinje cells by RT-PCR (positive and representative negative samples shown in Figure 10c), whereas we were able to detect PCP-2 (Purkinje cell protein 2) in all samples. While inconclusive, this could be a result of low levels of Cdk1 active transcription or a technical difficulty in detecting the transcript in this tissue type.

The expression of Cdk1 has not been previously associated with Purkinje cells, however, Purkinje cells do have a distinct transcriptional profile. In Cyclin D1 and D2 knockout mice Purkinje cells were found to be abnormally positioned resulting in problems with coordinated movement (Ciemerych et al. 2002). Moreover, cell cycle proteins, including Cyclins A, B, D and E along with Cdks 1, 2 and 4, have been shown to be expressed and form functional complexes in differentiated, post-mitotic neurons of the neocortex in adult mouse brains (Schmetsdorf et al. 2007). Under physiological conditions the expression of cell cycle related proteins may be associated with transcriptional or metabolic regulation (Tamaru et al. 1993; Miyajima et al. 1995; Schmetsdorf et al. 2005). However, in neurodegenerative disorders, such as Alzheimer's disease, an unscheduled up-regulation of cell cycle-associated proteins has linked cell cycle reactivation to neuronal cell death (Nagy et al. 1997; McShea et al. 1997).

In order to address the role of Cdk1 in Purkinje cells *in vivo*, we crossed the *Cdk1lox* allele to a Purkinje-specific Cre recombinase (Tg.*Pcp-2-Cre*)(Barski et al. 2000).

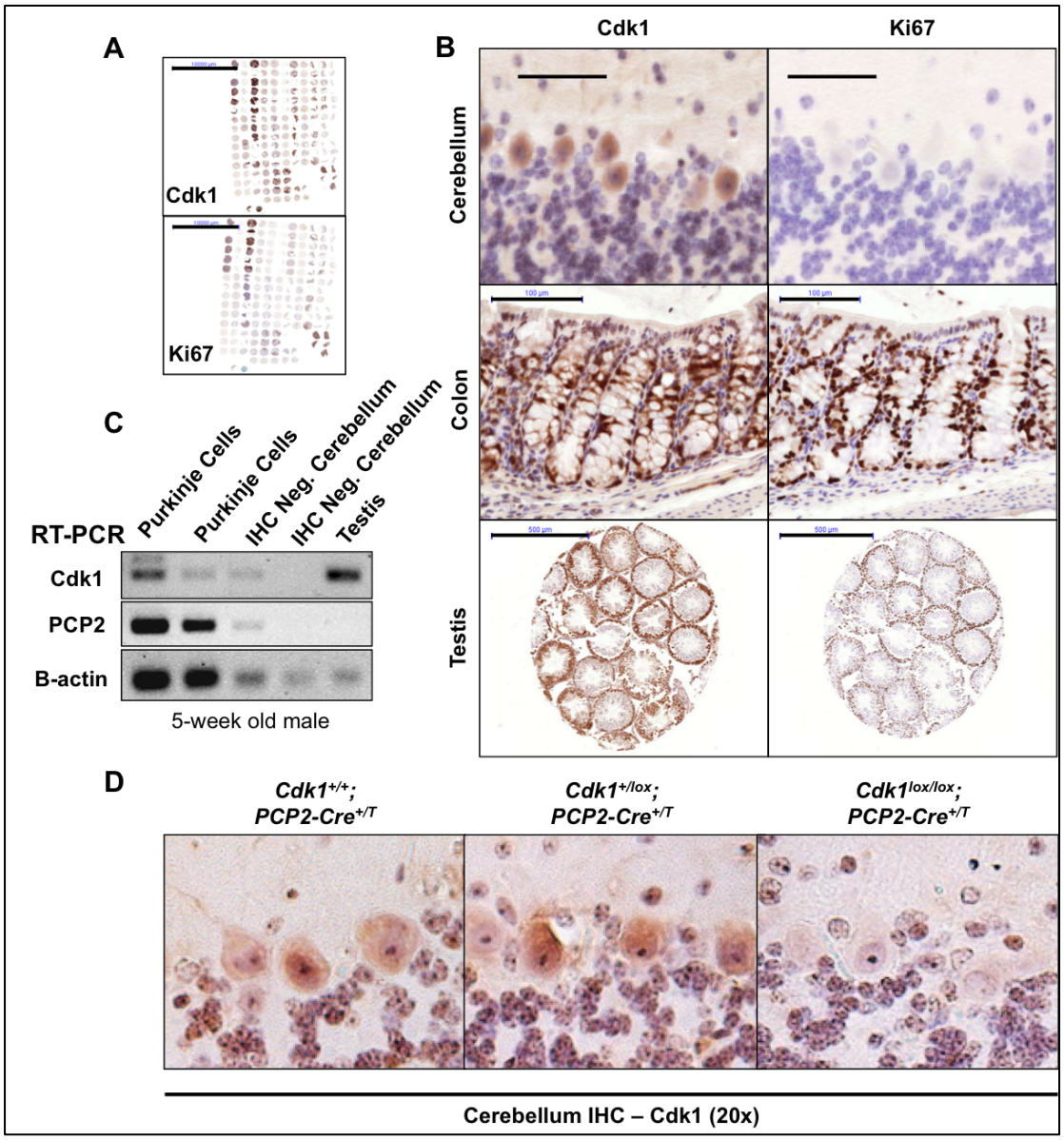

Figure 10: Cdk1 is expressed independently of the cell cycle in Purkinje cells of the cerebellum. A) Immunohistochemistry (IHC) of Cdk1 and Ki67 of consecutive sections of Tissue Microarray (TMA) samples, scale bars 10000µm. B) Cdk1 and Ki67 IHC of consecutive sections of Purkinje Cells of the Cerebellum (scale bars 50µm), Colon (scale bars 100µm) and the Testis (scale bars 500µm). C) Representative RT-PCR analysis of laser microdissected Purkinje Cells, neighboring Cdk1-negative brain tissue and testis for Cdk1, PCP-2 (Purkinje cell protein 2) and B-actin. D) Representative micrograhs of Cdk1 IHC on cerebellum sections from respective *Cdk1lox; Pcp2-Cre* (Purkinje-specific Cre) mice at 8 months of age.

Recombinase activity is first observed around postnatal day 6 and fully established two to three weeks after birth in the majority of Purkinje cells and some retinal bipolar neurons. We maintained *Cdk1$^{lox/lox}$; Tg.Pcp-2-Cre$^{+/T}$* mice until 8-9 months of age (n=8) and observed no obvious physiological or motor function phenotype as compared to WT or heterozygous littermate controls. We confirmed the ablation of Cdk1 in Purkinje cells by IHC (Figure 10d). However, in order to fully identify the role of Cdk1 expression in the

Purkinje cells of the cerebral cortex further physiological and motor-function tests would need to be performed. Due to the scope of this project, this line of investigation was not pursued further.

4.4.2 Role of Cdk1 in angiogenesis

Angiogenesis is the physiological process by which new blood vessels are formed from existing blood vessels and is required both in maintenance and repair of vasculature. In contrast to vasculogenesis, or *de novo* generation of blood vessels, angiogenesis creates new vessels from existing vasculature. There are two types of angiogenesis, sprouting angiogenesis and intussusceptive angiogenesis. Sprouting angiogenesis is characterized as having four phases: 1) Activation of endothelial cells which results in the alteration and partial degradation of the mother vessel's basement membrane allowing for endothelial cell projection into the connective tissue; 2) Parallel migration of polarized endothelial cells and formation of the capillary bud; 3) Basement membrane formation along the growing capillary bud; 4) Coverage of growing capillary bud by proliferating pericytes resulting in the formation of the new vessel. Intussusceptive angiogenesis is the formation of new vessels by splitting an existing vessel in two and is carried out in four phases: 1) The two opposing capillary walls establish a zone of contact; 2) Reorganization of the endothelial cell junctions creates a perforation in the vessel bilayer allowing growth factors and cells to enter the lumen; 3) A pericyte and myofibroblast core/pillar is formed between the two new vessels at the zone of contact, these cells will begin laying the collagen fibers to provide the extracellular matrix for vessel formation; 4) Finally, as the core grows the two daughter vessels will form. Intussusceptive angiogenesis occurs without a significant increase in the number of endothelial cells, thus without the need for cellular proliferation. Whereas sprouting angiogenesis does indeed require proliferation. Sprouting angiogenesis, where proliferating endothelial cells contribute to the growth of the new vessel, is the primary mechanism involved in physiological angiogenesis.

Angiogenesis is a process that is essential for most tumor formation, thus significant efforts have focused on determining mechanisms to block angiogenesis. The majority of research has surrounded growth factors which induce the activation of endothelial cells, such as vascular endothelial growth factor receptor (VEGFR), and have resulted in the development of inhibitors that are currently being used in the clinic (*e.g.* Pazopanib and Regorafenib). A study performed in a mouse model for p185BCR-Abl+ B-acute lymphoid leukemia found that Cdk6 forms part of a transcription complex that

induces expression of the tumor suppressor p16INK4a and the pro-angiogenic factor VEGF-A (Kollmann et al. 2013). In tumors lacking functional expression of p16INK4a, Cdk6 was able to promote tumor formation by stimulating proliferation as well as angiogenesis (Kollmann et al. 2013). These findings provide a link between cell cycle progression and angiogenesis, however further studies will be needed to fully elucidate the role of cellular proliferation in angiogenesis.

In order to assess the role of proliferation in angiogenesis directly, we targeted Cdk1 elimination in the endothelial compartment of mice and induced angiogenesis physiologically using a wound healing assay. We made use of the *Tie-2* driven tamoxifen-inducible Cre recombinase, *Tie2-CreERT2* knockin mouse (Rodrigo Dieguez-Hurtado and Sagrario Ortega unpublished data). Tie-2 is an angiopoietin tyrosine kinase receptor expressed on endothelial cells from embryogenesis through adulthood and is responsible for binding angiopoietin and inducing angiogenesis (Dumont et al. 1994; Suri et al. 1996; Puri et al. 1995; Sato et al. 1995; Wong et al. 1997). We crossed these mice to the conditional *Cdk1lox* mice and the reporter *Gt-Rosa26-lslLacZ* mice. First we assessed Cre recombinase activity by performing X-gal staining on the peritonea and diaphragms of *Cdk1lox* heterozygous and homozygous mice fed a tamoxifen-containing diet for five months. These tissues were analyzed for their dense microvasculature and tissue transparency in imaging. In both the heterozygous and wild-type mice we observed normal branching and density of microvasculature as well as complete induction of Cre recombinase activity in all vessels (Figure 11a). Given that angiogenesis is required for normal vascular homeostasis, this data could suggest that Cdk1, or endothelial cell proliferation, is in fact dispensable for normal vascular homeostasis. However, the *lacZ* reporter allele is only indirect evidence of *Cdk1lox* cleavage and we were unable to properly assess for *Cdk1lox* cleavage in the entire endothelial compartment, thus we cannot rule out the possibility of ineffective *Cdk1lox* cleavage.

A common and well-defined scenario where sprouting angiogenesis is actively induced is during the course of wound healing. A skin wound, when the epidermal and dermal layers are broken, induces an intricate biochemical cascade that will trigger the healing process. This process is initiated by hemostasis, or blood clotting, followed by inflammation, the growth of new tissue (proliferation) and remodeling of tissue (maturation). Angiogenesis specifically takes place during the proliferative stage to reconstruct the broken or lost vasculature in the wounded area and will initiate days after the injury lasting up to a couple months. In order to determine the role of Cdk1 in the

angiogenic response of vasculature during wound healing, we fed wild-type, heterozygous and homozygous *Cdk1lox* mice a Tamoxifen-containing diet *ad libidum* for a month prior to the assay.

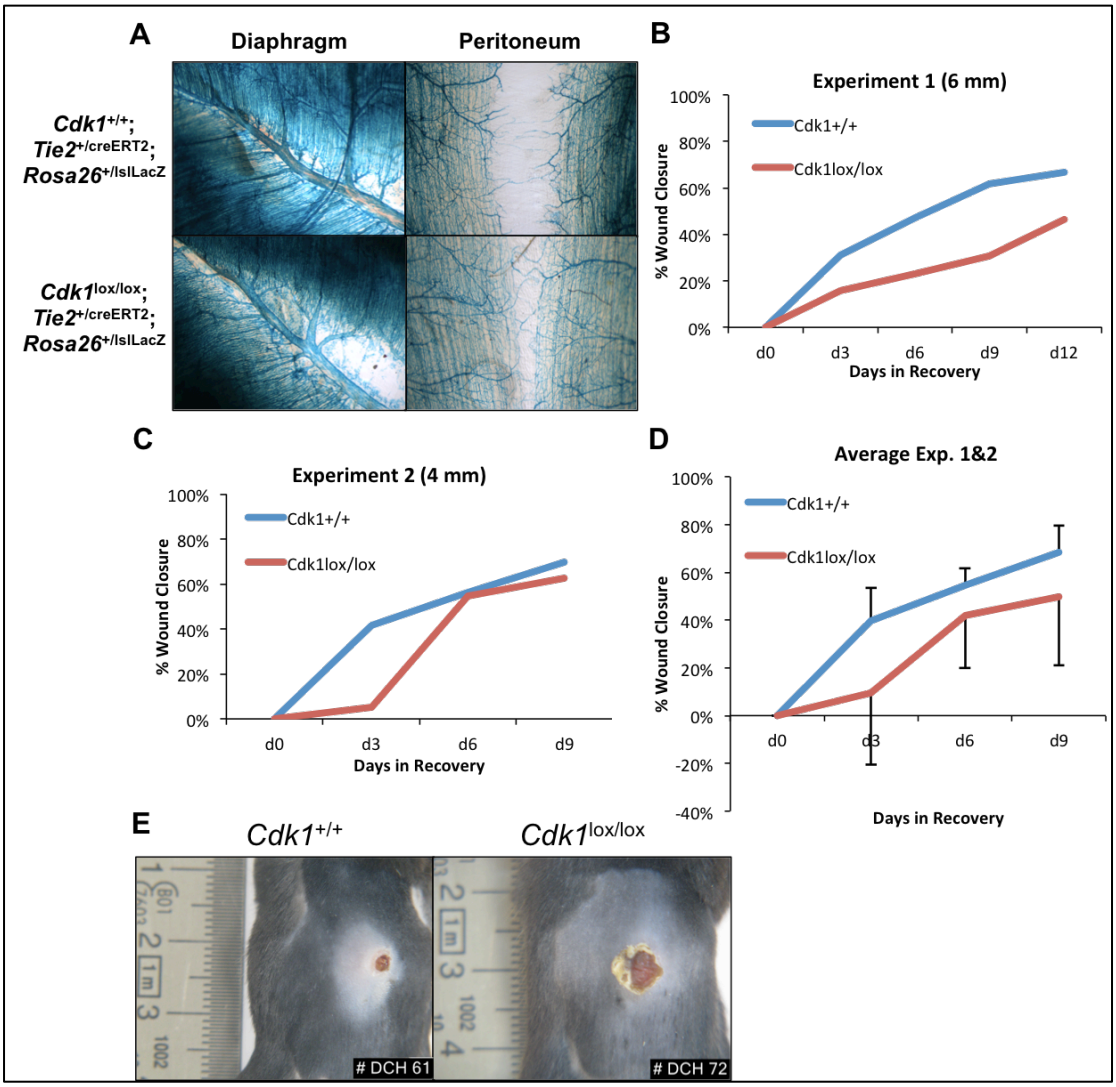

Figure 11: Role of Cdk1 in physiological angiogenesis. A) X-gal staining of diaphragm and peritonea of respective *Cdk1lox; Tie2-CreERT2; Rosa26lslLacZ* mice. B) Analysis of first wound healing experiment (4 mm wound size). C) Analysis of second wound healing experiment (6 mm wound size). D) Average of experiments 1 and 2. E) Representative images of wounds from experiment 1 at sacrifice (day 12 – d12) of $Cdk1^{+/+}$ and $Cdk1^{lox/lox}$ mice with endogenous *Tie2-CreERT2* and having been fed a Tamoxifen-containing diet for 1 month prior to assay (lower right-hand inset is mouse ID).

An initial experiment was performed utilizing a skin punch of 6 mm to induce circular wounds medially on the shaved back skins of 2 $Cdk1^{+/+}$ and 4 $Cdk1^{lox/lox}$ mice. The wounds were measured daily and collected as samples at day 12 to analyze molecular markers of angiogenesis. We observed a reduction in the kinetics of wound healing in both the heterozygous and homozygous *Cdk1lox* mice. An initial lag was observed at day

3, with 31.1% closure in the wild-type mice and 19% and 15.9% closure in the heterozygous and homozygous *Cdk1lox* mice. The mice depleted of Cdk1 were only able to reduce wound size on average by 46.4%, the heterozygous control achieved 59.2% wound closure, whereas the wild-type control reached 66.6% wound closure (Figure 11b,e).

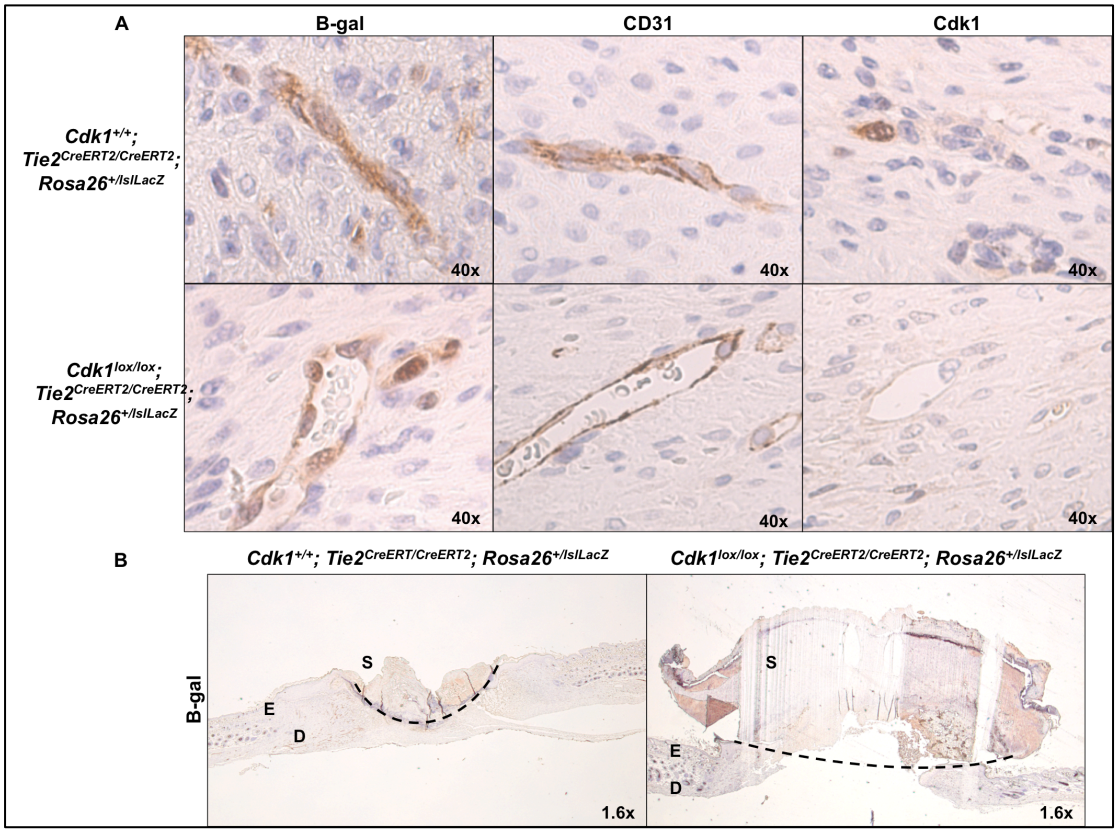

Figure 12: Ablation of Cdk1 in endothelial compartment delays wound healing. A) B-gal, CD31 and Cdk1 IHC of vasculature from consecutive tissue sections proximal to wound of respective mice. B) B-gal IHC of wound and neighboring skin of wild-type and homozygous *Cdk1lox* mice. Images were taken from samples in Experiment #1. (E: epidermis, D: Dermis, S: Scab, dotted line: division between wound/scab and epidermal and dermal regrowth).

Given these findings, we performed a second experiment where two, 4 mm circular wounds were made bilateral to the dorsal medial plane on the shaved back skins of 2 $Cdk1^{+/+}$ and 3 $Cdk1^{lox/lox}$ mice. We utilized smaller wounds in the second experiment so that we could induce two measurable wounds per mouse, maximize the data obtained and minimize variability per mouse. We also made four additional wounds, bilateral to the dorsal medial plane and inferior to the initial wounds, three and six days after the initial wounds so that we could obtain samples at earlier stages during the wound healing process. These additional wound measurements were not taken into consideration for the kinetics. When we look at the day 3 kinetics in the second experiment we observe a

stark delay in wound healing of the homozygous (5.3% closure) *Cdk1lox* mice as compared to the control wild-type (41.5% closure) mice (Figure 11c). However, overall at the time of sacrifice we only observed a 69.5% and 62.5% closure in wild-type and homozygous *Cdk1lox* mice respectively at day 9 (Figure 11c). When we averaged the percent wound closure between the experiments for the wild-type and homozygous *Cdk1lox* mice, we observe an overall delay in wound healing kinetics, suggesting that lack of Cdk1 results in a delayed or inefficient wound healing angiogenic response.

We performed immunohistochemical analysis of Cdk1, CD31 (an endothelial cell marker) and β-gal expression in the skin surrounding the wound and the neighboring tissue. We observed sufficient Cre recombinase activity to induce expression of the β-gal marker as well as deplete Cdk1 from the endothelial cells in the neighboring dermis of the wound (Figure 12a). We also observed that histopathologically the wild-type control animals displayed advanced wound healing, with significant regrowth of the epidermis and dermis below the wound, whereas in the homozygous *Cdk1lox* mice the scab is still present and skin regeneration has not occurred to the same extent (Figure 12b). These data taken together with the wound healing kinetics demonstrate that depletion of Cdk1 leads to delayed or impaired wound healing, further suggesting proliferation to be a key aspect of sprouting angiogenesis. Further studies will be needed to fully elucidate the molecular mechanisms involving Cdk1 in wound-induced angiogenesis.

4.4.3 Role of Cdk1 in tumor-driven angiogenesis

Given the initial findings we obtained with the wound healing assays and the importance of angiogenesis in tumor development and progression, we decided to target Cdk1 depletion in the endothelial compartment of mice with Tg.*MMTV-PyMT* driven mammary tumors. Breast tissue is highly vascularized and it has long been accepted that angiogenesis plays a pivotal role in breast neosplasms (Folkman 1971). Previous studies have demonstrated breast tumors to be highly vascularized with Tie2-positive endothelia (Peters et al. 1998). The transgenic mouse model *Tg.MMTV-PyMT* expresses the polyomavirus middle T antigen under the control of the murine mammary tumor virus promoter/enhancer (Guy et al. 1992). In this strain female carriers will develop palpable mammary tumors as early as 5 weeks of age (in FVB background) which are highly vascularized and can metastasize to the lung; while male carriers will also develop mammary tumors, albeit at a later age (Guy et al. 1992; Gao et al. 2008). We crossed

these mice to the *Cdk1lox, Tie2-CreERT2; Gt-Rosa26-LSL-LacZ* strain and maintained the *Tie2-CreERT2* in homozygosity, the *Gt-Rosa26-LSL-LacZ* in either homozygosity or heterozygosity and the *Tg.MMTV-PyMT* in heterozygosity. Given that the resulting genetic background would result in varied survival outcomes, we performed a Kaplan Meier survival analysis on female carriers of the *Tg.MMTV-PyMT* transgene and determined median survival to be 20 weeks of age with detectable hyperplasias at 10 weeks of age in our strain's genetic background (Figure 13a,b). We confirmed vascularity of *Tg.MMTV-PyMT* tumors by staining 10 week hyperplasias and neighboring tissue for CD31 (Figure 13c), observing positively stained vasculature associated with both tissue types.

We waited until mice developed palpable tumors and then fed $Cdk1^{+/+}$, $Cdk1^{+/lox}$, and $Cdk1^{lox/lox}$ animals a Tamoxifen-containing diet *ad libidum*. We confirmed Cre recombinase activity in the tumor vasculature by performing X-gal staining on tumor samples of animals fed a Tamoxifen-containing diet (Figure 13d). We then performed a Kaplan-Meier statistical analysis of survival on the sample cohorts and found that there was a increase in median survival of the $Cdk1^{lox/lox}$ animals (n=7) to 40.5 days post Tamoxifen diet, as compared with 25.5 and 20 days in the $Cdk1^{+/lox}$ (n=21) and $Cdk1^{+/+}$ (n=6) cohorts respectively (Figure 13e). Although we observed an increase in median survival, the number of animals analyzed for the $Cdk1^{lox/lox}$ genotype was limited to 7, and 6 in the $Cdk1^{+/+}$ genotype, and the variation we observed was too significant to faithfully draw any conclusions.

Given the inconclusiveness of our findings, we cannot rule out the potential for targeting proliferation in the endothelial compartment as a way to inhibit tumor-associated angiogenesis. However, tumors are capable of bypassing the need for physiological angiogenesis, which could provide the tumor an evasion mechanism for a approach of this kind. Evidence has shown that certain types of tumors (melanomas and gliomas) are capable of generating their own vasculature in a process termed vasculogenic mimicry (Maniotis et al. 1999; El Hallani et al. 2010; Schnegg et al. 2015; Liu et al. 2013). In this process tumor cells will mimic endothelial cells and form tumor associated vasculature. While, vasculogenic mimicry has yet to be thoroughly investigated in all tumor types, it is clear that tumors have multiple mechanisms to overcome failed angiogenesis. Thus, targeting Cdk1 in the endothelial compartment as an endeavor to thwart endothelial proliferation may not be sufficient in bypassing the capability of the tumor to generate and recruit necessary vasculature.

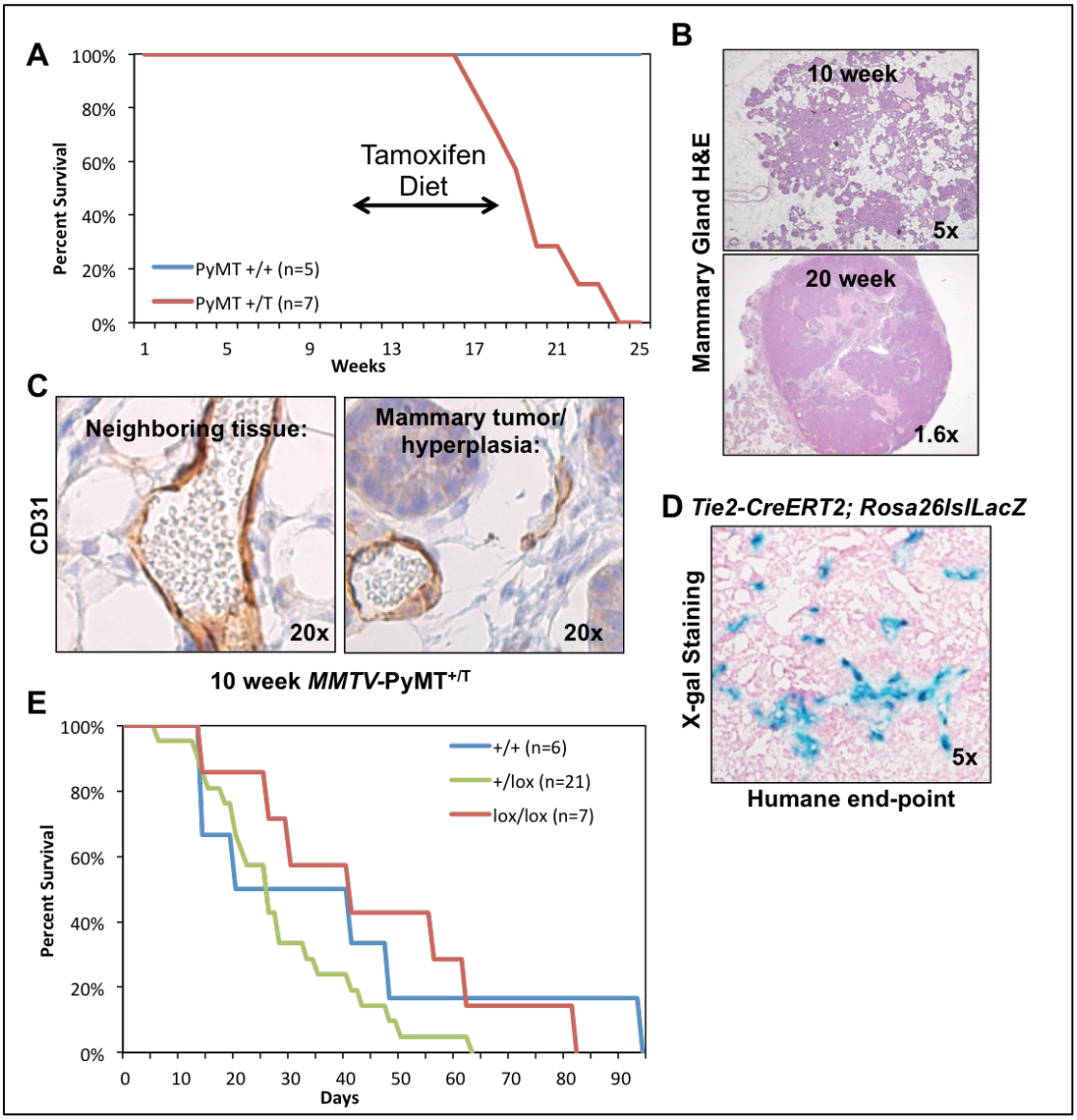

Figure 13: Targeting proliferation in endothelial compartment to inhibit tumor-associated angiogenesis. A) Kaplan-Meier survival curve in weeks of *Tg.MMTV-PyMT* in mixed genetic background (FVB/C57Bl/6J). "Tamoxifen Diet" refers to therapeutic treatment window. B) Representative image of 10 and 20 week PyMT mouse mammary hyperplasia and adenoma respectively. C) IHC of CD31 in 10-week hyperplasia and neighboring healthy mammary tissue. D) X-gal staining of 20 week tumor. E) Kaplan-Meier survival curve of all mice analyzed. F) Kaplan-Meier survival curve of mice analyzed removing outliers. G) Fold change in tumor burden during Tamoxifen-containing diet.

4.5 Cell cycle function of Cdk1

4.5.1 Cell cycle analysis in MEFs

We have so far observed the essential role of Cdk1 in early embryogenesis and adult homeostasis, particularly in proliferative tissues. Thus, to obtain a clear understanding of minute cell cycle changes upon elimination of Cdk1, we generated primary MEFs carrying the *Cdk1* conditional allele in combination with the *Tg.hUBC-*

CreERT2 transgene. We initially isolated wild-type, heterozygous and homozygous *Cdk1lox* genotypes and addressed the functionality of Cre recombinase activity in these cells by southern blot. To avoid the positive selection pressure of cells maintaining Cdk1 under proliferative conditions, cells were synchronized and maintained in G0 by serum starvation with 0.1% FBS for 72, 96 and 120 hours in the presence of 4-hydroxytamoxifen (4-OHT, a metabolite of Tamoxifen, was utilized in cell culture since Tamoxifen cannot be properly metabolized by the cells). We observed significant, but not complete cleavage of *Cdk1lox* alleles by southern blot analysis (Figure 14a).

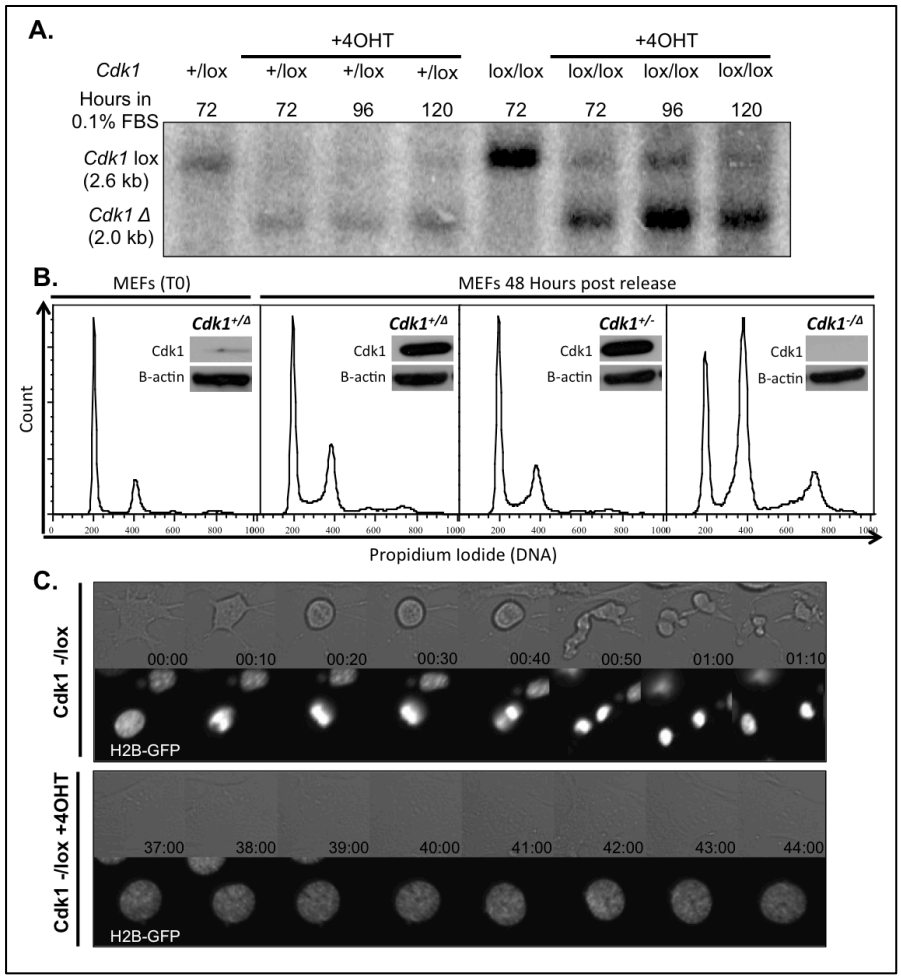

Figure 14: *Cdk1-null* MEFs arrest with a 4n DNA content and do not enter into mitosis. A) Southern blot analysis of *Cdk1lox* cleavage after serum starvation for 72, 96 and 120 hours respectively in the presence of 4-OHT containing medium. B) Cell cycle analysis by flow cytometry (DNA content by PI) and western blot analysis of protein expression from cell lysates at time of flow cytometry analysis (insets). C) Representative time-lapse images of serum starved (0.1% FBS for 96 hours) and stimulated (+10% FBS) *Cdk1-/lox* (no 4-OHT) vs. *Cdk1-/Δ* (+4-OHT) MEFs expressing H2B-GFP. Top panels, for each condition, show brightfield images and bottom field shows H2B-GFP fluorescence expression. Time stamps in upper panels of *Cdk1-/lox* cells represent time since entrance into mitosis (showing ten minute intervals), while *Cdk1-/Δ* time stamps are the time since serum starvation release (showing 1 hour intervals) (hh:mm).

Given this finding, we decided to include the *Cdk1-null* allele in conjunction with the *Cdk1lox* allele in an attempt to facilitate the elimination of the *Cdk1lox* allele. Indeed when we synchronized *Cdk1$^{-/lox}$; Tg.hUBC-CreERT2* cells in G0 by serum starvation for 72 hours and then stimulated their release into the cell cycle (with 10% FBS), we observed efficient cleavage of the *Cdk1lox* allele by western blot analysis of protein expression up to 48 hours post-release (Figure 14b-insets). We then compared the cell cycle kinetics of the *Cdk1-null* cells with germline heterozygous (*Cdk1$^{+/-}$; Tg.hUBC-CreERT2$^{+/T}$*) or induced heterozygous (*Cdk1$^{lox/-}$; Tg.hUBC-CreERT2$^{+/T}$*) control MEFs and observed that cells lacking Cdk1 were able to enter and progress through the S phase of the cell cycle arresting with a 4n DNA content (Figure 14b). Moreover, to ensure that cells were not entering mitosis, we performed time-lapse microscopy of synchronized cells expressing a histone H2B-GFP fluorescence marker to observe chromatin condensation. As compared to the heterozygous control cells, the cells lacking Cdk1 did not undergo chromatin condensation, nuclear envelope breakdown or mitotic entry (Figure 14c and supplemental videos).

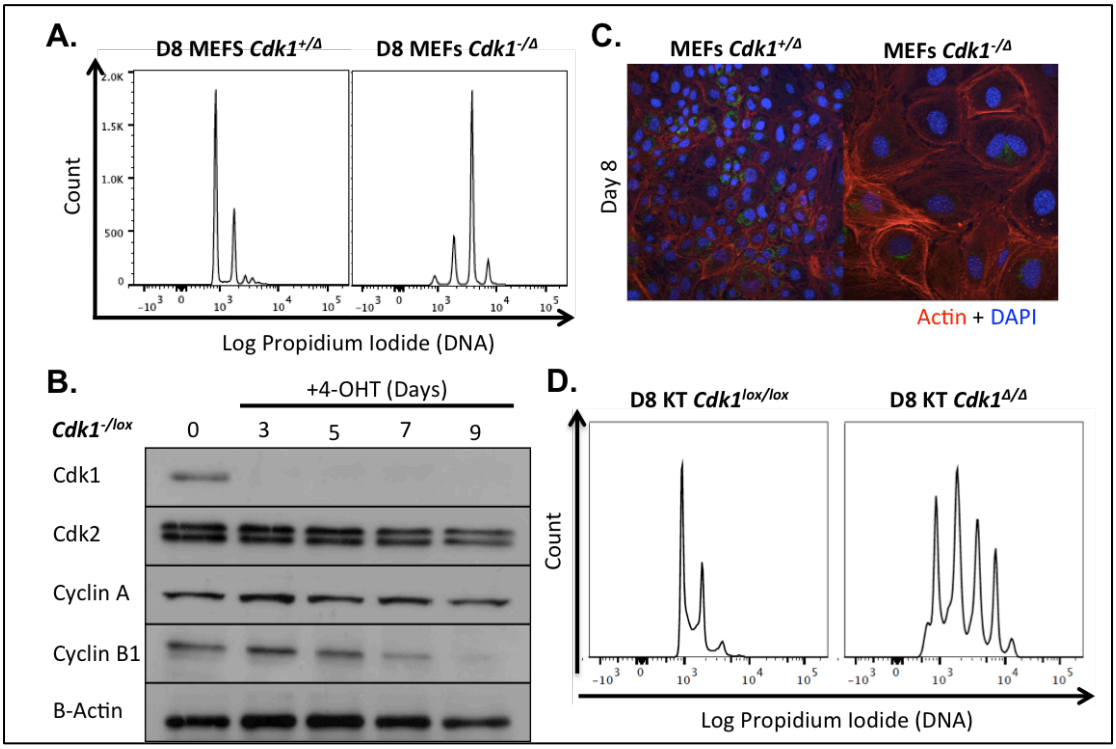

Figure 15: *Cdk1-null* differentiated cell types undergo multiple rounds of endoreplication. A) Cell cycle analysis of *Cdk1$^{+/\Delta}$* and *Cdk1$^{-/\Delta}$* MEFs with endogenous *Tg.hUBC-CreERT2* at day 8 of asynchronous culture in the presence of 4-OHT containing media. B) Western blot analysis of cell cycle proteins (Cdk1, Cdk2, Cyclin A, Cyclin B1 and B-Actin as a loading control) in *Cdk1$^{-/lox}$; Tg.hUBC-CreERT2$^{+/T}$* MEFs over time, post addition of 4-OHT to culture media (Days 0, 3 5, 7 and 9 respectively). C) Immunofluorescence of heterozygous and null *Cdk1lox; Tg.hUBC-CreERT2* cells at day 8 post-addition of 4-OHT to culture media. D) Cell cycle analysis of keratinocytes from *Cdk1$^{lox/lox}$; Tg.hUBC-CreERT2$^{+/T}$* animals, 8 days post-addition of 4-OHT to culture medium or in the absence of 4-OHT at respective time of culture.

To address the length of the cell cycle arrest we performed asynchronous depletion of Cdk1 and collected samples for flow cytometry analysis of cell cycle distribution 8 days post-addition of 4-OHT to the culture media. We observed that cells lacking Cdk1 underwent multiple rounds of endoreplication resulting in up to 16n ploidy (Figure 15a). Moreover, when we analyzed Cyclin B and A along with Cdk2 expression levels in these MEFs over time, we observed a gradual decrease of Cyclin B in cells lacking Cdk1 5-7 days post-addition of 4-OHT to culture media, whereas Cyclin A and Cdk2 protein levels remained mostly unchanged (Figure 15b). When we analyzed these cells by immunofluorescence staining of the DNA (DAPI) and actin (phalloidin) we observed cells to be larger both in cytoplasmic as well as nuclear size (Figure 15c). Taken together these results demonstrate that elimination of Cdk1 in MEFs results in cell cycle arrest at the G2-M transition and multiple rounds of endoreplication.

4.5.2 Cell cycle analysis in Keratinocytes

MEFs are commonly utilized in the analysis of molecular interactions and biochemistry as they are well characterized. In order to confirm our findings in a secondary primary cell type, we extracted keratinocytes from the tail skin of young *Cdk1lox; Tg.hUBC-CreERT2* mice. Cells were maintained in the presence of 4-OHT for 8 days and analyzed by flow cytometry for cell cycle distribution. Indeed we observed that upon ablation of Cdk1, keratinocytes also underwent multiple rounds of endoreplication reaching a ploidy of up to 32n (Figure 15d). These results further demonstrate that Cdk1 elimination results in G2-M cell cycle arrest and can induce multiple rounds of endoreplication in differentiated cell types.

4.5.3 Molecular analysis of G2-M cell cycle arrest upon depletion of Cdk1

Cdk1 has thoroughly been studied for the indispensable function it provides at the G2-M transition of the cell cycle. In all model systems only Cdk1 bound with Cyclin B1 has been capable of providing the substrate specificity as well as reach the kinetic activity necessary to surpass the restrictive threshold at the G2-M transition. Cdk1 activity is balanced through inhibitory phosphorylation by Wee1 and Myt-1 kinases as well as positively by the Cdc25 family of phosphatases. These are in turn negatively and positively regulated by Cdk1 itself respectively, creating a bi-stable switch able to provide the specific activity necessary for the cell to enter into mitosis. However, balance at the G2-M transition is also provided by Greatwall/Mastl kinase, via the phosphorylation of Arpp19 and alpha-Endosulfine (ENSA). Arpp19 and ENSA inhibit the PP2A family of

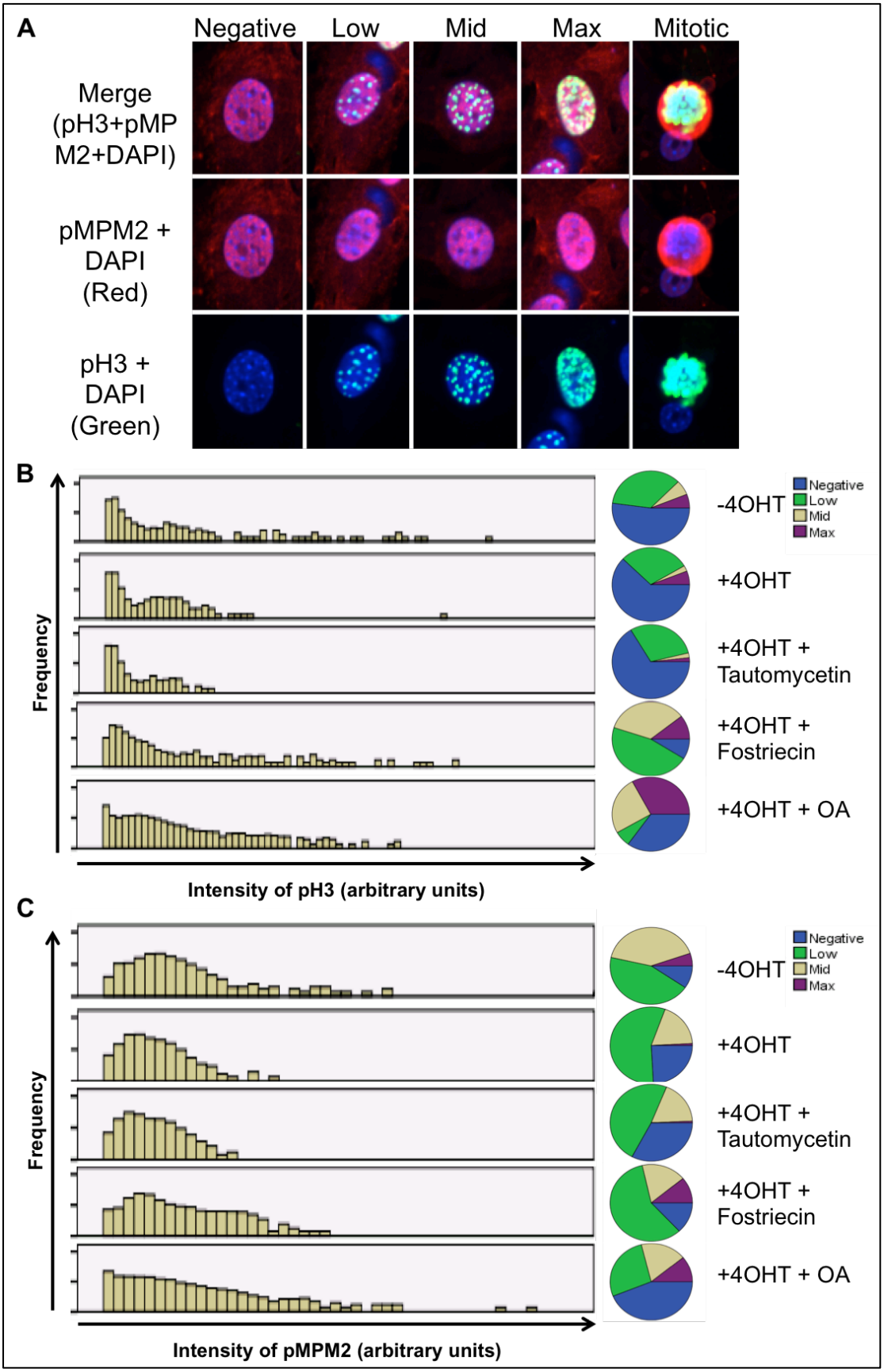

Figure 16: Inhibition of PP2A partially rescues G2-M cell cycle arrest in absence of Cdk1. A) Representative images of fluorescence signals within the 4 groups (negative, low, mid, max) and mitotic signal for phosphorylated Histone H3 (pH3 – Green) and phosphorylated MPM-2 (pMPM2 – Red). B) Intensity, frequency and quantification of pH3 in *Cdk1lox* MEFs with the respective treatments. C) Intensity, frequency and quantification of pMPM2 in *Cdk1lox* MEFs with the respective treatments. (OA: Okadaic Acid)

phosphatases (Mochida et al. 2010; Gharbi-Ayachi et al. 2010), which dephosphorylate the myriad of Cdk1 mitotic substrates necessary to enter into mitosis. Cdk1 itself activates Greatwall/Mastl, albeit indirectly, however the intricacies of this mechanism have yet to be fully elucidated (Domingo-Sananes et al. 2011). Thus at the G2-M transition of the cell cycle, there is a fine balance between mitotic kinase activity and inhibitory phosphatase activity.

Utilizing the *Cdk1lox; Tg.hUBC-CreERT2* cells, we set out to determine if cells can compensate for the lack of Cdk1 when mitotic inhibitory signals are diminished. To do this we made use of the high-throughput confocal microscope (Opera) and the previously tested experimental conditions for G2-M cell cycle arrest upon serum starvation and release in the absence of Cdk1. We utilized staining against phosphorylated histone H3 (pH3), which is phosphorylated on serine 10 during mitosis, as well as the monoclonal antibody recognizing phosphorylation of serine/threonine mitotic epitopes (pMPM-2) as readouts for mitotic entry. We performed the experiment by synchronizing cells by serum starvation and then stimulating re-entry into the cell cycle. At 36 hours post-release cells were treated with one of the following inhibitors: 1) Fostriecin, an antitumor antibiotic from *Streptomyces pulveraceous*, which shows inhibitory activity against protein phosphatase types 2A (PP2A) and 4 (PP4); 2) Tautomycetin, a selective inhibitor of protein phosphatase 1 (PP1) resulting in an inhibition of proliferation; 3) Okadaic Acid, a naturally occurring polyether toxin derived from marine dinoflagellates, *Prorocentrium spp.*, which acts as a reversible, potent and selective inhibitor of PP2A and PP1. All cells and conditions were treated with Vincristine 12 hours post-release, an anticancer drug that disrupts microtubules and can stably maintain a mitotic cell cycle arrest (Manchado et al. 2010), in order to capture all cells that entered into mitosis. Cells were then fixed and stained 48 hours post-release, processed by the Opera and analyzed using tailored scripts to detect nuclei and fluorescent intensity (as outlined in Materials and Methods and Figure 16a).

Using this system we confirmed that MEFs lacking Cdk1 do not enter into mitosis as there was no significant associated pH3 or pMPM-2 fluorescence signal detected (Figure 16b,c – second row). Cells lacking Cdk1 and treated with Tautomycetin also showed no induction of pH3 or pMPM-2 (Figure 16b,c – third row). However, we did observe a significant induction of pH3 and pMPM-2 in *Cdk1-null* cells treated with either Fostriecin or Okadaic Acid (Figure 16b,c – 4th and 5th rows respectively). These results demonstrate that when the inhibitory mechanisms counteracting pro-mitotic

kinase activity are disrupted, specifically PP2A, cells lacking Cdk1 have the capacity to enter into mitosis. Given the strong requirement for cylin-associated kinase activity at the G2-M transition, we hypothesize that other Cdks are capable of compensating for the loss of Cdl1.

4.6 Compensation for Cdk1 *in vivo*

While Cdk1 can compensate for the loss of interphase Cdks, a Cdk that can compensate for the absence of Cdk1 has yet to be described. If indeed there is no specialized function for Cdk1, but rather the functions of Cdk1 at the G2-M transition are solely due to the accumulation of Cdk-associated kinase activity; we may suggest that the ability of interphase Cdks to compensate for Cdk1 could be achieved by reducing Cdk-associated inhibitory signals or decreasing the kinase threshold required for mitotic entry. Indeed the observation that depletion of PP2A-associated phosphatase activity in G2 will allow for mitotic entry in cells lacking Cdk1, is a clear demonstration that of the cyclin-associated G2-M kinase activity threshold being lowered to facilitate mitotic entry. Similar evidence generated with shRNA against Cdk1 in wild-type, *p21-null* and DKO MEFs for *p21* and *Cdk2*, demonstrated the ability of *p21-null* MEFs to progress the cell cycle further into G2 or mitosis (as detected by pH3) when Cdk1 is depleted (Figure 17a,b). This was dependent upon Cdk2, as the DKO MEFs were unable to enter into mitosis (Figure 17b,c). These findings further support the cylin-assocated kinase threshold model of the cell cycle, where in the absence of a potent Cdk-inhibitor, p21, Cdk2 was capable of partially compensating for Cdk1 in promoting the G2-M transition.

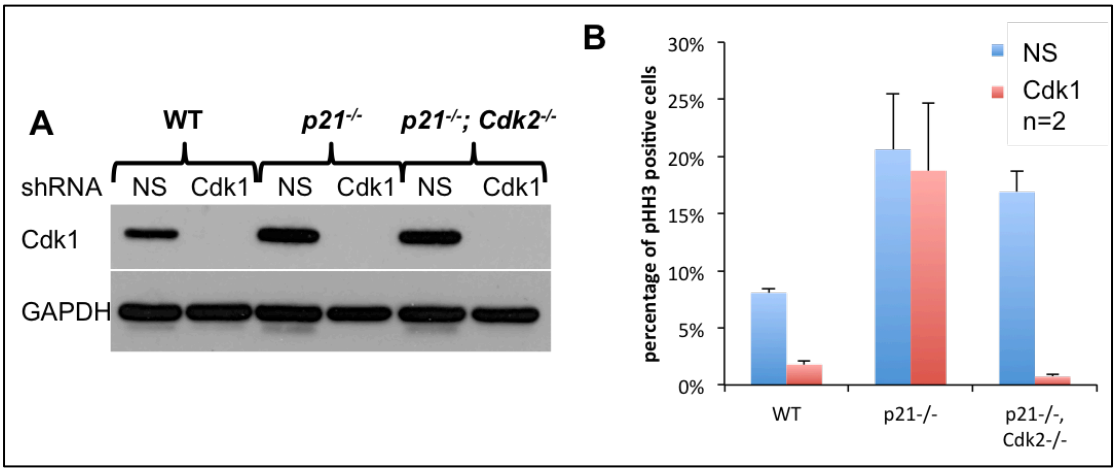

Figure 17: Partial rescue of G2-M cell cycle arrest in cells depleted of Cdk1 by concomitant absence of *p21*. A) Western blot of Cdk1 and GAPDH (loading control) for respective genotypes and shRNA (NS: non-specific control, Cdk1). B) pH3 quantification by IF for MEFs with respective genotypes, with and without Cdk1 inhibition. MEFs were synchronized by serum starvation (0.1% FBS for 72 hours) and released by stimulation with 10% FBS for 24h.

Therefore, with the aim to confirm this data *in vivo*, we generated *Cdk1; p21* double knockout embryos and followed their development *ex vivo* to see if they could rescue the *Cdk1-null* lethality. Indeed we were able to obtain embryos that progressed past the stage of *Cdk1*$^{-/-}$ embryonic arrest (E1.5-3.5), embryos formed morulae and blastocysts but began to die before hatching (Figure 18a). In fact, all of the *Cdk1*$^{-/-}$*; p21*$^{-/-}$ DKO embryos appeared to arrest and undergo cell death, being incapable of hatching from the *zona pelucidae* (Figure 18a).

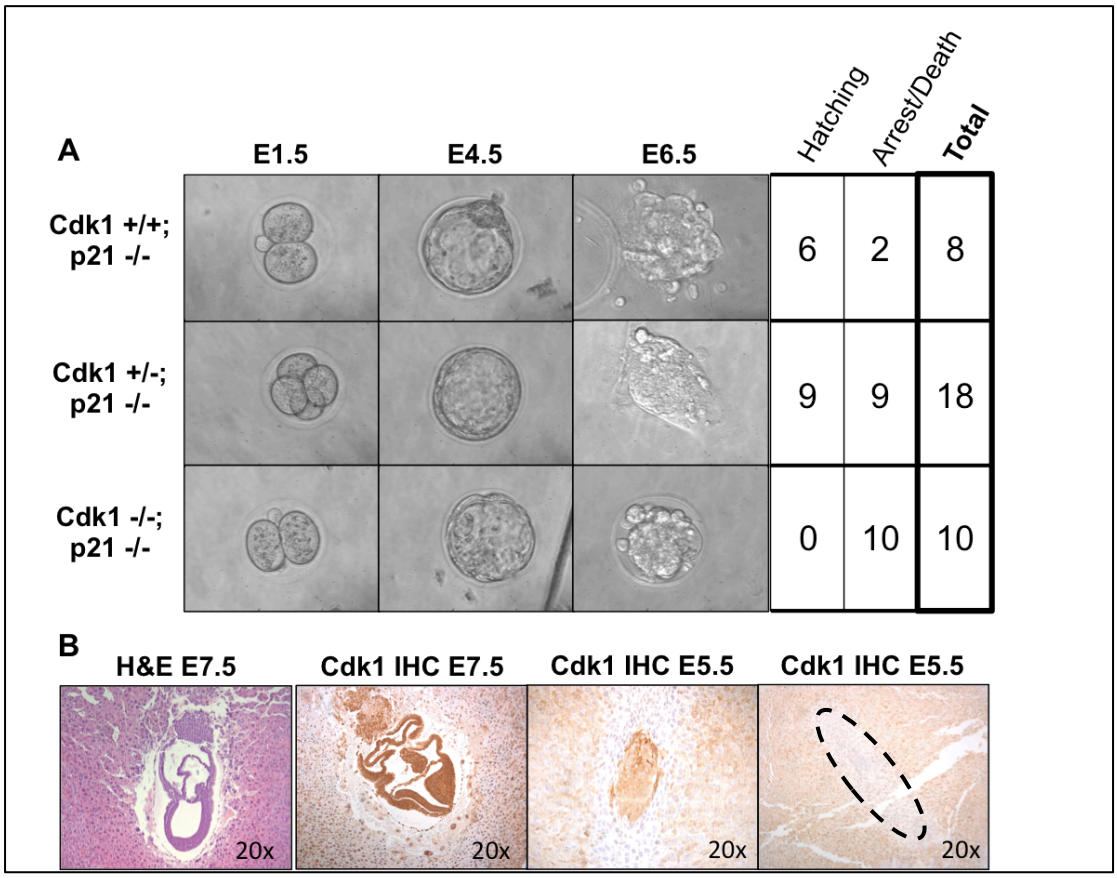

Figure 18: Early embryo *Cdk1-null* proliferative arrest is partially rescued in absence of p21. A) Representative images (at E1.5, E4.5 and E6.5 respective to days post-coitum) of embryos extracted at E1.5 and grown *in vitro* with respective genotypes. Table outlines number of embryos presenting with each phenotype (hatching or developmental arrest and embryonic death). B) Micrographs of Hematoxylin and Eosin (H&E - left panel) and Cdk1 IHC (right three panels) of decidua from *Cdk1; p21* crosses isolated at embryonic day 7.5 (E7.5 - left two panels) and E5.5 (right two panels). Last panel shows a Cdk1-negative staining zone in a decidua where no embryo was detected (outlined by dotted line)

To assess under more physiological conditions the observed rescue by *p21-null* in *Cdk1-null* embryonic proliferative arrest, we extracted *p21-null* decidua at E7.5 and E5.5 and performed immunohistochemical analysis of Cdk1 expression. We extracted 32 decidua at E7.5 and found 19 embryos that stained positive for Cdk1 (Table 3 and Figure 18b). The remaining decidua did not have detectable embryos (Figure 18b – last panel on

right). At E5.5 we extracted 14 decidua and found 9 embryos that all stained positive for Cdk1 (Table 2 and Figure 18b). These data demonstrate that *Cdk1-null; p21-null* (double knockout DKO) embryos can indeed progress further in embryonic development when compared to the *Cdk1*-KO embryos and thus are capable of compensating for a lack of Cdk1 up until peri-implantation stage of development. While the rescue is only partial, this is the first evidence *in vivo* of the mammalian cell cycle progressing in the absence of Cdk1.

	IHC + Cdk1	ND
E5.5	**9**	**5**
E7.5	**19**	**13**

Table 2: Decidua genotypes by IHC from *Cdk1; p21* crosses. Embryo genotypes as determined by IHC of Cdk1 in E5.5 and E7.5 decidua (ND: not detected).

4.7 Role of Cdk1 in embryonic and induced pluripotent stem cells

The lethality we observed in *Cdk1*$^{-/-}$ embryos at E3.5 is intriguing because it is at the first stage of major differentiation where the inner cell mass (ICM) and the trophoectoderm lineages are formed. In fact in the presence of wild-type *p21*, *Cdk1*$^{-/-}$ embryos do not undergo proper compaction, arresting between the 8-16 cell stage. The ICM is the source of ES cells and as previously discussed maintains a distinct cell cycle profile from that found in MEFs or Keratinocytes. Given the distinct cell cycle and limited cell cycle regulatory mechanisms present in ES cells(White & Dalton 2005; V. C. Li et al. 2012), we decided to analyze the role of Cdk1 in ES and iPS cell cycles.

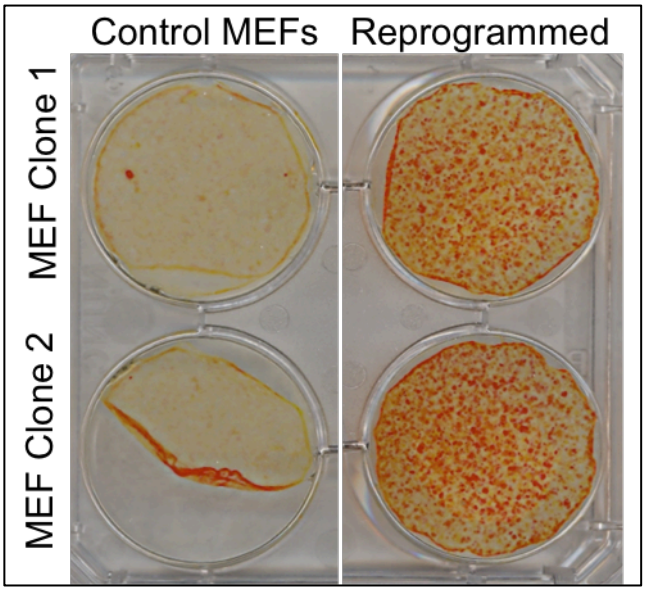

Figure 19: Alkaline phosphatase activity of 4F reprogrammed MEFs. Representative alkaline phosphatase activity staining (orange) in 4F reprogrammed MEFs (4F – Yamanaka 4 factors, Oct4, c-Myc, Klf4 and Sox2). Two independent clones shown for reprogrammed and control MEFs.

Induced pluripotent stem cells (iPS) are generated by exogenously inducing Oct4, Sox2, c-Myc and Klf4 transcription factor activity in MEFs until the expression becomes endogenous and the MEFs reprogram into pluripotent stem cells capable of forming self-renewable colonies, differentiating into the three germ layers, forming teratomas and contributing to chimera formation (Takahashi & Yamanaka 2006). We generated iPS cells from the *Cdk1lox*; *Tg.hUBC-CreERT2* MEFs and isolated ES cells from ICM outgrowths from E3.5 embryos of the *Cdk1lox; Tg.hUBC-CreERT2* mouse strain. The clones we isolated were positive for alkaline-phosphatase activity (Figure 19) which has been shown to be upregulated in pluripotent ES and iPS cells.

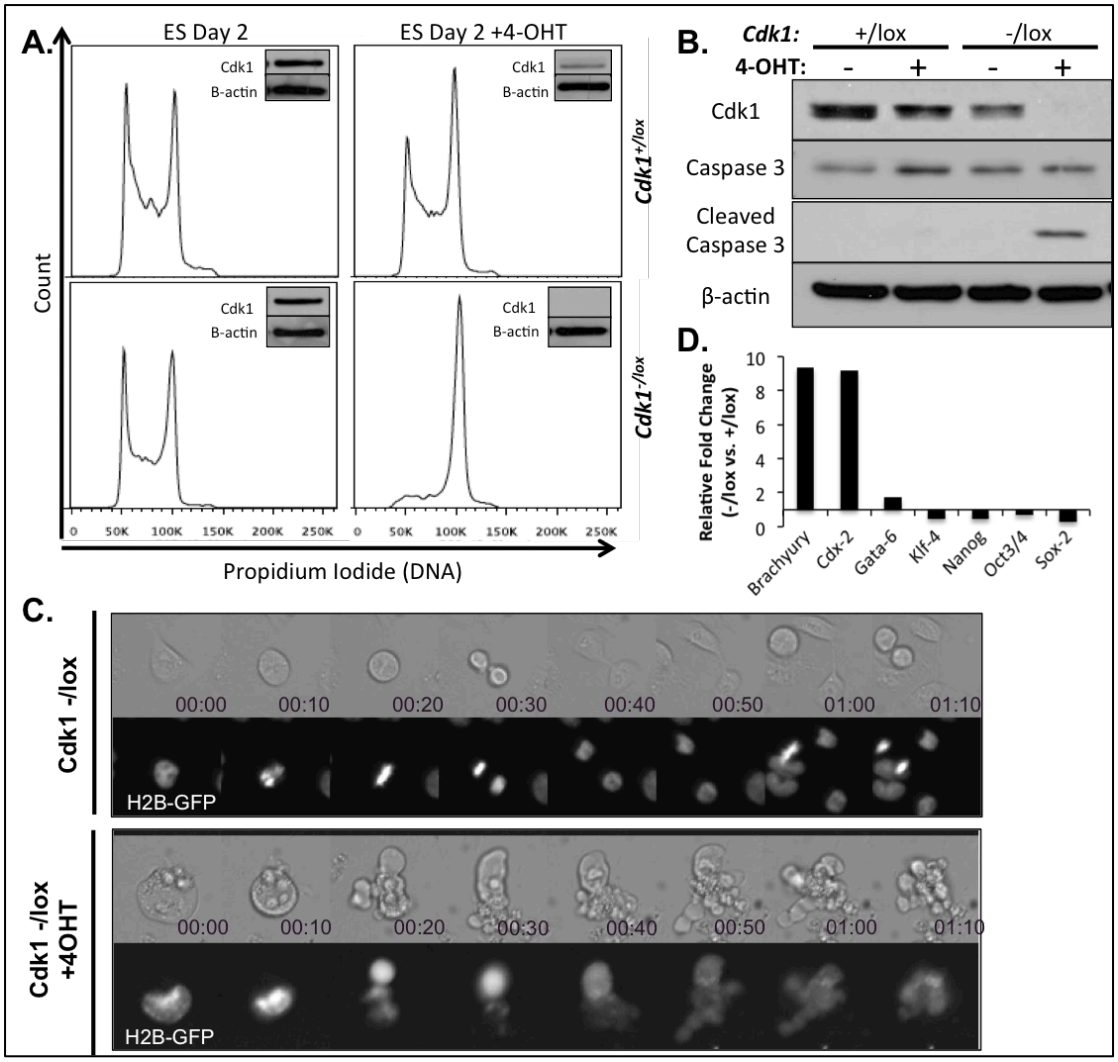

Figure 20: Cdk1 ablation in ES cells results in a transient G2-M cell cycle arrest, an upregulation of differentiation factors and apoptosis. A) Cell cycle (PI) and western blot analysis of ES cells. B) Western blot analysis of Caspase 3 activation upon depletion of Cdk1 by addition of 4-OHT to ES cell culture media for 48 hours. C) Time-lapse micrographs of *Cdk1*$^{-/lox}$*; Tg.hUBC-CreERT2*$^{+/T}$ ES cells in the absence and presence of 4-OHT. Top panel shows brightfield images and bottom panels, expression of exogenous H2B-GFP. Time stamps represent time since entry into mitosis/apoptosis respectively (hh:mm). D) RNA expression levels of stem and differentiation markers upon elimination of Cdk1 in ES cells (+4-OHT).

In order to address the role of Cdk1 in the ES and iPS cell cycle we treated asynchronous *Cdk1*$^{-/lox}$*; Tg.hUBC-CreERT2*$^{+/T}$ cells (and respective heterozygous controls) with 4-OHT over the course of 3 days. Given the rapid turnover of ES and iPS cells, we observed almost complete cleavage of Cdk1 by 48 hours post-treatment with 4-OHT (Figure 20a, b). When we analyzed cell cycle distribution by flow cytometry we observed that cells lacking Cdk1 arrested with a 4n DNA content (Figure 20a). Interestingly, almost the entire population arrested with a 4n DNA content in the iPS and ES cell clones lacking Cdk1, as compared to MEFs, where the majaroity of cells progressed on to endoreplicate. Moreover, the arrest we see in ES and iPS cells is temporal, with cells exiting the cell cycle and undergoing cell death (as observed by time-lapse microscopy) in a caspase-dependent manner (Figure 20b,c and supplemental videos). When we collected *Cdk1*$^{+/\Delta}$ and *Cdk1*$^{-/\Delta}$ samples after 48 hours of 4-OHT addition to culture media and performed quantitative RT-PCR, we found that expression of pluripotency genes was downregulated (Klf-4, Nanog, Oct3/4 and Sox2), along with an upregulation in early differentiation markers (Brachyury and Cdx2) upon ablation of Cdk1 (Figure 20d). Similar findings have been reported previously using siRNA against Cdk1 (Zhang et al. 2011). Taken together these findings demonstrate that Cdk1 elimination is lethal in pluripotent iPS and ES cells and that either Cdk1 or the continued progression of the cell cycle is necessary to maintain pluripotency.

In order to further elucidate the differential phenotype we observed between the MEFs and the ES and iPS cells, we performed an experiment where we cultured iPS cell clones under various conditions: 1) ES cell medium + FBS ; 2) ES cell medium + KSR; 3) ES cell medium + KSR (knockout serum replacement) + 2i (Gsk3B and Mek inhibitors). We utilized iPS clones as they are more sensitive to differentiation induced by culture media variations. KSR is more capable than FBS at maintaining iPS cell culture in a homogenous and pluripotent state. In addition, recent reports show that 2i culture media will further maintain cells in a "ground state" of pluripotency (Kanda et al. 2012; Marks et al. 2012). Therefore, the cells were grown under restrictive, highly pluripotent conditions (condition 1) or more permissive conditions for differentiation (condition 3). When we eliminated Cdk1 under these conditions we observed that cells maintained under pluripotent conditions would arrest transiently and undergo cell death, whereas the iPS clones grown in more permissive conditions would undergo endoreplication and generate cells with an 8n DNA content (Figure 21a). This suggests that the cell death phenotype we observed in the ES and iPS cell clones is due to a lethal effect of Cdk1

elimination in pluripotent cell types, which is also coherent with the *in vivo* data of early embryonic lethality.

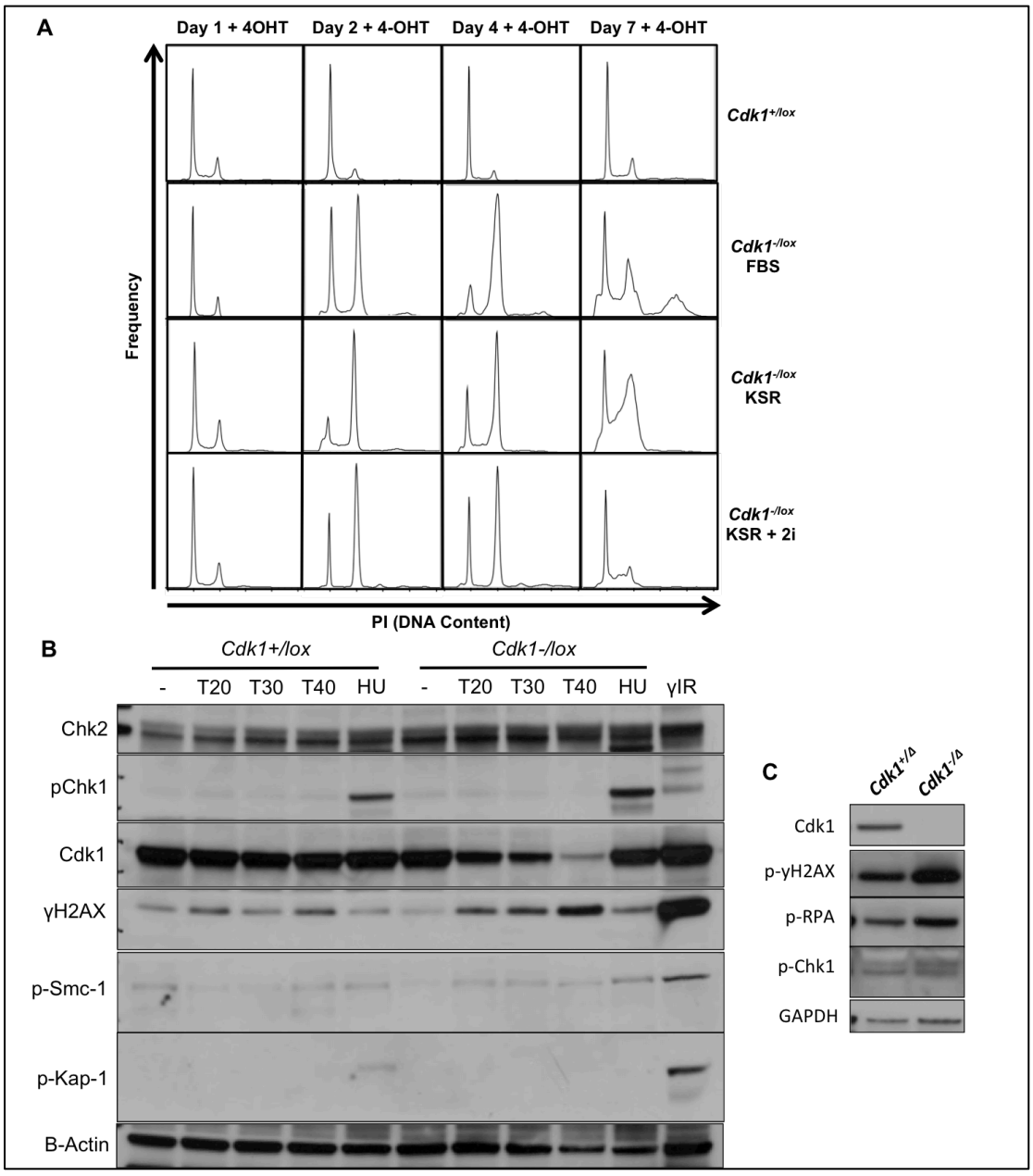

Figure 21: Apoptotic phenotype in ES cells is condition-dependent and not due to DNA DSBs. A) *Cdk1*$^{+/lox}$ and *Cdk1*$^{-/lox}$ ES cells with endogenous *Tg.bUBC-CreERT2* allele were grown in the presence of 4-OHT in Standard ES cell media supplemented with FBS, KSR or KSR + 2i and analyzed for DNA content (PI) by flow cytometry at 1, 2 4 and 7 days post-addition of 4-OHT to culture media. B) Western blot analysis of DDR regulatory proteins including Chk2, pChk2, Cdk1, γH2AX, pSmc-1, pKap-1 in ES cells upon ablation of Cdk1 by 4-OHT addition to media for 20, 30 and 40 hours (T20, T30 and T40 respectively), B-actin was used as the loading control. Positive controls of cells treated with HU (hydroxyurea) and irradiated (γIR) were included, along with a control of cells not treated with 4-OHT. C) Western blot analysis of γH2AX, Cdk1, pRPA, pChk1, and GAPDH as loading control.

In early *Cdk1-null* embryos we observed phosphorylated γH2AX (Figure 4), a molecular marker for DNA damage. Thus we hypothesized that Cdk1 elimination could

be resulting in an imbalance of Cdk-dependent DNA repair functions. Given that Cdks are induced in DNA repair, we assessed ES cell clones upon elimination of Cdk1 and did indeed observe an increase in phosphorylated γH2AX (a marker for DNA double strand breaks) by western blot (Figure 21b). However, when we assessed for activation of regulators of DNA double strand break (DSB) repair downstream of ATM (ataxia telangiectasia mutated), such as phosphorylated Chk2, Kap1 or Smc1, we found no activation of the pathway by western blot (Figure 21b). We also assessed for activation of replicative single strand break repair and observed no phosphorylation of Chk1, although we did see an increase in phosphorylated replication protein A (Rpa)(Figure 21c). Phosphorylated γH2AX on serine 139 can be associated with G2-M cell cycle arrest upon γ-IR (Tu et al. 2013) but can also be phosphorylated upon induction of caspase-dependent apoptosis (Rogakou et al. 2000). From these results we can conclude that the observed phosphorylation of γH2AX is induced by the elimination of Cdk1, however this is independent of DNA DSBs.

4.8 RNA Sequencing analysis of *Cdk1-null* MEFs and ES cells

In order to address the *Cdk1-null* observed lethality in embryonic cells versus differentiated cell types, we set out to analyze the expression profiles of *Cdk1-null* ES cells as compared to *Cdk1-null* MEFs. Human ES cells express a constitutively active form of the pro-apoptotic protein Bax (Dumitru et al. 2012) so that they are poised to rapidly induce apoptosis and cell death. While this mechanism has not been detailed in mouse ES cells, it is intuitive that embryonic cells would employ a failsafe mechanism to prevent development under adverse conditions. In order to gain further insight into the molecular mechanism that induces cell death in ES cells upon elimination of Cdk1, we performed RNA sequencing of G2-M arrested *Cdk1-null* ES cells and G2-M arrested *Cdk1-null* MEFs and compared to respective Cdk1 heterozygous control cells. We utilized MEFs since they are still embryonic cells and they reliably arrest at the G2-M phase of the cell cycle *in vitro*. Two clones were sequenced for each condition from 1 μg of RNA with an RNA integrity number of 10 and a single read of 40 base pairs was performed on the Illumina Genome Analyzer IIx (GAIIx). An average of 7,094,448 high quality reads were obtained per sample yielding an average of 284 Mbases. An average of 93.5% of bases had a quality greater than or equal to the Q30 as determined by the clusters passing filter (Table 3). Quality filtered sequence reads were aligned to the NCBI

m37 mouse assembly, April 2007, strain C57BL/6J. Similarities of expression data were compared and a principle component test was performed demonstrating that the MEF and ES cell samples were highly correlated and mapped together by cell type as was to be expected (Figure 22a and Table 4).

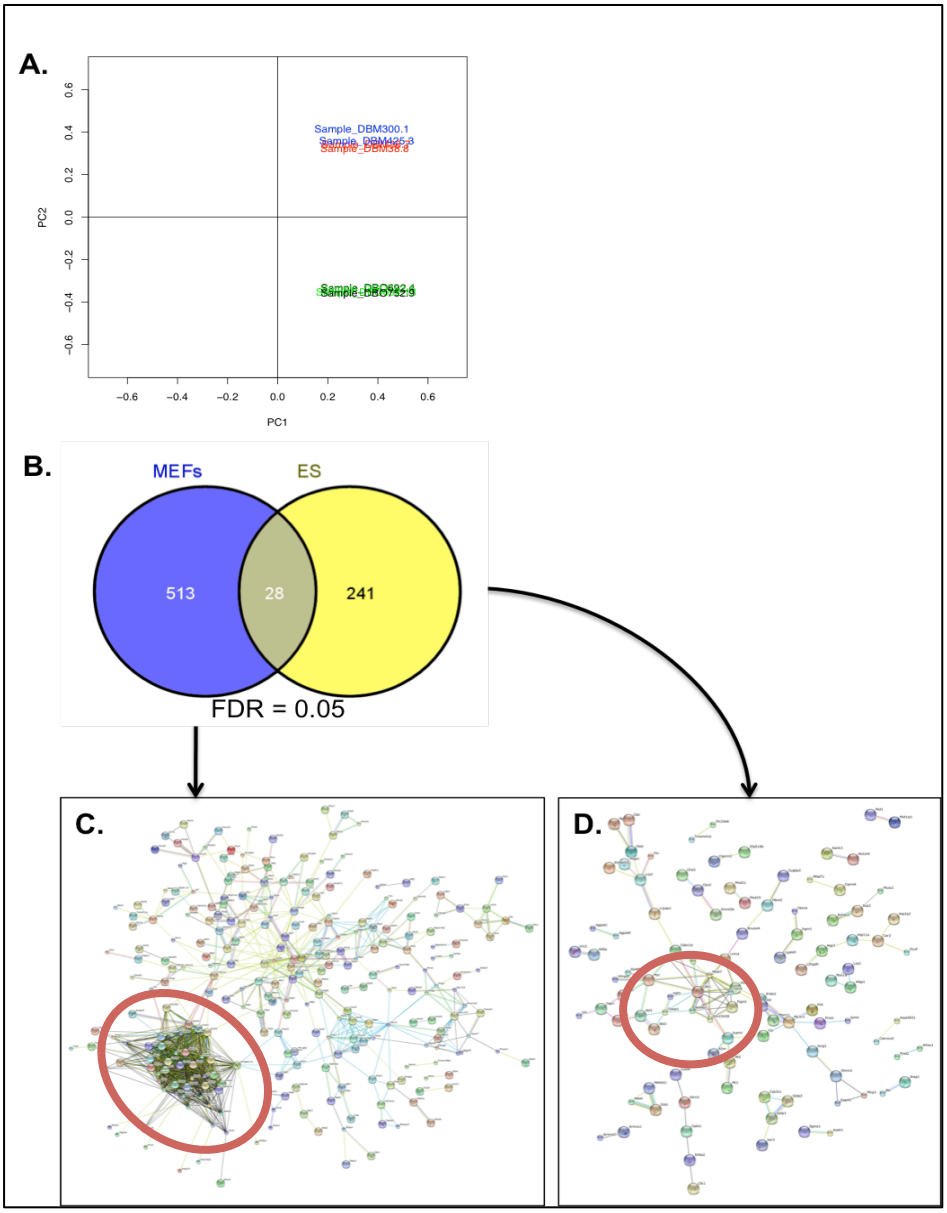

Figure 22: Upon Cdk1 elimination in MEFs and ES cells the Cell Cycle is the major node of differentially regulated genes. A) Principal component analysis of RNA sequencing analysis (Red: Het-MEFs, Blue: KO-MEFs, Light Green: Het-ES, Dark Green: KO-ES). B) Venn diagram of *Cdk1-null* MEF and ES cell differentially expressed gene set overlaps. C) String v9.2 analysis of MEF DEGs. D) String v9.2 analysis of ES cell DEGs. Red circles highlight Cdk1/Cell Cycle gene node.

We then performed expression analysis on the four populations: 1) *Cdk1*$^{+/\Delta}$*; Tg.hUBC-CreERT2*$^{+/T}$ ES cells (Het-ES); 2) *Cdk1*$^{\Delta/\Delta}$*; Tg.hUBC-CreERT2*$^{+/T}$ ES cells (KO-ES); *3) Cdk1*$^{+/\Delta}$*; Tg.hUBC-CreERT2*$^{+/T}$ MEFs (Het-MEF); 4) *Cdk1*$^{\Delta/\Delta}$*; Tg.hUBC-*

CreERT2$^{+/T}$ MEFs (KO-MEF). We first identified differentially expressed gene sets when comparing Het-ES vs. Het-MEF, KO-ES vs. KO-MEF, Het-ES vs. KO-ES and Het-MEF vs. KO-MEF (Supplemental File 1) and then performed gene set enrichment analysis (GSEA). Maintaining a false discovery rate (FDR) of less than 0.05 (Figure 22b) we utilized the significant DEGs in the Het-ES vs. KO-ES and the Het-MEF vs. KO-MEF conditions to identify known protein-protein interaction networks using the STRING database v9.1 (Franceschini et al. 2013). In the Het-ES vs. KO-ES analysis Cdk1 was a central node and we identified the GO biological processes of cell differentiation, cell cycle and cell death to be significantly enriched (Figure 22d).

Run type	read length	Sample ID	RIN	Barcode	Lane	Read	number of high quality reads (Clusters PF)	yield (Mbases)	% of reads mapped confidently % Align	% >=Q30 bases (PF)
Single Read	40	DBM300-1	10.0	ACAGTG	6	1	6,974,982	279	80.1	93.6
		DBM38-7	10.0	CGATGT	6	1	8,119,027	325	81.0	93.5
		DBM38-8	10.0	TGACCA	6	1	7,718,163	309	79.9	93.5
		DBM425-3	10.0	GCCAAT	6	1	5,393,083	216	80.7	93.3
		DBO692-13	10.0	CTTGTA	6	1	6,348,969	254	68.3	93.6
		DBO692-4	10.0	CAGATC	6	1	6,879,134	275	70.6	93.6
		DBO752-6	10.0	GTGAAA	6	1	8,146,092	326	71.9	93.7
		DBO752-9	10.0	CCGTCC	6	1	7,176,137	287	69.6	93.3

Table 3: RNA Sequencing Read Data (Q30). Run type, read length, sample ID, RNA Integrity Number, Barcode, Lane, Read, Number of high quality reads (Clusters PF), yield (Mbases), % of reads mapped confidently (% Align), % >= Q30 bases (PF). % Align (PF) is the percentage of filtered (Passing Filter) reads that were uniquely aligned to the reference. % >=Q30 bases (PF) is the yield of bases with Q30 or higher from clusters passing filter divided by total yield of clusters passing filter.

	DBM300.1	DBM425.3	DBM38.7	DBM38.8	DBO692.13	DBO752.6	DBO692.4	DBO752.9
DBM300.1	1	0.93208	0.91054	0.84102	0.65316	0.68216	0.68347	0.66813
DBM425.3	0.93208	1	0.93198	0.93169	0.71019	0.74521	0.74921	0.73140
DBM38.7	0.91054	0.93198	1	0.91095	0.72106	0.73092	0.73733	0.73312
DBM38.8	0.84102	0.93169	0.91095	1	0.71792	0.72416	0.72625	0.72499
DBO692.13	0.65316	0.71019	0.7210	0.71792	1	0.94375	0.93616	0.97237
DBO752.6	0.68216	0.74521	0.7309	0.72416	0.94375	1	0.98628	0.96934
DBO692.4	0.68347	0.74921	0.73733	0.72625	0.93616	0.98628	1	0.97572
DBO752.9	0.66813	0.73140	0.73312	0.72499	0.97237	0.96934	0.97572	1

Table 4: PC analysis of RNA Sequencing Samples. Principal component analysis of Het-MEFs (DBM38.7 & DBM38.8), KO-MEFs (DBM300.1 & DBM425.3), Het-ES (DBO692.4 & DBO752.9), and KO-ES (DBO692.13 & DBO752.6). The samples which have correlation values closest to 1.0 are the most similar.

Similar to the ES cells in the Het-MEF vs. KO-MEF analysis the cell cycle was a primary node and we identified the GO biological processes of cell differentiation, cell division and regulation of cell death to be significantly enriched (Figure 22c). These findings were similar to those found in the GSEA analysis, which included cell cycle associated pathway enrichment. This data was expected and confirmed our previously discussed results however we have yet to glean any insight into possible molecular mechanisms that differ between ES cells and MEFs that would result in the differential phenotype we observe.

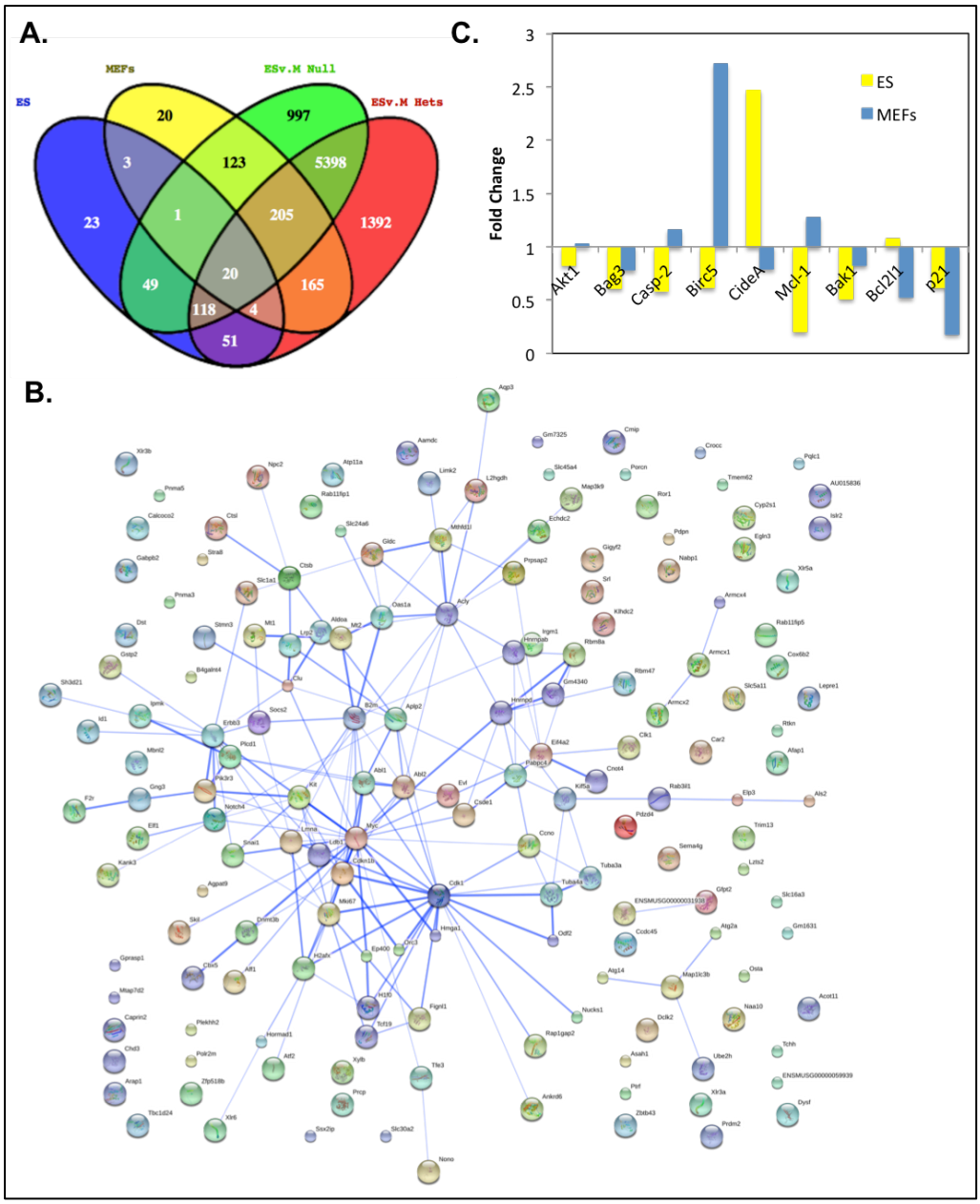

Figure 23: Common genes upon elimination of Cdk1 in MEFs and ES cells. A) Venn diagram of all four data sets. B) String analysis of genes from overlapping (169) genes between MEFs and ES cells upon elimination of Cdk1. C) qRT-PCR of ES vs. MEFs to validate significant genes.

With the aim of identifying significant regulators that differ between ES cells and MEFs we performed a VENN diagram analysis of the significant DEGs (Figure 23a). Comparing all four experimental conditions allowed us to identify differentially regulated genes specific to one or multiple experimental conditions. For example a gene upregulated in ES cells upon elimination of Cdk1 may also be upregulated in MEFs as compared to ES cells, suggesting that it could play a role in differentiation. Using the VENN diagram analysis we were able to generate gene lists specific to different conditions. We found that the cell cycle pathway and associated genes were linked to the majority of the conditions but specifically, in a list of 28 genes differentially regulated upon elimination of Cdk1 in both ES cells and MEFs, we identified Arpp19 to be upregulated upon elimination of Cdk1 (Table 5). Arpp19, is a PP2A inhibitor that aids in the regulation of the G2-M transition. Moreover, we associated a list of 169 genes found to be unique to ES cells and differentially regulated upon elimination of Cdk1. When we analyzed the list of 169 genes using the STRING database v9.1, we surprisingly found Cdk1 to be a central node in the model with cell cycle, cell differentiation and cell death interaction networks all significantly enriched (Figure 23b).

While assessing this data, Piotr Sicinski (Dana Farber Cancer Institute, Boston, USA) provided us a list of 84 genes known to be involved in apoptosis. We cross-referenced these genes to our RNA sequencing data obtained fold-change values for these genes (Figure 24). We found a handful of these genes of interest as they were either significantly differentially expressed in ES cells or MEFs upon ablation of Cdk1. We then performed RT-PCR to validate the differential expression of these genes (Figure 23c). We found that Akt1, Casp2, Bcl2l1, Birc5, CideA and Mcl1 were all differentially regulated between the ES and MEFs. Of particular interest we found that Birc5 (Survivin), an inhibitor of apoptosis is downregulated in ES cells while significantly upregulated in MEFs upon ablation of Cdk1. In a preliminary experiment where we transfected ES cells with wild-type Survivin, we find a rescue of the apoptotic phenotype and an increase in the number of *Cdk1-null* ES cells arrested in G2-M (Figure 25). Also of interest in this group of genes is CideA, a cell death activator that we found to be induced in ES cells and downregulated in MEFs upon ablation of Cdk1. Mcl1, a member of the Bcl-2 family of proteins, can be both an activator or inhibitor of apoptosis and we see that there is downregulation of Mcl1 in ES cells and upregulation in MEFs upon ablation of Cdk1. In contrast Bag3, Bak1 and p21 were all downregulated upon elimination of Cdk1 in both the ES cells and MEFs. Bag3 is a Bcl2-Associated

Gene ID	Gene Function
Hist1h2bc	Alcoholism|Viral carcinogenesis|Systemic lupus erythematosus
Slc9a3r2	Aldosterone-regulated sodium reabsorption
Nars	Aminoacyl-tRNA biosynthesis
Ephx2	Arachidonic acid metabolism|Metabolic pathways|Peroxisome
Ptpn11	Jak-STAT signaling pathway|Renal cell carcinoma|Chronic myeloid leukemia
Plod2	Lysine degradation
Ngfrap1	Neurotrophin signaling pathway
Ncoa4	Pathways in cancer|Thyroid cancer
Sorbs1	PPAR signaling pathway|Adherens junction|Insulin signaling pathway
Sulf2	sulfatase 2
Anxa6	Annexin A6, calcium signaling
Arid4b	AT rich interactive domain 4b (Rbp1-like), transcription factor (Rb)
Psrc1	transcriptional target of p53 and p73, microtubule binding, cell cycle
Schip1	PDGF signaling, estrogen signaling, Fos
Gm14431	KRAB box and zinc finger C2H2 type domain containing protein
Nusap1	microtubule binding, cell cycle, mitosis
Mum1l1	cell division, growth and differentiation (putative chromatin binding site)
Arpp19	G2-M transition, cell cycle, mitosis, protein phosphatase inhibitor activity
Mtap7d1	MAP7 domain containing 1, Foxp3-interactor
Epb4.1l1	tight-junctions and AMPA signaling
Ppp1r18	protein phosphatase 1, regulatory subunit 18, interactor of Foxp3
Fhl1	delta-notch signaling pathway, differentiation, negative reg. of cell cycle
Cgnl1	cingulin-like 1, actin cytoskeleton, cell junction
Cd24a	CD24a antigen, hematopoietic cell lineage
Txnip	immune system (oxidative stress, apoptosis and cancer)
Dbnl	debrin-like, Apoptosis
St5	suppression of tumorigenicity 5, positive activator of Erk1 and Erk2

Table 5: Cell cycle genes significantly differentially regulated between ES and MEFs upon elimination of Cdk1. Gene IDs and their annotated functions

Athanogene 3 protein that interacts with and inhibits Hsp70/Hsc70 chaperone activity promoting the release of its substrates and can be antiapoptotic. Bak1, Bcl2-Antagonist/Killer 1, interacts with and inhibits the anti-apoptotic activity of Bcl2 and induces mitochondrial release of cytochrome c, thus inducing apoptosis. Of interest among these genes is p21, since we observed *in vivo* that the loss of p21 was capable partially rescuing early embryonic lethality of *Cdk1-null* embryos, it is unclear why p21 RNA levels are downregulated upon ablation of Cdk1. These data provide an initial indication as to the molecular mechansisms differentiating ES cells and MEFs.

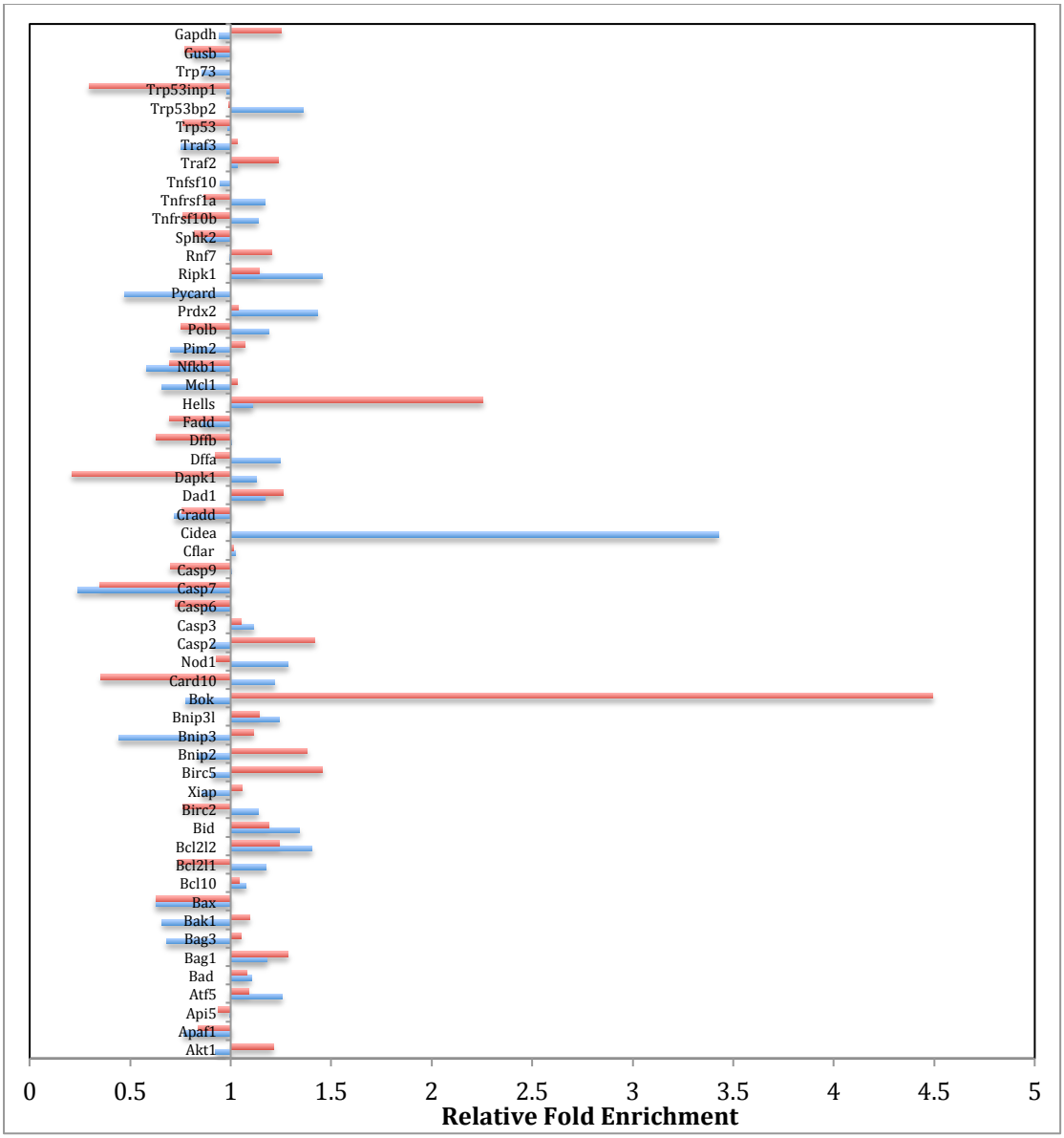

Figure 24: Relative expression of apoptotic gene set in ES cells and MEFs upon ablation of Cdk1. Fold change values were obtained from differentially expressed data sets of Het-ES vs. KO-ES and HetMEF vs. KO-MEFs for each gene respectively.

Taken together the RNA sequencing data provides a functionally relevant data

set to address novel G2-M regulators, cell cycle arrest, pluripotency and cell death pathways. Moreover, our findings were consistent with what we observed *in vitro* and provide support to the experimental data we have obtained thus far. Further analysis of molecular pathways and regulators is ongoing to be able to elucidate the molecular mechanism responsible for inducing cell death in ES cells upon elimination of Cdk1.

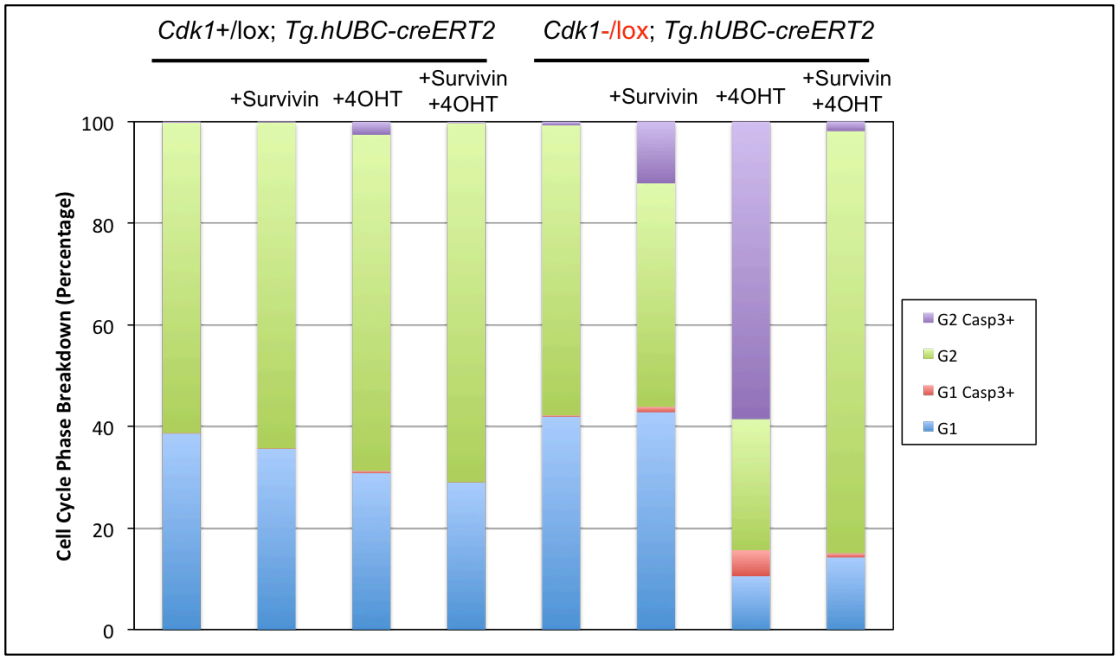

Figure 25: Rescue of ES cell apoptosis upon ablation of Cdk1 and exogenous expression of Survivin. *Cdk1*$^{+/lox}$*; Tg.hUBC-CreERT2*$^{+/T}$ and *Cdk1*$^{-/lox}$*; Tg.hUBC-CreERT2*$^{+/T}$ ES cell clones were transfected with wild-type Survivin and treated with 4-OHT for 48h. Cells were then analyzed by flow cytometry for cell cycle (DNA content) and Caspase 3 positivity (Casp3). Here we show a representation of cell cycle breakdown between G1 (2n) and G2 (>2n) and the relative Caspase 3 positive subset.

4.9 Cdk1 elimination in hematopoietic stem cells

We have observed thus far that eliminating Cdk1 in vivo results in embryonic and adult mouse lethality, an arrest of proliferative tissues in the cell cycle at the G2-M transition and ongoing endoreplication, as well as transient cell cycle arrest followed by apoptosis in ES and iPS cells. In collaboration with Rebeca Sanchez and José Carlos Segovia (CIEMAT, Madrid, Spain), we set out to determine whether the cell death phenotype is specific to embryonic stem cells or can also be observed in adult stem cell compartments. We analyzed hematopoietic stem cells (HSC), which reside in the bone marrow of adult mammals and are a well characterized source of adult stem cells. Thus, we isolated the bone marrow from *Cdk1lox; Tg.hUBC-CreERT2* mice and sorted out the LSK (Lin$^-$, Sca1$^+$ and cKit$^+$) , the Sca1 and cKit double negatives, and the granulocyte and monocyte progenitors (GMP) populations. LSK cells comprise both the long-term

and short-term hematopoietic stem cell populations and are capable of self-renewal and giving rise to all hematopoietic cell lineages. The Sca1 and cKit double negative cells or hematopoietic precursor cell (HPC) is more mature and no longer capable of self-renewal, however still maintains the ability to generate either lymphoid or myeloid lineages. The GMP population is lineage committed and can only generate monocytes or granulocytes.

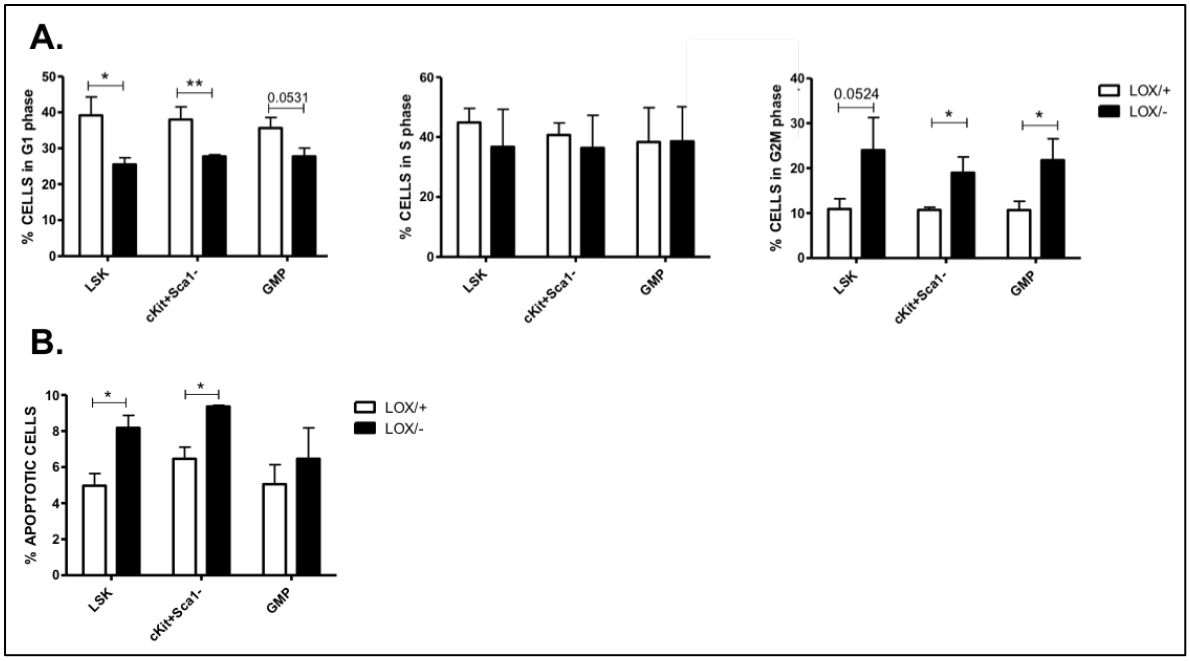

Figure 26: Elimination of Cdk1 in HSC populations results in G2-M cell cycle arrest and apoptosis. Analysis of HSC cell cycle and apoptosis upon ablation of Cdk1. A) G1, S and G2 percentages in LSK, cKit and GMP cell populations after treatment with 4-OHT for five days (white bars are Cdk1 heterozygous cells and black bars are *Cdk1-null* cells). B) Percentage of apoptotic cells in LSK, cKit and GMP cell populations after 5 days of treatment with 4-OHT.

Cells were stimulated to proliferate and grown *in vitro* following standard HSC growth protocols to maintain stemness (see Materials and Methods) in the presence or absence of 4-OHT to induce endogenous Cre recombinase and cleavage of the *Cdk1lox* allele. Cells were then analyzed by flow cytometry at day 3 post-addition of 4-OHT for DNA content (cell cycle profile) and 7AAD (7-amino-actinomycin D) viability stain. In all cells depleted of Cdk1 we observed a statistically significant induction of G2-M (4n DNA content) cell cycle arrest (Figure 26a). In the LSK and the HPC cell populations, we observed a significant decrease in the percentage of cells in G1 (with a 2n DNA content)(Figure 26a). Since our analysis of the cell cycle was performed 5 days after addition of Tamoxifen, the decrease in number of cells found in G1 could be attributed to a greater number of cells entering the cell cycle but not continuing to cycle, either due

to a cell cycle arrest or cell death. Indeed, we observed a significant increase in apoptosis in the LSK and HPC cell populations, while the GMP population was viable and able to maintain the cell cycle arrest (Figure 26b). These data are congruent with our findings in embryonic stem cells and further demonstrate that Cdk1 is essential for maintaining both adult and embryonic stem cell viability.

4.10 Therapeutic potential of targeting Cdk1

4.10.1 Teratomas

Teratomas are tumors with tissue components deriving from more than one germ layer. They can occur physiologically or can be generated by injecting ES cell lines into Nude mice. In order to address the feasibility of targeting Cdk1 elimination in stem cells of a tumor compartment, we generated teratomas from the *Cdk1lox; Tg.hUBC-CreERT2* ES cell lines. Once tumors were palpable we fed mice a Tamoxifen-containing diet *ad libidum* for 5 days. Tumor samples were then collected and processed by immunohistochemistry. We observed teratoma formation with contribution from all three germ layers from the ES cell lines utilized (Figure 27a). We then stained for yH2AX in the teratomas by immunofluorescence and observed an induction of yH2AX positive staining in teratomas depleted of Cdk1 (Figure 27b). While this data is preliminary, it suggests that therapeutic targeting of Cdk1 can induce apoptosis of tumor-associated stem cells. Ongoing experiments are currently being conducted to address this further.

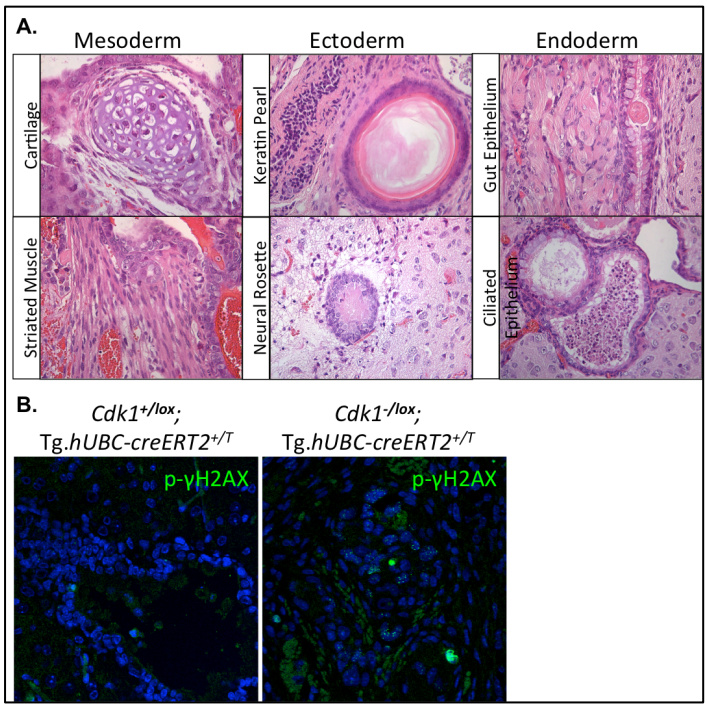

Figure 27: Cdk1 elimination in teratomas induces phosphorylation of yH2AX. A) Generation of all three germ layers in *Cdk1*$^{-/lox}$*; Tg.hUBC-CreERT2*$^{+/T}$ ES cell derived teratomas. B) Phosporylated yH2AX positive staining in *Cdk1*$^{+/-}$ *and Cdk1-null* teratomas.

4.10.2 Mammary Tumor Cancer Stem Cells

Cdk1 inhibitors have been thoroughly tested in the clinic, however their toxic systemic effects outweigh their efficacy. Taken together, our findings show that Cdk1 depletion results in a cell cycle arrest in lineage committed and differentiated cell types, and a transient cell cycle arrest followed by rapid apoptosis in stem cells. We hypothesized that temporal inhibition of Cdk1 in a tumor environment will induce apoptosis of the cancer stem cells and prime the tumoral cells for standard therapy. Recent findings have described a method for the isolation of mouse mammary tumor stem cells by FACS (Ma et al. 2012). Using the Tg.MMTV-PyMT mouse mammary tumor model they isolated the Lin-CD44lowCD24+CD29+CD49f+Sca-1low surface marker expressing population and identified these cells to be able to differentiate *in vitro*, form clonal populations *in vitro*, and initiate tumor formation when transplanted *in vivo* with 1 x 10^3 being the limiting number of cells necessary to induce tumor formation (Ma et al. 2012). Thus, using our *Cdk1lox; Tg.MMTV-PyMT* mice, we have isolated tumoral cell lines. When we infected asynchronouos cell lines with Ad-Cre we observed cells undergoing multiple rounds of endoreplication upon elimination of Cdk1 (Figure 28a). When we analyze the same cell lines by FACS analysis for the previously defined stem cell marker profile and apoptosis, we observe an induction of apoptosis in the cancer stem cell pool (Figure 28b). This data suggests that while differentiated tumoral cells will arrest in the cell cycle and undergo endoreplication upon elimination of Cdk1, transiently targeting Cdk1 in a tumoral population can eliminate cancer stem cells. This data is only preliminary but taken together with our previous findings both *in vitro* and *in vivo* we believe that targeting Cdk1 temporally in tumor cell populations, would act to eliminate cancer stem cells while priming the tumoral cell population for further treatment via irradiation or chemotherapy.

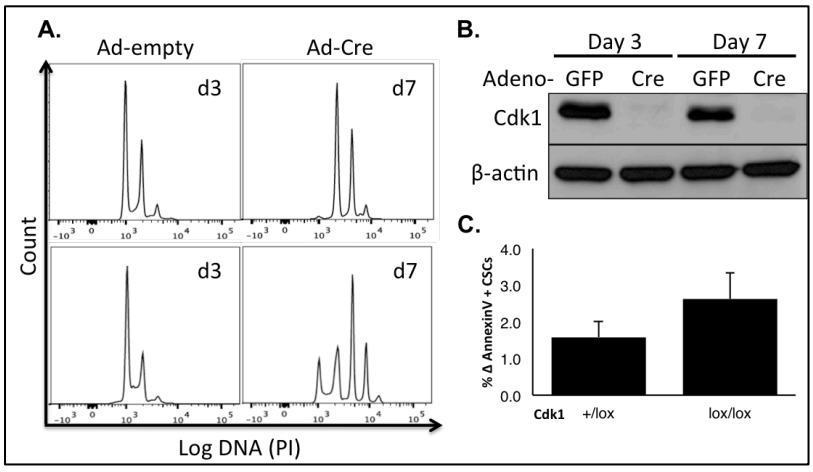

Figure 28: Cdk1 elimination in tumor cell populations can induce cell cycle arrest, endoreplication and apoptosis. A) Cell cycle analysis of *Tg.MMTV-PyMT* tumoral cell lines infected with Ad-GFP or Ad-Cre-GFP and analyzed 3 and 7 days post infection. B) Western blot analysis of tumor cell populations for Cdk1. C) Induction of apoptosis (AnnexinV +) in CSC population by FACS analysis.

5. Discussion

5.1 Cdk1 is essential in mouse embryogenesis and viability

The mammalian cell cycle is regulated by multiple Cdks and Cyclins, including Cdks 1, 2, 4 and 6 and Cyclins A, B, D and E. Over the past two decades genetic studies have provided insight into the connection between these cell cycle regulators and mammalian development, homeostasis and viability. Through these studies the interphase Cdks were found to be dispensable for life, albeit each Cdk was found to have cell-specific functions including: pancreatic β-cell proliferation (*Cdk4*), hematopoietic regulation (*Cdk6*) and essential functions in meiosis (*Cdk2*) (Rane et al. 1999; Ortega et al. 2003; Malumbres et al. 2004; Berthet et al. 2003; Tsutsui et al. 1999). Given that the Cdk provides the kinase activity of the Cdk-Cyclin heterodimeric cell cycle regulatory unit and the cyclin provides substrate specificity, these initial findings led to the understanding that the interphase Cdks were capable of compensating for eachother in maintaining essential cell cycle progression and homeostasis. Indeed when compound knockout models were generated, more severe phenotypes were observed. *Cdk2* and *Cdk4* DKO mice completed embryonic development but died shortly after birth, whereas *Cdk4* and *Cdk6* DKO mice died late in embryogenesis (Barrière et al. 2007; Malumbres et al. 2004). Lastly, a TKO mouse was generated lacking all interphase Cdks: *Cdk2, Cdk4, Cdk6* as well as *Cdk3* (due to an endogenous mutation). These mice were able to undergo embryogenesis until midgestation (E13.5-15.5) when they began to die and Cdk1 was found capable of providing all essential cell cycle associated kinase activity necessary (Santamaría et al. 2007). These final studies confirmed that the interphase Cdks are dispensable for the essential mammalian mitotic cell cycle and that Cdk1 is capable of compensating for their loss.

When similar studies were performed with the Cyclins the phenotypes were generally similar but some important distinctions were unveiled. Cyclin D1, D2 and D3 combined knockout resulted in lethality at E16.5 with hematopoietic defects (Kozar et al. 2004). Cyclin E1 and E2 individual knockouts were viable but combined knockout resulted in lethality at E11.5 (Geng et al. 2003; Parisi et al. 2003). However, this phenotype was due to an inability of trophoblast giant cells to increase in ploidy resulting in abnormal placental development. The lethality of Cyclin E KO embryos was able to be rescued by tetraploid complementation (Eggan et al. 2001; Tanaka et al. 1997) prolonging life to E15.5-18.5 (Geng et al. 2003; Parisi et al. 2003). Cyclin A1 knockouts were viable but the males were infertile, while Cyclin A2 knockout mice were lethal at E5.5 (Liu et al. 1998; Murphy et al. 1997). Cyclin B2 knockouts were viable with no

obvious defects, whereas elimination of Cyclin B1 resulted in early embryonic lethality, prior to E10 (Brandeis et al. 1998).

When we compare with the E13.4-15.5 lethality observed in the Cdk TKO model, elimination of all Cyclin D was less lethal allowing embryos to develop up to E16.5, while the loss of all Cyclin E resulted in lethality at E11.5, two days earlier than the Cdk TKO model. This disparity can be explained by the respective roles of Cyclin D and E in G1 and S phase. The tetraploid complementation rescue of Cyclin E KOs clearly demonstrates the essential role of Cyclin E in development of the extraembryonic placenta, while highlighting the ability of the remaining Cyclins to compensate for embryonic development until E15.5-18.5, when KO embryos die due to cardiovascular abnormalities, the same as Cyclin D KOs (Kozar et al. 2004; Geng et al. 2003; Parisi et al. 2003). Thus, when we do not account for the placental defects of Cyclin E KOs, both Cyclin D and Cyclin E KO mice display less lethality than their corresponding Cdk KOs. This may be explained by the ability of Cyclin A to compensate for the loss of Cyclins D and E in early embryonic development.

In contrast, when we examine the lethality of Cyclin A2 KO mice, the phenotype is starkly different from that of its corresponding Cdk. Cdk2 is the primary Cdk known to associate with Cyclin A, and yet, while Cyclin A2 KO mice die at E5.5, Cdk2 KO mice show no obvious phenotype, aside from male infertility (Ortega et al. 2003). This dichotomy was a surprise to the research community at the time and demonstrates that Cyclin A2 is essential for mammalian cell cycle progression and embryonic development whereas Cdk2 is dispensable.

Another disparity that Cdk2 KO mice give prominence to is the trophoblast giant cell phenotype of Cyclin E KO mice. Cdk2 also associates with Cyclin E and the ability of Cdk2 KO mice to develop without the need for tetraploid complementation demonstrates that the role of Cyclin E in trophoblast giant cells is specific to Cyclin E as this defect is not even present in the TKO Cdk model, where Cdk1 can compensate for the loss Cdk2 binding with Cyclin E and Cyclin A2. Trophoblast stem cells differentiate into trophoblast giant cells and undergo rapid endocycles up to 1000n DNA content and result in placentation (Cross 2005). The mechanism by which endocycles occur is through the inhibition of Cdk1 and ability of Cdk2-Cyclin E complexes to initiate DNA synthesis. The Cdk2-Cyclin E complexes form a transitory ternary complex with the CKIs $p21^{Cip1}$, $p27^{Kip1}$ and $p57^{Kip1}$, whose expression fluctuate allowing for Cdk1 and Cdk2 inhibition for proper endocycle progression. Indeed it is the fluctuation of $p57^{Kip1}$

specifically that regulates the Cdk activity associated with trophoblast giant cell endocycles (Ullah et al. 2008; Zhang et al. 1998). However, not all cyclin-Cdk complexes have the same sensitivity towards CKIs and the role of Cyclin E in directing ternary complex formation must be critical to trophoblast giant cell endoreplication (Parisi et al. 2003). In MEFs lacking Cdk2, there was no detected Cyclin E-associated kinase activity (Ortega et al. 2003), however, Cdk1 was found to form complexes with Cyclin E in whole embryo lysates of *Cdk2-null* embryos (Santamaría et al. 2007). Thus in Cyclin E KO trophoblast stem cells, Cdk1/2-Cyclin A complexes form, which are unable to inhibit CKI activity or form the ternary complexes necessary to induce endoreplication and differentiation, whereas in Cdk2 KO trophoblast stem cells Cyclin E is still present and capable of driving endoreplication.

Finally, when we consider the Cyclin B1 knockout, while the analysis of embryonic lethality was not fully elucidated, it was clear that Cyclin B1 nullizygous embryos were not present at E10 and therefore must have died before reaching that stage of development (Brandeis et al. 1998). Further studies into the role of Cyclin B1 in early embryogenesis and cell cycle regulation is merited. Cyclin A2 and B1 are expressed primarily during S and G2 phases of the cell cycle. Both bind and interact with Cdk1, while Cyclin A2 can also bind Cdk2. Given that Cdk1 was able to compensate for the lack of interphase Cdks in the TKO model, it stands to logic that the loss of its partner Cyclins would result in a similar phenotype as that observed when Cdk1 was eliminated. Indeed the gene trap disruption of *Cdk1* resulted in early embryonic lethality (Santamaría et al. 2007) and our findings as well as those published by Diril and colleagues (Diril et al. 2012) corroborate these results with *Cdk1-null* embryos dying before implantation. In fact the inability for *Cdk1-null* embryos to develop into blastocysts and *in vitro* complete initial cell divisions clearly demonstrates that elimination of the mitotic kinase is essential for cell cycle progression. Whereas in the case of Cyclin A2, embryos can progress up to later stages of development, past implantation (Murphy et al. 1997).

While expression of the zygote genome occurs as early as the two cell stage, early embryogenesis is know to be supported, if not driven by the presence of maternal mRNAs. These maternal mRNAs are present in the oocytes and maintain their levels until peri-implation (Bachvarova & De Leon 1980). Thus the disparity we see in developmental potential of *Cdk1-null* embryos *in vitro* vs. *in vivo* may be due to the stability of the maternal mRNAs under the stresses of *in vitro* culture. In fact in the Cyclin A2 nullizygous embryos, Cyclin A2 expression was detected in early morula-blastocyst

stage embryos by immunofluorescence, which could only be from the translation of maternal mRNAs (Murphy et al. 1997). Moreover, it has been demonstrated that ES cells lacking both Cyclin A1 and Cyclin A2 are not viable (Kalaszczynska et al. 2009). These findings are similar to those we present here where ES cells depleted of Cdk1 are unable to proliferate and die via apoptosis. Given that ES cells represent the cells that form the embryo proper and *in utero* maternal mRNA can drive development up until peri-implantation, these findings when considered together demonstrate that Cyclin A2 and Cdk1 are essential for early embryonic cell cycles and viability. We can also postulate that the early embryonic cell cycles may be more dependent on Cyclin A2, as the maternal mRNA can maintain embryo development further than in the case of *Cdk1-null* embryos, however embryonic stem cells require both Cyclin A2 and Cdk1.

5.2 Threshold model of cell cycle progression

Initial belief in the cell cycle field was that higher organisms had developed multiple, functionally-specific Cdk homologues from the single yeast Cdk in order to provide the required layers of complexity appropriate and each playing a pivitol role in regulating proper cell cycle progression. Indeed, the finding that Cdk2 was dispensable for mouse development and homeostasis (Ortega et al. 2003) was not expected from the research community, and partially disproved the idea that greater organismal complexity required a higher level of molecular regulation. This idea grew ever weaker, as Cdks 4 and 6 were also found to be dispensable to the cell cycle (Rane et al. 1999; Malumbres et al. 2004). Combined genetic ablation of interphase Cdks (Barrière et al. 2007; Malumbres et al. 2004) further proved that higher organisms did not require an additional layer of regulation. Finally, when all mammalian interphase Cdks (2, 3, 4 and 6) were eliminated and embryonic development progressed (Santamaría et al. 2007), the added complexity of essential mammalian cell cycle regulatory mechanisms was definitively called into question. How could a complex mammalian cell cycle progress with a single Cdk? What is the specific purpose of the interphase Cdks in essential mammalian cell cycle progression?

During these years, a study in yeast demonstrated the ability to manipulate the cell into specific phases of the cell cycle based on the amount of Cdk-associated kinase activity alone (Coudreuse & Nurse 2010). By generating a yeast strain mutant for mitotic cyclin homologues cig1, cig2 and puc1 and expressing a cyclin B homologue cdc13 fused with a linker to a temperature- and analogue-sensitive cdc2 mutant, the authors were able

to interrogate the autonomous function of cdc13-cdc2 to drive the cell cycle and if this progression could be mediated by distinct thresholds of cdc2 activity. Indeed, the authors were able to artificially modulate the activity of the cdc13-cdc2 molecule and progress the cell through S and M phases of the cell cycle (Coudreuse & Nurse 2010). Moreover, the authors establish that the different phases of the mitotic cell cycle operate independently from each other and can be defined by specific Cdk activity thresholds (Coudreuse & Nurse 2010). These findings when taken together with those from the triple interphase Cdk knockout model strongly demonstrate that the cell cycle is a basic function of cellular physiology and that the mechanisms that regulate the essential cell cycle are shared across species, in particular the Cdk-associated kinase activity threshold model of cell cycle regulation.

Herein we have presented the generation of a conditional knockout mouse model for Cdk1. We have demonstrated that elimination of Cdk1 in adult tissue homeostasis is lethal and that Cdk1 is essential for early embryonic development. During the course of this research a similar model was published by Diril and collegues, where they observed early embryonic lethality at E3.5 and full recovery from partial hepatectomy via endoreplication and cell expansion, rather than proliferative recovery (Diril et al. 2012). Moreover, in vitro data demonstrated that cells lacking Cdk1 would arrest with a 4n DNA content (at the G2-M transition) and undergo multiple rounds of endoreplication (Diril et al. 2012). These data confirm and support the findings that we present here, demonstrating that Cdk1 elimination is lethal for mouse development and adult homeostasis.

When we consider this data in light of the Cdk-associated kinase activity threshold model of cell cycle regulation, it is curious as to why another one of the many interphase Cdks would not compensate for the lack of Cdk1. The threshold model is based on steadily increasing Cdk-associated kinase activity throughout interphase, followed by a significant peak of Cdk1-associated kinase activity at the G2-M transition and later a depletion of all Cdk activity during mitosis. The Cdk-associated kinase activity is constantly regulated by a system of bistable switches, through phosphatases that dephosphorylate Cdk substrates, kinases that inhibit Cdk activity, and Cdk-inhibitors such as p21 (Domingo-Sananes et al. 2011). Given that the expression and activation of Cdk1 is specific to the G2-M transition of the cell cycle and its binding with Cyclin B, we hypothesized that the inherent regulatory mechanisms inhibiting interphase Cdks to prevent unscheduled mitotic entry may act in concert with a lack of Cdk1 to inhibit

interphase Cdks more aggressively. We tested this hypothesis both *in vivo* with *Cdk1; p21* DKO mice and *in vitro* with phosphatase inhibitors. *In vivo* we observed a clear and substantial rescue of early embryonic *Cdk1-null* proliferative arrest and lethality in embryos also lacking *p21*. Albeit the rescue was not functionally viable past implantation (E5.5), the absence of Cdk1 was compensated for in the maintenance of the essential embryonic cell cycle. *In vitro*, utilizing *Cdk1-null* MEFs and a high-throughput screening mechanism for controlled mitotic entry, we observed that phosphatase inhibitors (specifically against PP2A) were capable of advancing *Cdk1-null* MEFs into mitosis.

Taken together our data support the threshold model of cell cycle regulation, where a single Cdk is capable of maintaining the essential cell cycle. Competitive regulatory mechanisms that are in place to prevent unscheduled cellular division maintain interphase Cdks at bay in the absence of Cdk1. However, upon elimination or depletion of these factors, other Cdks are capable of compensating for the absence of Cdk1. Further research will be needed to determine the Cdk responsible for rescue of the *Cdk1-null* phenotype, however, given expression and activity patterns, we believe that Cdk2 is responsible for this observed compensation. We have generated TKO mice for *Cdk1; Cdk2; p21* and are currently in the process of assessing this both *in vivo* and *in vitro*.

5.3 Tissue specific functions of *Cdk1*

Previous genetic studies have identified tissue-specific cell cycle-independent functions of cell cycle proteins, including the interphase Cdks. Namely, Cdk2 in prophase I of the meiotic cell cycle (Ortega et al. 2003), Cdk4 in β-islet pancreatic cells (Rane et al. 1999) and Cdk6 in hematopoiesis (Malumbres et al. 2004). In order to address the second aim of this thesis, we investigated the role of Cdk1 in both Purkinje cells of the cerebellum as well as the endothelial compartment during angiogenesis.

We decided to assess the role of Cdk1 in the Purkinje cells of the cerebellum due to our observation that Cdk1 was expressed in these cells independently of Ki67. Analysis was unable to either confirm expression of Cdk1 by RT-PCR or identify obvious motor function defects in mice depleted of Cdk1 in the Purkinje cells alone. Further investigation would be needed to fully address the potential role for Cdk1 expression in these cells.

Given the importance of angiogenesis in tumor growth and dissemination, there are many studies investigating the potential for inhibiting angiogenesis to thwart tumor growth. Sprouting angiogenesis, the primary form of angiogenesis requires heavily on the

induction of proliferation in the endothelial cell compartment. Therefore, we sought to address the role of proliferation in physiological angiogenesis (wound healing) as well as pathological angiogenesis (*Tg.MMTV-PyMT*). In both cases we saw minimal effects upon eliminating Cdk1 in the endothelial compartment during angiogenesis. In the wound healing assay, we observed a significant delay in initial wound closure kinetics as well as a delayed healing process. During wound healing the initial response is inflammation and debriding of the exposed area. This is quickly followed by an induction of angiogenesis that will form new vessels in the damaged tissue allowing tissue perfusion and aiding in the healing process. Given that we observed a delay in wound healing in mice lacking Cdk1 in the endothelial vasculature, we can propose that the delay was due to an inability for proper induction of angiogenesis. There are two primary types of angiogenesis, sprouting (proliferative) and intussusceptive (branching). The former requires proliferation of endothelial cells which grow out of the mother vessel to form a new vessel. The latter is a division and reorganization of the existing vessel architecture in order to provide vasculature to the area in need. It is possible that the delay we observed was due to the time necessary in order to activate intussusceptive angiogenesis, however, further studies would be necessary to fully explore this theory.

We next utilized the *Tg.MMTV-PyMT* mammary tumor model in conjunction with the endothelial-specific tamoxifen-inducible Cre recombinase to study how targeting endothelial cell proliferation can affect tumor growth. The *Tg.MMTV-PyMT* tumor model develops highly vascularized tumors. In our analysis, we observed a minimal increase in overall survival, thus we cannot conclude that targeting Cdk1 in vascular angiogenesis is a viable therapeutic option. However, given the inherent variability of tumor growth within the model further analysis would be needed. Indeed control animals that did not develop tumors but were fed a Tamoxifen-containing diet *ad libidum* to assess endothelial homeostasis upon depletion of Cdk1, presented with no obvious phenotypic defects. Physiological angiogenesis is required in normal tissue homeostasis and can be induced during muscle activity. Therefore, while a more comprehensive analysis would need to be performed to fully address the role of Cdk1 in physiological angiogenesis, our data suggest that endothelial proliferation is not a standard requirement for homeostatic angiogenesis. Moreover, we cannot rule out the potential for other mechanisms of angiogenesis, such as vasculogenic mimicry, which has been documented in several tumor types, and intussusceptive angiogenesis. Our data present preliminary evidence that inhibiting proliferation in the endothelial compartment

may in fact delay angiogenesis, however further investigation is required.

5.4 Cell cycle function of Cdk1

As has been previously reported (Diril et al. 2012), when we eliminated Cdk1 in MEFs we observed an arrest of cells with a 4n DNA content (at the G2-M transition), followed by multiple rounds of endoreplication. These cells would arrest indefinitely without entering into mitosis reaching up to 16n and 32n ploidy. We confirmed this data in primary keratinocytes as well. Thus, differentiated cells lacking Cdk1 can progress through interphase without any cell cycle defects, but cannot independently enter into mitosis. Interestingly, when we observe cell cycle proteins, Cyclin B1 levels remain constant and then slightly decline, even in the absesnce of Cdk1, suggesting that another Cdk may initially be stabilizing Cyclin B1 and preventing its degradation. Overall the cell cycle effects of eliminating Cdk1 in MEFs were to be expected as Cdk1 has been studied thoroughly using shRNA, small molecule inhibitors and genetics (Diril et al. 2012).

When we analyzed the effect of eliminating Cdk1 in other cell types, such as keratinocytes and *Tg.MMTV-PyMT* tumoral cell lines, we observed similar results to the MEFs. Ablation of Cdk1 in these cell types will result in an arrest at the G2-M phase transition, followed by endoreplication. As was previously discussed, the ability of cells to undergo endoreplication upon elimination of Cdk1 is not surprising as this is a requirement in cells, such as trophoblast giant cells, that naturally undergo endoreplication (Ullah et al. 2008; Zhang et al. 1998). However, what remains unclear is if this is a phenotype observed in cells that naturally have a predisposition to endoreplicate or whether the elimination of Cdk1 in all proliferating cell types will result in endoreplication. Given that cells of the *Cdk1-null* early embryo were unable to sustain viability, eventually dying, we decided to look at early embryonic cell cycles.

The role of Cdk1 in early embryonic development was interesting since the embryonic cell cycle is quite distinct being biphasic between S and M phases, with little regulation and believed to be driven by constitutively high levels of Cyclins and Cdks (White & Dalton 2005). When we assessed the role of Cdk1 in the embryonic stem cell cycle, similar to the MEFs, we observed a cell cycle arrest at the G2-M transition. However, the arrest was transient followed by phosphorylation of γH2AX and induction of caspase-dependent apoptosis. This is similar to previous results using the Cdk1 inhibitor RO3306, where ES cells treated with the inhibitor underwent a transient G2-M arrest followed by cell death (Ullah et al. 2008). We further analyzed the apoptotic

phenotype and determined it to be independent of DDR. We cannot rule out that elimination of Cdk1 results in DNA damage, as we still observe a strong induction of γH2AX. Phosphorylated γH2AX can also be associated to apoptosis directly (Rogakou et al. 2000). Moreover, the phenotype in ES and iPS cells is similar to what is observed *in vivo*. Previous evidence has shown, that early embryos are capable of maintaining a cell cycle arrest *ex vivo*, as is the case in the *Cdc20-null* embryos (Manchado et al. 2010), whereas the *Cdk1-null* embryos undergo apoptosis and cannot maintain a stable cell cycle arrest.

In order to elucidate the molecular mechanisms behind ES cell death and MEFs ability to arrest and undergo endoreplicaiton, we performed RNA sequencing of ES and MEFs in the presence or absence of Cdk1. In line with expectations, we observed Cdk1 and cell cycle pathways to be differentially expressed in both the MEFs and the ES cells. We were able to identify Arpp19 to be significantly upregulated upon ablation of Cdk1. This could be expected as Arpp19 served to inhibit PP2A phosphatase activity against Cdk1 substrates, since there is no Cdk1 activity the cell has no requirement for PP2A activity. We also observed an induction of apoptotic and cell death pathways in *Cdk1-null* ES cell populations. When we further analyzed specific gene sets, we found Survivin to be downregulated in ES cells but conversely upregulated in MEFs. Survivin is a member of the chromosome passenger complex, can activate the SAC and is phosphorylated by Cdk1-Cyclin B1 (Tsukahara et al. 2010). Aside from the cell cycle functions of Survivin, it is also involved in apoptosis and phosphorylation by Cdk1 on threonine 34 has been shown to inhibit its mitotic activity and enhance its anti-apoptotic activity (Barrett et al. 2009). Given that Cdk1 is known to phosphorylate Survivin we believe that the differential expression we observe in MEFs and ES cells may partially explain the difference in response to Cdk1 elimination. In fact a recent study has linked high expression levels of Survivin in human ES cells to pluripotency (Mull et al. 2014). Moreover, in esophageal cancers and hepatocellular carcinomas Oct4 was shown to induce expression of Survivin, promoting cancer cell proliferation and correlating with poor prognosis (C. Li et al. 2012; Cao et al. 2013). We are currently investigating this further in order to delineate the connection between Survivin and Cdk1 in ES cell viability and cell cycle regulation.

Aside from the understanding the difference between the observed phenotype in stem and differentiated cells upon elimination of Cdk1, the RNA sequencing data that we have obtained can also be utilized in order to gain a better understanding of the

regulatory mechanisms in place during the G2-M transition in all cell types. We have generated a list of genes that are significantly differentially regulated in both the ES cells and the MEFs upon elimination of Cdk1. We have curated this list to obtain a more finite number of genes of interest. Moreover, given the comparison between ES cells and MEFs, our data also provide an inherent analysis of pluripotency. With the VENN diagram analysis we have been able to sort out the genes that are differentially regulated due to cell cycle changes (upon elimination of Cdk1) and generate a list of genes that are differentially regulated between ES cells and MEFs under all circumstances. One caveat with our data is that proliferation has been associated with pluripotency While our analysis of the RNA sequencing data is not complete, the continued analysis will surely provide a valued asset to the stem cell and cell cycle fields as well as further insight into the regulatory mechanisms controlling the G2-M cell cycle transition and cell fate decisions during proliferation.

Lastly, in order to determine the role of Cdk1 ablation in other stem cell compartments we analyzed HSC populations as well as teratomas from the previously mentioned ES cell clones. We found similar data to that found in the ES cells. Interestingly, the LSK and c-Kit+ HSC populations both resulted in an increase in apoptosis as compared to the GMP population. In the teratomas, we were able to identify an increase in phosphorylated yH2AX upon ablation of Cdk1. Taken together these data demonstrate that elimination of Cdk1 in a stem cell compartment *in vivo* will result in apoptosis, whereas differentiated cells will arrest and undergo endoreplication.

5.4 Therapeutic potential of targeting Cdk1

Aside from the previously discussed potential therapeutic approach in vascular endothelia, given the differential phenotype observed between stem and differentiated cell types we wanted to determine if targeting the cancer stem cell population could be therapeutically advantageous. Indeed, we observed an increase in apoptosis in the CSCs from *Tg.MMTV-PyMT* tumors lacking Cdk1. Moreover, the remaining cell population undergoes cell cycle arrest and endoreplication. These findings are preliminary evidence demonstrating a therapeutic potential for already existing Cdk1-inhibitors (RO-3306).

Indeed, therapeutic targeting of Cdk1 would need to be thoroughly investigated as initial studies demonstrated significant toxic complications due to therapy, as would be expected given the results we have presented here. However, the advancement of tissue and cell-specific drug delivery methods are advancing and may soon become a reality in

the clinic. If one could direct the Cdk1-inhibitor to a specific cell and tissue type to eliminate the CSC population, the remainder of the tumor could be targeted with chemotherapy, radiation therapy or surgery with less risk for recurrence. Systemic delivery of Cdk1 inhibitors would need to be on a strict dosing schedule to avoid toxic complications. However, if targeting Cdk1 in the CSC population, while arresting the remainder of the tumoral cells at the G2-M transition would be viable, one could quite effectively target complete tumor elimination.

6. Conclusions

The conclusions obtained from this work were the following:

1. *Cdk1-null* embryos present with a proliferative arrest, followed by lethality at 8-16 cell stage of development, demonstrating the essential role for Cdk1 in early embryonic cell cycles and development.
2. The *Tg.hUBC-CreERT2* tamoxifen-inducible Cre recombinase is more efficient and expressed in a more homogenous and ubiquitous manner than the *RERT*.
3. Cdk1 is essential for adult mouse homeostasis. Adult mice lacking Cdk1 cannot thrive, proliferative tissue compartments arrest and undergo atrophy, resulting in malnourishment, weight-loss and death.
4. Loss of p21 is capable of rescuing *Cdk1-null* early embryonic lethality up to a later developmental stage.
5. Differentiated mitotic cells lacking Cdk1 arrest with a 4n DNA content at the G2-M transition, undergo multiple rounds of endoreplication but are incapable of traversing mitosis.
6. Inhibition of PP2A phosphatase activity is capable of rescuing *Cdk1-null* cell cycle arrest and induce progression of cell cycle into late G2 or early mitosis.
7. Cdk1 is dispensable for endothelial homeostasis, while depletion of Cdk1 in the endothelial vasculature diminishes physiological angiogenesis potential but does not completely block angiogenesis.
8. Elimination of Cdk1 in a stem cell compartment will induce caspase-dependent apoptosis and phosphorylation of yH2AX.

Las conclusions más relevantes de esta tesis son las siguientes:

1. Los embriones nulos de Cdk1 se presentan con una parada proliferativa, seguida por letalidad al estado de desarollo de 8-16 celulas, demostrando el papel esencial de Cdk1 en los ciclos celulares embrionarios tempranos y en el desarrollo.
2. El *Tg.hUBC-CreERT2* Cre recombinasa inducible por Tamoxifen es más eficiente y expresada de manera más omogenio y ubiquo que el RERT.
3. Cdk1 es esencial para la homeostasis del ratón adulto. Ratones adultos carentes de Cdk1 no pueden desarrollarse con salud, los tejidos proliferativos se paran y sufren atrofia, resultando en malnutrición, pérdida de peso y muerte.
4. La pérdida de p21 es capaz de rescatar la letalidad embrionaria temprana debida a la falta de Cdk1 hasta un estadio posterior del desarrollo.
5. Las células mitóticas diferenciadas carentes de Cdk1 se paran con un contenido de ADN 4n en la transición G2-M, sufren múltiples rondas de endoreplicación pero son incapaces de atravesar la mitosis.
6. La inhibición de la actividad fosfatasa de PP2A es capaz de rescatar parcialmente la detención del ciclo celular en células nulas de Cdk1 e inducir la entrada en mitosis.
7. Cdk1 es dispensable por la homeostasis vascular, mientras su eliminación en la vasculatura endotelial disminuye el potencial angiogénico fisiológico pero no bloquea su desarrollo.
8. La eliminación de Cdk1 en compartimentos de células madre induce apoptosis dependiente de caspasa y fosforilación de yH2AX.

Bibliography

Anderson, N.G. et al., 1991. Raf-1 is a potential substrate for mitogen-activated protein kinase in vivo. *The Biochemical journal*, 277 (Pt 2, pp.573–576.

Bachvarova, R. & De Leon, V., 1980. Polyadenylated RNA of mouse ova and loss of maternal RNA in early development. *Developmental biology*, 74(1), pp.1–8.

Barrett, R.M. a, Osborne, T.P. & Wheatley, S.P., 2009. Phosphorylation of survivin at threonine 34 inhibits its mitotic function and enhances its cytoprotective activity. *Cell Cycle*, 8(2), pp.278–283.

Barrière, C. et al., 2007. Mice thrive without Cdk4 and Cdk2. *Molecular oncology*, 1(1), pp.72–83.

Barski, J.J., Dethleffsen, K. & Meyer, M., 2000. Cre recombinase expression in cerebellar Purkinje cells. *Genesis (New York, N.Y. : 2000)*, 28(3-4), pp.93–98.

Bashir, T. et al., 2004. Control of the SCFSkp2-Cks1 ubiquitin ligase by the APC/CCdh1 ubiquitin ligase. *Nature*, 428(6979), pp.190–193.

Berthet, C. et al., 2003. Cdk2 Knockout Mice Are Viable. *Current Biology*, 13(20), pp.1775–1785.

Bollen, M. et al., 2010. The extended PP1 toolkit: designed to create specificity. *Trends in biochemical sciences*, 35(8), pp.450–458.

Brandeis, M. et al., 1998. Cyclin B2-null mice develop normally and are fertile whereas cyclin B1-null mice die in utero. *Proceedings of the National Academy of Sciences of the United States of America*, 95(April), pp.4344–4349.

Brocard, J. et al., 1997. Spatio-temporally controlled site-specific somatic mutagenesis in the mouse. *Proceedings of the National Academy of Sciences of the United States of America*, 94(26), pp.14559–14563.

Brown, N. et al., 2007. Cyclin B and Cyclin A Confer Different Substrate Recognition Properties on Cdk2. *Cell Cycle*, 6(11), pp.1350–1359.

Bryja, V. et al., 2008. Lineage specific composition of cyclin D-CDK4/CDK6-p27 complexes reveals distinct functions of CDK4, CDK6 and individual D-type cyclins in differentiating cells of embryonic origin. *Cell proliferation*, 41(6), pp.875–893.

Campisi, J. et al., 1982. Restriction point control of cell growth by a labile protein: evidence for increased stability in transformed cells. *Proceedings of the National Academy of Sciences of the United States of America*, 79(2), pp.436–440.

Cao, L. et al., 2013. OCT4 increases BIRC5 and CCND1 expression and promotes cancer progression in hepatocellular carcinoma. *BMC cancer*, 13(1), p.82.

Chen, J. et al., 1995. Separate domains of p21 involved in the inhibition of Cdk kinase and PCNA. *Nature*, 374(6520), pp.386–388.

Ciemerych, M. a et al., 2002. Development of mice expressing a single D-type cyclin Development of mice expressing a single D-type cyclin. , 5, pp.3277–3289.

Clausen, B.E. et al., 1999. Conditional gene targeting in macrophages and granulocytes using LysMcre mice. *Transgenic research*, 8(4), pp.265–277.

Cooke, C.A. et al., 1993. Mapping DNA within the mammalian kinetochore. *The Journal of cell biology*, 120(5), pp.1083–1091.

Coudreuse, D. & Nurse, P., 2010. Driving the cell cycle with a minimal CDK control network. *Nature*, 468(7327), pp.1074–9.

Cross, J.C., 2005. How to make a placenta: mechanisms of trophoblast cell differentiation in mice--a review. *Placenta*, 26 Suppl A, pp.S3–9.

Daksis, J.I. et al., 1994. Myc induces cyclin D1 expression in the absence of de novo protein synthesis and links mitogen-stimulated signal transduction to the cell cycle. *Oncogene*, 9(12), pp.3635–3645.

Diril, M.K. et al., 2012. Cyclin-dependent kinase 1 (Cdk1) is essential for cell division and suppression of DNA re-replication but not for liver regeneration. *PNAS*, 109(10).

Domingo-Sananes, M.R. et al., 2011. Switches and latches: a biochemical tug-of-war between the kinases and phosphatases that control mitosis. *Philosophical transactions of the Royal Society of London. Series B, Biological sciences*, 366(1584), pp.3584–3594.

Dou, Q.P. et al., 1993. Cyclin E and cyclin A as candidates for the restriction point protein. *Cancer Research*, 53(7), pp.1493–1497.

Dumitru, R. et al., 2012. Human Embryonic Stem Cells Have Constitutively Active Bax at the Golgi and Are Primed to Undergo Rapid Apoptosis. *Molecular Cell*, 46(5), pp.573–583.

Dumont, D.J. et al., 1994. Dominant-negative and targeted null mutations in the endothelial receptor tyrosine kinase, tek, reveal a critical role in vasculogenesis of the embryo. *Genes and Development*, 8(16), pp.1897–1909.

Dunn, J.M. et al., 1988. Identification of germline and somatic mutations affecting the retinoblastoma gene. *Science (New York, N.Y.)*, 241(4874), pp.1797–1800.

Eggan, K. et al., 2001. Hybrid vigor, fetal overgrowth, and viability of mice derived by nuclear cloning and tetraploid embryo complementation. *Proceedings of the National Academy of Sciences of the United States of America*, 98(11), pp.6209–6214.

Ewen, M.E. et al., 1993. Functional interactions of the retinoblastoma protein with mammalian D-type cyclins. *Cell*, 73(3), pp.487–497.

Faast, R. et al., 2004. Cdk6-cyclin D3 activity in murine ES cells is resistant to inhibition by p16(INK4a). *Oncogene*, 23(2), pp.491–502.

Folkman, J., 1971. Tumor Angiogenesis: Therapeutic Implications. *New England Journal of Medicine*, 285(21), pp.1182–1186.

Forde, A. et al., 2002. Temporal Cre-mediated recombination exclusively in endothelial cells using Tie2 regulatory elements. *Genesis (New York, N.Y. : 2000)*, 33(4), pp.191–197.

Franceschini, A. et al., 2013. STRING v9.1: Protein-protein interaction networks, with increased coverage and integration. *Nucleic Acids Research*, 41(D1), pp.808–815.

Gao, D. et al., 2008. Endothelial Progenitor Cells Control the Angiogenic Switch in Mouse Lung Metastasis. *Science* , 319 (5860), pp.195–198.

Gavet, O. & Pines, J., 2010a. Activation of cyclin B1-Cdk1 synchronizes events in the nucleus and the cytoplasm at mitosis. *The Journal of cell biology*, 189(2), pp.247–59.

Gavet, O. & Pines, J., 2010b. Progressive activation of CyclinB1-Cdk1 coordinates entry to mitosis. *Developmental cell*, 18(4), pp.533–43.

Geng, Y. et al., 2003. Cyclin E ablation in the mouse. *Cell*, 114(4), pp.431–443.

Gharbi-Ayachi, A. et al., 2010. The substrate of Greatwall kinase, Arpp19, controls mitosis by inhibiting protein phosphatase 2A. *Science (New York, N.Y.)*, 330(6011), pp.1673–7.

Gibbs, J.B. et al., 1988. Purification of ras GTPase activating protein from bovine brain. *Proceedings of the National Academy of Sciences of the United States of America*, 85(14), pp.5026–5030.

Gille, H. et al., 1995. ERK phosphorylation potentiates Elk-1-mediated ternary complex formation and transactivation. *The EMBO journal*, 14(5), pp.951–962.

Goldfarb, M. et al., 1982. Isolation and preliminary characterization of a human transforming gene from T24 bladder carcinoma cells. *Nature*, 296(5856), pp.404–409.

Gould, K.L. & Nurse, P., 1989. Tyrosine phosphorylation of the fission yeast cdc2+ protein kinase regulates entry into mitosis. *Nature*, 342(6245), pp.39–45.

Guerra, C. et al., 2003. Tumor induction by an endogenous K-ras oncogene is highly dependent on cellular context. *Cancer cell*, 4(2), pp.111–20.

Guy, C.T., Cardiff, R.D. & Muller, W.J., 1992. Induction of mammary tumors by expression of polyomavirus middle T oncogene: a transgenic mouse model for metastatic disease. *Molecular and cellular biology*, 12(3), pp.954–961.

El Hallani, S. et al., 2010. A new alternative mechanism in glioblastoma vascularization: tubular vasculogenic mimicry. *Brain : a journal of neurology*, 133(Pt 4), pp.973–982.

Harrington, E.A., Bruce, J.L. & Dyson, N., 1998. pRB plays an essential role in cell cycle arrest induced by DNA damage. *Proceedings of the National Academy of Sciences of the United States of America*, 95(September), pp.11945–11950.

Helin, K. et al., 1993. Heterodimerization of the transcription factors E2F-1 and DP-1 leads to cooperative trans-activation. *Genes and Development*, 7, pp.1850–1861.

Hendrickx, A. et al., 2009. Docking motif-guided mapping of the interactome of protein phosphatase-1. *Chemistry & biology*, 16(4), pp.365–371.

Hiebert, S.W. et al., 1992. The interaction of RB with E2F coincides with an inhibition of the transcriptional activity of E2F. *Genes & development*, 6, pp.177–185.

Jackman, M. et al., 2003. Active cyclin B1-Cdk1 first appears on centrosomes in prophase. *Nat Cell Biol*, 5(2), pp.143–148.

Jones, S.M. & Kazlauskas, a, 2001. Growth-factor-dependent mitogenesis requires two distinct phases of signalling. *Nature cell biology*, 3(2), pp.165–172.

Kalaszczynska, I. et al., 2009. Cyclin A - Redundant in Fibroblasts, Essential in Hematopoietic and Embryonal Stem Cells. *Cell*, 138(2), pp.352–365.

Kanda, A. et al., 2012. Establishment of ES cells from inbred strain mice by dual inhibition (2i). *The Journal of reproduction and development*, 58(1), pp.77–83.

Keenan, S.M., Bellone, C. & Baldassare, J.J., 2001. Cyclin-dependent Kinase 2 Nucleocytoplasmic Translocation Is Regulated by Extracellular Regulated Kinase. *Journal of Biological Chemistry*, 276(25), pp.22404–22409.

Kim, Y. et al., 2009. Cyclin-dependent kinase 2-associating protein 1 commits murine embryonic stem cell differentiation through retinoblastoma protein regulation. *The Journal of biological chemistry*, 284(35), pp.23405–23414.

Koledova, Z. et al., 2010. Cdk2 inhibition prolongs G1 phase progression in mouse embryonic stem cells. *Stem cells and development*, 19(2), pp.181–194.

Kollmann, K. et al., 2013. A kinase-independent function of CDK6 links the cell cycle to tumor angiogenesis. *Cancer cell*, 24(2), pp.167–181.

Kolupaeva, V. & Janssens, V., 2012. PP1 and PP2A phosphatases: cooperating partners in modulating retinoblastoma protein activation. *FEBS J.*

Kozar, K. et al., 2004. Mouse development and cell proliferation in the absence of D-cyclins. *Cell*, 118(4), pp.477–491.

Lawson, K.A., Meneses, J.J. & Pedersen, R.A., 1991. Clonal analysis of epiblast fate during germ layer formation in the mouse embryo. *Development (Cambridge, England)*, 113(3), pp.891–911.

Lee, J.O., Russo, A.A. & Pavletich, N.P., 1998. Structure of the retinoblastoma tumour-suppressor pocket domain bound to a peptide from HPV E7. *Nature*, 391(6670), pp.859–865.

Lents, N.H. et al., 2002. Stimulation of the Raf/MEK/ERK cascade is necessary and sufficient for activation and Thr-160 phosphorylation of a nuclear-targeted CDK2. *Journal of Biological Chemistry*, 277(49), pp.47469–47475.

Li, C. et al., 2012. OCT4 Positively Regulates Survivin Expression to Promote Cancer Cell Proliferation and Leads to Poor Prognosis in Esophageal Squamous Cell Carcinoma. *PLoS ONE*, 7(11), pp.1–10.

Li, V.C., Ballabeni, A. & Kirschner, M.W., 2012. Gap 1 phase length and mouse embryonic stem. *PNAS*, 109(31), pp.12550–12555.

Lichti, U., Anders, J. & Yuspa, S.H., 2008. Isolation and short-term culture of primary keratinocytes, hair follicle populations and dermal cells from newborn mice and keratinocytes from adult mice for in vitro analysis and for grafting to immunodeficient mice. *Nature protocols*, 3(5), pp.799–810.

Lindqvist, A., Rodriguez-Bravo, V. & Medema, R.H., 2009. The decision to enter mitosis: feedback and redundancy in the mitotic entry network. *The Journal of cell biology*, 185(2), pp.193–202.

Liu, D. et al., 1998. Cyclin A1 is required for meiosis in the male mouse. *Nature genetics*, 20(4), pp.377–380.

Liu, T.J. et al., 2013. CD133+ cells with cancer stem cell characteristics associates with vasculogenic mimicry in triple-negative breast cancer. *Oncogene*, 32(5), pp.544–553.

Ma, J. et al., 2012. Characterization of mammary cancer stem cells in the MMTV-PyMT mouse model. *Tumour biology : the journal of the International Society for Oncodevelopmental Biology and Medicine*, 33(6), pp.1983–1996.

Malumbres, M. et al., 2009. Cyclin-dependent kinases: a family portrait. *Nature cell biology*, 11(11), pp.1275–1276.

Malumbres, M. et al., 1997. Isolation of high molecular weight DNA for reliable genotyping of transgenic mice. *BioTechniques*, 22(6), pp.1114–1119.

Malumbres, M. et al., 2004. Mammalian Cells Cycle without the D-Type Cyclin-Dependent Kinases Cdk4 and Cdk6. *Cell*, 118, pp.493–504.

Manchado, E. et al., 2010. Targeting mitotic exit leads to tumor regression in vivo: Modulation by Cdk1, Mastl, and the PP2A/B55α,δ phosphatase. *Cancer cell*, 18(6), pp.641–54.

Maniotis, A.J. et al., 1999. Vascular channel formation by human melanoma cells in vivo and in vitro: vasculogenic mimicry. *The American journal of pathology*, 155(3), pp.739–752.

Mao, X., Fujiwara, Y. & Orkin, S.H., 1999. Improved reporter strain for monitoring Cre recombinase-mediated DNA excisions in mice. *Proceedings of the National Academy of Sciences of the United States of America*, 96(9), pp.5037–5042.

Marks, H. et al., 2012. The transcriptional and epigenomic foundations of ground state pluripotency. *Cell*, 149(3), pp.590–604.

Martín, A. et al., 2005. Cdk2 is dispensable for cell cycle inhibition and tumor suppression mediated by p27(Kip1) and p21(Cip1). *Cancer cell*, 7(6), pp.591–8.

McShea, A. et al., 1997. Abnormal expression of the cell cycle regulators P16 and CDK4 in Alzheimer's disease. *The American journal of pathology*, 150(6), pp.1933–1939.

Méndez, J. & Stillman, B., 2000. Chromatin association of human origin recognition complex, cdc6, and minichromosome maintenance proteins during the cell cycle: assembly of prereplication complexes in late mitosis. *Molecular and cellular biology*, 20(22), pp.8602–8612.

Merchant, A.M. et al., 1997. A lesion in the DNA replication initiation factor Mcm10 induces pausing of elongation forks through chromosomal replication origins in Saccharomyces cerevisiae. *Molecular and cellular biology*, 17(6), pp.3261–3271.

Merrick, K. a et al., 2008. Distinct activation pathways confer cyclin-binding specificity on Cdk1 and Cdk2 in human cells. *Molecular cell*, 32(5), pp.662–72.

Miyajima, M., Nornes, H.O. & Neuman, T., 1995. Cyclin E is expressed in neurons and forms complexes with cdk5. *Neuroreport*, 6(8), pp.1130–1132.

Mochida, S. et al., 2010. Greatwall phosphorylates an inhibitor of protein phosphatase 2A that is essential for mitosis. *Science (New York, N.Y.)*, 330(6011), pp.1670–3.

Moyer, S.E., Lewis, P.W. & Botchan, M.R., 2006. Isolation of the Cdc45/Mcm2-7/GINS (CMG) complex, a candidate for the eukaryotic DNA replication fork helicase. *Proceedings of the National Academy of Sciences of the United States of America*, 103(27), pp.10236–10241.

Mull, A.N., Klar, A. & Navara, C.S., 2014. Differential localization and high expression of SURVIVIN splice variants in human embryonic stem cells but not in differentiated cells implicate a role for SURVIVIN in pluripotency. *Stem cell research*, 12(2), pp.539–549.

Murphy, L.O. et al., 2002. Molecular interpretation of ERK signal duration by immediate early gene products. *Nature cell biology*, 4(8), pp.556–564.

Murphy, L.O., Mackeigan, J.P. & Blenis, J., 2004. A Network of Immediate Early Gene Products Propagates Subtle Differences in Mitogen-Activated Protein Kinase Signal Amplitude and Duration A Network of Immediate Early Gene Products Propagates Subtle Differences in Mitogen-Activated Protein Kinase Signal. *Molecular and Cellular Biology*, 24(1), p.144.

Murphy, M. et al., 1997. Delayed early embryonic lethality following disruption of the murine cyclin A2 gene. *Nature genetics*, 15(1), pp.83–86.

Nagy, Z. et al., 1997. Cell cycle markers in the hippocampus in Alzheimer's disease. *Acta neuropathologica*, 94(1), pp.6–15.

Nevins, J.R., 1992. E2F: A Link Between the Rb Tumor Suppressor Protein and Viral Oncoproteins. *Science (New York, N.Y.)*, 258, pp.424–427.

Nguyen, V.Q., Co, C. & Li, J.J., 2001. Cyclin-dependent kinases prevent DNA re-replication through multiple mechanisms. *Nature*, 411(6841), pp.1068–1073.

Noble, M.E.M. et al., 1997. The cyclin box fold: protein recognition in cell-cycle and transcription control. *Trends in Biochemical Sciences*, 22(12), pp.482–487.

Novak, B. et al., 2010. Regulated protein kinases and phosphatases in cell cycle decicions. *Curr Opin Cell Biol*, 22(6), pp.801–808.

Nurse, P., 1990. Universal control mechanism regulating onset of M-phase. *Nature*, 344(6266), pp.503–508.

O'Farrell, P.H., Stumpff, J. & Su, T.T., 2004. Embryonic cleavage cycles: how is a mouse like a fly? *Current biology : CB*, 14(1), pp.R35–45.

Orford, K.W. & Scadden, D.T., 2008. Deconstructing stem cell self-renewal: genetic insights into cell-cycle regulation. *Nature reviews. Genetics*, 9(2), pp.115–28.

Ortega, S. et al., 2003. Cyclin-dependent kinase 2 is essential for meiosis but not for mitotic cell division in mice. *Nature genetics*, 35(1), pp.25–31.

Panniers, R. & Henshaw, E.C., 1983. A GDP/GTP exchange factor essential for eukaryotic initiation factor 2 cycling in Ehrlich ascites tumor cells and its regulation by eukaryotic initiation factor 2 phosphorylation. *The Journal of biological chemistry*, 258(13), pp.7928–7934.

Pardee, a B., 1974. A restriction point for control of normal animal cell proliferation. *Proceedings of the National Academy of Sciences of the United States of America*, 71(4), pp.1286–1290.

Parisi, T. et al., 2003. Cyclins E1 and E2 are required for endoreplication in placental trophoblast giant cells. *EMBO Journal*, 22(18), pp.4794–4803.

Peters, K.G. et al., 1998. Expression of Tie2/Tek in breast tumour vasculature provides a new marker for evaluation of tumour angiogenesis. *British journal of cancer*, 77(1), pp.51–56.

Pulciani, S. et al., 1982. Oncogenes in human tumor cell lines: molecular cloning of a transforming gene from human bladder carcinoma cells. *Proceedings of the National Academy of Sciences of the United States of America*, 79(9), pp.2845–2849.

Puri, M.C. et al., 1995. The receptor tyrosine kinase TIE is required for integrity and survival of vascular endothelial cells. *The EMBO journal*, 14(23), pp.5884–5891.

Quelle, D.E. et al., 1995. Alternative reading frames of the INK4a tumor suppressor gene encode two unrelated proteins capable of inducing cell cycle arrest. *Cell*, 83(6), pp.993–1000.

Rane, S.G. et al., 1999. Loss of Cdk4 expression causes insulin-deficient diabetes and Cdk4 activation results in beta-islet cell hyperplasia. *Nature genetics*, 22(1), pp.44–52.

Rapp, U.R. et al., 1983. Structure and biological activity of v-raf, a unique oncogene transduced by a retrovirus. *Proceedings of the National Academy of Sciences of the United States of America*, 80(14), pp.4218–4222.

Robinson, M.J. & Cobb, M.H., 1997. Mitogen-activated protein kinase pathways. *Current Opinion in Cell Biology*, 9(2), pp.180–186.

Rodríguez, C., Buchholz, F. & Galloway, J., 2000. High-efficiency deleter mice show that FLPe is an alternative to Cre-loxP. *Nature …*, 25(june), pp.139–140.

Rogakou, E.P. et al., 2000. Initiation of DNA fragmentation during apoptosis induces phosphorylation of H2AX histone at serine 139. *Journal of Biological Chemistry*, 275(13), pp.9390–9395.

Ruzankina, Y. et al., 2007. Deletion of the Developmentally Essential Gene ATR in Adult Mice. *Cell Stem Cell*, 1(1), pp.113–126.

Salomoni, P. & Calegari, F., 2010. Cell cycle control of mammalian neural stem cells: putting a speed limit on G1. *Trends in cell biology*, 20(5), pp.233–243.

Santamaría, D. et al., 2007. Cdk1 is sufficient to drive the mammalian cell cycle. *Nature*, 448(7155), pp.811–5.

Sato, T.N. et al., 1995. Distinct roles of the receptor tyrosine kinases Tie-1 and Tie-2 in blood vessel formation. *Nature*, 376(6535), pp.70–74.

Savatier, P., Huang, S. & Szekely, L., 1994. Contrasting patterns of retinoblastoma protein expression in mouse embryonic stem cells and embryonic fibroblasts. *Oncogene*, 9, pp.809–818.

Schmetsdorf, S., Gartner, U. & Arendt, T., 2007. Constitutive expression of functionally active cyclin-dependent kinases and their binding partners suggests noncanonical functions of cell cycle regulators in differentiated neurons. *Cerebral cortex (New York, N.Y. : 1991)*, 17(8), pp.1821–1829.

Schmetsdorf, S., Gartner, U. & Arendt, T., 2005. Expression of cell cycle-related proteins in developing and adult mouse hippocampus. *International journal of developmental neuroscience : the official journal of the International Society for Developmental Neuroscience*, 23(1), pp.101–112.

Schnegg, C.I. et al., 2015. Induction of Vasculogenic Mimicry Overrides VEGF-A Silencing and Enriches Stem-like Cancer Cells in Melanoma. *Cancer research*, 75(8), pp.1682–1690.

Scholzen, T. & Gerdes, J., 2000. The Ki-67 protein: from the known and the unknown. *Journal of cellular physiology*, 182(3), pp.311–322.

Scolnick, E.M., Papageorge, a G. & Shih, T.Y., 1979. Guanine nucleotide-binding activity as an assay for src protein of rat-derived murine sarcoma viruses. *Proceedings of the National Academy of Sciences of the United States of America*, 76(10), pp.5355–5359.

Serrano, M., Hannon, G.J. & Beach, D., 1993. A new regulatory motif in cell-cycle control causing specific inhibition of cyclin D/CDK4. *Nature*, 366(6456), pp.704–707.

Seth, A. et al., 1991. A phosphorylation site located in the NH2-terminal domain of c-Myc increases transactivation of gene expression. *Journal of Biological Chemistry*, 266(35), pp.23521–23524.

Shi, Y., 2009. Serine/threonine phosphatases: mechanism through structure. *Cell*, 139(3), pp.468–484.

Shih, C. & Weinberg, R. a, 1982. Isolation of a transforming sequence from a human bladder carcinoma cell line. *Cell*, 29(1), pp.161–169.

Singh, A.M. & Dalton, S., 2009. The cell cycle and Myc intersect with mechanisms that regulate pluripotency and reprogramming. *Cell stem cell*, 5(2), pp.141–149.

Sisken, J.E. & Morasca, L., 1965. Intrapopulation kinetics of the mitotic cycle. *Journal of Cell Biology*, 25, pp.179–189.

Slupe, A.M., Merrill, R.A. & Strack, S., 2011. Determinants for Substrate Specificity of Protein Phosphatase 2A. *Enzyme research*, 2011, p.398751.

Solomon, M.J., Lee, T. & Kirschner, M.W., 1992. Role of phosphorylation in p34cdc2 activation: identification of an activating kinase. *Molecular biology of the cell*, 3(1), pp.13–27.

Spencer, S.L. et al., 2013. The proliferation-quiescence decision is controlled by a bifurcation in CDK2 activity at mitotic exit. *Cell*, 155(2), pp.369–383.

Stead, E. et al., 2002. Pluripotent cell division cycles are driven by ectopic Cdk2, cyclin A/E and E2F activities. *Oncogene*, 21(54), pp.8320–8333.

Suri, C. et al., 1996. Requisite role of angiopoietin-1, a ligand for the TIE2 receptor, during embryonic angiogenesis. *Cell*, 87(7), pp.1171–1180.

Takahashi, K. & Yamanaka, S., 2006. Induction of Pluripotent Stem Cells from Mouse Embryonic and Adult Fibroblast Cultures by Defined Factors. *Cell*, 126(4), pp.663–676.

Tamaru, T. et al., 1993. Identification of cells expressing a D type G1 cyclin in matured brain: Implication for its role in neuronal function. *Neuroscience Letters*, 153(2), pp.169–172.

Tanaka, M. et al., 1997. Mash2 acts cell autonomously in mouse spongiotrophoblast development. *Developmental biology*, 190(1), pp.55–65.

Tiedt, R. et al., 2007. Pf4-Cre transgenic mice allow the generation of lineage-restricted gene knockouts for studying megakaryocyte and platelet function in vivo. *Blood*, 109(4), pp.1503–1506.

Tobey, R. a. & Ley, K.D., 1970. Regulation of initiation of DNA synthesis in Chinese hamster cells. I. Production of stable, reversible G1-arrested populations in suspension culture. *Journal of Cell Biology*, 46(1), pp.151–157.

Todaro, G.J., Lazar, G.K. & Green, H., 1965. The initiation of cell division in a contact-inhibited mammalian cell line. *Journal of cellular physiology*, 66(3), pp.325–333.

Trakala, M. et al., 2015. Functional Reprogramming of Polyploidization in Megakaryocytes. *Developmental Cell*, 32(2), pp.155–167.

Tsai, S.-Y. et al., 2008. Mouse Development with a Single E2F Activator. *October*, 28(30), pp.4439–4448.

Tsukahara, T., Tanno, Y. & Watanabe, Y., 2010. Phosphorylation of the CPC by Cdk1 promotes chromosome bi-orientation. *Nature*, 467(7316), pp.719–723.

Tsutsui, T. et al., 1999. Targeted disruption of CDK4 delays cell cycle entry with enhanced p27(Kip1) activity. *Molecular and cellular biology*, 19(10), pp.7011–7019.

Tu, W.-Z. et al., 2013. γH2AX foci formation in the absence of DNA damage: Mitotic H2AX phosphorylation is mediated by the DNA-PKcs/CHK2 pathway. *FEBS Letters*, 587(21), pp.3437–3443.

Ullah, Z. et al., 2008. Differentiation of trophoblast stem cells into giant cells is triggered by p57/Kip2 inhibition of CDK1 activity. *Genes & development*, 22(21), pp.3024–36.

Volmat, V. et al., 2001. The nucleus, a site for signal termination by sequestration and inactivation of p42/p44 MAP kinases. *Journal of cell science*, 114(Pt 19), pp.3433–3443.

Walsh, S., Margolis, S.S. & Kornbluth, S., 2003. Phosphorylation of the cyclin b1 cytoplasmic retention sequence by mitogen-activated protein kinase and Plx. *Molecular cancer research : MCR*, 1(February), pp.280–289.

White, J. & Dalton, S., 2005. Cell cycle control of embryonic stem cells. *Stem cell reviews*, 1(2), pp.131–138.

Williams, R.S., Shohet, R. V & Stillman, B., 1997. A human protein related to yeast Cdc6p. *Proceedings of the National Academy of Sciences of the United States of America*, 94(1), pp.142–147.

Wong, A.L. et al., 1997. Tie2 expression and phosphorylation in angiogenic and quiescent adult tissues. *Circulation research*, 81(4), pp.567–574.

Wong, J. V. et al., 2011. Network calisthenics: Control of E2F dynamics in cell cycle entry. *Cell Cycle*, 10(February 2015), pp.3086–3094.

Wuarin, J. et al., 2002. Stable association of mitotic Cyclin B/Cdc2 to replication origins prevents endoreduplication. *Cell*, 111, pp.419–431.

Yamamoto, T. et al., 2006. Continuous ERK Activation Downregulates Antiproliferative Genes throughout G1 Phase to Allow Cell-Cycle Progression. *Current Biology*, 16(12), pp.1171–1182.

Ye, X., Zhu, C. & Harper, J.W., 2001. A premature-termination mutation in the Mus musculus cyclin-dependent kinase 3 gene. *Proceedings of the National Academy of Sciences of the United States of America*, 98(4), pp.1682–1686.

Yeeles, J.T.P. et al., 2015. Regulated eukaryotic DNA replication origin firing with purified proteins. *Nature*, 519(7544), pp.431–435.

Zambrowicz, B.P. et al., 1997. Disruption of overlapping transcripts in the ROSA beta geo 26 gene trap strain leads to widespread expression of beta-galactosidase in

mouse embryos and hematopoietic cells. *Proceedings of the National Academy of Sciences of the United States of America*, 94(8), pp.3789–3794.

Zhang, P. et al., 1998. Cooperation between the Cdk inhibitors p27(KIP1) and p57(KRP2) in the control of tissue growth and development. *Genes and Development*, 12(20), pp.3162–3167.

Zhang, W.W. et al., 2011. Cdk1 is required for the self-renewal of mouse embryonic stem cells. *Journal of cellular biochemistry*, 112(3), pp.942–8.

Zhu, W. et al., 2007. Mcm10 and And-1/CTF4 recruit DNA polymerase alpha to chromatin for initiation of DNA replication. *Genes & development*, 21(18), pp.2288–2299.

Zielke, N., Edgar, B.A. & Depamphilis, M.L., 2015. Endoreplication. , pp.1–16.

Appendix 1

Supplementary Figures

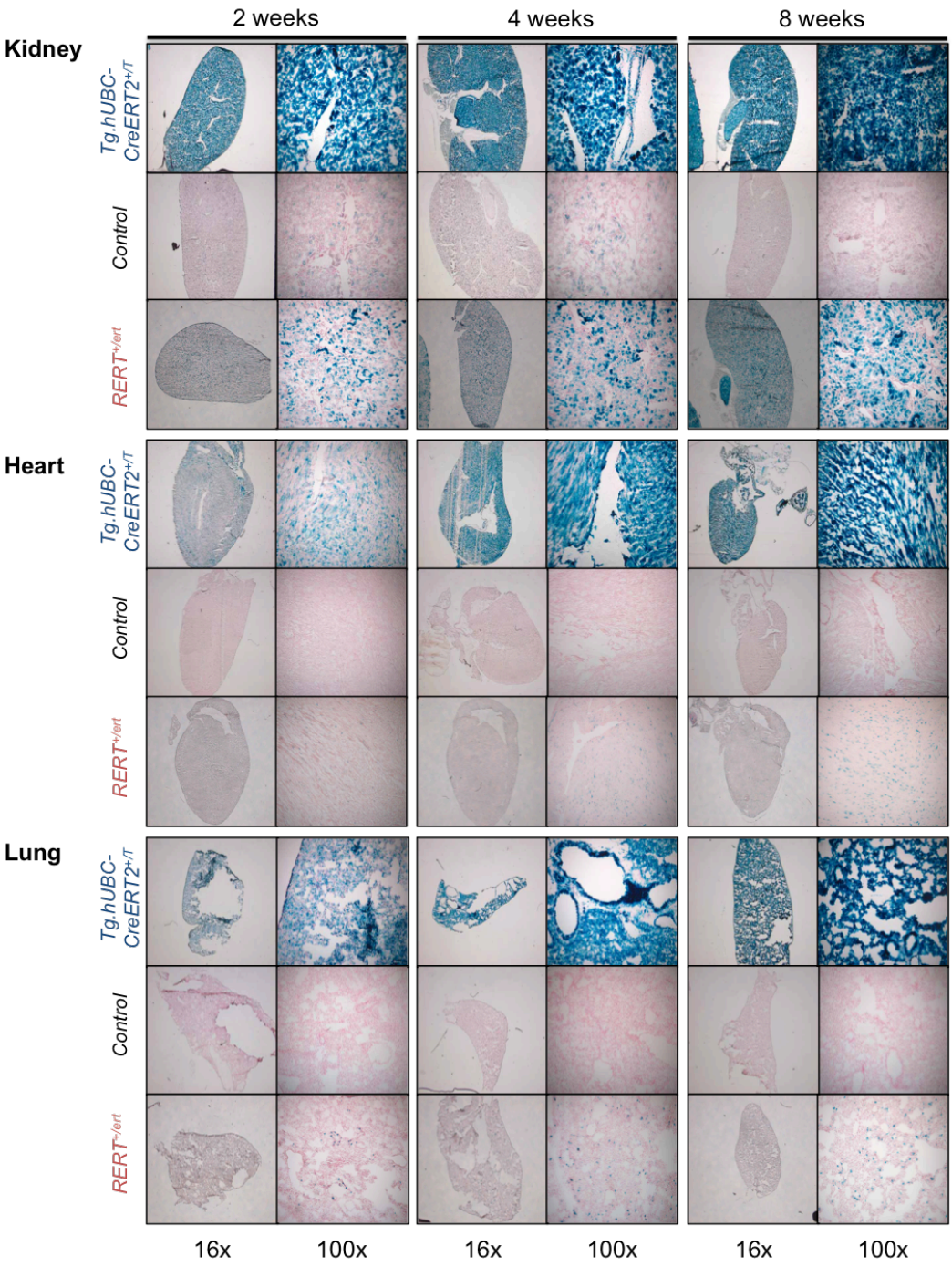

Supplemental Figure 1a: Comparison of *RERT* and *Tg.hUBC-CreERT2* inducible Cre mice. Kidney, heart and lung samples from *Rosa26lslsLacZ, Tg.hUBC-CreERT2; Rosa26lslLacZ; RERT*, or *Rosa26lslLacZ* controls at 2, 4 and 8 weeks of Tamoxifen-containing diet *ad libidum*.

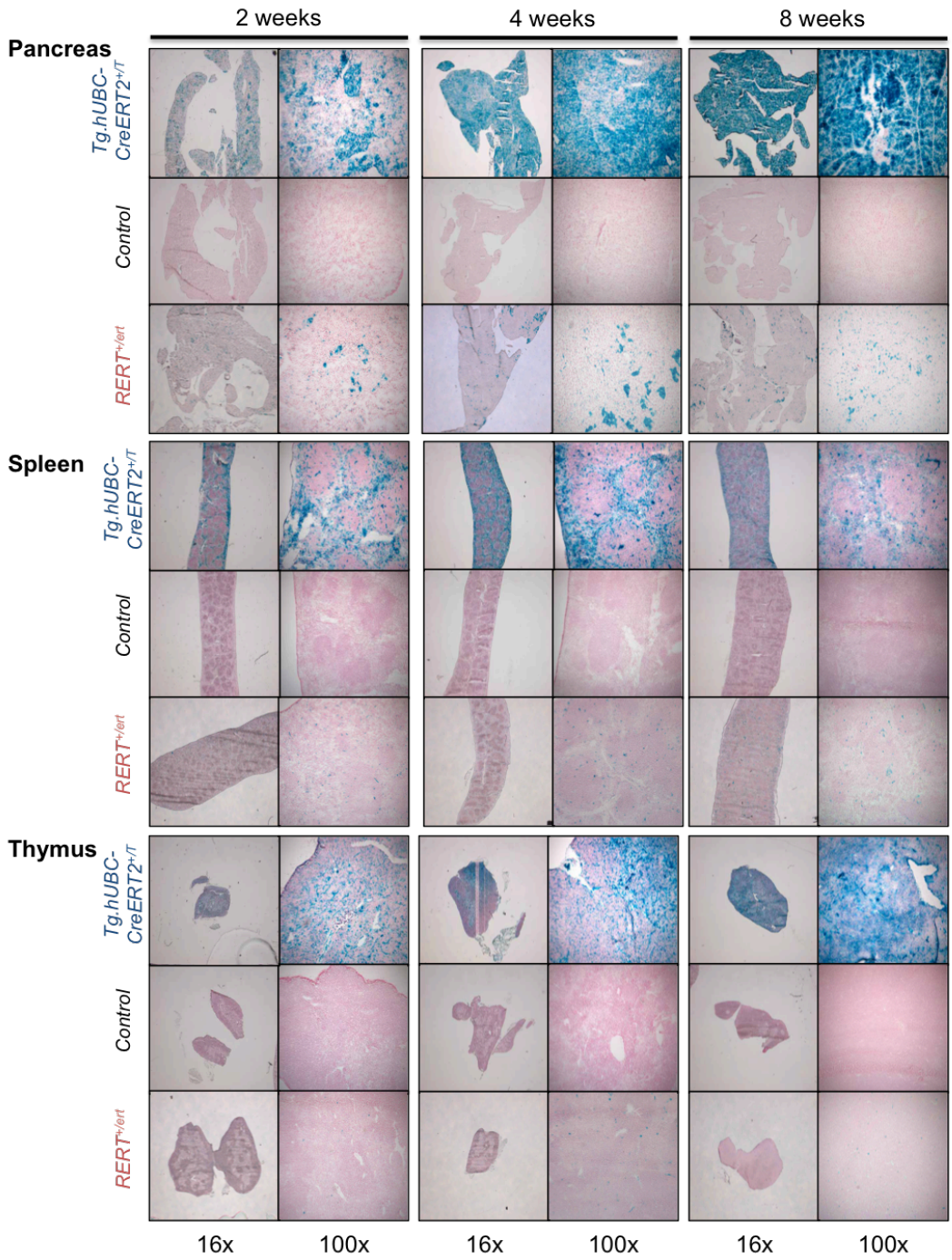

Supplemental Figure 1b: Comparison of *RERT* and *Tg.hUBC-CreERT2* inducible Cre mice. Pancreas, spleen and thymus samples from *Rosa26lslsLacZ, Tg.hUBC-CreERT2; Rosa26lslLacZ; RERT*, or *Rosa26lslLacZ* controls at 2, 4 and 8 weeks of Tamoxifen-containing diet *ad libidum*.

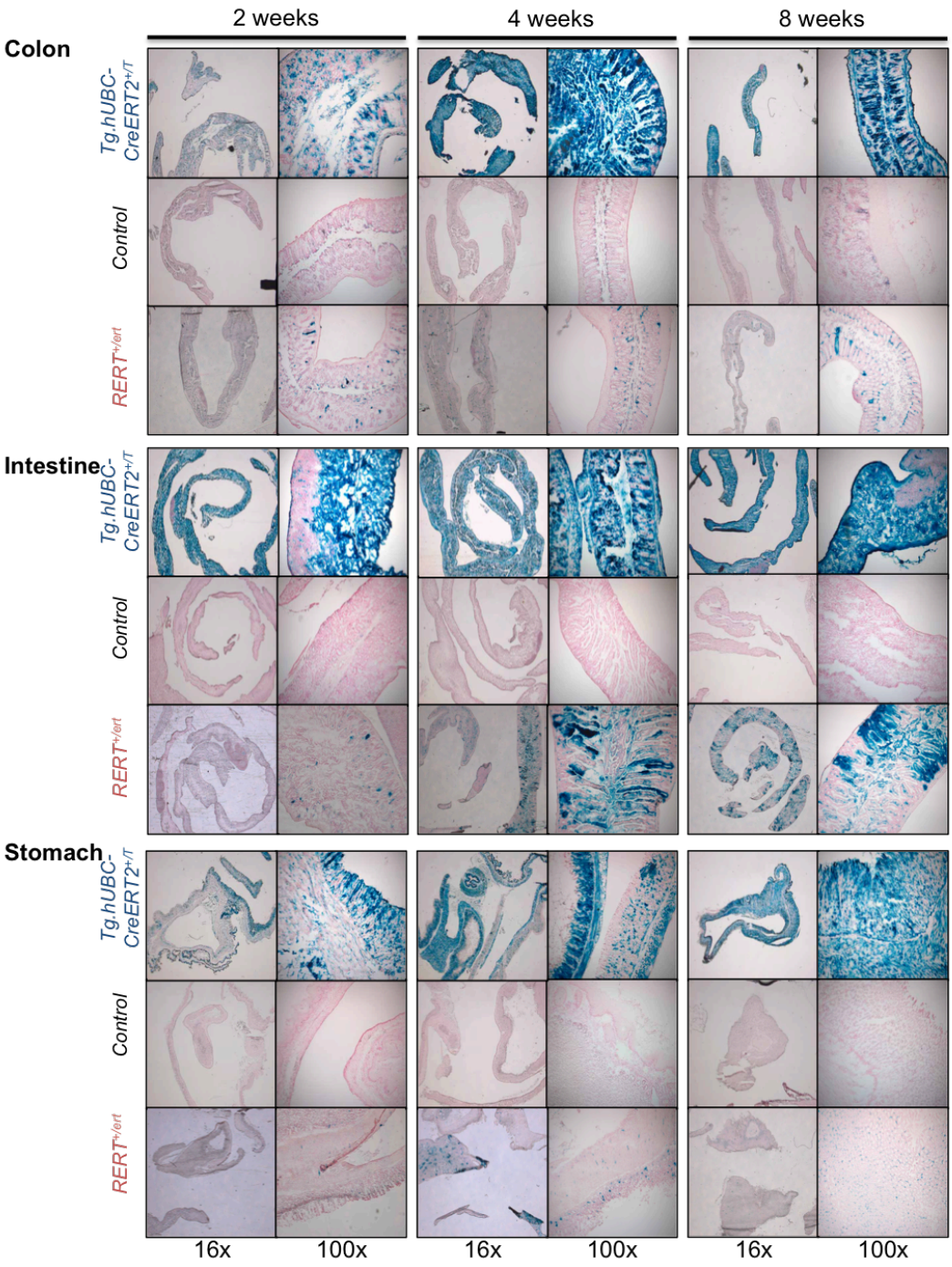

Supplemental Figure 1c: Comparison of *RERT* and *Tg.hUBC-CreERT2* inducible Cre mice. Colon, intestine and stomach samples from *Rosa26lslLacZ, Tg.hUBC-CreERT2; Rosa26lslLacZ; RERT*, or *Rosa26lslLacZ* controls at 2, 4 and 8 weeks of Tamoxifen-containing diet *ad libidum.*

Appendix 2

Publications

© 2015. Published by The Company of Biologists Ltd | Journal of Cell Science (2015) 128, 88–99 doi:10.1242/jcs.154922

RESEARCH ARTICLE

CDK2 regulates nuclear envelope protein dynamics and telomere attachment in mouse meiotic prophase

Alberto Viera[1], Manfred Alsheimer[2], Rocío Gómez[1], Inés Berenguer[1], Sagrario Ortega[3], Catherine E. Symonds[4], David Santamaría[4], Ricardo Benavente[2] and José A. Suja[1,*]

ABSTRACT

In most organisms, telomeres attach to the nuclear envelope at the onset of meiosis to promote the crucial processes of pairing, recombination and synapsis during prophase I. This attachment of meiotic telomeres is mediated by the specific distribution of several nuclear envelope components that interact with the attachment plates of the synaptonemal complex. We have determined by immunofluorescence and electron microscopy that the ablation of the kinase CDK2 alters the nuclear envelope in mouse spermatocytes, and that the proteins SUN1, KASH5 (also known as CCDC155) and lamin C2 show an abnormal cap-like distribution facing the centrosome. Strikingly, some telomeres are not attached to the nuclear envelope but remain at the nuclear interior where they are associated with SUN1 and with nuclear-envelope-detached vesicles. We also demonstrate that mouse testis CDK2 phosphorylates SUN1 *in vitro*. We propose that during mammalian prophase I the kinase CDK2 is a key factor governing the structure of the nuclear envelope and the telomere-led chromosome movements essential for homolog pairing.

KEY WORDS: Meiosis, CDK2, SUN1, Telomere, Nuclear envelope

INTRODUCTION

Meiosis represents a specialized type of cell division characterized by the existence of a single round of DNA replication, followed by two rounds of chromosome segregation. In most sexually reproducing organisms, homologous chromosomes must correctly achieve the processes of pairing, recombination and synapsis during the meiotic prophase I in order to prompt the further generation of haploid cells. The tethering of telomeres to the nuclear envelope is considered a prerequisite that facilitates and mediates the initiation and accomplishment of these processes (Koszul and Kleckner, 2009; Kracklauer et al., 2013; Scherthan, 2007; Zickler and Kleckner, 1998). The attachment of telomeres to the nucleoplasmic face of the inner nuclear membrane (INM) of the nuclear envelope occurs at the leptotene stage of meiotic prophase I. These anchoring sites represent nuclear envelope bridges linking the cytoskeleton and the nucleoskeleton that mediate the chromosomal movements during prophase I stages (Koszul and Kleckner, 2009; Kracklauer et al., 2013). In animals and fungi, telomeres move on the inner surface of the nuclear envelope and become clustered at a certain nuclear region, adjacent to the centrosome, creating a bouquet-like arrangement of chromosomes during zygotene. Afterwards, telomeres disperse along the nuclear envelope during the pachytene and diplotene stages until their detachment at the transition between diakinesis and prometaphase I.

As shown in recent years, the proper tethering of telomeres to the nuclear envelope is not only mediated by telomeric DNA and the attachment plates of the axial elements and lateral elements of the synaptonemal complex, but by their interactions with other protein components (Alsheimer, 2009). In this regard, the evolutionarily conserved SUN-domain-containing proteins present at the INM are required to tether the telomeres to the nuclear envelope through their interaction with adaptor proteins that mediate their association to the telomeres at the attachment plates (Alsheimer, 2009; Hiraoka and Dernburg, 2009; Koszul and Kleckner, 2009). Moreover, SUN domain proteins interact at the perinuclear space of the nuclear envelope with KASH domain proteins, located at the outer nuclear membrane, to form the so-called LINC complexes that connect the nucleoskeleton and the cytoskeleton (Starr and Fridolfsson, 2010). Thus, SUN domain proteins provide a link to nucleoskeleton structures, such as the nuclear lamina, whereas KASH domain proteins connect to the microtubule or actin-based cytoskeleton. Consistent with this arrangement, it has been recently reported that in mouse meiosis KASH5 associates with SUN1 and SUN2, and with cytoplasmic dynein (Horn et al., 2013; Link et al., 2014; Morimoto et al., 2012). Interestingly, it has also been recently demonstrated that different serine/threonine protein kinases phosphorylate the nucleoplasmic domain of SUN1 at the meiotic nuclear envelope in the nematode *Caenorhabditis elegans*, and that these modifications are required for telomere movement and attachment to the centrosome (Labella et al., 2011; Penkner et al., 2009; Sato et al., 2009).

Cyclin-dependent kinases (CDKs) are a group of serine/threonine protein kinases, highly conserved from yeast to humans, which participate in the regulation and progression of the cell cycle and the subsequent cell division. In recent years, however, it has become evident that CDKs demonstrate a high level of functional redundancy. In this context, the only CDK that seems to be essential for the cell cycle is CDK1, the so-called ‘mitotic kinase’, whose deletion causes cell cycle arrest (Santamaría et al., 2007). In contrast, it has been reported that the previously considered master regulator of cell cycle progression in mammals, namely CDK2, is dispensable for mitotic cell cycle progression and division (Berthet et al., 2003; Ortega et al., 2003; Tetsu and McCormick, 2003). However, a possible role of CDK2 in meiosis arose from the finding that it

[1]Unidad de Biología Celular, Departamento de Biología, Facultad de Ciencias, Universidad Autónoma de Madrid, E-28049 Madrid, Spain. [2]Department of Cell and Developmental Biology, Biocenter, University of Würzburg, D-97074 Würzburg, Germany. [3]Biotechnology Program, Centro Nacional de Investigaciones Oncológicas, E-28029 Madrid, Spain. [4]Molecular Oncology Program, Centro Nacional de Investigaciones Oncológicas, E-28029 Madrid, Spain.

*Author for correspondence (jose.suja@uam.es)

Received 11 April 2014; Accepted 27 October 2014

Journal of Cell Science (2015) 128, 88–99 doi:10.1242/jcs.154922

locates at telomeres and at late recombination nodules throughout meiotic prophase I (Ashley et al., 2001). Indeed, the essential role of CDK2 in gametogenesis was demonstrated from the evidence that *Cdk2*$^{-/-}$ mice were infertile, with complete penetrance (Berthet et al., 2003; Ortega et al., 2003). Accordingly, in *Cdk2*$^{-/-}$ male mice, meiosis arrests in prophase I, triggering the apoptotic pathway in the spermatocytes, which results in the absence of further meiotic stages (Berthet et al., 2003; Ortega et al., 2003). In a previous study, we reported that in male mouse meiosis CDK2 was required for recombination, proper homolog pairing and synapsis, and sex-body formation (Viera et al., 2009). Moreover, we described that in *Cdk2*$^{-/-}$ mutant spermatocytes some telomeres did not attach accurately to the nuclear envelope during prophase I stages, and suggested that this could lead to extensive non-homologous synapsis (Viera et al., 2009).

In the present study, we have performed a detailed analysis of possible modifications in the structure and composition of the nuclear envelope in *Cdk2*$^{-/-}$ spermatocytes. For this purpose, we have investigated the organization of the nuclear envelope as well as the presence, distribution and dynamics of representative nuclear envelope protein components by using immunofluorescence and electron microscopy. Furthermore, we have tested whether mouse testis CDK2 is able to phosphorylate SUN1 *in vitro*. According to our results, we propose and discuss the putative participation of CDK2 in maintaining the structure and dynamics of the nuclear envelope, as well as its role in driving the attachment of meiotic telomeres to the nuclear envelope and in chromosome movement and bouquet formation, in male mouse meiosis.

RESULTS

Cdk2$^{-/-}$ spermatocytes display an anomalous distribution of SUN1

We have previously described that in the most advanced meiotic prophase I stage found in *Cdk2*$^{-/-}$ male mice, i.e. in pachytene-like spermatocytes, some telomeres seemed to be in the nuclear interior and thus were not attached to the nuclear envelope (Viera et al., 2009). Given that it has been proposed that SUN domain proteins present at the INM are involved in the anchoring of telomeres to the nuclear envelope in meiocytes from several species (Alsheimer, 2009; Hiraoka and Dernburg, 2009; Koszul and Kleckner, 2009; Kracklauer et al., 2013), we compared the pattern of distribution of SUN1 in wild-type and *Cdk2*$^{-/-}$ spermatocytes. To this end, we made a double-immunolabeling of SUN1 and SYCP3, a structural protein component of the axial and lateral elements of the synaptonemal complex, to define meiotic staging during prophase I. We used the squashing technique because it preserves the nuclear volume and chromosome condensation, and positioning inside spermatocyte nuclei (Page et al., 1998; Parra et al., 2002). In wild-type leptotene spermatocytes, SUN1 appeared as small spots at the nuclear envelope (Fig. 1A,B), whereas at zygotene most SUN1 spots were present at the ends of axial and lateral elements giving a bouquet-like arrangement (Fig. 1C,D). In pachytene spermatocytes, all SUN1 signals appeared at the ends of synaptonemal complexes, the attachment plates, associated with the nuclear envelope (Fig. 1E,F). Strikingly, in all prophase I *Cdk2*$^{-/-}$ spermatocytes SUN1 was mainly observed as a polarized cap-shaped continuous labeling at the nuclear envelope (Fig. 1G–L). Given that it is known that SUN1 participates in the attachment of the centrosome to the nucleus (Tzur et al., 2006), we studied whether the polarization of SUN1 in mutant spermatocytes was related to the distribution of the centrosome. To address this, we performed a double-immunolabeling of SYCP3 and pericentrin, a component of the pericentriolar material present at the centrosome, and also of pericentrin and SUN1. Our results showed that the centrosome was always located near the nuclei as an unaltered ‘cloud’ from leptotene up to pachytene both in wild-type and mutant spermatocytes (supplementary material Fig. S1A–J). Interestingly, the SUN1 cap present in all mutant spermatocytes was always facing the centrosome (Fig. 1M,N; supplementary material Fig. S1K–N). These results suggest that in the absence of CDK2 the protein SUN1 is still able to become mostly polarized at the INM near the centrosome, as occurs when it associates to telomeres during the bouquet-like arrangement in wild-type zygotene nuclei. However, SUN1 is unable to redistribute along the nuclear envelope in pachytene-like mutant spermatocytes, as occurs in wild-type pachytene spermatocytes when it associates to the attachment plates.

Surprisingly, in addition to the remarkable anomalous and persisting polarization of SUN1 at the nuclear periphery, it also appeared as small foci at the nuclear interior in all prophase I stages in *Cdk2*$^{-/-}$ individuals (Fig. 1G–L). Therefore, we next analyzed the possible spatial relationship between internal SUN1 foci and internal telomeres. A triple-immunolabeling of SUN1, TRF1, a telomeric protein, and SYCP3 demonstrated that all internal SUN1 foci were associated with internal TRF1 signals (Fig. 1O,P). However, some internal TRF1 signals actually did not colocalize with SUN1 (Fig. 1O,P). This association of SUN1 with internal telomeres denoted an internal localization of the transmembrane protein SUN1, which is remarkable and without precedent in the literature. Given that several SUN1 foci could be detected in a given *Cdk2*$^{-/-}$ spermatocyte, we scored the number of internal SUN1 foci in ten squashed nuclei of each prophase I stage, in two different *Cdk2*$^{-/-}$ individuals, after the immunolabeling of SUN1 and SYCP3. Our results demonstrated the presence of one up to four internal SUN1 signals in each analyzed spermatocyte (Fig. 2A). In this sense, 50% of leptotene spermatocytes presented a single SUN1 internal signal, whereas the percentages of spermatocytes with two or three internal SUN1 foci were 30% and 15%, respectively. Remarkably, only 5% of leptotene spermatocytes presented four SUN1 foci at their nuclear interior. By contrast, only 20% of zygotene and pachytene-like spermatocytes displayed only one internal SUN1 signal, whereas four foci were present in other 20% of spermatocytes. These observations prompted us to analyze the organization of the nuclear periphery in wild-type and *Cdk2*$^{-/-}$ spermatocytes by electron microscopy. In wild-type pachytene spermatocytes, telomeres were attached to the nuclear envelope through the attachment plates, disk-shaped electron-dense plates at the ends of the lateral elements of the synaptonemal complex (Esponda and Giménez-Martin, 1972; Liebe et al., 2004) (Fig. 3A). At the attachment sites, both nuclear envelope membranes were thicker and associated with fibrils that bridge the perinuclear space. These fibrils were in apparent continuity with cytoplasmic fibrils that associated with the outer nuclear membrane (Fig. 3A). According to current models, the fibrils in the perinuclear space correspond, at least in part, to SUN proteins, whereas the cytoplasmic fibrils might represent KASH domain proteins (Schmitt et al., 2007). In mutant pachytene-like spermatocytes, we found normally attached telomeres (Fig. 3B). However, other telomeres in the same nucleus did not attach to the INM through attachment plates, but the ends of the lateral elements contacted laterally with the INM (Fig. 3C). In other cases, the ends of the lateral elements contacted with one or two membrane vesicles of ~200 nm in diameter, that were apparently detaching from the INM (Fig. 3D,E,G).

Journal of Cell Science (2015) 128, 88–99 doi:10.1242/jcs.154922

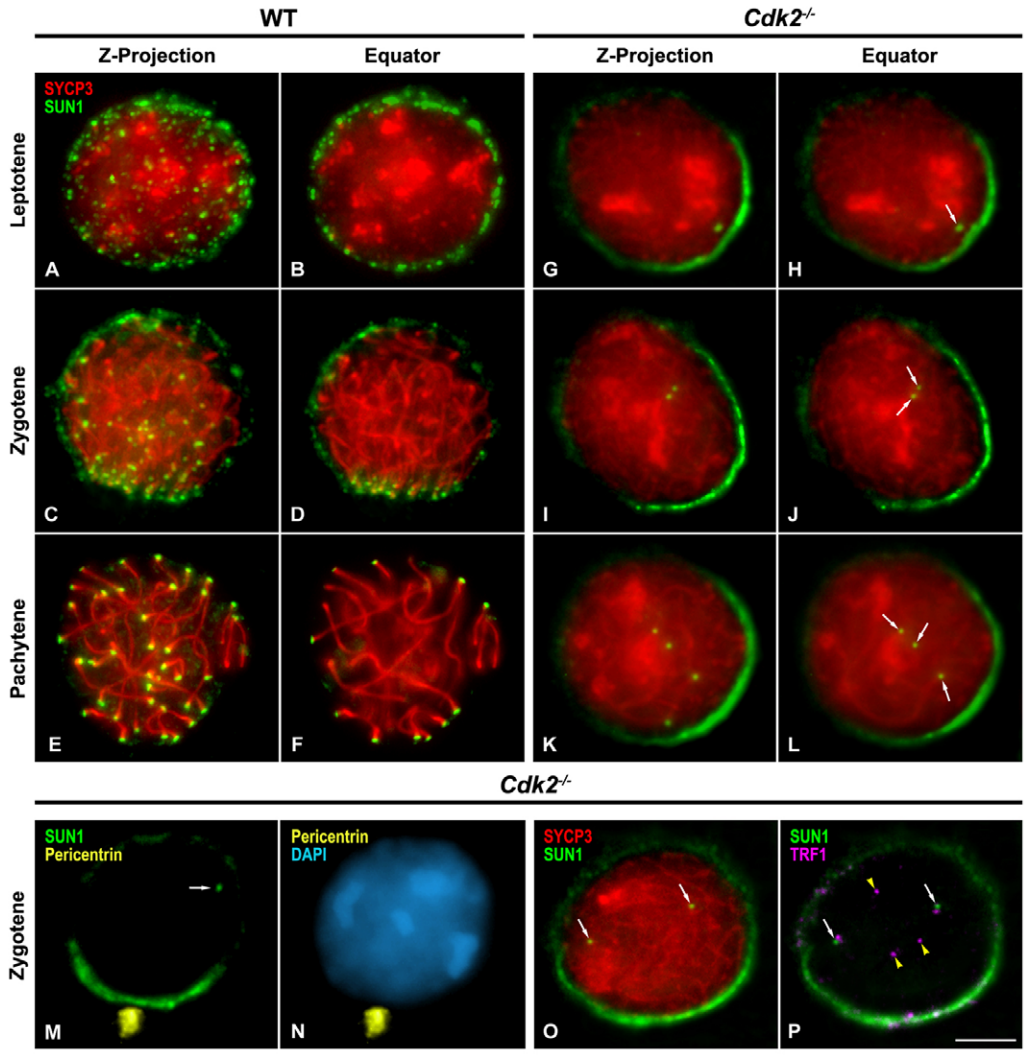

Fig. 1. SUN1 distribution at the nuclear envelope is disturbed in *Cdk2*$^{-/-}$ spermatocytes. (A–L) Double-immunolabeling of SUN1 (green) and SYCP3 (red) on squashed wild-type (A–F) and *Cdk2*$^{-/-}$ (G–L) prophase I spermatocytes. The first and third columns correspond to the *z*-projection of all the focal planes throughout a wild-type and *Cdk2*$^{-/-}$ spermatocyte nucleus, respectively. The second and fourth columns present the partial *z*-projections of 15 focal planes throughout the equatorial region of the same spermatocytes. (A,B) Wild-type (WT) leptotene nucleus. SUN1 appears as spots uniformly distributed at the nuclear periphery. (C,D) WT zygotene nucleus. Most SUN1 spots are polarized at the nuclear envelope reflecting a bouquet-like telomere arrangement. (E,F) WT pachytene nucleus. SUN1 is observed at the synaptonemal complex ends at the nuclear periphery. (G–L) *Cdk2*$^{-/-}$ prophase I nuclei. From leptotene on SUN1 is always found as a continuous and polarized cap-like labeling at the nuclear envelope . Note that SUN1 also appears as small foci (arrows) in the nuclear interior. (M,N) Double-immunolabeling of SUN1 (green) and pericentrin (yellow) on a zygotene *Cdk2*$^{-/-}$ spermatocyte. The SUN1 cap faces the pericentrin-labeled centrosome. Note one internal SUN1 spot (arrow). (O,P) Triple-immunolabeling of SUN1 (green), TRF1 (purple) and SYCP3 (red) on a zygotene *Cdk2*$^{-/-}$ spermatocyte. Both images are partial *z*-projections of 15 focal planes throughout the equatorial region. Two internal SUN1 foci (white arrows) are near telomeric TRF1 signals, and three internal telomeric signals (yellow arrowheads) do not colocalize with SUN1 spots. Scale bar: 5 μm.

Interestingly, we also found that the ends of lateral elements or synaptonemal complexes in internal nuclear regions were attached to vesicles that were obviously separated from the nuclear envelope (Fig. 3F,H,I). To our knowledge this is the first description of telomere-associated vesicles in the nuclear interior of meiotic cells.

Taking into account our results, we wondered whether CDK2 could participate in the anchoring of the attachment plates of the synaptonemal complex to the nuclear envelope, taking into account that CDK2 has been cytologically detected at telomeres in mouse prophase I spermatocytes (Ashley et al., 2001). For this purpose, we analyzed by electron microscopy the telomeric location of CDK2 in wild-type pachytene spermatocytes. We found that CDK2 labeling was positioned over the attachment plates that were associated with the INM (Fig. 4A). Given that in *C. elegans* meiocytes SUN1 is phosphorylated by serine/threonine protein kinases (Labella et al., 2011; Penkner et al., 2009; Sato et al., 2009), we subsequently tested whether SUN1 might be a substrate for CDK2 phosphorylation in mouse. In order to directly test this possibility we performed an *in vitro* kinase assay using the N-terminal domain (amino acids 1–243) of SUN1 as a substrate. Interestingly, CDK2 immunoprecipitated from wild-type testis extracts could efficiently phosphorylate recombinant SUN1 (Fig. 4B). Thus, at least *in vitro*, SUN1 is a substrate for mouse testis CDK2 phosphorylation.

Taken together, our results suggest that CDK2-mediated phosphorylation of SUN1 is involved in its accurate distribution

Journal of Cell Science (2015) 128, 88–99 doi:10.1242/jcs.154922

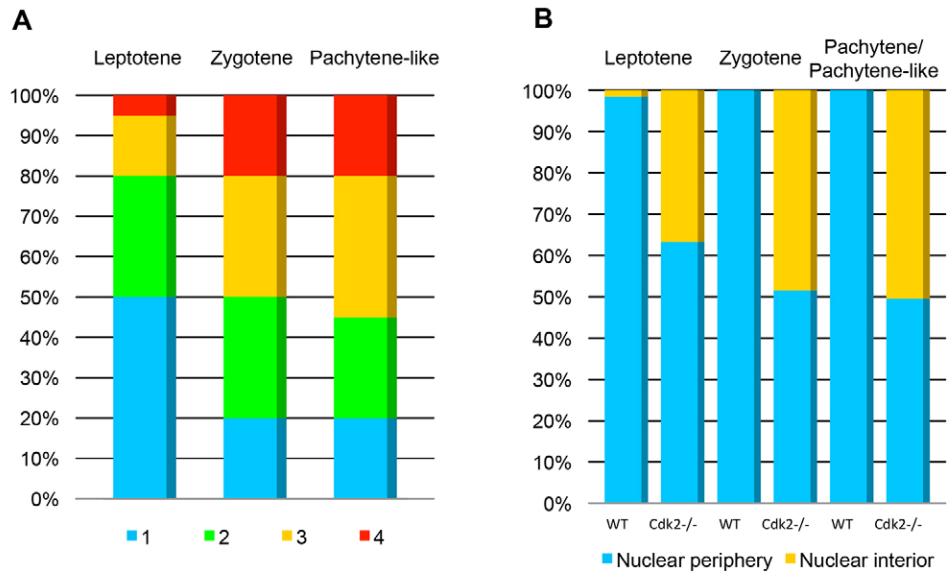

Fig. 2. Percentages of internal SUN1 foci and telomeres.
(A) Percentages of internal SUN1 foci in *Cdk2*$^{-/-}$ spermatocytes . The presence of internal SUN1 signals within a nucleus was scored in 20 squashed spermatocytes for each prophase I stage in *Cdk2*$^{-/-}$ individuals. The graphic representation corresponds to the percentage of nuclei showing one (blue), two (green), three (yellow) or four (red) internal SUN1 foci.
(B) Percentages of non-attached telomeres in wild-type and *Cdk2*$^{-/-}$ spermatocytes. The position of telomeres within a nucleus was scored in 20 squashed spermatocytes for each prophase I stage in wild-type (WT) and *Cdk2*$^{-/-}$ individuals. The graphic representation corresponds with the percentage of telomeres found at the nuclear periphery (blue) or at the nuclear interior (yellow).

	Number of internal SUN1 foci:			
	1	2	3	4
Leptotene	50%	30%	15%	5%
Zygotene	20%	30%	30%	20%
Pachytene-like	20%	25%	35%	20%

	Telomere attachment			
	Wild-type		*Cdk2*$^{-/-}$	
	Nuclear periphery	Nuclear interior	Nuclear periphery	Nuclear interior
Leptotene	98.41%	1.59%	63.28%	36.72%
Zygotene	100%	0%	51.52%	48.48%
Pachytene/ Pachytene-like	100%	0%	49.48%	50.53%

and association to the attachment plates found at the ends of axial and lateral elements during prophase I. Thus, in the absence of CDK2 some telomeres are tethered to the nuclear envelope in early prophase I stages, but some of them can detach from the nuclear envelope peeling off vesicles derived from the INM, accounting for the presence of SUN1 at internal telomeres (see below).

KASH5 distribution is disrupted in *Cdk2*$^{-/-}$ spermatocytes

In mouse spermatocytes, SUN1 interacts with KASH5 to form LINC complexes associated to the telomeres (Horn et al., 2013; Morimoto et al., 2012). Thus, in wild-type pachytene spermatocytes both SUN1 and KASH5 signals localized at the ends of synaptonemal complexes attached to the nuclear envelope (Fig. 5A–D). Given that the accurate localization of KASH5 during meiosis is disturbed in the absence of SUN1 (Horn et al., 2013; Morimoto et al., 2012), and that we found a cap-shaped polarization of SUN1 in *Cdk2*$^{-/-}$ spermatocytes, we then analyzed the relative distribution of SUN1 and KASH5 in *Cdk2*$^{-/-}$ individuals. *Cdk2*$^{-/-}$ spermatocytes, from leptotene up to the pachytene-like stage, displayed a polarized SUN1 labeling at the nuclear envelope (Fig. 5E,I,M), which was also observed for KASH5 (Fig. 5F,J,N). Indeed, both proteins mostly colocalized at the cap-shaped arrangement (Fig. 5G,K,O). Nevertheless, whereas SUN1 was additionally detected as discrete dots positioned at the nuclear interior, KASH5 was not detectable inside the nuclei (Fig. 5H,L,P). Our observations indicate that CDK2 drives the proper distribution of SUN1 at telomeres in mouse spermatocytes, and that the polarization of SUN1 at the nuclear envelope, in the absence of CDK2, determines the altered distribution of its interacting protein KASH5.

Cdk2$^{-/-}$ spermatocytes show a disturbed distribution of nuclear envelope components

Given that we had observed that SUN1, as an INM protein, was polarized at the nuclear envelope in *Cdk2*$^{-/-}$ spermatocytes, we then explored whether the structure of the nuclear lamina was similarly impaired. To verify this, we performed double-immunolabeling experiments of SYCP3 with LAP2, another INM integral protein, or lamin C2, a meiosis-specific isoform of lamin A that appears at the docking sites for meiotic telomeres in the nuclear envelope (Alsheimer and Benavente, 1996; Alsheimer et al., 1999). In wild-type prophase I spermatocytes, LAP2 always appeared to be homogeneously distributed at the nuclear envelope (supplementary material Fig. S2A–F), whereas in *Cdk2*$^{-/-}$ prophase I spermatocytes we never observed LAP2 labeling at the nuclear envelope (supplementary material Fig. S2G–L). Nevertheless, in *Cdk2*$^{-/-}$ individuals, LAP2 was able to locate to the nuclear envelope in testicular somatic cells (supplementary material Fig. S2M–P), which are frequently found in squashed preparations of seminiferous tubules. Lamin C2 showed a rather homogeneous distribution at the nuclear envelope of wild-type spermatocytes during leptotene and zygotene (Fig. 6A–D), but it

Journal of Cell Science (2015) 128, 88–99 doi:10.1242/jcs.154922

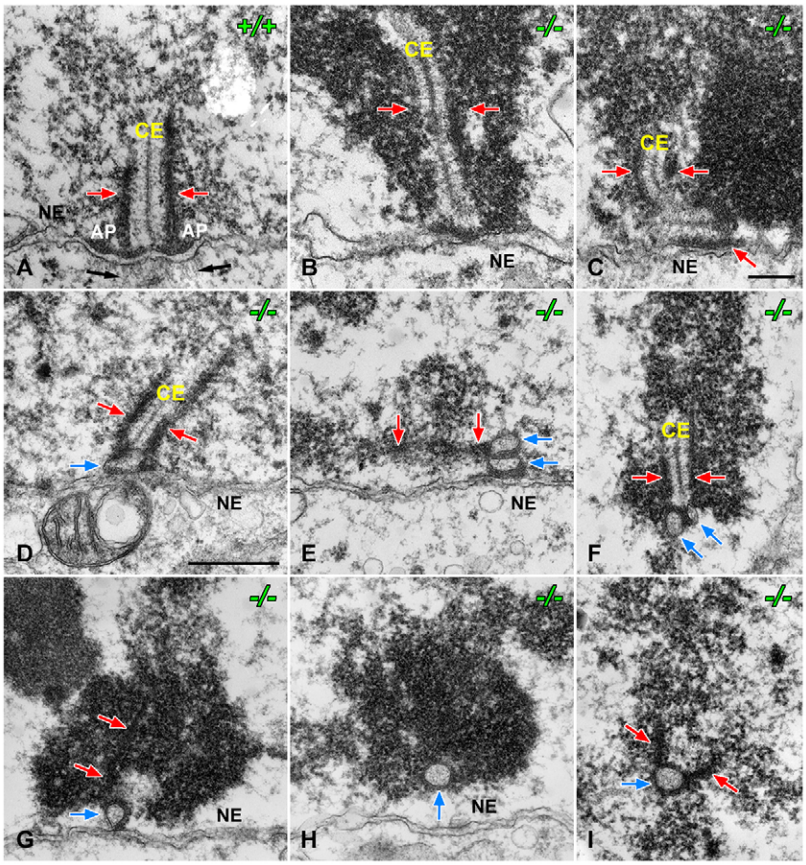

Fig. 3. Internal telomeres are associated with membrane vesicles in *Cdk2*$^{-/-}$ spermatocytes. (A–I) Electron micrographs showing telomere attachments in wild-type (+/+) pachytene nuclei (A) and in pachytene-like (−/−) mutant nuclei (B–I). (A) End of a synaptonemal complex attached to the nuclear envelope (NE) showing the central element (CE), the two lateral elements (red arrows) and their association to the INM through the attachment plates (AP). Thin fibrils attaching to the cytoplasmic side of the nuclear envelope are indicated (black arrows). (B–I) In mutant spermatocytes some telomere regions appear rather normal (B) whereas in other cases one of the lateral elements (red arrows) interacts laterally with the INM (C). Some other telomere regions appear to be associated with one or two membrane vesicles (blue arrows) either associated to the INM (D,E,G) or lying at the nuclear interior (F,H,I). Scale bars: 200 nm (A–C); 500 nm (D–I).

showed a patchy distribution in pachytene (Fig. 6E,F; see also Alsheimer et al., 1999). Surprisingly, in all *Cdk2*$^{-/-}$ prophase I spermatocytes lamin C2 appeared to be polarized showing a cap-shaped labeling at the nuclear envelope (Fig. 6G–L). Given that this labeling is similar to that found for SUN1 in mutant spermatocytes, we co-detected lamin C2 and SUN1 to assess whether these proteins colocalized at the nuclear envelope cap. Our observations demonstrated that indeed both proteins colocalized at the aberrant nuclear envelope cap in mutant spermatocytes (Fig. 6M–P). Interestingly, some lamin C2 foci were detected at the nuclear interior, however, these foci never colocalized with internal SUN1 foci (Fig. 6N–P). These results demonstrate that, in the absence of CDK2, the distribution of SUN1 at the INM and the structure of the nuclear lamina are severely disturbed, with a complete lack of LAP2.

Taking into account the drastic alterations in the distribution of the nuclear envelope proteins SUN1, KASH5, LAP2 and lamin C2 in *Cdk2*$^{-/-}$ spermatocytes, we also explored whether the distribution of nuclear pore complexes (NPCs) was also affected. For this purpose we performed a double-immunolabeling of SYCP3 and RanGAP1, a Ran GTPase-activating protein that localizes at the cytoplasmic filaments of NPCs (Mahajan et al., 1997), in both wild-type and *Cdk2*$^{-/-}$ prophase I spermatocytes. We observed that RanGAP1 was distributed as discontinuous patches along the nuclear envelope in wild-type prophase I spermatocytes. Accordingly, the projections of equatorial focal planes revealed a discontinuous ring surrounding the nuclei of these spermatocytes (supplementary material Fig. S3A–F). Likewise, a homogeneous patchy distribution of NPCs was observed in *Cdk2*$^{-/-}$ prophase I spermatocytes (supplementary material Fig. S3G–L). Thus, the absence of CDK2 does not affect the distribution of NPCs.

Telomere tethering to the nuclear envelope is altered in *Cdk2*$^{-/-}$ spermatocytes

The abnormal cap-shaped distribution of several nuclear envelope components in *Cdk2*$^{-/-}$ spermatocytes prompted us to investigate telomere dynamics at the nuclear envelope in these individuals. For this purpose, we determined the distribution and behavior of telomeres in both wild-type and *Cdk2*$^{-/-}$ spermatocytes during early prophase I stages by a double-immunolabeling of the telomeric protein TRF1 and SYCP3 (Fig. 7). In wild-type spermatocytes, telomeric TRF1 signals were discernible at the ends of the developing axial elements, as revealed by the anti-SYCP3 antibody during leptotene (Fig. 7A). The *z*-projections of all focal planes throughout these nuclei showed a homogeneous nuclear distribution of telomeres. Progressively, most telomere signals were polarized at a discrete nuclear region during zygotene denoting a bouquet-like arrangement (Fig. 7C). In pachytene spermatocytes, telomeres redistributed along the nuclear envelope and the bouquet-like arrangement was disorganized (Fig. 7E). In *Cdk2*$^{-/-}$ spermatocytes, TRF1 signals appeared to be dispersed at the nuclear envelope and they never presented a polarized distribution (Fig. 7G,I,K), and thus a bouquet-like arrangement was never observed in zygotene nuclei (Fig. 7I). This observation corroborates our previous proposal that in *Cdk2*$^{-/-}$ spermatocytes the presence of telomeres that did not attach to the nuclear envelope might

Journal of Cell Science (2015) 128, 88–99 doi:10.1242/jcs.154922

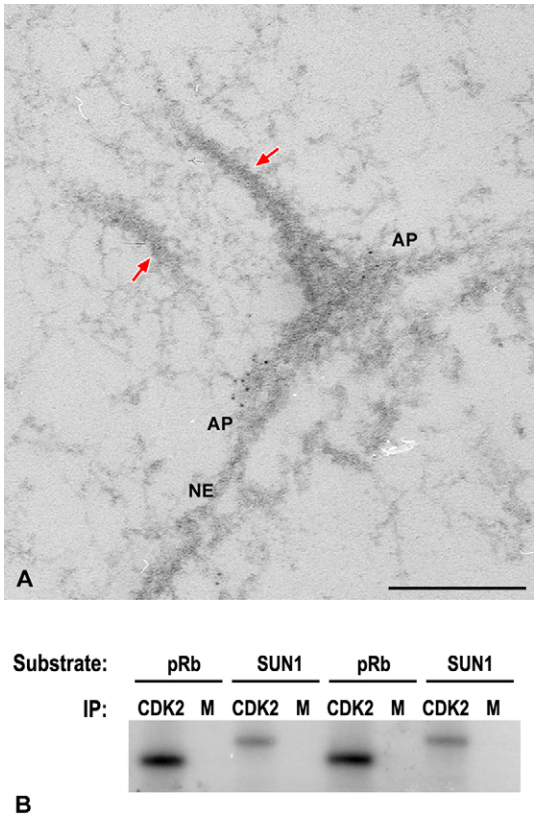

Fig. 4. CDK2 locates at the attachment plates and phosphorylates SUN1 *in vitro*. (A) Immunogold EM examination of CDK2 in wild-type (+/+) mouse pachytene spermatocytes. CDK2 locates at the attachment plates (AP) of the lateral elements (red arrows) that are connected with the INM of the nuclear envelope (NE). Scale bar: 200 nm. (B) *In vitro* kinase assay. Kinase activity associated with CDK2 immunoprecipitates obtained from 8-week-old wild-type testis extracts. Recombinant SUN1 (amino acids 1–243) together with the canonical CDK substrate pRb (amino acids 773–928) were used in parallel. Results from two independent experiments are shown. M, mock immunoprecipitate.

prompt the absence of bouquet formation, which ultimately leads to the extensive non-homologous pairing found (Viera et al., 2009).

Taking into account our previous observation of internal telomeres in *Cdk2*$^{-/-}$ spermatocytes (Viera et al., 2009) and the presence of SUN1 signals at internal telomeres associated with membrane vesicles, we next investigated the origin of the failures in telomere attachment to the nuclear envelope. To determine whether the internal telomeres found in *Cdk2*$^{-/-}$ pachytene-like spermatocytes arise by either their detachment from the nuclear envelope, tearing SUN1-containing membrane vesicles, or by their inability to attach to the nuclear envelope during preceding meiotic stages, we analyzed early prophase I stages in wild-type and *Cdk2*$^{-/-}$ spermatocytes. To address this, we estimated the location of telomeres (either peripheral or internal) in ten nuclei of each prophase I stage in two different individuals for each genotype (wild-type and *Cdk2*$^{-/-}$) after the immunostaining of TRF1 and SYCP3. The analyses of partial projections corresponding to the equatorial regions of wild-type prophase I spermatocytes demonstrated that 1.59% of the TRF1 telomere signals were present at the nuclear interior in leptotene nuclei (Fig. 7A,B; Fig. 2B). These internal telomeric signals were no longer observed in wild-type zygotene and pachytene nuclei (Fig. 7C–F; Fig. 2B). By contrast, in *Cdk2*$^{-/-}$ spermatocytes a high percentage of internal telomeric signals were always observed in leptotene (36.72%), zygotene (48.48%) and pachytene-like (50.52%) spermatocyte nuclei, respectively (Fig. 7G–L; Fig. 2B).

We also wondered whether the internal TRF1 signals that we observed in *Cdk2*$^{-/-}$ spermatocytes corresponded to proximal telomeres (located at the chromosome centromeric end) or distal telomeres (located at the non-centromeric end), given that mouse chromosomes are telocentric. To examine this, we performed both a double-immunolabeling of centromeres and SYCP3 (Fig. 8), and a triple detection of telomeres, centromeres, and SYCP3 (supplementary material Fig. S4). Our results showed that in wild-type spermatocytes the centromeres were located at the nuclear periphery from leptotene up to pachytene (Fig. 8A–F; supplementary material Fig. S4A–D). However, in *Cdk2*$^{-/-}$ spermatocytes the centromere signals were found, not only at the nuclear periphery, but also at the nuclear interior in all prophase I stages (Fig. 8G–L; supplementary material Fig. S4E–P). The simultaneous labeling of centromeres and telomeres showed that in mutant spermatocytes both the proximal telomeres, with TRF1 and ACA signals, and the distal telomeres, only with TRF1 signals, were likewise present at the nuclear interior at all prophase I stages (supplementary material Fig. S4E–P). Taken together, our results indicate that in the absence of CDK2 some telomeres, independently of their proximal or distal chromosomal position, are unable to attach to the nuclear envelope during leptotene and remain at the nuclear interior in later prophase I stages, and a bouquet-like arrangement is not reached. Moreover, the presence of intranuclear telomeres associated with nuclear-envelope-derived membrane vesicles (Fig. 3D–I) and with SUN1 (Fig. 1P) indicates that some attached telomeres have detached from the nuclear envelope in the course of meiotic prophase I.

DISCUSSION

CDK2 regulates SUN1 distribution at the meiotic nuclear envelope

SUN1 is a member of the SUN domain protein family that is known to participate in the attachment of meiotic telomeres to the INM of the nuclear envelope (Alsheimer, 2009; Hiraoka and Dernburg, 2009; Koszul and Kleckner, 2009; Kracklauer et al., 2013). In wild-type mice, SUN1 is enriched at discrete nuclear envelope docking sites that physically connect the telomeres of meiotic chromosomes to the nuclear envelope (Ding et al., 2007). By contrast, we found that in the *Cdk2*$^{-/-}$ background most SUN1 arranges into a cap-like structure polarized at the nuclear envelope region facing the centrosome. This result therefore indicates that CDK2 is not essential for the association of SUN1 to the INM. Interestingly, we have additionally observed that the SUN1 cap at the nuclear envelope is detected in all prophase I stages in these mutant spermatocytes. This finding suggests that SUN1 is able to load to the INM, but that it cannot disperse to discrete regions in the absence of CDK2. Accordingly, we suggest that during mammalian meiosis CDK2 regulates the lateral diffusion of SUN1 along the nuclear envelope. Our data demonstrate at the ultrastructural level that CDK2 locates at the attachment plates of the synaptonemal complex, where SUN1 participates in telomere anchoring to the nuclear envelope (Ding et al., 2007), and that mouse testis CDK2 phosphorylates SUN1 *in vitro*. Thus, the cytological and biochemical data together indicate that the phosphorylation of the nucleoplasmic domain of

Journal of Cell Science (2015) 128, 88–99 doi:10.1242/jcs.154922

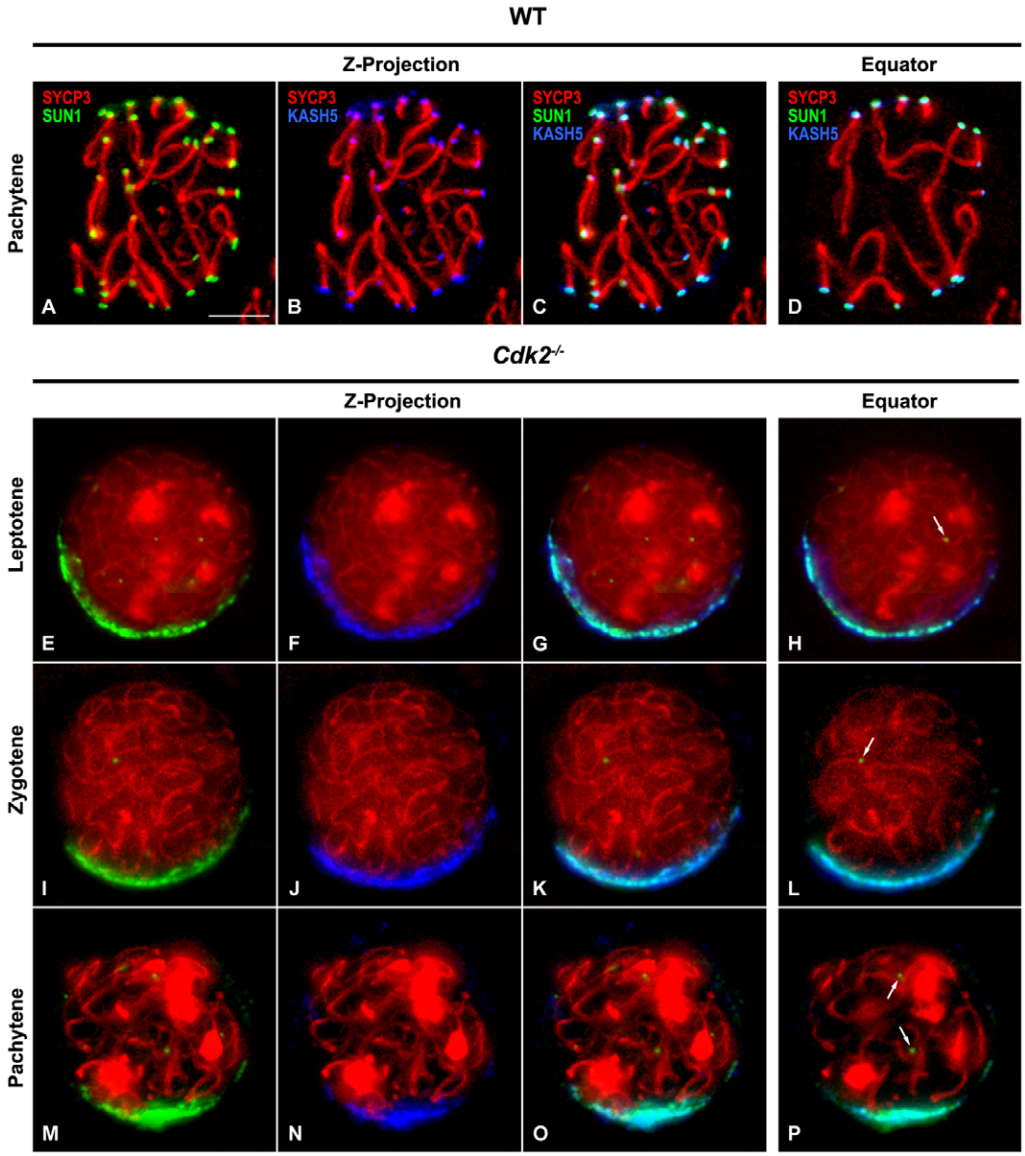

Fig. 5. SUN1 and KASH distribution in *Cdk2*$^{-/-}$ spermatocytes. Triple-immunolabeling of SUN1 (green), KASH5 (blue) and SYCP3 (red) on pachytene wild-type (WT) (A–D) and prophase I *Cdk2*$^{-/-}$ (E–P) squashed spermatocytes. The first three columns correspond to the *z*-projection of all the focal planes throughout a nucleus. The fourth column presents the partial *z*-projections of 15 focal planes throughout the equatorial region of the same nuclei. (A–D) WT pachytene nucleus. SUN1 and KASH5 are positioned at discrete sites of the nuclear envelope, coincident with the attachment plates of the synaptonemal complex, and thus they are detected at the nuclear periphery. (E–P) *Cdk2*$^{-/-}$ prophase I spermatocytes. In all prophase I stages, SUN1 and KASH5 are invariably distributed as a continuous and polarized cap-like arrangement at the nuclear envelope. Although SUN1 also appears as small foci (arrows) at the nuclear interior, KASH5 is not detectable at these foci. Scale bar: 5 µm.

SUN1 by CDK2 could be an important step in regulating SUN1 distribution along the nuclear envelope in spermatocytes. Interestingly, two recent studies have reported that the kinases CHK-2 and PLK-2, by phosphorylating the nucleoplasmic domain of SUN-1 during *C. elegans* meiosis, do not regulate telomere attachment, but the telomere movement along the nuclear envelope and homolog pairing (Labella et al., 2011; Penkner et al., 2009; Sato et al., 2009). Similarly, in mouse meiosis CDK2 could be responsible for phosphorylating SUN1 to direct the lateral diffusion of these LINC complexes and then move telomeres along the nuclear envelope. Accordingly, in *Cdk2*$^{-/-}$ individuals the KASH domain protein that interacts with SUN1 to form meiotic LINC complexes, namely KASH5, presents an altered distribution, which is coincident with SUN1 at the nuclear envelope. Thus, our data indicate that CDK2 is dispensable for the interaction of SUN1 and KASH5 at LINC complexes, and support recent reports stating that in male mouse meiosis the localization of KASH5 is to some extent dependent on SUN1 (Horn et al., 2013; Link et al., 2014; Morimoto et al., 2012). Indeed, it has been demonstrated that in mouse meiosis SUN1–KASH5 complexes are necessary to promote chromosome pairing, and the proper progression of prophase I, by generating a nucleocytoplasmic bridge connecting telomeres to microtubules (Horn et al., 2013; Link et al., 2014; Morimoto et al., 2012). Consequently, the defective distribution of LINC complexes along the nuclear envelope of *Cdk2*$^{-/-}$ spermatocytes results in a lack of telomere and chromosome movements, which would promote failures in homologue pairing, accounting for the defective synapsis previously reported in these individuals (Viera et al., 2009). Therefore, we propose that CDK2 is needed to transfer the microtubule-dependent cytoplasmic forces to move telomeres along the meiotic nuclear envelope.

CDK2 regulates the structure of the prophase I nuclear envelope

Our results show that in the absence of CDK2 the lamin-associated protein LAP2 is not detected at the nuclear envelope during prophase I. By contrast, in *Cdk2*$^{-/-}$ mutants LAP2 is still detected at the nuclear envelope of somatic testicular cells, as in rat testis (Schmitt et al., 2007). These results thus suggest that CDK2 might be involved in the regulatory mechanism that allows the association of LAP2 to the INM during meiosis.

Journal of Cell Science (2015) 128, 88–99 doi:10.1242/jcs.154922

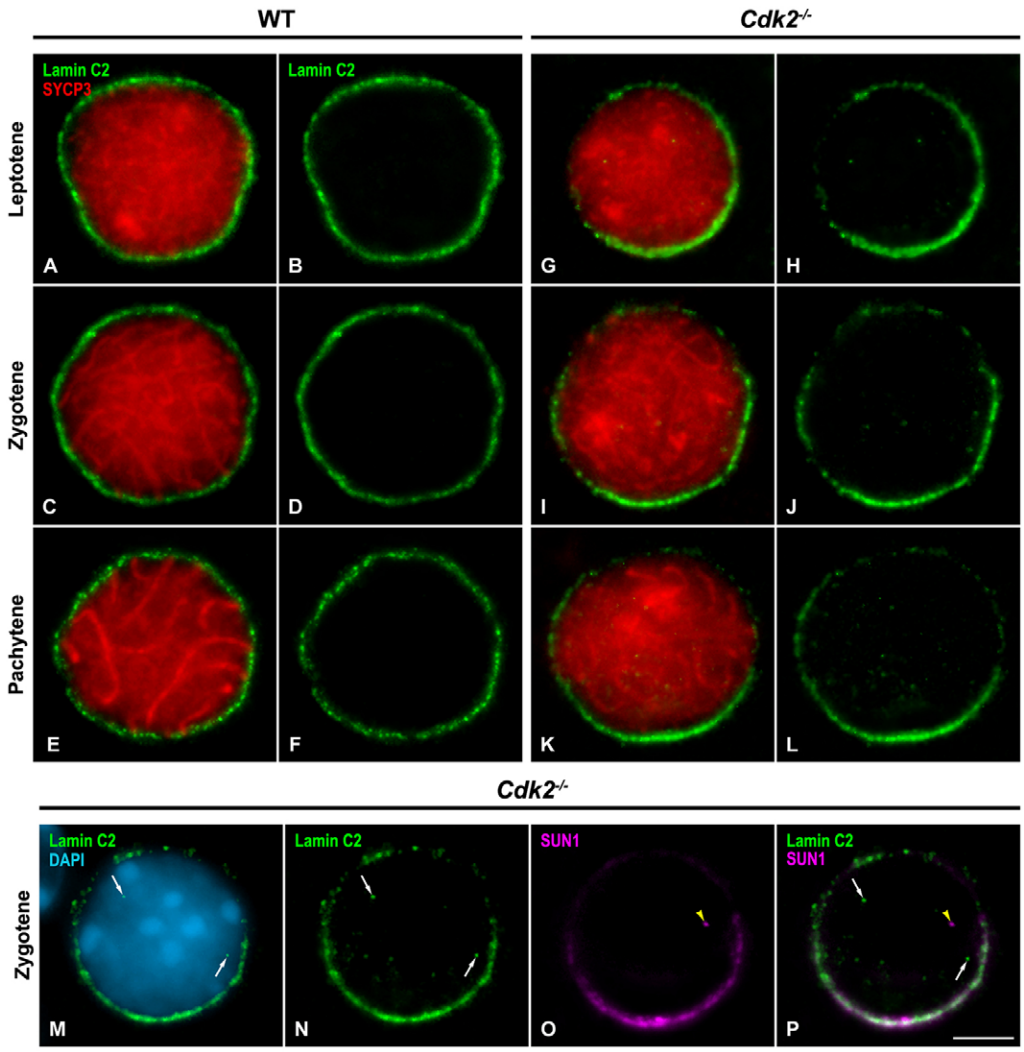

Fig. 6. Lamin C2 distribution is disturbed in *Cdk2*$^{-/-}$ spermatocytes. (A–L) Double-immunolabeling of lamin C2 (green) and SYCP3 (red) on squashed wild-type (WT) (A–F) and *Cdk2*$^{-/-}$ (G–L) prophase I spermatocytes. The images correspond to the partial *z*-projections of 15 focal planes throughout the equatorial region of each spermatocyte. (A–F) WT prophase I nuclei. Lamin C2 is uniformly distributed at the nuclear envelope. (G–L) *Cdk2*$^{-/-}$ prophase I nuclei. Lamin C2 appears to be polarized, showing a cap-shaped labeling at the nuclear envelope. (M–P) Equatorial *z*-projection of a squashed *Cdk2*$^{-/-}$ zygotene nucleus double-immunolabelled for lamin C2 (green) and SUN1 (purple) and chromatin counterstaining with DAPI (blue). Lamin C2 and SUN1 colocalize showing a cap-like distribution at the nuclear envelope. Some internal lamin C2 spots (white arrows) are observed but they do not colocalize with SUN1 internal focus (yellow arrowhead). Scale bar: 5 µm.

Consequently, it should be addressed in further investigations whether CDK2 participates in the regulation of the phosphorylation pathway of LAP2 during mammalian meiosis.

We have also found that in *Cdk2*$^{-/-}$ spermatocytes the distribution of lamin C2 at the nuclear envelope is disturbed. Indeed, lamin C2 unusually shows a cap-like distribution facing the centrosome. Given that in mammals the meiotic A-type lamin, lamin C2, is exclusively expressed during prophase I (Alsheimer and Benavente, 1996; Furukawa et al., 1994; Smith and Benavente, 1992), it can be assumed that CDK2 is involved in the assembly of the meiosis-specific nuclear lamina. In the *Cdk2*$^{-/-}$ background, the distribution of lamin C2 at the nuclear envelope during meiosis is surprisingly coincident with that observed for SUN1. SUN1 and its paralog SUN2 are present at the INM of the nuclear envelope in both somatic and germ cells, and they are able to interact with A-type lamins directly through their nucleoplasmic domain (Alsheimer, 2009; Gerace and Huber, 2012; Tzur et al., 2006). During mouse meiosis, SUN1, SUN2 and lamin C2 appear to be enriched at the attachment sites of telomeres to the nuclear envelope (Alsheimer et al., 1999; Alsheimer et al., 2000; Ding et al., 2007; Schmitt et al., 2007). Hypothetically, two possible pathways can determine the altered distribution of SUN1 and lamin C2 in *Cdk2*$^{-/-}$ spermatocytes. One possibility is that CDK2 regulates the localization of SUN1 and lamin C2 in an independent manner, and that its ablation alters the distribution of both proteins individually. Alternatively, CDK2 might participate in a pathway that regulates only one of these proteins, either SUN1 or lamin C2, one of which determines the dynamics of the other. In this sense, it has been recently demonstrated, in somatic cells, that the interaction of SUN1 with lamin A is disrupted after the phosphorylation of SUN1 by CDK1 or PLK1 (Patel et al., 2014). However, previous reports have demonstrated that mutant mice lacking SUN1 do not present an altered organization of the lamin-B-based nuclear lamina during meiosis (Ding et al., 2007), and conversely, the absence of lamin C2 does not promote a modification of SUN1 or SUN2 distribution at telomeres (Link et al., 2013; Schmitt et al., 2007). Indeed, despite the fact that it has been demonstrated that in somatic cells SUN1 presents an extremely strong interaction with A-type lamins, SUN1 localization at the nuclear envelope is independent of lamin A (Crisp et al., 2006). Moreover, in *Cdk2*$^{-/-}$ spermatocytes all the internal SUN1 foci were associated with internal telomeres, whereas the internal lamin C2 signals were never located at internal telomeres or close to internal SUN1 foci. Taking into account our data, and previous results, it can be assumed that the localization of SUN1 and lamin C2 at meiotic telomere attachment sites is independent from each other. However, we suggest that CDK2-mediated phosphorylation

Journal of Cell Science (2015) 128, 88–99 doi:10.1242/jcs.154922

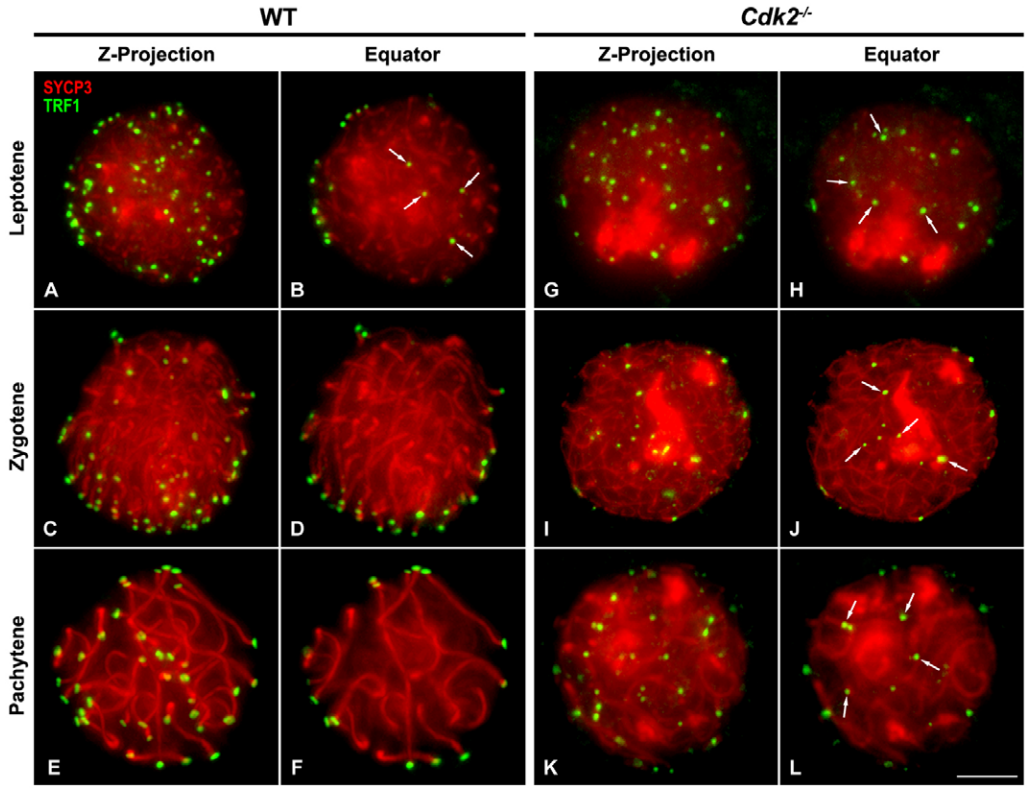

Fig. 7. Telomeres do not attach accurately to the nuclear envelope in *Cdk2*$^{-/-}$ spermatocytes. Double-immunolabeling of TRF1 (green) and SYCP3 (red) on squashed wild-type (WT) (A–F) and *Cdk2*$^{-/-}$ (G–L) prophase I spermatocytes. The first and third columns correspond to *z*-projections of all focal planes throughout a nucleus. The second and fourth columns show the partial *z*-projections of 15 focal planes throughout the equatorial region of the same nuclei. (A,B) WT leptotene nucleus. Some telomeric TRF1 signals (arrows) are evident at the nuclear interior. (C–F) WT zygotene and pachytene nuclei. No internal TRF1 signals are observed. Note the bouquet-like arrangement of most telomeres associated to the nuclear envelope in the zygotene nucleus, and the telomere signals at the synaptonemal complex ends in pachytene. (G–L) *Cdk2*$^{-/-}$ prophase I nuclei. Internal TRF1 signals (arrows) are evident in all prophase I nuclei. The bouquet-like arrangement of telomeres is not observed in zygotene nuclei. Scale bar: 5 μm.

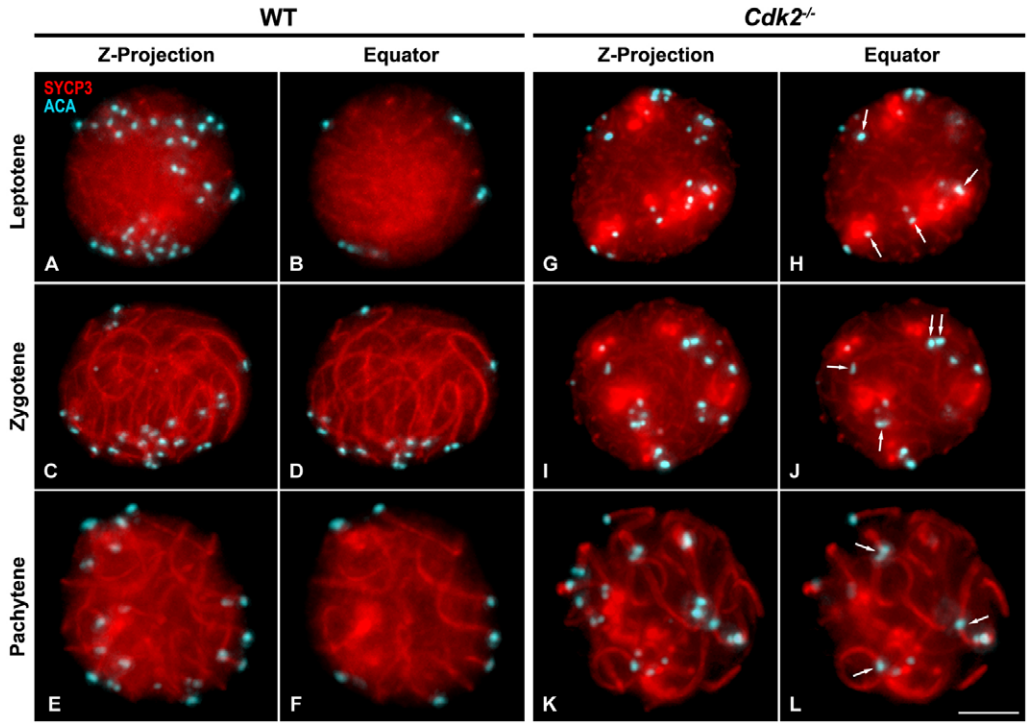

Fig. 8. Centromere distribution is disturbed in *Cdk2*$^{-/-}$ spermatocytes. Double-immunolabeling of centromeres (ACA, blue) and SYCP3 (red) on squashed wild-type (WT) (A–F) and *Cdk2*$^{-/-}$ (G–L) prophase I spermatocytes. The first and third columns correspond to the *z*-projection of all the focal planes throughout a WT and *Cdk2*$^{-/-}$ spermatocyte, respectively. The second and fourth columns present the partial *z*-projections of 15 focal planes throughout the equatorial region of the same nuclei. (A–F) WT leptotene, zygotene and pachytene nuclei. Centromere signals at one of the ends of axial and lateral elements are located at the nuclear periphery from leptotene up to pachytene. Note the bouquet-like arrangement of centromeres, indirectly labeling the proximal chromosome ends, in the zygotene nucleus. (G–L) *Cdk2*$^{-/}$ prophase I nuclei. Some centromere signals (arrows), representing proximal telomere ends, lie at the nuclear interior from leptotene up to the pachytene-like stage. Scale bar: 5 μm.

might specifically promote the positioning of lamin C2 at the nuclear envelope, and/or its redistribution to the telomere-docking sites, as occurs for SUN1. The bulk of our results therefore demonstrate that the ablation of CDK2 causes a severe disruption in the structure of the meiotic nuclear envelope in mouse spermatocytes. Thus, we propose CDK2 as an essential kinase, the first one described in mammals, which regulates the assembly and dynamics of the nuclear envelope during meiotic prophase I.

CDK2 mediates meiotic telomere attachment and dynamics

Meiotic telomere attachment to the nuclear envelope and their further clustering at a discrete region, which ensures the bouquet-like arrangement of chromosomes, represents a shared feature among a variety of species to facilitate the proper achievement of homology search, recombination and synapsis (Koszul and Kleckner, 2009; Scherthan, 2007; Zickler and Kleckner, 1998). In this sense, our data indicate that the absence of CDK2 inhibits the formation of the bouquet-like arrangement in spermatocytes, which could account for the defects in the processes of homolog pairing, recombination and synapsis previously reported (Viera et al., 2009). Surprisingly, in fifth and sixth generation telomerase-deficient mice (*Terc*$^{-/-}$), in which telomeric DNA repeats shortened down to below detection levels (Franco et al., 2002), and in shelterin protein *Rap1*-knockout mice (Scherthan et al., 2011), telomeres are still able to properly attach to the nuclear envelope. In striking contrast, in mice defective for SUN1, telomeres are frequently found at the nuclear interior during prophase I, revealing the importance of non-telomeric proteins for meiotic telomere attachment (Ding et al., 2007; Link et al., 2014). Given that CDK2 locates at late recombination nodules and at telomeres during mouse prophase I (Ashley et al., 2001; Viera et al., 2009), it has been proposed that CDK2 participates in the organization of the Holliday junction intermediates and telomeric DNA t-loops, which share structural similarities (Ashley et al., 2001). Indeed, in *Cdk2*$^{-/-}$ spermatocytes late recombination nodules were never found (Viera et al., 2009), but defects in the tethering of meiotic telomeres to the nuclear envelope, ring chromosomes and chromosome end-to-end fusions have been reported, indicating a putative participation of CDK2 in telomere capping (Viera et al., 2009). In the present study, we demonstrate by electron microscopy the presence of CDK2 at the attachment plates of the synaptonemal complex, suggesting a possible participation of CDK2 in meiotic telomere attachment. Moreover, we found that in *Cdk2*$^{-/-}$ spermatocytes a high percentage of telomeres were lying at the nuclear interior in leptotene (37.72%), and that this percentage was increased in zygotene and pachytene-like spermatocytes (48.48% and 50.52%, respectively). Thus, we speculate that at least two non-mutually exclusive events might lead to the appearance of internal telomeres in the absence of CDK2. The first one implies that some telomeres are unable to attach to the nuclear envelope during leptotene, and therefore remain in the nucleoplasm in further prophase I stages, as described in knockout mouse models for *Smc1b*$^{-/-}$ and *Sun1*$^{-/-}$ mice (Adelfalk et al., 2009; Ding et al., 2007). An alternative, and more fascinating possibility, consists in the detachment of telomeres that were initially attached to the nuclear envelope, accounting for the increase in the rate of non-attached telomeres in zygotene and pachytene-like nuclei. It is widely accepted that several chromosome functions can be governed by mechanical stresses transmitted along the chromosome axes (Kleckner et al., 2004). In this regard, physical tensions generated by the ongoing heterologous synapsis in *Cdk2*$^{-/-}$ spermatocytes might spread along chromosomes up to the telomeres, forcing their detachment from the nuclear envelope. This possibility is strongly supported by the presence of SUN1 and membrane vesicles, probably peeled off the INM of the nuclear envelope, at the internal telomeres found in *Cdk2*$^{-/-}$ spermatocytes. Indeed, the fact that the number of internal SUN1 foci increased during prophase I progression, as synapsis proceeds, also reinforces this proposal. In this context, it has been shown that SUN1 persists at the axial and lateral elements ends on spread spermatocytes after a harsh preparative technique that disrupts the nuclear envelope (Adelfalk et al., 2009; Ding et al., 2007; Morimoto et al., 2012). Accordingly, SUN1 at detached telomeres in *Cdk2*$^{-/-}$ spermatocytes could bring with them vesicles derived from the nuclear envelope. Based on our data, we propose that either or both events would finally disrupt chromosome movements, and the formation of a bouquet-like arrangement, and explain the meiotic defects previously found in *Cdk2*$^{-/-}$ spermatocytes (Viera et al., 2009). However, a detailed analysis of meiotic telomere attachment to the nuclear envelope in other mouse models displaying non-homologous synapsis would clarify whether this is a particular phenotype of the *Cdk2*$^{-/-}$ background, or by contrast if it represents a general consequence of non-homologous synapsis.

In summary, our results point to CDK2 as a key factor governing the assembly, structure and dynamics of the meiotic nuclear envelope in mice. Moreover, CDK2 is essential for the accurate attachment of meiotic telomeres to the nuclear envelope and chromosome movements in prophase I.

MATERIALS AND METHODS

Ethics statement

Animals were kept under SPF barrier conditions at the CNIO animal facility. Animals were handled according to relevant regulatory standards and experiments were approved by the Universidad Autónoma de Madrid Ethics Committee.

Immunofluorescence microscopy

Adult male C57BL/6 mice (wild-type) and adult *Cdk2*$^{-/-}$ mice (Ortega et al., 2003) were used for this study. Testes were removed, detunicated and seminiferous tubules then processed for squashing as previously described (Page et al., 1998; Parra et al., 2002). After fixation, the squashed spermatocyte preparations were rinsed three times for 5 min in PBS, and incubated overnight at 4℃ with the corresponding primary antibodies diluted in PBS. To detect SYCP3, we employed either a mouse monoclonal antibody (Abcam, ab-12452) or a rabbit polyclonal serum A1 (a gift from Christa Heyting, Wageningen University, Wageningen, The Netherlands) at a 1:100 dilution. To detect SUN1, we used an affinity-purified guinea pig polyclonal antibody raised against a peptide corresponding to amino acids 428–722 of mouse SUN1 (Adelfalk et al., 2009) at a 1:30 dilution. The centrosome was revealed by using a rabbit polyclonal anti-pericentrin antibody generated against the residues 100–600 of mouse pericentrin 1 (Abcam, ab-4448) at a 1:10 dilution. TRF1 was detected with a rabbit polyclonal serum (Alpha Diagnostic International, TRF 12-S), raised against mouse TRF1, at a 1:50 dilution. KASH5 was detected with a rabbit polyclonal antibody generated against the amino acid residues 242–688 of mouse KASH5 (Link et al., 2014), following previous reports (Morimoto et al., 2012), at a 1:30 dilution. The mouse monoclonal 13d4 antibody (Alsheimer et al., 1998) was used to reveal LAP-2 at a 1:10 dilution. To detect lamin C2 we employed either a rabbit polyclonal antibody raised against the amino acids 231–340 of human lamin A (Santa Cruz Biotechnology, sc-20681) that also recognizes lamin C2 in mouse spermatocytes (Jahn et al., 2010) or an affinity-purified rabbit polyclonal antibody generated against mouse A-type lamins (Jahn et al., 2010) at a 1:10 dilution. Centromeres were revealed with a human anti-centromere antibody (ACA) (Antibodies Incorporated, 15-235) at a 1:50 dilution. A goat anti-RanGAP1 antibody

(Pichler et al., 2002) was employed to detect RanGAP1 (a gift from Frauke Melchior, Zentrum für Molekulare Biologie der Universität Heidelberg, Heidelberg, Germany) at a 1:10 dilution.

Following three washes in PBS, the slides were incubated for 30 min at room temperature with secondary antibodies diluted in PBS. The appropriated combinations of the following secondary antibodies were employed for simultaneous double- or triple-immunolabeling: a fluorescein isothiocyanate (FITC)-conjugated donkey anti-mouse IgG antibody (Jackson) at a 1:150 dilution, a Texas-Red-conjugated donkey anti-mouse ML IgG antibody (Jackson) at a 1:150 dilution, a FITC-conjugated donkey anti-rabbit ML IgG antibody (Jackson) at a 1:150 dilution, a Texas-Red-conjugated donkey anti-rabbit ML IgG antibody (Jackson) at a 1:150 dilution, a FITC-conjugated goat anti-human IgG antibody (Jackson) at a 1:150 dilution, a FITC-conjugated donkey anti-guinea-pig ML IgG antibody (Jackson) at a 1:150 dilution, a Texas-Red-conjugated donkey anti-guinea-pig ML IgG antibody (Jackson) at a 1:150 dilution, and a FITC-conjugated donkey anti-goat ML IgG antibody (Jackson) at a 1:40 dilution. Subsequently, slides were rinsed in PBS, and, in double-immunolabeling experiments, counterstained for 3 min with 5 µg/ml DAPI. After a final rinse in PBS, the slides were mounted in Vectashield (Vector Laboratories) and sealed with nail varnish.

Observations were performed using an Olympus BX61 microscope equipped with a motorized *z*-axis and epifluorescence optics. Image stacks comprising 65 focal planes across the entire spermatocyte nuclei were captured with an Olympus DP71 digital camera controlled by the analySIS software (Soft Imaging System). The complete image stacks were used to analyze the relative distribution of the proteins at a given entire nucleus and for estimating the percentages that are presented at the results section. For a better presentation of the results in the figures, stacks were subsequently processed for obtaining complete *z*-projections (65 focal planes) or partial *z*-projections (15 focal planes along the equator of the nucleus) using the public domain software ImageJ (National Institutes of Health). Final images were processed with Adobe Photoshop 7.0 software.

Transmission electron microscopy and immunogold electron microscopy

Electron microscopy was performed according to standard procedures (Schramm et al., 2011). Testes of wild-type and *Cdk2*$^{-/-}$ mice were fixed for 2 h at 4℃ in 2.5% glutaraldehyde in 50 mM cacodylate buffer. Then, samples were washed in cacodylate buffer and postfixed in 1% osmium tetroxide for 1 h at 4℃. After rinsing several times in water, samples were dehydrated in an ethanol series and embedded in Epon. Ultrathin sections were stained with uranyl acetate and lead citrate. Observations were performed in a Zeiss EM-10 transmission electron microscope operated at 80 kV. For immunoelectron microscopy we proceeded as previously described (Schramm et al., 2011). Briefly, 10-µm mouse testis cryosections were fixed with acetone for 10 min at −20℃ and air dried. Incubation with a rabbit anti-CDK2 antibody (Abcam, ab-7954), at a 1:50 dilution in PBS, was carried out in a humidified chamber for 4 h at room temperature. After two rinses in PBS, sections were fixed for 10 min in 2% formaldehyde and blocked with 50 mM NH_4Cl. A goat anti-rabbit secondary antibody conjugated to 6-nm-gold particles (Dianova) was incubated overnight at 4℃ and samples were washed subsequently in PBS. Samples were fixed for 30 min in 2.5% glutaraldehyde and post-fixed in 2% osmium tetroxide. After rinsing three times with H_2O, samples were dehydrated in an ethanol series and embedded in Epon. Ultrathin sections were stained with uranyl acetate and lead citrate according to standard procedures.

In vitro kinase assay

For the *in vitro* kinase assay, we proceeded as previously reported (Martín et al., 2005). Briefly, testis lysates were prepared with the Precellys 24 tissue homogenizer (Bertin technologies) in immunoprecipitation buffer (0.5% Nonidet p-40; 50 mM Tris-HCl pH 7.5; 50 mM NaCl) supplemented with the protease inhibitor cocktail (Roche). Lysates were clarified by centrifugation and 500 µg were incubated overnight at 4℃ with 2 µg of a rabbit anti-CDK2 antibody (Santa Cruz Biotechnology, sc-163) followed by precipitation with protein-A–sepharose beads for 2 h. Immunoprecipitates were washed three times with 1 ml of immunoprecipitation buffer and three times with kinase buffer (50 mM Hepes pH 7.5; 50 mM urea; 10 mM $MgCl_2$; 5 mM $MnCl_2$; 1 mM DTT). The beads were suspended in 30 µl of kinase buffer containing 1 µg substrate; either His-tagged Sun1 (amino acids 1–243) or retinoblastoma protein (pRb) (amino acids 773–928, Upstate, 12-439); 30 µM ATP and 10 µCi of [γ-^{32}P] ATP (Perkin Elmer, 6000Ci/mmol). After incubation for 30 min at 30℃ with occasional mixing the samples were boiled with SDS/PAGE sample buffer and separated by electrophoresis. Phosphorylated proteins were visualized with a phosphoimager (Storm 820; Molecular Dynamics) after overnight exposure.

Acknowledgements

We express our sincere thanks to Christa Heyting and Frauke Melchior for providing antibodies. We also thank Miriam García and Isabel Blanco, from the Animal Facility at the CNIO, for their help with mouse maintenance, and Lorena Barreras for her technical assistance.

Competing interests

The authors declare no competing interests.

Author contributions

A.V. and J.A.S. conceived and designed the experiments. A.V., M.A., C.E.S., R.B. and J.A.S. performed the experiments. A.V., M.A. R.G., I.B., S.O., C.E.S., D.S., R.B. and J.A.S. analyzed the data. A.V. and J.A.S. wrote the paper and all authors revised the manuscript.

Funding

This work was supported by the Ministerio de Ciencia e Innovación (Spain) [grant number BFU2009-10987/BCM to A.V.] and the Ministerio de Economía y Competitividad (Spain) [grant number SAF2011-28842-C02-01 from to J.A.S.]. M.A. and R.B. are supported by grants of the Priority Program SPP 1384 'Mechanisms of genome haploidization' of the German Science Foundation (DFG) and the Graduate School 'Organogenesis' of the University of Würzburg (Germany). I.B. is supported by a predoctoral fellowship from Ministerio de Economía y Competitividad (Spain). C.E.S. is supported by a grant from the 'La Caixa'/CNIO International Ph.D. Fellowship Program sponsored by 'La Caixa' Foundation (Spain).

Supplementary material

Supplementary material available online at
http://jcs.biologists.org/lookup/suppl/doi:10.1242/jcs.154922/-/DC1

References

Adelfalk, C., Janschek, J., Revenkova, E., Blei, C., Liebe, B., Göb, E., Alsheimer, M., Benavente, R., de Boer, E., Novak, I. et al. (2009). Cohesin SMC1beta protects telomeres in meiocytes. *J. Cell Biol.* **187**, 185-199.

Alsheimer, M. (2009). The dance floor of meiosis: evolutionary conservation of nuclear envelope attachment and dynamics of meiotic telomeres. *Genome Dyn.* **5**, 81-93.

Alsheimer, M. and Benavente, R. (1996). Change of karyoskeleton during mammalian spermatogenesis: expression pattern of nuclear lamin C2 and its regulation. *Exp. Cell Res.* **228**, 181-188.

Alsheimer, M., Fecher, E. and Benavente, R. (1998). Nuclear envelope remodelling during rat spermiogenesis: distribution and expression pattern of LAP2/thymopoietins. *J. Cell Sci.* **111**, 2227-2234.

Alsheimer, M., von Glasenapp, E., Hock, R. and Benavente, R. (1999). Architecture of the nuclear periphery of rat pachytene spermatocytes: distribution of nuclear envelope proteins in relation to synaptonemal complex attachment sites. *Mol. Biol. Cell* **10**, 1235-1245.

Alsheimer, M., von Glasenapp, E., Schnolzer, M., Heid, H. and Benavente, R. (2000). Meiotic lamin C2: the unique amino-terminal hexapeptide GNAEGR is essential for nuclear envelope association. *Proc. Natl. Acad. Sci. USA* **97**, 13120-13125.

Ashley, T., Walpita, D. and de Rooij, D. G. (2001). Localization of two mammalian cyclin dependent kinases during mammalian meiosis. *J. Cell Sci.* **114**, 685-693.

Berthet, C., Aleem, E., Coppola, V., Tessarollo, L. and Kaldis, P. (2003). Cdk2 knockout mice are viable. *Curr. Biol.* **13**, 1775-1785.

Crisp, M., Liu, Q., Roux, K., Rattner, J. B., Shanahan, C., Burke, B., Stahl, P. D. and Hodzic, D. (2006). Coupling of the nucleus and cytoplasm: role of the LINC complex. *J. Cell Biol.* **172**, 41-53.

Ding, X., Xu, R., Yu, J., Xu, T., Zhuang, Y. and Han, M. (2007). SUN1 is required for telomere attachment to nuclear envelope and gametogenesis in mice. *Dev. Cell* **12**, 863-872.

Esponda, P. and Giménez-Martín, G. (1972). The attachment of the synaptonemal complex to the nuclear envelope. An ultrastructural and cytochemical analysis. *Chromosoma* **38**, 405-417.
Franco, S., Alsheimer, M., Herrera, E., Benavente, R. and Blasco, M. A. (2002). Mammalian meiotic telomeres: composition and ultrastructure in telomerase-deficient mice. *Eur. J. Cell Biol.* **81**, 335-340.
Furukawa, K., Inagaki, H. and Hotta, Y. (1994). Identification and cloning of an mRNA coding for a germ cell-specific A-type lamin in mice. *Exp. Cell Res.* **212**, 426-430.
Gerace, L. and Huber, M. D. (2012). Nuclear lamina at the crossroads of the cytoplasm and nucleus. *J. Struct. Biol.* **177**, 24-31.
Hiraoka, Y. and Dernburg, A. F. (2009). The SUN rises on meiotic chromosome dynamics. *Dev. Cell* **17**, 598-605.
Horn, H. F., Kim, D. I., Wright, G. D., Wong, E. S., Stewart, C. L., Burke, B. and Roux, K. J. (2013). A mammalian KASH domain protein coupling meiotic chromosomes to the cytoskeleton. *J. Cell Biol.* **202**, 1023-1039.
Jahn, D., Schramm, S., Benavente, R. and Alsheimer, M. (2010). Dynamic properties of meiosis-specific lamin C2 and its impact on nuclear envelope integrity. *Nucleus* **1**, 273-283.
Kleckner, N., Zickler, D., Jones, G. H., Dekker, J., Padmore, R., Henle, J. and Hutchinson, J. (2004). A mechanical basis for chromosome function. *Proc. Natl. Acad. Sci. USA* **101**, 12592-12597.
Koszul, R. and Kleckner, N. (2009). Dynamic chromosome movements during meiosis: a way to eliminate unwanted connections? *Trends Cell Biol.* **19**, 716-724.
Kracklauer, M. P., Link, J. and Alsheimer, M. (2013). LINCing the nuclear envelope to gametogenesis. *Curr. Top. Dev. Biol.* **102**, 127-157.
Labella, S., Woglar, A., Jantsch, V. and Zetka, M. (2011). Polo kinases establish links between meiotic chromosomes and cytoskeletal forces essential for homolog pairing. *Dev. Cell* **21**, 948-958.
Liebe, B., Alsheimer, M., Höög, C., Benavente, R. and Scherthan, H. (2004). Telomere attachment, meiotic chromosome condensation, pairing, and bouquet stage duration are modified in spermatocytes lacking axial elements. *Mol. Biol. Cell* **15**, 827-837.
Link, J., Jahn, D., Schmitt, J., Göb, E., Baar, J., Ortega, S., Benavente, R. and Alsheimer, M. (2013). The meiotic nuclear lamina regulates chromosome dynamics and promotes efficient homologous recombination in the mouse. *PLoS Genet.* **9**, e1003261.
Link, J., Leubner, M., Schmitt, J., Göb, E., Benavente, R., Jeang, K. T., Xu, R. and Alsheimer, M. (2014). Analysis of meiosis in SUN1 deficient mice reveals a distinct role of SUN2 in mammalian meiotic LINC complex formation and function. *PLoS Genet.* **10**, e1004099.
Mahajan, R., Delphin, C., Guan, T., Gerace, L. and Melchior, F. (1997). A small ubiquitin-related polypeptide involved in targeting RanGAP1 to nuclear pore complex protein RanBP2. *Cell* **88**, 97-107.
Martín, A., Odajima, J., Hunt, S. L., Dubus, P., Ortega, S., Malumbres, M. and Barbacid, M. (2005). Cdk2 is dispensable for cell cycle inhibition and tumor suppression mediated by p27(Kip1) and p21(Cip1). *Cancer Cell* **7**, 591-598.
Morimoto, A., Shibuya, H., Zhu, X., Kim, J., Ishiguro, K., Han, M. and Watanabe, Y. (2012). A conserved KASH domain protein associates with telomeres, SUN1, and dynactin during mammalian meiosis. *J. Cell Biol.* **198**, 165-172.
Ortega, S., Prieto, I., Odajima, J., Martín, A., Dubus, P., Sotillo, R., Barbero, J. L., Malumbres, M. and Barbacid, M. (2003). Cyclin-dependent kinase 2 is essential for meiosis but not for mitotic cell division in mice. *Nat. Genet.* **35**, 25-31.
Page, J., Suja, J. A., Santos, J. L. and Rufas, J. S. (1998). Squash procedure for protein immunolocalization in meiotic cells. *Chromosome Res.* **6**, 639-642.
Parra, M. T., Page, J., Yen, T. J., He, D., Valdeolmillos, A., Rufas, J. S. and Suja, J. A. (2002). Expression and behaviour of CENP-E at kinetochores during mouse spermatogenesis. *Chromosoma* **111**, 53-61.
Patel, J. T., Bottrill, A., Prosser, S. L., Jayaraman, S., Straatman, K., Fry, A. M. and Shackleton, S. (2014). Mitotic phosphorylation of SUN1 loosens its connection with the nuclear lamina while the LINC complex remains intact. *Nucleus* **5**, 462-473.
Penkner, A. M., Fridkin, A., Gloggnitzer, J., Baudrimont, A., Machacek, T., Woglar, A., Csaszar, E., Pasierbek, P., Ammerer, G., Gruenbaum, Y. et al. (2009). Meiotic chromosome homology search involves modifications of the nuclear envelope protein Matefin/SUN-1. *Cell* **139**, 920-933.
Pichler, A., Gast, A., Seeler, J. S., Dejean, A. and Melchior, F. (2002). The nucleoporin RanBP2 has SUMO1 E3 ligase activity. *Cell* **108**, 109-120.
Santamaría, D., Barrière, C., Cerqueira, A., Hunt, S., Tardy, C., Newton, K., Cáceres, J. F., Dubus, P., Malumbres, M. and Barbacid, M. (2007). Cdk1 is sufficient to drive the mammalian cell cycle. *Nature* **448**, 811-815.
Sato, A., Isaac, B., Phillips, C. M., Rillo, R., Carlton, P. M., Wynne, D. J., Kasad, R. A. and Dernburg, A. F. (2009). Cytoskeletal forces span the nuclear envelope to coordinate meiotic chromosome pairing and synapsis. *Cell* **139**, 907-919.
Scherthan, H. (2007). Telomere attachment and clustering during meiosis. *Cell. Mol. Life Sci.* **64**, 117-124.
Scherthan, H., Sfeir, A. and de Lange, T. (2011). Rap1-independent telomere attachment and bouquet formation in mammalian meiosis. *Chromosoma* **120**, 151-157.
Schmitt, J., Benavente, R., Hodzic, D., Höög, C., Stewart, C. L. and Alsheimer, M. (2007). Transmembrane protein Sun2 is involved in tethering mammalian meiotic telomeres to the nuclear envelope. *Proc. Natl. Acad. Sci. USA* **104**, 7426-7431.
Schramm, S., Fraune, J., Naumann, R., Hernandez-Hernandez, A., Höög, C., Cooke, H. J., Alsheimer, M. and Benavente, R. (2011). A novel mouse synaptonemal complex protein is essential for loading of central element proteins, recombination, and fertility. *PLoS Genet.* **7**, e1002088.
Smith, A. and Benavente, R. (1992). Identification of a short nuclear lamin protein selectively expressed during meiotic stages of rat spermatogenesis. *Differentiation* **52**, 55-60.
Starr, D. A. and Fridolfsson, H. N. (2010). Interactions between nuclei and the cytoskeleton are mediated by SUN-KASH nuclear-envelope bridges. *Annu. Rev. Cell Dev. Biol.* **26**, 421-444.
Tetsu, O. and McCormick, F. (2003). Proliferation of cancer cells despite CDK2 inhibition. *Cancer Cell* **3**, 233-245.
Tzur, Y. B., Wilson, K. L. and Gruenbaum, Y. (2006). SUN-domain proteins: 'Velcro' that links the nucleoskeleton to the cytoskeleton. *Nat. Rev. Mol. Cell Biol.* **7**, 782-788.
Viera, A., Rufas, J. S., Martínez, I., Barbero, J. L., Ortega, S. and Suja, J. A. (2009). CDK2 is required for proper homologous pairing, recombination and sex-body formation during male mouse meiosis. *J. Cell Sci.* **122**, 2149-2159.
Zickler, D. and Kleckner, N. (1998). The leptotene-zygotene transition of meiosis. *Annu. Rev. Genet.* **32**, 619-697.

Supplementary Information

CDK2 regulates nuclear envelope protein dynamics and telomere attachment in mouse meiotic prophase

Alberto Viera, Manfred Alsheimer, Rocío Gómez, Inés Berenguer, Sagrario Ortega, Catherine E. Symonds, David Santamaría, Ricardo Benavente, and José A. Suja

Figure S1

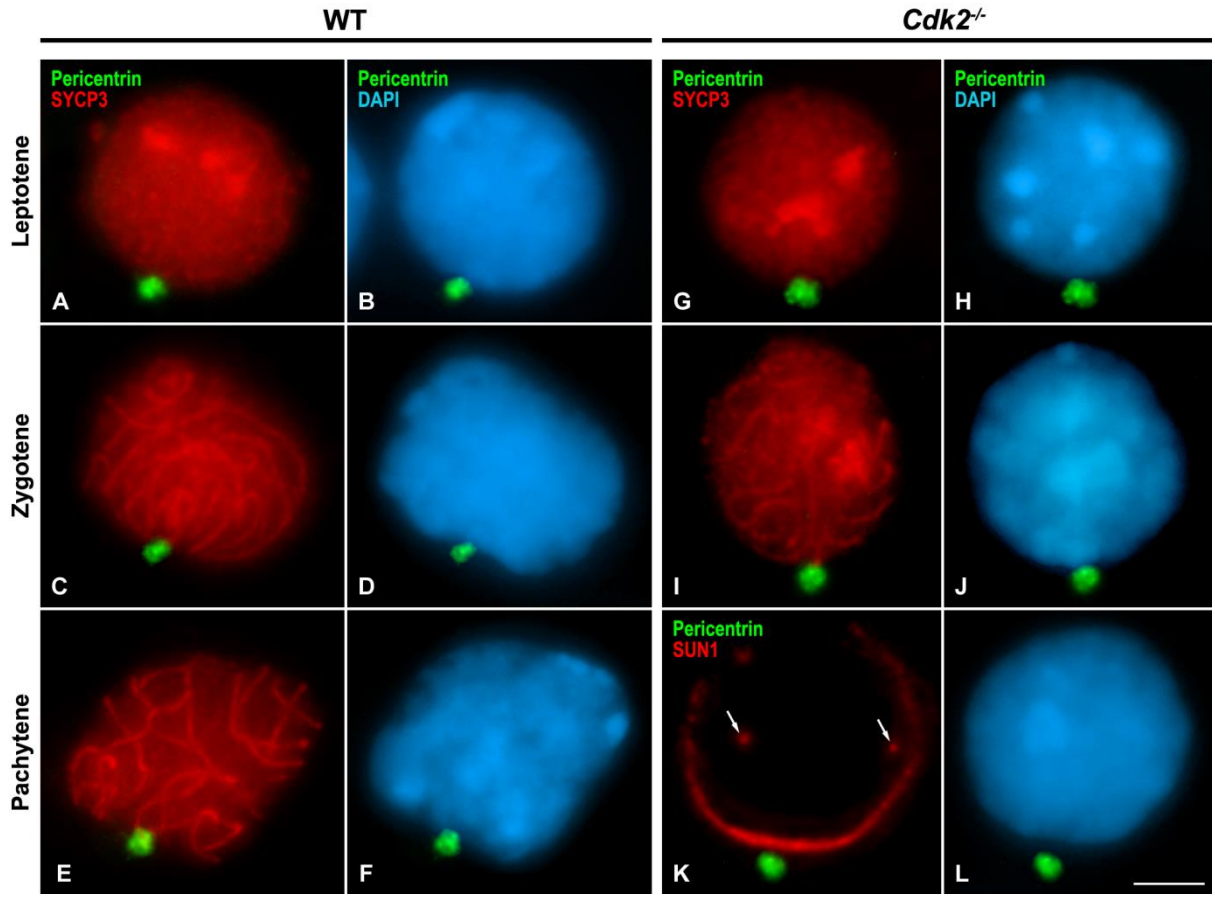

Fig. S1. Centrosome distribution in wild-type and *Cdk2*$^{-/-}$ spermatocytes. (A-J) Double-immunolabeling of pericentrin (green) and SYCP3 (red) and chromatin counterstaining with DAPI (blue) on squashed wild-type (A-F) and *Cdk2*$^{-/-}$ (G-J) prophase I spermatocytes. The images correspond to the partial Z-projections of 15 focal planes throughout the equatorial region of each spermatocyte. (A-F) WT prophase I nuclei. The centrosome (pericentrin staining) appears as a cloud near the nucleus. (G-J) *Cdk2*$^{-/-}$ leptotene and zygotene nuclei. The centrosome appears as a cloud near the nucleus. (K, L) Double-immunolabeling of pericentrin (green) and SUN1 (red) and chromatin counterstaining with DAPI (blue) on a squashed *Cdk2*$^{-/-}$ pachytene-like spermatocyte. The SUN1 cap-like labeling at the NE is always found facing the centrosome. Note internal SUN1 signals (arrows). Scale bar: 5 μm.

Figure S2

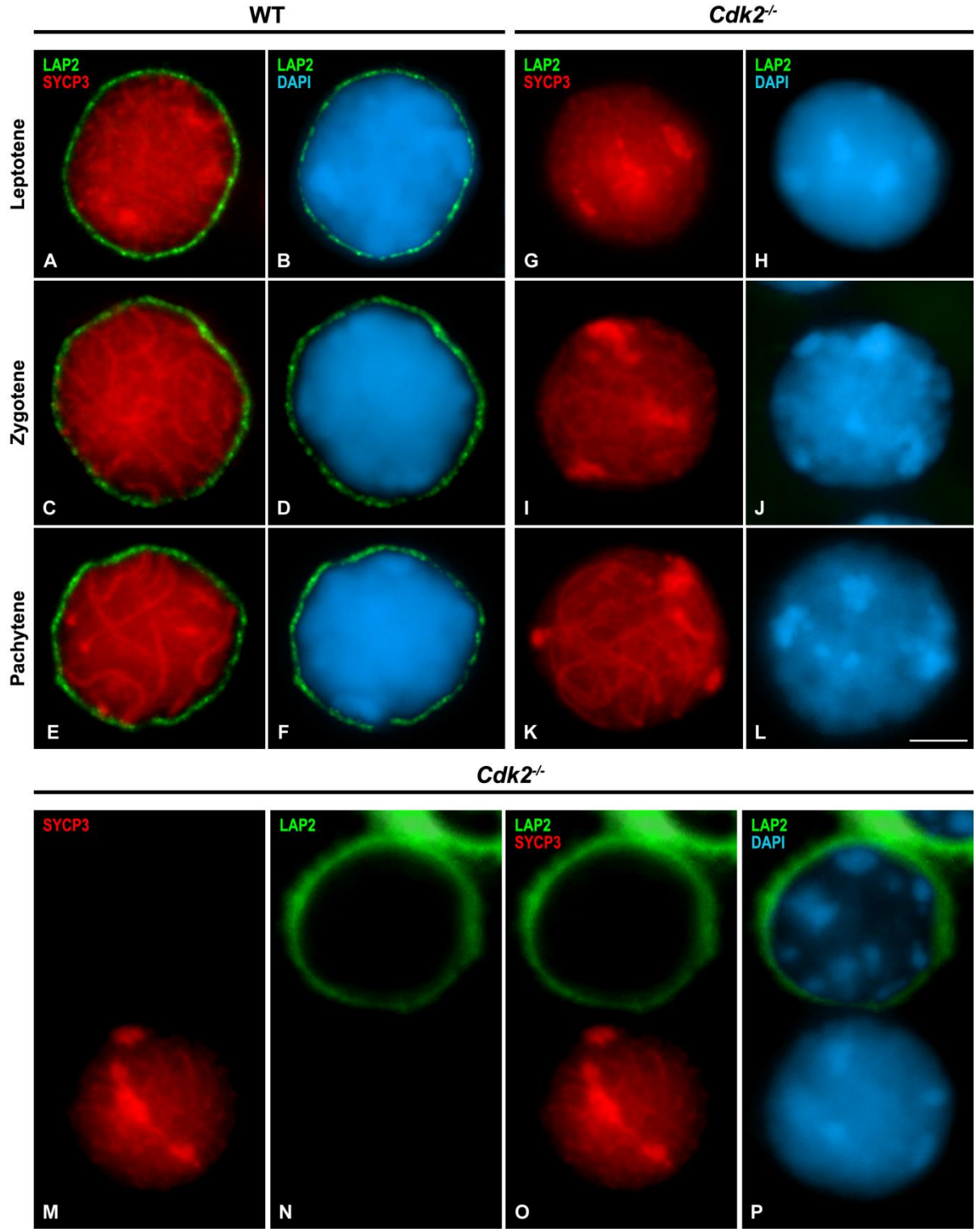

Fig. S2. LAP2 does not assemble at the NE in *Cdk2*$^{-/-}$ spermatocytes. Double-immunolabeling of LAP2 (green) and SYCP3 (red) and chromatin counterstaining with DAPI (blue) on squashed wild-type (A-F) and *Cdk2*$^{-/-}$ (G-P) prophase I spermatocytes. Images are partial Z-projections of 15 focal planes throughout the equatorial region of each spermatocyte. (A-F) WT prophase I nuclei. LAP2 appears uniformly distributed at the NE. (G-L) *Cdk2*$^{-/-}$ prophase I nuclei. LAP2 is not detected at the NE. (M-P) *Cdk2*$^{-/-}$ testicular somatic cell (top) and prophase I spermatocyte (bottom). LAP2 locates at the NE in a somatic cell, but it is absent at the NE of the spermatocyte. Scale bar: 5 μm.

Figure S3

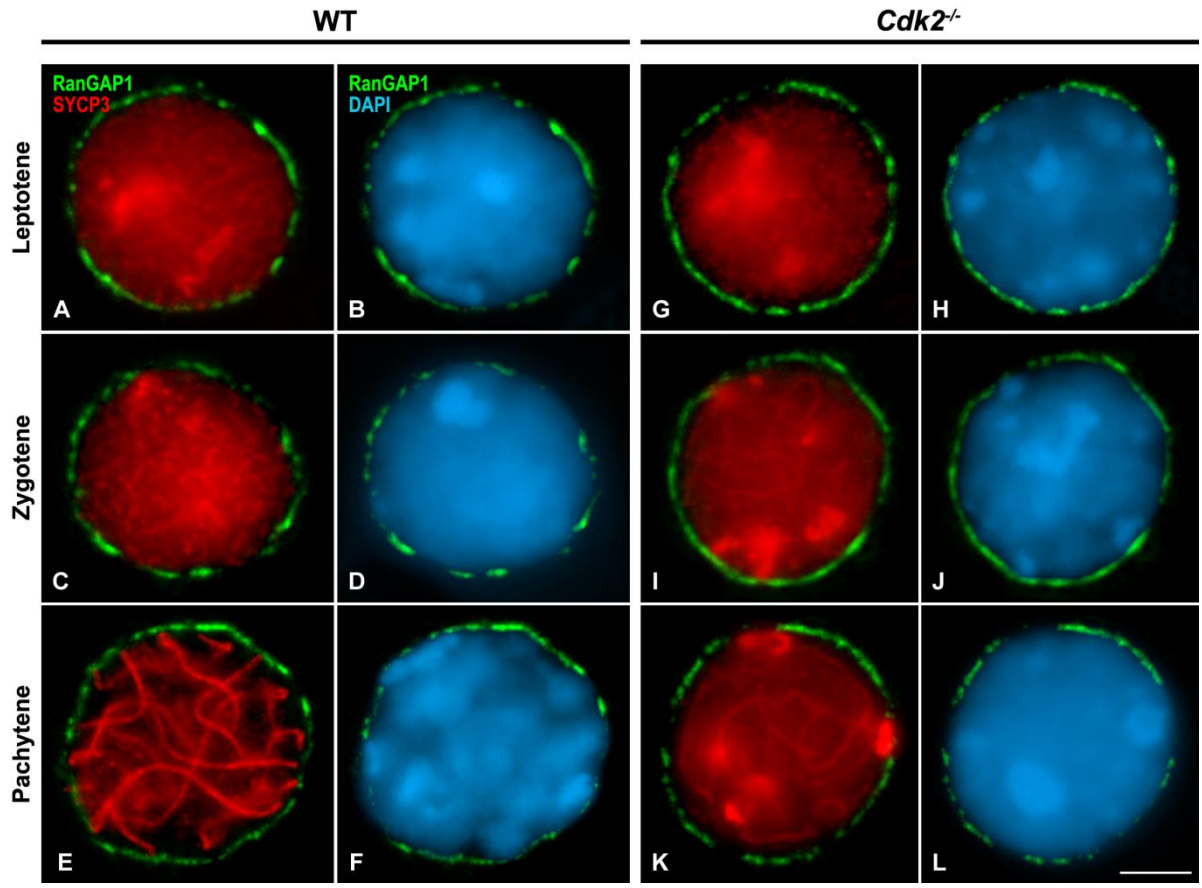

Fig. S3. The distribution of nuclear pore complexes is not modified in Cdk2-/- spermatocytes. Double-immunolabeling of RanGAP1 (green) and SYCP3 (red) and chromatin counterstaining with DAPI (blue) on squashed wild-type (A-F) and Cdk2-/- (G-L) prophase I spermatocytes. Images are partial Z-projections of 15 focal planes throughout the equatorial region of each spermatocyte. RanGAP1 appears as small spots at the NE both in WT and Cdk2-/- prophase I spermatocytes. Scale bar: 5 μm.

Figure S4

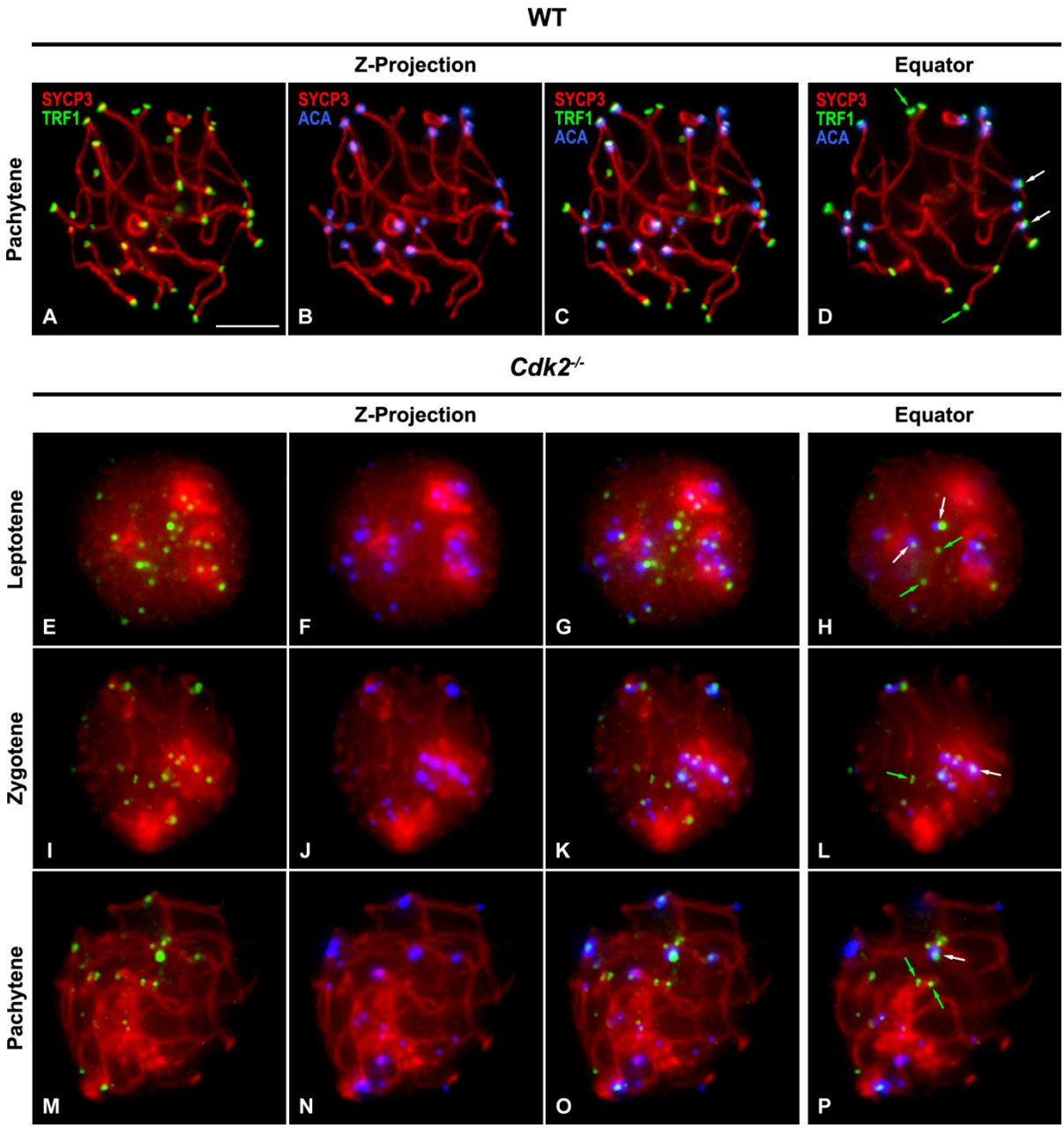

Fig. S4. Telomere and centromere distribution in Cdk2-/- spermatocytes. Triple-immunolabeling of telomeres (TRF1, green), centromeres (ACA, blue) and SYCP3 (red) on pachytene wild-type (A-D) and prophase I Cdk2-/- (E-P) squashed spermatocytes. The first three columns correspond to the Z-projection of all the focal planes throughout a nucleus. The fourth column presents the partial Z-projections of 15 focal planes throughout the equatorial region of the same nuclei. (A-D) WT pachytene nucleus. All the proximal telomeres (white arrows), with telomere and centromere signals, and the distal telomeres (green arrows), with only telomere signals, are located at the nuclear periphery. (E-P) Cdk2-/- prophase I nuclei. Both proximal telomeres (white arrows) and distal telomeres (green arrows) can be found at the nuclear interior in all prophase I stages. Scale bar: 5 μm.

Article

Developmental Cell

Functional Reprogramming of Polyploidization in Megakaryocytes

Graphical Abstract

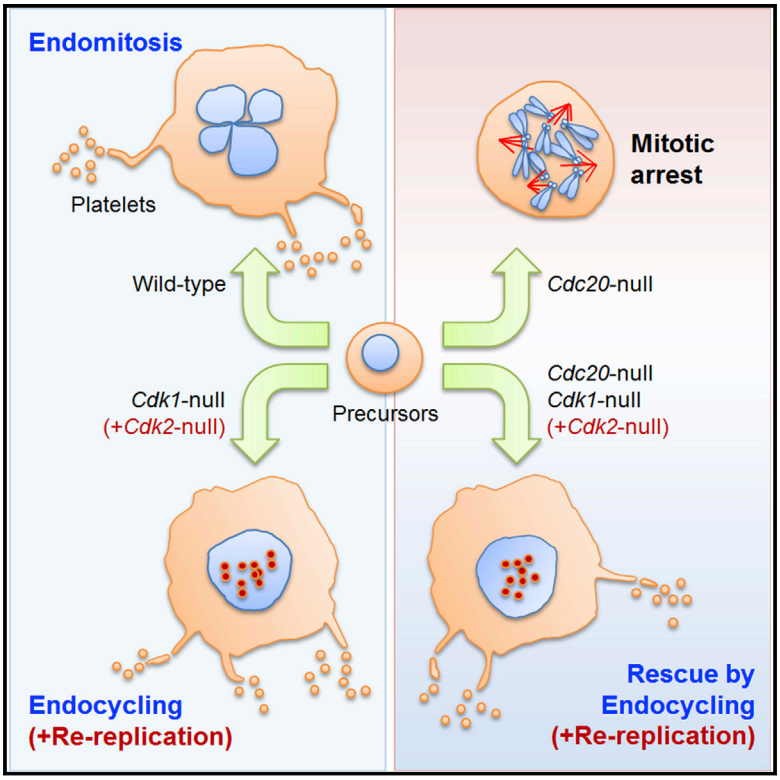

Highlights

- Ablation of Cdc20 compromises endomitosis during megakaryocyte polyploidization
- Megakaryocytes can generate platelets in the absence of endomitosis
- Cdk2 is essential to prevent re-replication in the absence of Cdk1 in vivo
- Different polyploidization mechanisms are functionally interchangeable

Authors

Marianna Trakala,
Sara Rodríguez-Acebes, ...,
Juan Méndez, Marcos Malumbres

Correspondence

malumbres@cnio.es

In Brief

Polyploidization normally occurs as part of a developmental program in which cells increase their ploidy without cell division. Although different cell types use specific polyploidization mechanisms, Trakala et al. now show that megakaryocytes can use different types of unconventional cell cycles to become polyploid without losing cell functionality in vivo.

Trakala et al., 2015, Developmental Cell *32*, 155–167
January 26, 2015
http://dx.doi.org/10.1016/j.devcel.2014.12.015

Developmental Cell
Article

Functional Reprogramming of Polyploidization in Megakaryocytes

Marianna Trakala,[1] Sara Rodríguez-Acebes,[2] María Maroto,[1] Catherine E. Symonds,[3] David Santamaría,[3] Sagrario Ortega,[4] Mariano Barbacid,[3] Juan Méndez,[2] and Marcos Malumbres[1,*]
[1]Cell Division and Cancer Group, Spanish National Cancer Research Centre (CNIO), 28029 Madrid, Spain
[2]DNA Replication Group, CNIO, 28029 Madrid, Spain
[3]Experimental Oncology Group, CNIO, 28029 Madrid, Spain
[4]Transgenic Unit, CNIO, 28029 Madrid, Spain
*Correspondence: malumbres@cnio.es
http://dx.doi.org/10.1016/j.devcel.2014.12.015

SUMMARY

Polyploidization is a natural process that frequently accompanies differentiation; its deregulation is linked to genomic instability and cancer. Despite its relevance, why cells select different polyploidization mechanisms is unknown. Here we report a systematic genetic analysis of endomitosis, a process in which megakaryocytes become polyploid by entering mitosis but aborting anaphase. Whereas ablation of the APC/C cofactor Cdc20 results in mitotic arrest and severe thrombocytopenia, lack of the kinases Aurora-B, Cdk1, or Cdk2 does not affect megakaryocyte polyploidization or platelet levels. Ablation of Cdk1 forces a switch to endocycles without mitosis, whereas polyploidization in the absence of Cdk1 and Cdk2 occurs in the presence of aberrant re-replication events. Importantly, ablation of these kinases rescues the defects in Cdc20 null megakaryocytes. These findings suggest that endomitosis can be functionally replaced by alternative polyploidization mechanisms in vivo and provide the cellular basis for therapeutic approaches aimed to discriminate mitotic and polyploid cells.

INTRODUCTION

Variation in ploidy is commonly found in multiple organisms and polyploid cells are an essential part of the developmental program in many different species (Edgar et al., 2014). In most cases, developmentally programmed polyploidy is an irreversible process linked to terminal cell differentiation and the acquisition of new functional capabilities. In addition, polyploidy has been proposed to buffer the genome against genetic damage (Pandit et al., 2013). Somatic polyploidy can be achieved through multiple modifications of the basic cell division cycle. These special cycles include endocycles, originally described as a process in which rounds of DNA replication occur while mitosis is completely bypassed (successive DNA synthesis and gap phases), or endomitosis, an atypical cell cycle in which cells undergo an aberrant mitosis in the absence of segregation of the previously duplicated genomes. The term ''endoreplication'' is often used either to refer to endocycles or more widely to include diverse polyploidization mechanisms and will not be used here to avoid confusion. Both endocycles and endomitosis lead to uniform and integral duplication of the genome in mammals (Sher et al., 2013). Other processes, such as re-replication, lead to nonuniform increased ploidy, as a consequence of alteration in the regulatory modules that impose a single round of DNA replication per cell cycle, and normally lead to cell death (Arias and Walter, 2007).

Polyploidization is an essential part of the programmed developmental process required for the formation of placental trophoblast giant cells, which use endocycles to achieve chromatin-values (C-value, a multiple of the DNA content of the unreplicated haploid chromosome complement) of >1,000. Similarly, bone marrow megakaryocytes can reach up to 128C in humans or 64C in the mouse through endomitotic cell cycles. Whereas endocycling is characterized by low expression of mitotic genes, and low cyclin-dependent kinase (Cdk) activity, mitotic genes are normally expressed during endomitosis in megakaryocytes (Edgar and Orr-Weaver, 2001; Sher et al., 2013). Megakaryocytes are the largest (50–100 μm) cells in the bone marrow and they produce platelets by fractionation of the cytoplasm after a terminal differentiation process in which the cytoplasmic volume increases in parallel with ploidy (Thon and Italiano, 2012). Polyploidization in megakaryocytes occurs in the presence of an aberrant mitosis in which cells do not undergo cleavage furrow formation after the 4N stage, and they skip late anaphase and cytokinesis, suggesting that segregation of chromosomes is not necessary for megakaryocyte maturation and platelet formation (Geddis et al., 2007; Kaushansky, 2008; Lordier et al., 2008; Ravid et al., 2002; Wen et al., 2009). The increase in cell volume likely helps to generate a large amount of mRNA and protein necessary to be packaged into platelets (Zimmet and Ravid, 2000). To what extent ploidy and platelet formation are linked is not well established (Machlus and Italiano, 2013), and why polyploidy in these cells is specifically achieved through abortive mitosis is presently unclear.

The variation in polyploidization mechanisms raises the question of whether these unconventional cycles have functional links with the differentiation of specific cell types or they simply represent alternative processes to increase ploidy. In addition, inhibition of multiple mitotic kinases such as Aurora A or Aurora B does not impair polyploidization in cultured megakaryocytes (Lordier et al., 2010; Wen et al., 2012), an observation that, while opening

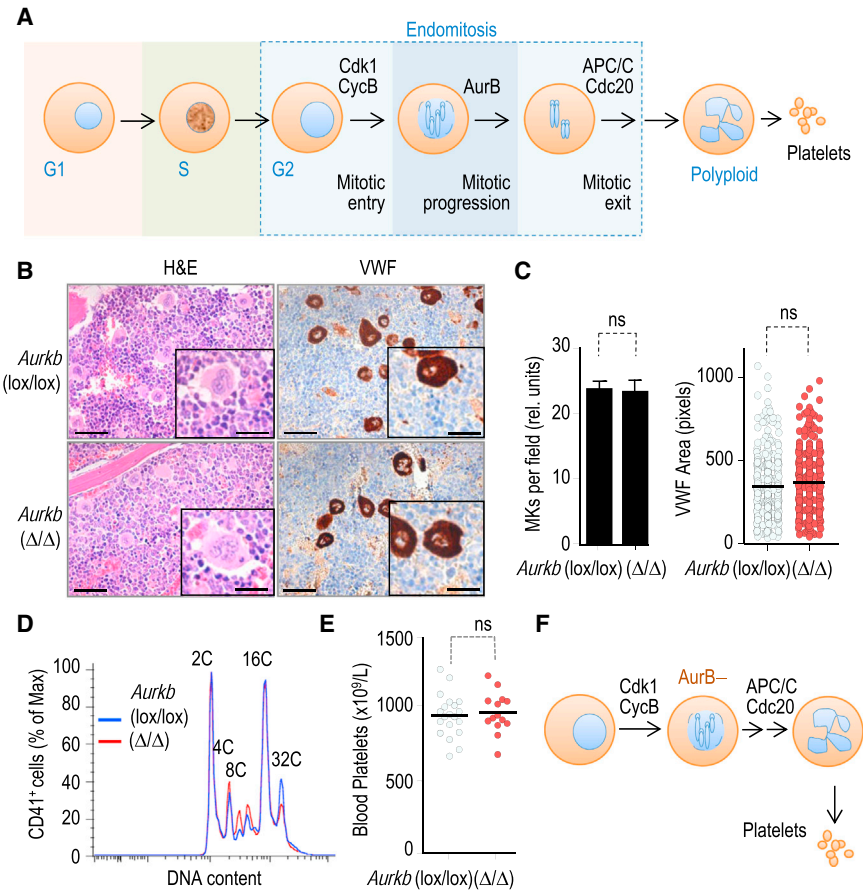

Figure 1. Aurora-B Is Dispensable for Megakaryopoiesis and Platelet Formation

(A) Schematic representation of the role of the molecules discussed in this work during endomitosis.

(B) Bone marrow sections from 12-week-old mice were stained with hematoxylin and eosin (H&E) or treated for immunohistochemical staining of Von Willebrand factor (VWF). Scale bars represent 50 μm (insets, 20 μm).

(C) Pf4-Cre; *Aurkb*(Δ/Δ) mice show normal megakaryocyte number (MKs per 40× microscopic field) and VWF staining (relative VWF signal per cell). At least 300 megakaryocytes from three different animals per genotype were counted. Data are mean ± SEM (ns; not significant; $p > 0.05$; Student's t test).

(D) Ploidy distribution (after DAPI staining) of CD41+ bone marrow cells.

(E) Blood platelet levels from 8- to 12-week-old *Aurkb*(Δ/Δ) and control mice (ns; not significant; $p > 0.05$; Student's t test).

(F) Schematic representation of mitotic progression in the absence of Aurora B.

See also Figure S1.

RESULTS

Aurora B Is Dispensable for Megakaryocyte Development

To understand the requirements for specific mitotic regulators during megakaryocyte development, we made use of transgenic mice expressing Cre recombinase under the platelet factor 4 (Pf4) promoter (Tiedt et al., 2007). In this model, Cre is expressed in megakaryocyte progenitors and mature megakaryocytes with preference for polyploid (≥8C) cells (Figure S1 available online).

Aurora B is a mitotic kinase whose ablation results in a normal mitotic entry but a premature exit from mitosis without being able to segregate chromosomes, resulting in tetraploidy (Fernández-Miranda et al., 2011; Trakala et al., 2013). Specific genetic ablation of the murine *Aurkb* gene in megakaryocytes (Figure S1) resulted in normal survival and no overt defects during development or adulthood of Pf4-Cre; *Aurkb*(Δ/Δ) (from now on *Aurkb*(Δ/Δ)) mice. These mutant mice displayed fully mature megakaryocytes in the bone marrow as indicated by Von Willebrand factor (VWF) staining (Figure 1B). The absolute number of megakaryocytes and the level of VWF staining per cell was not altered (Figure 1C), and we found no significant differences in the ploidy distribution of cells positive for the megakaryocytic marker CD41 (Figure 1D). In *Aurkb*(Δ/Δ) mice, hematopoietic progenitors displayed normal differentiation kinetics toward CD41+ cells when stimulated with thrombopoietin (TPO), and mature megakaryocytes were able to shed platelets (Figure S1). Accordingly, we found no differences in blood platelet levels in *Aurkb*(Δ/Δ) mice (Figure 1E), indicating a complete maturation, terminal differentiation and full functionality of these mutant megakaryocytes (Figure 1F).

new therapeutic opportunities in cancer (Krause and Crispino, 2013), illustrates our limited understanding on how polyploidization is modulated. We have analyzed in this work new mouse strains lacking selected key proteins involved in mitotic entry (Cdks; Figure 1A), mitotic progression (Aurora B), or mitotic exit (the anaphase-promoting complex [APC/C] cofactor Cdc20) during megakaryocyte maturation in vivo. Our results confirm that Aurora B, a kinase essential for proper attachment of microtubules to kinetochores (Nezi and Musacchio, 2009), is not required for megakaryocyte maturation (Lordier et al., 2010). However, genetic ablation of Cdc20 results in mitotic arrest and severe thrombocytopenia indicating that endomitosis is the major megakaryocyte polyploidization mechanism in vivo. Importantly, genetic ablation of Cdk1, an enzyme essential for mitosis, prevents endomitosis but does not impair platelet formation, as a consequence of reprogramming from endomitosis to endocycles that alternate DNA synthesis and gap phases. Similarly, concomitant ablation of Cdk1 and Cdk2 results in aberrant re-replication without dramatically affecting platelet levels. Furthermore, the loss of Cdk1 or the concomitant ablation of both Cdk1 and Cdk2 can significantly rescue proplatelet formation and platelet levels in Cdc20 null mice. These results suggest that reprogramming from endomitosis to other unconventional cell cycles in vivo is compatible with megakaryocyte function, even in the presence of re-replication, a dangerous process in which DNA is unevenly replicated.

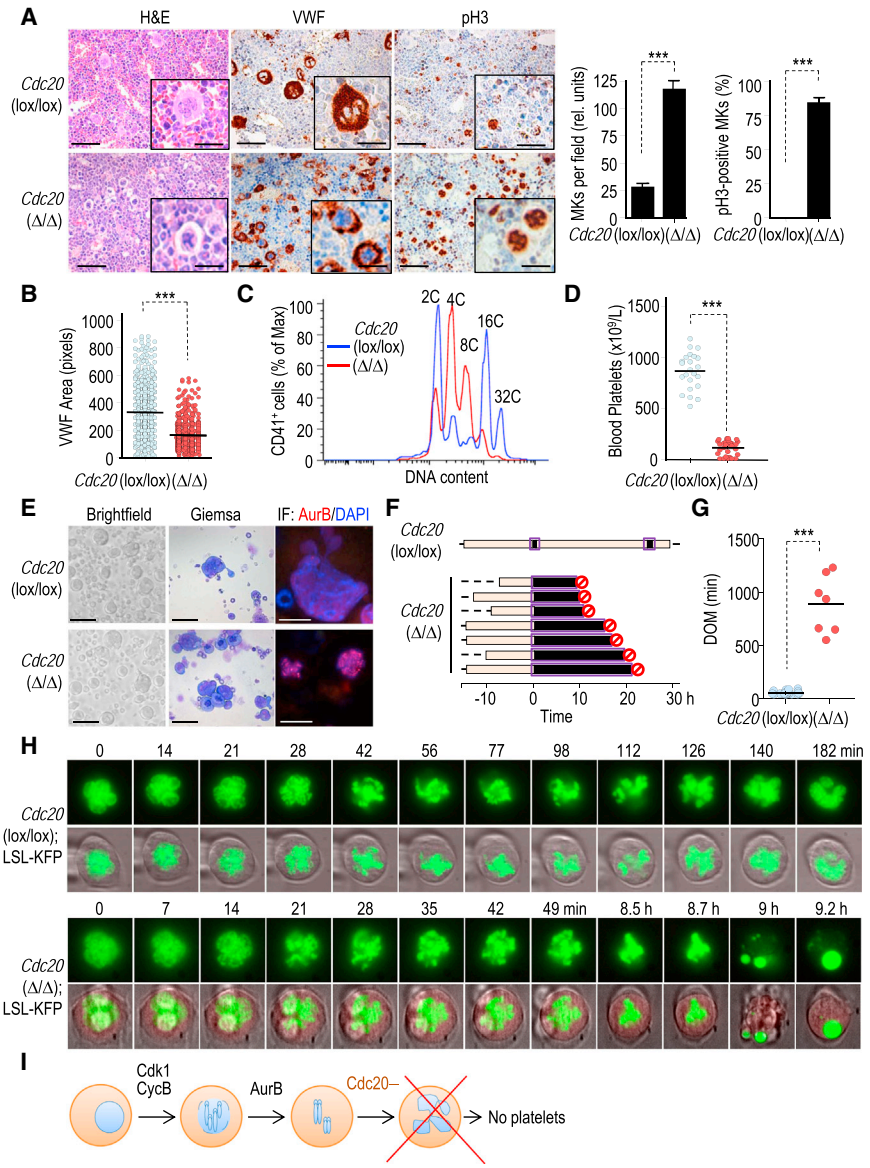

Figure 2. Cdc20 Is Essential for Megakaryocyte Maturation and Platelet Production

(A) Hematoxylin and eosin (H&E) and immunohistochemical staining for Von Willebrand factor (VWF) and phosphorylation of histone H3 (pH3) in 12-week-old mice. Scale bars represent 50 μm (insets, 20 μm). The abundance of megakaryocytes (mean ± SEM megakaryocyte per 40× microscopy field) and the percentage of mitotic cells (mean ± SEM) are indicated in the histograms. n = 250 cells from three mice per genotype.

(B) Quantification of VWF signal in Cdc20 null and control megakaryocytes. n = 250 cells from three mice per genotype.

(C) Ploidy distribution of bone marrow CD41+ cells after DAPI staining.

(D) Blood platelet levels from 8- to 12-week-old *Cdc20*(Δ/Δ) and control.

(E) Bone marrow cells were stimulated with TPO for 3 days. Micrographs represent bright-field and Giemsa staining, and immunofluorescence (IF) for Aurora B (red; DAPI is in blue). Scale bars represent 50 μm or 20 μm (IF).

(F) Cell fate of Cdc20-deficient megakaryocytes. Every row represents a single cell and purple frames depict endomitosis. Time 0 is set to mitotic entry (DNA condensation). Interphase is shown in pale brown and mitosis in black. Cell death is represented by a red circle. Only a control cell (top) is shown as an example.

(G) Duration of mitosis (DOM) in minutes estimated by the analysis of individual cells by time-lapse microscopy. In *Cdc20*(Δ/Δ) megakaryocytes, the DOM is considered from DNA condensation until cells die in mitosis.

(H) Representative time-lapse images of bone marrow-derived megakaryocytes stably expressing histone H2B-GFP (green). Red in *Cdc20*(Δ/Δ) megakaryocytes corresponds to Katushka fluorescent protein (KFP), which is expressed in a Cre-dependent manner.

(I) Scheme representing the essential role of Cdc20 for endomitotic exit in megakaryocytes. The Student's t test was used for statistics in (A), (B), (D), and (G). ***$p < 0.001$.

See also Figure S2.

APC/C-Cdc20 Is Essential for Endomitotic Exit in Megakaryocytes

The APC/C-Cdc20 complex is an E3-ubiquitin ligase whose activity is essential for exiting the mitotic cycle by triggering the degradation of the Cdk1 activator cyclin B1 (Peters, 2006). Thus, Cdc20 ablation does not have any effect in interphase or mitotic entry but cells are trapped in mitosis in the absence of APC/C-Cdc20 activity (Manchado et al., 2010). Specific genetic ablation of Cdc20 in megakaryocytes (Figure S2) resulted in a dramatic phenotype characterized by lack of mature cells and a significant increase in progenitors and small megakaryocytes in the bone marrow (Figure 2A) and the spleen (Figure S2), a phenotype commonly induced by lack of circulating platelets. *Cdc20*(Δ/Δ) megakaryocytes were characterized by reduced VWF staining (Figures 2A and 2B) and abundant mitotic figures in the presence of phosphorylated histone H3, suggesting mitotic arrest of mid-size megakaryocytes in the absence of Cdc20 (Figure 2A). In addition, the 16C and 32C populations were almost absent whereas 4–8C megakaryocytes were more abundant (Figures 2A and 2C), likely as a consequence of the terminal accumulation of mitotic 8C cells as a result of Cdc20 ablation in 2–4C cells. Accordingly, *Cdc20*(Δ/Δ) mutant mice presented severe thrombocytopenia ($108.4 \pm 70.8 \times 10^9$ platelets/l versus 781.6 ± 171.0 [mean ± SD] in control mice; $p < 0.001$; Student's t test; Figure 2D), thus confirming a critical role for Cdc20 in megakaryocyte function.

We next analyzed the cellular effect of megakaryocyte-specific ablation of Cdc20 using bone marrow progenitors stimulated in vitro with TPO. Three days after stimulation, mutant megakaryocytes were smaller than control cells, presented condensed DNA, and were positive for mitotic markers suggesting mitotic arrest in vitro (Figure 2E). We then transduced these megakaryocytes with lentiviral vectors expressing histone H2B fused to the green fluorescent protein (H2B-GFP). As depicted

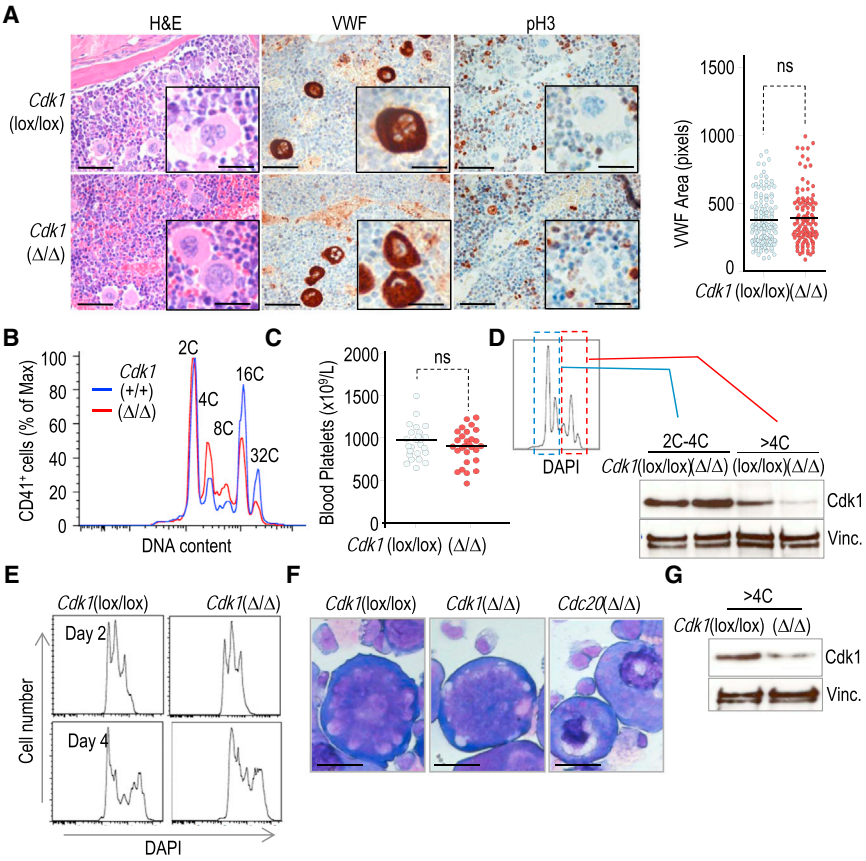

Figure 3. Normal Megakaryocyte Function in the Absence of Cdk1

(A) Bone marrow sections from *Cdk1*(lox/lox) and *Cdk1*(Δ/Δ) mice stained with hematoxylin and eosin (H&E) or after immunodetection of Von Willebrand factor (VWF) or phosphorylation of histone H3 (pH3). Scale bars represent 50 μm (insets 20 μm). VWF signal per cell is quantified in the histogram.

(B) Ploidy distribution of bone marrow CD41+ cells after DAPI staining. A representative image out of three separate experiments is shown.

(C) Blood platelet levels in *Cdk1*(lox/lox) and *Cdk1*(Δ/Δ) mice.

(D) Immunodetection of Cdk1 in freshly isolated megakaryocytes (CD41+ cells) from bone marrow. Megakaryocytes were stained with Hoechst and CD41+ cells were sorted according the DNA content into two populations (2C–4C) and (>4C). Vinculin was used as a loading control.

(E) DNA content of CD41+ bone marrow derived >4C megakaryocytes at days 2 and 4 during polyploidization upon TPO stimulation.

(F) Giemsa staining of the indicated megakaryocytes 4 days after TPO stimulation in vitro. Scale bars represent 50 μm.

(G) Immunodetection of Cdk1 in bone marrow-derived >4C megakaryocytes after stimulation ex vivo with TPO for 3 days. Vinculin is used as a loading control. In (A) and (C), ns, not significant (Student's t test).

in Figures 2F–2H, control *Cdc20*(lox/lox) megakaryocytes underwent typical endomitotic cycles in which cells displayed condensed DNA for approximately 1–2 hr and exited mitosis in the absence of chromosome segregation. Similar assays were performed in Pf4-Cre; *Cdc20*(Δ/Δ); LSL-KFP megakaryocytes in which the activity of Cre resulted in *Cdc20* ablation and the expression of Katushka fluorescent proteins (KFP) as a result of the excision of a LoxP-STOP-loxP cassette (Figure S1). These *Cdc20*(Δ/Δ) megakaryocytes displayed normal entry into endomitosis but arrested with condensed chromosomes at 10–24 hr until cell death (Figures 2G and 2H). Although we cannot discard another unknown function for Cdc20 in platelet formation, these data are indicative of the essential relevance of Cdc20 during endomitotic exit, resulting in lack of platelets due to mitotic arrest in low-intermediate ploidy Cdc20 null megakaryocytes (Figure 2I).

Cdk1 Is Essential for Endomitosis but Dispensable for Megakaryopoiesis

By definition, endomitotic cells do enter into mitosis and exit without segregation, whereas endoreplicating cells completely skip mitosis, frequently as a consequence of Cdk1 inhibition (Zielke et al., 2013). We therefore eliminated Cdk1 activity in megakaryocytes to prevent mitotic entry. The resulting Pf4-Cre; *Cdk1*(Δ/Δ) mice did not display major defects in megakaryocyte number, morphology, or VWF staining in adult mice (Figure 3A). Similarly, the ratio of highly polyploid (16C–32C) megakaryocytes was partially reduced (Figure 3B), although the number of platelets in peripheral blood was similar to that of control littermates (Figure 3C). Whereas Aurora B and Cdc20 protein levels are controlled by cell cycle-regulated ubiquitin-dependent proteolysis (Peters, 2006), Cdk1 is more stable raising the possibility that its depletion was not efficient in this system. However, we confirmed that Cdk1 protein levels were significantly reduced in mature (>4C) bone marrow *Cdk1*(Δ/Δ) megakaryocytes (Figure 3D). After incubation of bone marrow progenitors with TPO in vitro, *Cdk1*(Δ/Δ) megakaryocytes also accumulated normal levels of ploidy (Figure 3E) and displayed a normal morphology whereas, as a control, *Cdc20*(Δ/Δ) megakaryocytes presented smaller nuclei with condensed DNA (Figure 3F). Similar depletion in Cdk1 protein levels was obtained in this assay (Figure 3G). Therefore, the lack of an obvious phenotype in platelet production was not likely due to inefficient ablation of Cdk1 in these genetic models.

To understand the cellular basis of these observations, we monitored polyplodization in *Cdk1*(Δ/Δ) megakaryocyte precursors by time-lapse microscopy. Bone marrow progenitors were transduced with lentiviral vectors expressing lamin-CFP to stain nuclear envelope, and H2B-GFP to label chromatin. In addition, we used a vector expressing geminin-mCherry, a DNA replication regulator induced in S phase and degraded in an APC/C-dependent manner during mitotic or endomitotic exit (Sakaue-Sawano et al., 2008, 2013). Using these markers, together with the quantification of nuclear and cellular volumes, endocycles can be readily monitored in wild-type megakaryocytes

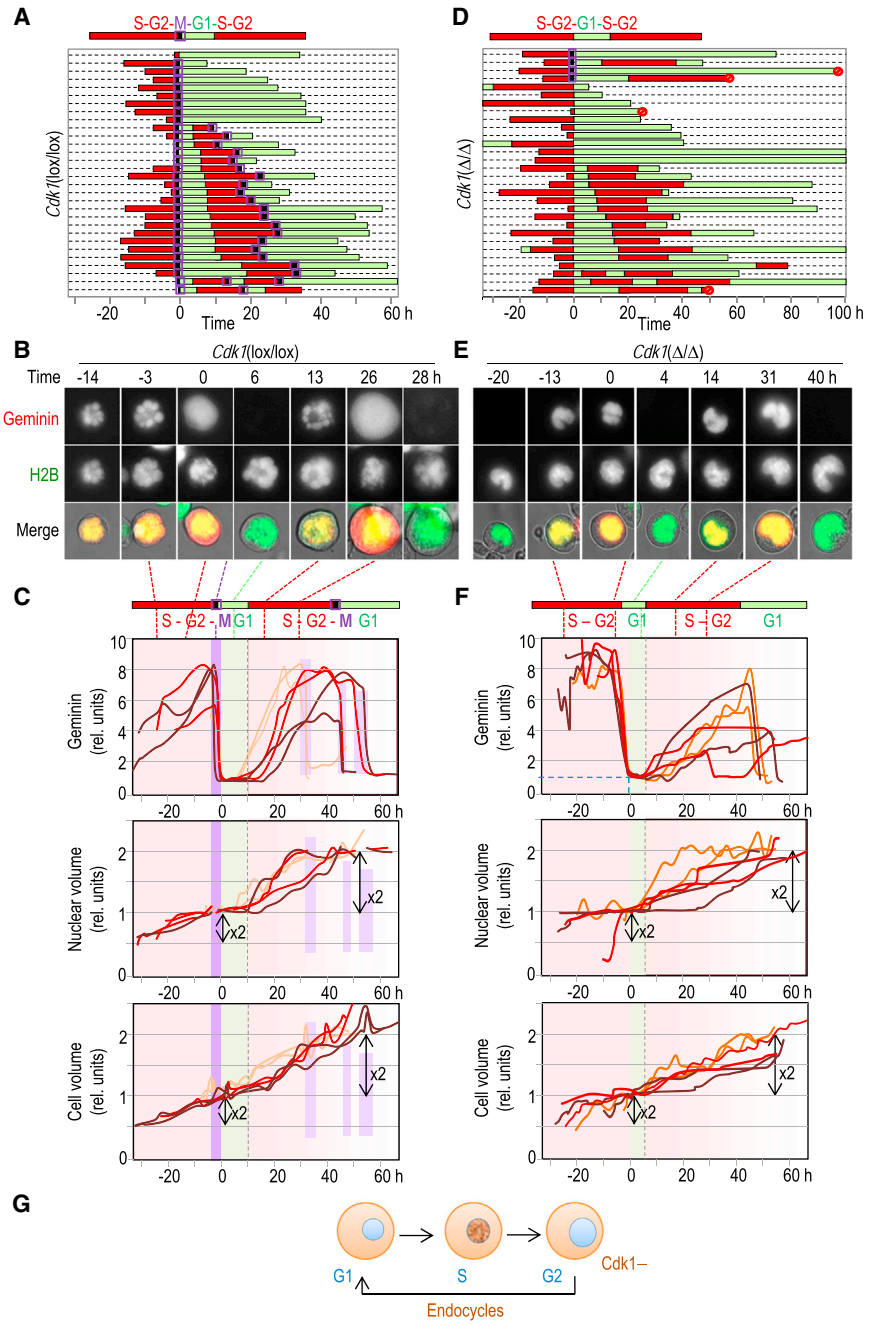

Figure 4. Lack of Cdk1 Results in Endoreplicative Polyploidization

(A) Cell fate of control bone marrow-derived megakaryocytes during approximately 5 days in the presence of TPO. Individual cells, stably expressing H2B-GFP (green) and Geminin-mCherry (red), were recorded with time-lapse microscopy. The red frame stands for S–G2 phases (geminin^{high}), whereas green frames represent G1 (geminin^{low}). Endomitosis is illustrated as a black box surrounded by a purple frame.

(B) Representative immunofluorescences of an individual control cell during endomitosis.

(C) Quantification of geminin fluorescent intensity, nuclear volume, and cell volume in individual control cells. Each line represents an individual cell and purple frames depict endomitosis. Black arrows indicate the 2-fold increase in nuclear and cellular volume between two geminin^{high} phases.

(D) Cell fate (similar to A) of individual cells derived from *Cdk1*(Δ/Δ) bone marrow-derived megakaryocytes. In most cells, geminin is degraded in the absence of mitosis. Red circles indicate cell death.

(E) Representative images of an individual *Cdk1*(Δ/Δ) megakaryocyte in which geminin is degraded in the absence of nuclear envelope breakdown or mitosis.

(F) Quantification of the temporal profiles of geminin fluorescent intensity, nuclear volume and cell volume in *Cdk1*(Δ/Δ) megakaryocytes. Each line represents an individual cell. Black arrows highlight the 2-fold increase of nuclear and cellular volume between two geminin^{high} phases even in the absence of endomitosis.

(G) Schematic representation of endocycles lacking mitotic phases in the absence of Cdk1.

See also Figures S3 and S4.

(Figure S3). Control megakaryocytes were recorded for several days and the behavior of individual cells is depicted in Figure 4A. Most control megakaryocytes were characterized by abortive mitosis (condensed chromosomes and pan-cellular geminin signal), degradation of geminin (geminin^{low} phase), followed in most cases by re-expression of geminin (geminin^{high}), and a new endomitotic phase (Figures 4A–4C). The histone signal (Figure S3) and nuclear volume (Figure 4C) similarly increased ~2-fold during the geminin^{high} phase, suggesting DNA replication in each of these endocycles. Cell volumes also increased during this process without clearly correlating with any particular phase (Figure 4C).

In most *Cdk1*(Δ/Δ) megakaryocytes, however, geminin was degraded in the absence of endomitosis (Figures 4D–4F). In these cells, geminin displayed an exclusive nuclear localization in agreement with the maintenance of the nuclear envelope (as detected by lamin signal; Figure S4) and the lack of chromosome condensation (as monitored by histone signal; Figures 4E and S4). Yet, geminin was degraded and cells underwent additional cycles characterized by the oscillation in geminin levels in the absence of mitosis. Interestingly, histone H2B-GFP signal (Figure S4) and nuclear volume (Figure 4F) increased ~2-fold in each of these endocycles, suggesting the presence of DNA replication throughout the geminin^{high} phase. Due to the difficulties in directly monitoring Cdk1 ablation in these individual cells, we also used the LSL-KFP allele as a surrogate marker for Cre activity. Approximately 70% of Pf4-Cre; *Cdk1*(Δ/Δ); LSL-KFP cells positive for the Katushka signal (an indication of Cre activity in polyploid cells; see Figure S1) underwent cycles in which geminin was degraded in the absence of endomitosis (S-G-S cycles), whereas all control Pf4-Cre; *Cdk1*(+/+); LSL-KFP cells underwent typical

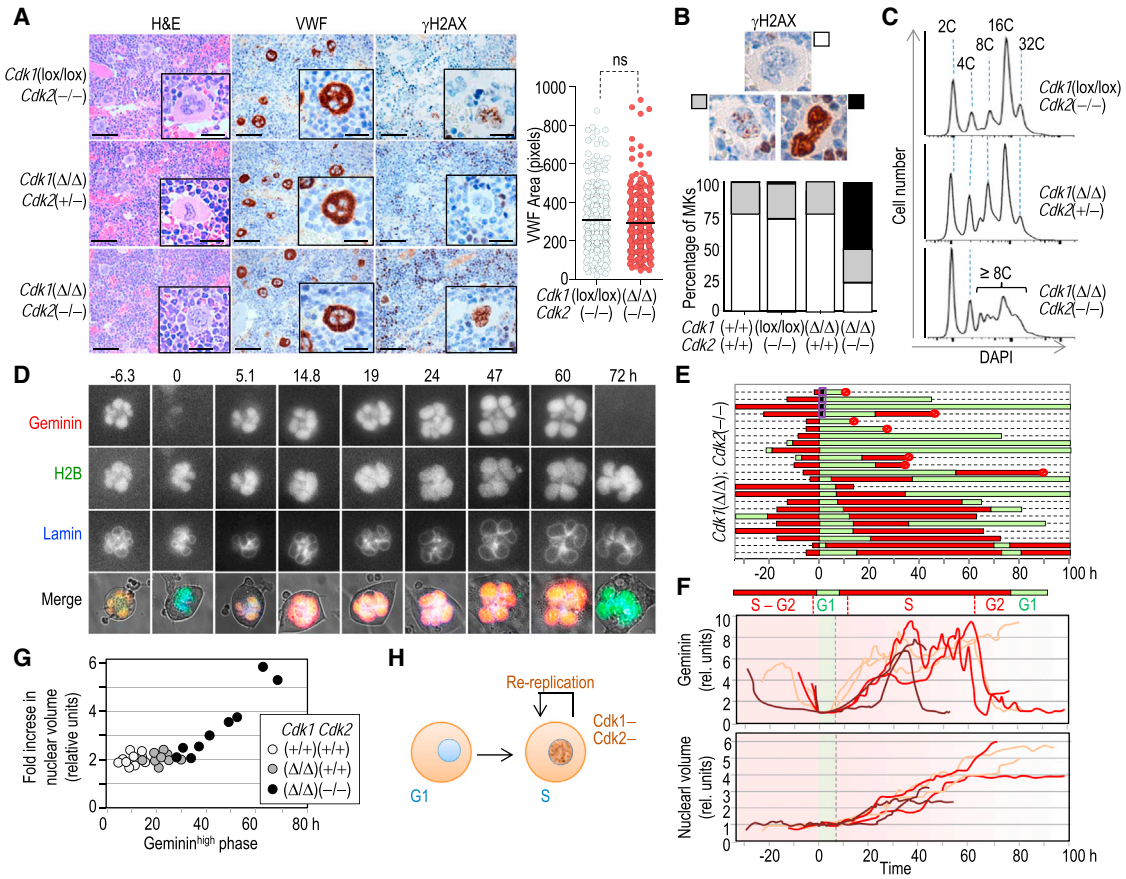

Figure 5. Lack of Cdk1 and Cdk2 Does Not Prevent Megakaryocyte Function despite Abnormal DNA Replication

(A) Representative bone marrow sections after staining with hematoxylin and eosin (H&E) or immunohistochemical staining for Von Willebrand factor (VWF) and phosphorylation of H2AX (γH2AX). Scale bars represent 50 μm (insets 20 μm). The quantification of the VWF signal per megakaryocyte is plotted for the indicated genotypes (ns, not significant; Student's t test).

(B) Quantification of megakaryocytes negative for γH2AX (empty box) or displaying a spotted pattern (gray boxes) or strong pan-nuclear staining (filled boxed) of γH2AX in the indicated genotypes.

(C) Ploidy distribution inside the bone marrow CD41+ population after DAPI staining. Plots are representative of three different experiments. The discrete peaks corresponding to different DNA content are indicated (2C–32C). The bracket indicates the diffuse pattern of high ploidy (>8C) *Cdk1*(Δ/Δ); *Cdk2*(−/−) megakaryocytes.

(D) Time-lapse microscopy of *Cdk1*(Δ/Δ); *Cdk2*(−/−) bone marrow-derived megakaryocytes after stimulation with TPO. Cells stably expressed histone H2B-GFP (red), lamin-CFP (blue), and geminin-mCherry (red). The cell increased nuclear size while maintaining its lobule organization.

(E) Cell fate of multiple individual *Cdk1*(Δ/Δ); *Cdk2*(−/−) megakaryocytes. Red and green boxes represent S–G2 (geminin^{high}) or G1 (geminin^{low}) phases. Endomitosis is illustrated as a black box surrounded by a purple frame and red circles represent cell death.

(F) Quantification of the temporal profiles of geminin fluorescence intensity and nuclear volume in *Cdk1*(Δ/Δ); *Cdk2*(−/−) megakaryocytes.

(G) Plot representing fold increase in nuclear volume versus geminin^{high} phase length in individual megakaryocytes with the indicated genotypes.

(H) A model suggesting that absence of Cdk1 and Cdk2 leads to increased ploidy by re-replication in megakaryocytes.

endomitotic cycles (Figure S4). The fact that the increase in ploidy was similar in wild-type and *Cdk1*(Δ/Δ) cells (Figures 4C and 4F) indicates that megakaryocytes are able to polyploidize using endocycling as an alternative route to endomitosis in the absence of Cdk1 (Figure 4G).

Cdk2 Prevents Re-replication in the Absence of Cdk1

We next used Cdk2-deficient mice to test the contribution of this kinase that is highly related to Cdk1 (Malumbres et al., 2009), but whose relevance to somatic cell cycles is not clear due to the lack of mitotic phenotypes in Cdk2-deficient mice (Malumbres and Barbacid, 2009; Ortega et al., 2003). In the absence of Cdk2 (Figure S5), megakaryocytes displayed normal morphology (Figure 5A) and platelet number (943.3 ± 137.6 × 10^9 platelets/L versus 852.3 ± 134.4 in wild-type littermates; $p > 0.05$, Student's t test). Similarly, lack of Cdk2 did not dramatically alter megakaryocyte maturation (Figure 5A) or platelet numbers in a *Cdk1*(Δ/Δ) background (739 ± 56.6 × 10^9 platelets/L in *Cdk1*(Δ/Δ); *Cdk2*(−/−) versus 863.4 3 ± 179.6 in *Cdk1*(Δ/Δ); *Cdk2*(+/+) littermates; $p > 0.05$, Student's t test). Unexpectedly, genetic ablation of Cdk2 in a Cdk1 null background resulted in pan-nuclear phosphorylation of H2AX (γH2AX) in megakaryocytes. Whereas γH2AX is usually found in a light, scattered pattern during normal DNA replication,

strong pan-nuclear staining is indicative of a response to DNA damage. Wild-type megakaryocytes or cells deficient in Cdk1 or Cdk2 displayed a scattered pattern in ~25% of the cells. However, *Cdk1*(Δ/Δ); *Cdk2*(−/−) megakaryocytes displayed an additional 52% of cells with strong pan-nuclear γH2AX staining, suggesting abnormal replication events (Figures 5A and 5B). These data correlated with abnormal ploidy in *Cdk1*(Δ/Δ); *Cdk2*(−/−) megakaryocytes in which the sharp peaks representing the 8C, 16C, and 32C populations were substituted with a continuous distribution of high ploidy cells, a phenotype frequently attributed to re-replication (Figure 5C).

Cdk1(Δ/Δ); *Cdk2*(−/−) megakaryocytes also presented geminin^{low} and geminin^{high} phases without evidences for mitosis in most cases (Figures 5D and 5E). Interestingly, the duration of many geminin^{high} phases was longer when compared to wild-type or *Cdk1*(Δ/Δ) cells (Figures 5D–5G), and the increase in nuclear volume per geminin^{high} phase in *Cdk1*(Δ/Δ); *Cdk2*(−/−) megakaryocytes was higher than 2-fold, and correlated (R^2 = 0.887) with the length of the individual geminin^{high} phases (Figure 5G). The fact that the increase in nuclear size was higher than expected and did not correspond to discrete genome doublings is consistent with a phenomenon known as re-replication in which the original DNA is copied more than once within each S phase (Figure 5H).

Cdk1 and Cdk2 Ablation Rescues Platelet Defects in the Absence of Cdc20

Because inactivation of Cdk1 or Cdk1 plus Cdk2 may trigger polyploidization in the absence of endomitosis, we hypothesized that lack of Cdks could rescue the mitotic-specific defects observed in Cdc20 null megakaryocytes by reprogramming the polyploidization process thus bypassing the mitotic arrest. We therefore generated Pf4-Cre; *Cdc20*(Δ/Δ); *Cdk1*(Δ/Δ) or Pf4-Cre; *Cdc20*(Δ/Δ); *Cdk1*(Δ/Δ); *Cdk2*(−/−) mutant mice. Whereas genetic ablation of Cdc20 was characterized by the presence of small megakaryocytes frequently arrested in mitosis, simultaneous ablation of Cdk1 allowed the accumulation of big megakaryocytes with increased VWF signal (Figures 6A and 6B) and ploidy (Figure 6C), suggesting a partial rescue in the maturation of these cells. Strikingly, concomitant ablation of Cdk1 and Cdk2 in a Cdc20 background led to an improved rescue in the maturation of megakaryocytes (Figures 6A and 6B). The rescue in ploidy was also improved because these triple mutant mice displayed clear 16C and 32C peaks in the presence of a significant number of cells with intermediate ploidy content (Figure 6C). These triple mutants displayed clear polyploid peaks what were not as evident in re-replicative *Cdk1*(Δ/Δ); *Cdk2*(−/−) megakaryocytes (Figure 5C). As detected by flow cytometry studies, ~17% of triple mutant cells were positive for the mitotic marker phospho-histone H3, an observation that likely reflects a partial mitotic arrest imposed by lack of Cdc20 in low-ploidy cells that may still express Cdk1 or Cdk2 (Figure S5). Yet, the percentage of cells with intermediate levels of ploidy (different from an exact multiple of the normal diploid number) was increased in *Cdc20*(Δ/Δ); *Cdk1*(Δ/Δ); *Cdk2*(−/−) triple mutants to levels close to those observed in *Cdk1*(Δ/Δ); *Cdk2*(−/−) double mutants (Figure S5). Overall, the percentage of mitotic megakaryocytes was significantly reduced in *Cdc20*(Δ/Δ); *Cdk1*(Δ/Δ) and *Cdc20*(Δ/Δ); *Cdk1*(Δ/Δ); *Cdk2*(−/−) mutant mice (Figure 6D), suggesting that Cdk1 null or Cdk1;Cdk2 null megakaryocytes were able either to exit from the mitotic arrest imposed by lack of Cdc20, or to polyploidize and form platelets in a endomitotic-independent manner. Time-lapse microscopy analysis indicated that no megakaryocyte was able to exit from the mitotic arrest imposed by Cdc20 ablation as a viable cell (Figure S5). However, about half of viable cells were able to start polyploidization cycles in the absence of mitosis suggesting that maturation of these cells was mediated by alternative polyploidization mechanisms. The reprogramming was also suggested by careful examination of nuclear morphology in vivo. Whereas wild-type (or Cdk2 null) megakaryocytes displayed typical complex nuclei characterized by the presence of multiple lobules (as a result of abortive chromosome segregation), *Cdk1*(Δ/Δ) or *Cdk1*(Δ/Δ); *Cdk2*(−/−) megakaryocytes (either in a wild-type or Cdc20 null background) were frequently mono- or binucleated (Figure 6E), supporting the hypothesis of a polyploidization mechanism different from endomitosis in vivo.

The presence of pan-nuclear staining of γH2AX in *Cdc20*(Δ/Δ); *Cdk1*(Δ/Δ); *Cdk2*(−/−) also indicated replicative defects in triple mutant mice that were not present in *Cdc20*(Δ/Δ); *Cdk1*(Δ/Δ) megakaryocytes (Figure 6A). We therefore tested whether these defects could be due to re-replication in the absence of both Cdk1 and Cdk2 by using an adaptation of DNA fiber spreading assays (Neelsen et al., 2013) to monitor re-replication on single DNA molecules from megakaryocytes. Cells were sequentially incubated with CldU and IdU, a technique commonly used to distinguish moving forks, origin firing and termination events. In this protocol, the overlap in these signals on the same replication track is indicative of re-replication events caused by two or more rounds of activation of the same replication origin. As shown in Figure 7A, the levels of re-replication were below 5% in wild-type megakaryocytes as well as in Cdk1- or Cdk2-single mutants in agreement with previous data in other control cultures (Dorn et al., 2009; Neelsen et al., 2013). However, about 15%–17% of labeled DNA replication tracks from both *Cdk1*(Δ/Δ); *Cdk2*(−/−) and *Cdc20*(Δ/Δ); *Cdk1*(Δ/Δ); *Cdk2*(−/−) megakaryocytes corresponded to re-replication events, indicating a potential loss of control over origin licensing in the absence of these two kinases.

Alternative Polyploidy Cycles Can Drive Proplatelet and Platelet Formation

To understand whether megakaryocytes were functional in the presence of alternative polyploidization mechanisms, we next performed proplatelet formation assays ex vivo. Five days after TPO-induced differentiation of bone marrow progenitors, 24% ± 2% (mean ± SEM) of wild-type endomitotic megakaryocytes were able to form proplatelets (Figure 7B). *Cdk1*(Δ/Δ) megakaryocytes displayed a similar percentage of proplatelet-bearing cells (21% ± 2%; Figures 7B and 7C). As a negative control, only 0.9% ± 0.5% of *Cdc20*(Δ/Δ) megakaryocytes were able to form proplatelets. Importantly, concomitant ablation of Cdk1 in a Cdc20 null background led to a significant rescue of proplatelet formation (7.0% ± 0.4%) and this was further improved in *Cdc20*(Δ/Δ); *Cdk1*(Δ/Δ); *Cdk2*(−/−) triple mutant cultures (16% ± 3.5%; Figures 7B and 7C).

In agreement with these data, genetic ablation of Cdk1 was able to significantly rescue thrombocytopenia in Cdc20 null

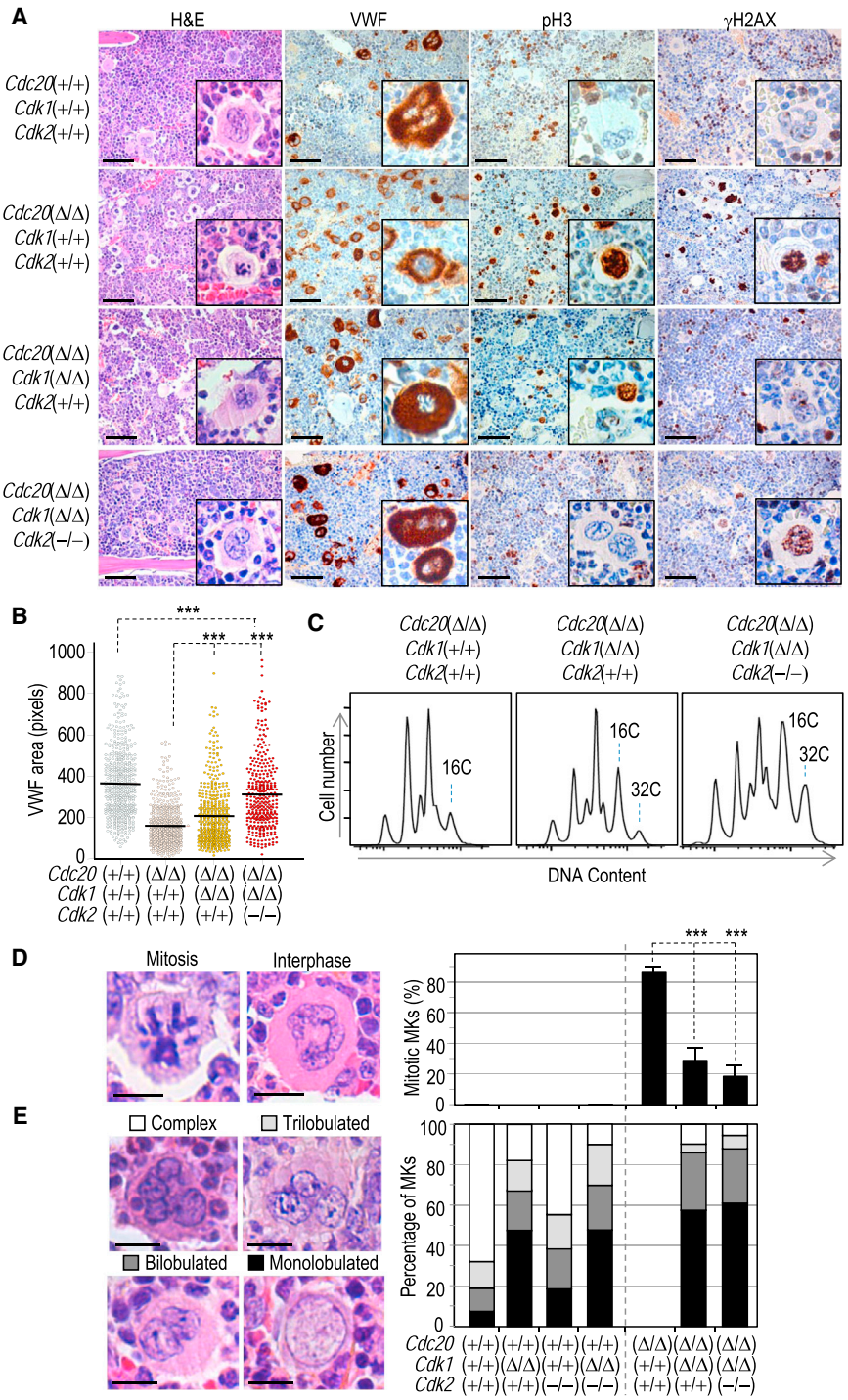

Figure 6. Reprogramming Polyploidization Rescue Defects in Cdc20-Deficient Megakaryocytes

(A) Representative bone marrow sections from the indicated animals after staining with hematoxylin and eosin (H&E) or immunohistochemical staining for Von Willebrand factor (VWF), phospho-histone H3 (pH3), or phosphorylated H2AX (γH2AX).

(B) Distribution of VWF signal per megakaryocyte. Each dot represents an individual cell. n = 400 cells and three mice per genotype. Student's t test, ***$p < 0.001$.

(C) Ploidy distribution inside the bone marrow CD41+ population after DAPI staining. The plot is representative from three separate experiments. Triple mutant bone marrows contain some polyploid mitotic cells, in agreement with a partial mitotic arrest imposed by Cdc20 loss, and a significant percentage of cells with intermediate levels of ploidy (Figure S5).

(D) Quantification of the mitotic index in megakaryocytes of the indicated genotypes. A representative image or interphasic and mitotic megakaryocytes is shown.

(E) Quantification of interphasic nuclear shape in megakaryocytes of the indicated genotypes. Cdc20 null megakaryocytes are not included because these cells are arrested in mitosis. At least 350 cells from three different animals were analyzed per genotype in (D) and (E). Data are mean ± SEM; ***$p < 0.001$; Student's t test.

See also Figure S5.

mice. The mean number of circulating platelets increased from 114 ± 79 × 10^9 platelets/L in *Cdc20*(Δ/Δ) animals to 376 ± 18 × 10^9 platelets/L in *Cdc20*(Δ/Δ); *Cdk1*(Δ/Δ) double-mutant mice (Figure 7D). Interestingly, concomitant ablation of one or two alleles of Cdk2 further improved this rescue (598 ± 42 × 10^9 platelets/L in *Cdc20*(Δ/Δ); *Cdk1*(Δ/Δ); *Cdk2*(−/−) triple mutants). Altogether, these results indicate that alternative polyploidization mechanisms can result in functional megakaryocytes in vivo even in the presence of re-replication events (Figure 7E).

DISCUSSION

Polyploidization provides an evolutionarily conserved mechanism for postmitotic cell growth in unicellular and multicellular organisms (Edgar et al., 2014; Pandit et al., 2013). The increase in ploidy can be achieved by variants of the cell cycle that have been analyzed in detail in *Drosophila* and *Arabidopsis* due to the availability of multiple genetic models (Edgar et al., 2014). In the mouse, polyploidization has been mostly studied in trophoblast giant cells and hepatocytes, two cell types that undergo endocycling or acytokinetic mitosis. In trophoblast giant cells, mitosis is prevented by inhibition of Cdk1 activity by multiple mechanisms such as induction of the $p57^{Kip2}$ Cdk inhibitor, or by enhanced APC/C-Cdh1 activity that results in the ubiquitin-dependent degradation of mitotic cyclins (García-Higuera et al., 2008; Ullah et al., 2008; Zielke et al., 2013).

Early assays in stimulated megakaryocytes in vitro concluded that polyploidization in these cells is achieved by endomitotic cycles in which cells skip the later stages of mitosis and

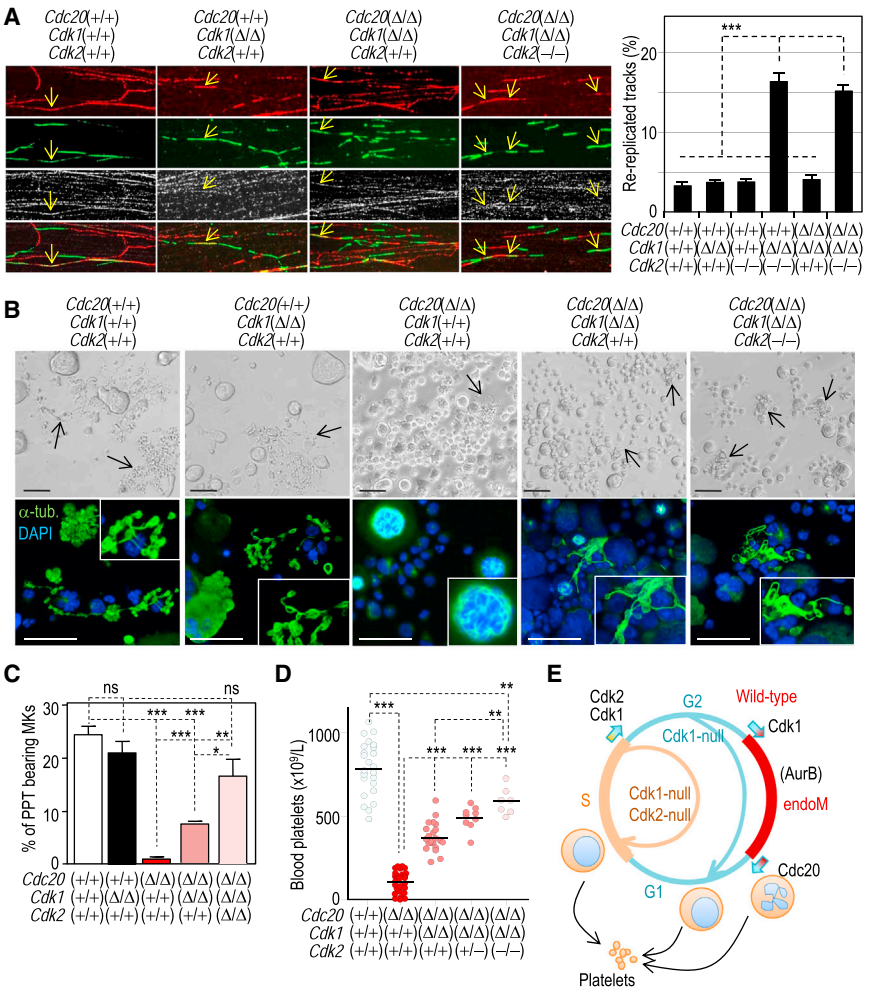

Figure 7. Functional Polyploidization in the Absence of Cdk1 or Cdk1 and Cdk2

(A) Representative pictures of two independent DNA fiber stretch assays in bone marrow-derived megakaryocytes on day 4 after TPO stimulation. In re-replicated tracks, the green (IdU) and red (CldU) signals overlap resulting in a yellow signal. Fiber integrity was monitored with an anti-ssDNA antibody (white). The percentage of re-replicated tracks in the indicated genotypes is indicated. For each sample at least 500 measurements were performed. Data represent mean ± SEM.

(B) Pro-platelet (PPT; arrows) formation in bone marrow-derived megakaryocytes analyzed 5 days after TPO stimulation. Bottom: samples were stained for α-tubulin (green) and DNA (DAPI; blue).

(C) The percentage of PPT-forming megakaryocytes was estimated by counting cells exhibiting 1 or more cytoplasmic protrusions with areas of platelet swellings as it is indicated by black arrows in (B). At least 300 cells were analyzed per group. Data represent mean ± SEM.

(D) Blood platelet levels in 8- to 14-week-old mice with the indicated genotypes. Each dot represents an individual animal. In (A), (C), and (D), Student's t test; ns, not significant. *$p < 0.5$; **$p < 0.01$; ***$p < 0.001$.

(E) A model indicating the mechanisms for polyploidization in wild-type megakaryocytes (G1-S-G2-endoM) or megakaryocytes deficient in Cdk1 (G-S-G) or Cdk1; Cdk2 double mutants (re-replication in S phase).

cytokinesis (reviewed in Ravid et al., 2002). Recent data using time-lapse microscopy indicates different dynamics in furrow formation between low- and high-ploidy megakaryocytes (Lordier et al., 2008; Papadantonakis et al., 2008). The resulting cells usually display a single polylobulated nucleus as a consequence of chromosome decondensation and nuclear envelope re-formation after aborted anaphase. The fact that more than 80% of mature megakaryocytes arrest in mitosis in the absence of Cdc20 (Figure 2) supports the notion that endomitosis is the major polyploidization mechanism for megakaryocytes in vivo. The requirements for other mitotic regulators are unclear and separate observations in the past suggested contradictory data on the relevance of the expression of several mitotic regulators such as Cdk-cyclin complexes or mitotic regulators during endomitosis (Vitrat et al., 1998; Zhang et al., 1996). Recent data indicate that mature megakaryocytes do not display a major defect in the expression of the mitotic machinery (Sher et al., 2013), although differences in specific RhoA exchange factors or non-muscle myosins may explain defects in furrow formation in high-ploidy megakaryocytes (Gao et al., 2012; Lordier et al., 2008, 2012). Aurora B, an enzyme essential for error correction during microtubule-kinetochore attachment, is dispensable for megakaryocytes in vivo (Figure 1), in agreement with previous data showing that chemical inhibition of this kinase does not prevent polyploidization and maturation of these cells (Lordier et al., 2010; Wen et al., 2012). Thus, whereas most mitotic genes are expressed in megakaryocytes, some of them may be dispensable due to the lack of ordered separation of chromosomes during mitotic exit.

Here, we have found that genetic ablation of Cdk1 results in bypass of mitosis in megakaryocytes (Figures 3 and 4), a process that has also been observed in some cell lines (Hochegger et al., 2007) or in hepatocytes (Diril et al., 2012), a cell type known to undergo endocycling upon different stress conditions (Gupta, 2000). Importantly, Cdk1-deficient megakaryocytes not only can increase ploidy using endocycles, but also generate normal levels of proplatelets in vitro and platelets in vivo (Figures 3, 4, and 7).

Unconventional cell cycles such as endomitosis or endocycles maintain a mechanism to enable the oscillation in Cdk and APC/C activity, thus ensuring the periodic relicensing of DNA for replication. Loss of this control leads to re-replication (also known as over-replication), a process in which some origins can be relicensed and refired before the whole genome has been duplicated once, resulting in genome compositions that differ from multiples of the normal ploidy (Arias and Walter, 2007). Apart from its physiological role in the amplification of specific genes during the development of the *Drosophila* ovary (Calvi et al., 1998; Claycomb et al., 2004), re-replication is

considered an aberrant process that does not appear to occur as part of any developmental program in mammals. Pioneering experiments by Nurse and colleagues showed that Cdks play a dual role in triggering replication initiation and limiting DNA replication to a single round per cell cycle by inhibiting relicensing of origins within a single S phase (Broek et al., 1991; Dahmann et al., 1995). In mammals, both Cdk1 and Cdk2 can prevent the function of the replication complex by phosphorylating multiple regulators such as Cdt1, Cdc6, Orc1, or MCM proteins, or by preventing polymerase activity (reviewed in Zhu, 2004). Depletion of Cdk1 and/or Cdk2 has been linked to re-replication phenomena in cell lines although in many cases these data are confusing given the use of different nomenclature or the lack of direct techniques, such as DNA fiber analysis to monitor these changes. Whereas Cdk1 is essential for the mammalian cell cycle (Diril et al., 2012; Santamaría et al., 2007), Cdk2 ablation in somatic cells does not result in major defects in the mitotic cell cycle, likely as a consequence of compensation by other Cdks (Berthet et al., 2003; Ortega et al., 2003). Interestingly, concomitant ablation of these two Cdks in megakaryocytes results in re-replication events, a phenomenon that cannot be easily repaired and leads to DNA breaks and apoptosis in other cell types (Arias and Walter, 2007; Neelsen et al., 2013). In *Drosophila*, polyploidy occurs in the absence of DNA-damage induced apoptosis (Hassel et al., 2014; Mehrotra et al., 2008). Similarly, megakaryocytes seem to be tolerant to the aberrant ploidy resulting from re-replication, probably as a consequence of the upregulation of prosurvival proteins to progress safely through proplatelet formation and platelet shedding (Josefsson et al., 2011). Thus, Cdk1;Cdk2-deficient megakaryocytes provide a model for functional re-replication in mammals.

These data also suggest that, although Cdk1 and Cdk2 may eventually participate in triggering DNA replication in mammalian cells (Moore et al., 2003; Santamaría et al., 2007), they are both dispensable for S phase entry, at least in the presence of other interphase Cdks. Although dispensable for G1/S transition, our work indicates that Cdk2 is essential to prevent re-replication in the absence of Cdk1, an interesting observation given the lack of essential functions for this protein in mammals (Berthet et al., 2003; Malumbres and Barbacid, 2009; Ortega et al., 2003), and the possible use of Cdk1/Cdk2 inhibitors to trigger lethal re-replication in tumor cells.

Strikingly, by modulating Cdk activity in megakaryocytes in vivo, we found that alternative polyploidization mechanisms besides endomitosis can lead to highly polyploid and mature megakaryocytes. The fact that reprogrammed megakaryocytes are functional even in the presence of DNA damage and absence of discrete ploidy peaks (Figure 5), suggests that the major, if not the only, function of polyploidization is to increase cell size for platelet generation (Thon and Italiano, 2012). Because endomitosis is one of the modified cell cycles least variant from the archetypal cell cycle, a simple interpretation suggests that megakaryocytes (which do not reach the higher ploidy levels observed in other cells such as trophoblast giant cells; >1,000C) simply select the smaller degeneration of the mitotic cell cycle required for expansion of progenitors to become polyploid. The slight defects in platelet levels in Cdk1- or Cdk1; Cdk2 null mice and the incomplete rescue induced by lack of these kinases in Cdc20-deficient mice may indicate that, although endocycling or re-replication can be functionally used during megakaryocyte polyploidization, they may be less efficient than endomitosis. As an attractive possibility, it has been recently proposed that the multilobulated nuclei generated during mitosis may participate in the establishment of the forces required for membrane fragmentation during the formation of proplatelets (Eckly et al., 2014).

In addition to its critical role as part of developmental or stress programs, polyploidization can also be a quick route to aneuploidy and genome instability (Davoli and de Lange, 2011; Pandit et al., 2013). Recent data have shown that inhibition of Aurora kinases as well as Cdk1 or Cdk2 in megakaryocytic leukemia cells leads not only to increased ploidy, but also to the expression of differentiation markers (Wen et al., 2012). Thus, polyploidization not only accompanies, but also can actually trigger the differentiation process in megakaryocytes. Because Cdk1 is essential for mitosis in all cells tested, it can be expected that the differentiation process induced by Cdk1 inhibition (Wen et al., 2012) is actually mediated by endocycling rather than endomitosis, although this has not been tested in detail. The fact that mitotic kinases such as Aurora A, Aurora B, or Cdk1 are not required for the function of endomitotic or endocycling cells, while being essential for mitotic cell cycles, opens new avenues in the use of inhibitors against these proteins in therapeutic approaches against specific human cancers (Krause and Crispino, 2013).

EXPERIMENTAL PROCEDURES

Mouse Colony and Histological Analysis

Mice deficient in Aurora-B (Fernández-Miranda et al., 2011), Cdc20 (Manchado et al., 2010), or Cdk2 (Ortega et al., 2003), and the Pf4-Cre (Tiedt et al., 2007) and LSL-Katushka (Diéguez-Hurtado et al., 2011) tool lines have been described previously (Supplemental Experimental Procedures). Expression of Cre in bone marrow cells does not alter polyploidization of megakaryocytes (Wen et al., 2009). The Cdk1 conditionally allele will be reported elsewhere (C.E.S, D.S., and M.B., unpublished data). Mice were housed in the pathogen-free animal facility of the Centro Nacional de Investigaciones Oncológicas (Madrid) following the animal care standards of the institution. All animal protocols were approved by the local committee for animal care and research. The following antibodies were used for immunohistochemistry in tissue sections: von Willebrand factor (FVIII, Dako; 1:2000), phospho-histone H3 (Ser10; Millipore; 1:2000) or γ-H2AX (Ser139, Millipore; 1:2,000). For quantification, paraffin sections stained with anti-VWF were examined using an Olympus BX51 microscope equipped with objective lenses (40/0.75, 20/0.4, 10/0.25, and 4/0.1). The relative amount of pixels positive for VWF was used as a score.

Cytometry

Flow cytometric analysis of DNA content and surface markers of megakaryocytes was determined by staining either whole bone marrow cells or hematopoietic progenitor cultures from 0 to 5 days in the presence of TPO with fluorescein isothiocyanate (FITC)-conjugated anti-CD41 antibody (BD Biosciences) followed by fixation with 4% paraformaldehyde at room temperature for 30 min followed by staining with 2 μg/ml 4′,6-diamidino-2-phenylindole (DAPI; Sigma-Aldrich) or 5 μg/ml Hoechst (Sigma-Aldrich) for 1 hr. See also the Supplemental Experimental Procedures.

Megakaryocyte Differentiation and Functional Assays

Cells from the bone marrow or fetal liver were isolated as indicated in the Supplemental Experimental Procedures. Lin^- cells were grown in Dulbecco's modified Eagle's medium (DMEM; GIBCO) supplemented with antibiotics

and 10% fetal bovine serum (FBS), and stimulated with 50–100 ng/ml murine TPO (PeproTech) during at least 5 days. For functional assays, the cell population was enriched in mature megakaryocytes either by using a 1.5%/3% BSA gradient under gravity (1 × *g*) for 45 min or by cell sorting using CD41 staining after 4–5 days of culture in the presence of TPO. Proplatelet formation assays were performed essentially as described previously (Bluteau et al., 2014).

Protein Analysis and Immunofluorescence

For immunodetection in protein lysates, proteins were separated on SDS-PAGE, transferred to nitrocellulose membranes (BioRad), and probed using specific primary antibodies against Cdk1 (Santa Cruz Biotechnology; 1:500) and vinculin (Sigma; 1:3,000) as a loading control. For immunofluorescence, cells were fixed with 4% paraformaldehyde in PBS for 10 min at 37°C, permeabilized with PBS-Triton 0.15% for 2 min at 37°C, blocked with 3% BSA, and subsequently incubated 1–3 hr with the primary antibody against Aurora B (Abcam; 1:200) or α-tubulin (Sigma; 1:2,000). Matching secondary antibodies with different Alexa dyes (488, 594, 647; Molecular Probes) and DAPI (Prolong Gold antifade; Invitrogen) were used for depiction of the nuclei. Image acquisition was performed using either a confocal ultra-spectral microscope (Leica TCS-SP5) or a Leica DMI fluorescence 6000B microscope.

Time-Lapse Microscopy

Cells were transduced with lentiviruses or retroviruses encoding histone H2B-GFP, lamin A-CFP (a gift from V. Andrés, CNIC, Madrid), and geminin-mCherry (Abe et al., 2013). Transduced cells were then plated on eight-well glass-bottom dishes (Ibidi) embedded in methylcellulose containing Iscove's modified Dulbecco's medium with 2% FBS and 100 ng/ml murine TPO, to minimize cell movement. Time-lapse acquisition was performed with a Leica DMI 6000B microscope equipped with a 63×/1.5 N.A. objective lens or DeltaVision RT imaging system (Applied Precision; IX70/71; Olympus) equipped with a Plan Apochromatic 40×/1.42 N.A. objective lens, and maintained at 37°C in a humidified CO_2 chamber. Images were acquired every 7 min for up to 10 days. Quantitative analysis was performed with ImageJ software.

DNA Fiber Assay

For the analysis of DNA replication in stretched DNA fibers, cells were processed using a protocol modified from Neelsen et al., 2013. Essentially, cells were incubated in presence of 50 μM CldU (5-clorodeoxyuridine) for 2 hr and pulsed for 30 min with 250 μM IdU (5-iododeoxyuridine). One drop containing 500–700 cells was placed on a microscope slide and cells were lysed with the addition of 10 μl lysis buffer (0.5% SDS, Tris [pH 7.4], EDTA 50 mM) for 6 min at room temperature. Slides were tilted at a 10°–15° angle to allow the DNA suspension to run slowly down the slide. Slides were air-dried and fixed in 3:1 v/v methanol:acetic acid. Following DNA denaturation with 2.5 M HCl for 30 min, DNA fibers were washed and blocked with PBS, 1% BSA, 0.1% Triton X-100, and incubated with primary antibodies against CldU and IdU (Abcam and Becton Dickinson; 1:100). Matching secondary antibodies conjugated to Alexa dyes (488, 594, 647) were used for signal depiction. Single-stranded DNA (ssDNA) was stained with a specific antibody (anti-ssDNA mouse monoclonal IgG2a; Millipore) to ensure the analysis of individual fibers. Image acquisition was performed using a Leica DMI fluorescence 6000B microscope. At least 500 replication tracks containing green signal were scored in each condition, and the percentage of re-replication events (yellow tracks) in the total population of green tracks was analyzed.

Statistical Analysis

Statistical analysis was carried out using Prism 5 (GraphPad). All statistical tests were performed using two-sided, unpaired Student's t tests, or the Fisher's exact test. Data with $p < 0.05$ were considered statistically significant.

SUPPLEMENTAL INFORMATION

Supplemental Information includes Supplemental Experimental Procedures and five figures and can be found with this article online at http://dx.doi.org/10.1016/j.devcel.2014.12.015.

AUTHOR CONTRIBUTIONS

M.T. performed most cellular and mouse experiments. M. Maroto helped with the quantification of histological samples. M.T., S.R.-A., and J.M. performed re-replication analyses in stretched DNA fibers. C.E.S, D.S., and M.B. generated the *Cdk1*(lox) allele and S.O. generated the Katushka allele. M. Malumbres conceived and supervised the project. M.T. and M. Malumbres analyzed the data and wrote the manuscript.

ACKNOWLEDGMENTS

We are fully indebted to V. Andrés (CNIC, Madrid, Spain) and A. Miyawaki (RIKEN, Saitama, Japan) for reagents. We thank Ana Pérez for technical help, Lola Martínez and Diego Megías (CNIO) for help with cytometry and microscopy analysis, members of the Comparative Pathology and Transgenic Units of the CNIO for excellent technical support, and Sara Leceta and Sheila Rueda for help with animal management. We also thank Miguel Torres and Guadalupe Sabio (CNIC) for help with blood counters. M.T. received a fellowship from the Foundation La Caixa. This work was funded by grants from the Foundation Ramón Areces, Spanish Ministry of Economy and Competitiveness (MINECO; SAF2012-38215 to M.Malumbres, SAF2010-18765 to S.O., and BFU2010-21467 and CSD2007-00015 to J.M.), Red Temática CellSYS (BFU2014-52125-REDT) and Red Consolider OncoBIO (SAF2014-57791-REDC), the OncoCycle Programme (S2010/BMD-2470 to M. Malumbres and M.B.) from the Comunidad de Madrid, and the European Union Seventh Framework Programme (MitoSys project; HEALTH-F5-2010-241548 to M. Malumbres).

Received: July 7, 2014
Revised: October 31, 2014
Accepted: December 17, 2014
Published: January 26, 2015

REFERENCES

Abe, T., Sakaue-Sawano, A., Kiyonari, H., Shioi, G., Inoue, K., Horiuchi, T., Nakao, K., Miyawaki, A., Aizawa, S., and Fujimori, T. (2013). Visualization of cell cycle in mouse embryos with Fucci2 reporter directed by Rosa26 promoter. Development *140*, 237–246.

Arias, E.E., and Walter, J.C. (2007). Strength in numbers: preventing rereplication via multiple mechanisms in eukaryotic cells. Genes Dev. *21*, 497–518.

Berthet, C., Aleem, E., Coppola, V., Tessarollo, L., and Kaldis, P. (2003). Cdk2 knockout mice are viable. Curr. Biol. *13*, 1775–1785.

Bluteau, D., Balduini, A., Balayn, N., Currao, M., Nurden, P., Deswarte, C., Leverger, G., Noris, P., Perrotta, S., Solary, E., et al. (2014). Thrombocytopenia-associated mutations in the ANKRD26 regulatory region induce MAPK hyperactivation. J. Clin. Invest. *124*, 580–591.

Broek, D., Bartlett, R., Crawford, K., and Nurse, P. (1991). Involvement of p34cdc2 in establishing the dependency of S phase on mitosis. Nature *349*, 388–393.

Calvi, B.R., Lilly, M.A., and Spradling, A.C. (1998). Cell cycle control of chorion gene amplification. Genes Dev. *12*, 734–744.

Claycomb, J.M., Benasutti, M., Bosco, G., Fenger, D.D., and Orr-Weaver, T.L. (2004). Gene amplification as a developmental strategy: isolation of two developmental amplicons in Drosophila. Dev. Cell *6*, 145–155.

Dahmann, C., Diffley, J.F., and Nasmyth, K.A. (1995). S-phase-promoting cyclin-dependent kinases prevent re-replication by inhibiting the transition of replication origins to a pre-replicative state. Curr. Biol. *5*, 1257–1269.

Davoli, T., and de Lange, T. (2011). The causes and consequences of polyploidy in normal development and cancer. Annu. Rev. Cell Dev. Biol. *27*, 585–610.

Diéguez-Hurtado, R., Martín, J., Martínez-Corral, I., Martínez, M.D., Megías, D., Olmeda, D., and Ortega, S. (2011). A Cre-reporter transgenic mouse expressing the far-red fluorescent protein Katushka. Genesis *49*, 36–45.

Diril, M.K., Ratnacaram, C.K., Padmakumar, V.C., Du, T., Wasser, M., Coppola, V., Tessarollo, L., and Kaldis, P. (2012). Cyclin-dependent kinase 1 (Cdk1) is essential for cell division and suppression of DNA re-replication but not for liver regeneration. Proc. Natl. Acad. Sci. USA *109*, 3826–3831.

Dorn, E.S., Chastain, P.D., 2nd, Hall, J.R., and Cook, J.G. (2009). Analysis of re-replication from deregulated origin licensing by DNA fiber spreading. Nucleic Acids Res. *37*, 60–69.

Eckly, A., Heijnen, H., Pertuy, F., Geerts, W., Proamer, F., Rinckel, J.Y., Léon, C., Lanza, F., and Gachet, C. (2014). Biogenesis of the demarcation membrane system (DMS) in megakaryocytes. Blood *123*, 921–930.

Edgar, B.A., and Orr-Weaver, T.L. (2001). Endoreplication cell cycles: more for less. Cell *105*, 297–306.

Edgar, B.A., Zielke, N., and Gutierrez, C. (2014). Endocycles: a recurrent evolutionary innovation for post-mitotic cell growth. Nat. Rev. Mol. Cell Biol. *15*, 197–210.

Fernández-Miranda, G., Trakala, M., Martín, J., Escobar, B., González, A., Ghyselinck, N.B., Ortega, S., Cañamero, M., Pérez de Castro, I., and Malumbres, M. (2011). Genetic disruption of aurora B uncovers an essential role for aurora C during early mammalian development. Development *138*, 2661–2672.

Gao, Y., Smith, E., Ker, E., Campbell, P., Cheng, E.C., Zou, S., Lin, S., Wang, L., Halene, S., and Krause, D.S. (2012). Role of RhoA-specific guanine exchange factors in regulation of endomitosis in megakaryocytes. Dev. Cell *22*, 573–584.

García-Higuera, I., Manchado, E., Dubus, P., Cañamero, M., Méndez, J., Moreno, S., and Malumbres, M. (2008). Genomic stability and tumour suppression by the APC/C cofactor Cdh1. Nat. Cell Biol. *10*, 802–811.

Geddis, A.E., Fox, N.E., Tkachenko, E., and Kaushansky, K. (2007). Endomitotic megakaryocytes that form a bipolar spindle exhibit cleavage furrow ingression followed by furrow regression. Cell Cycle *6*, 455–460.

Gupta, S. (2000). Hepatic polyploidy and liver growth control. Semin. Cancer Biol. *10*, 161–171.

Hassel, C., Zhang, B., Dixon, M., and Calvi, B.R. (2014). Induction of endocycles represses apoptosis independently of differentiation and predisposes cells to genome instability. Development *141*, 112–123.

Hochegger, H., Dejsuphong, D., Sonoda, E., Saberi, A., Rajendra, E., Kirk, J., Hunt, T., and Takeda, S. (2007). An essential role for Cdk1 in S phase control is revealed via chemical genetics in vertebrate cells. J. Cell Biol. *178*, 257–268.

Josefsson, E.C., James, C., Henley, K.J., Debrincat, M.A., Rogers, K.L., Dowling, M.R., White, M.J., Kruse, E.A., Lane, R.M., Ellis, S., et al. (2011). Megakaryocytes possess a functional intrinsic apoptosis pathway that must be restrained to survive and produce platelets. J. Exp. Med. *208*, 2017–2031.

Kaushansky, K. (2008). Historical review: megakaryopoiesis and thrombopoiesis. Blood *111*, 981–986.

Krause, D.S., and Crispino, J.D. (2013). Molecular pathways: induction of polyploidy as a novel differentiation therapy for leukemia. Clin. Cancer Res. *19*, 6084–6088.

Lordier, L., Jalil, A., Aurade, F., Larbret, F., Larghero, J., Debili, N., Vainchenker, W., and Chang, Y. (2008). Megakaryocyte endomitosis is a failure of late cytokinesis related to defects in the contractile ring and Rho/Rock signaling. Blood *112*, 3164–3174.

Lordier, L., Chang, Y., Jalil, A., Aurade, F., Garçon, L., Lécluse, Y., Larbret, F., Kawashima, T., Kitamura, T., Larghero, J., et al. (2010). Aurora B is dispensable for megakaryocyte polyploidization, but contributes to the endomitotic process. Blood *116*, 2345–2355.

Lordier, L., Bluteau, D., Jalil, A., Legrand, C., Pan, J., Rameau, P., Jouni, D., Bluteau, O., Mercher, T., Leon, C., et al. (2012). RUNX1-induced silencing of non-muscle myosin heavy chain IIB contributes to megakaryocyte polyploidization. Nat. Commun. *3*, 717.

Machlus, K.R., and Italiano, J.E., Jr. (2013). The incredible journey: From megakaryocyte development to platelet formation. J. Cell Biol. *201*, 785–796.

Malumbres, M., and Barbacid, M. (2009). Cell cycle, CDKs and cancer: a changing paradigm. Nat. Rev. Cancer *9*, 153–166.

Malumbres, M., Harlow, E., Hunt, T., Hunter, T., Lahti, J.M., Manning, G., Morgan, D.O., Tsai, L.H., and Wolgemuth, D.J. (2009). Cyclin-dependent kinases: a family portrait. Nat. Cell Biol. *11*, 1275–1276.

Manchado, E., Guillamot, M., de Cárcer, G., Eguren, M., Trickey, M., García-Higuera, I., Moreno, S., Yamano, H., Cañamero, M., and Malumbres, M. (2010). Targeting mitotic exit leads to tumor regression in vivo: modulation by Cdk1, Mastl, and the PP2A/B55α,δ phosphatase. Cancer Cell *18*, 641–654.

Mehrotra, S., Maqbool, S.B., Kolpakas, A., Murnen, K., and Calvi, B.R. (2008). Endocycling cells do not apoptose in response to DNA rereplication genotoxic stress. Genes Dev. *22*, 3158–3171.

Moore, J.D., Kirk, J.A., and Hunt, T. (2003). Unmasking the S-phase-promoting potential of cyclin B1. Science *300*, 987–990.

Neelsen, K.J., Zanini, I.M., Mijic, S., Herrador, R., Zellweger, R., Ray Chaudhuri, A., Creavin, K.D., Blow, J.J., and Lopes, M. (2013). Deregulated origin licensing leads to chromosomal breaks by rereplication of a gapped DNA template. Genes Dev. *27*, 2537–2542.

Nezi, L., and Musacchio, A. (2009). Sister chromatid tension and the spindle assembly checkpoint. Curr. Opin. Cell Biol. *21*, 785–795.

Ortega, S., Prieto, I., Odajima, J., Martín, A., Dubus, P., Sotillo, R., Barbero, J.L., Malumbres, M., and Barbacid, M. (2003). Cyclin-dependent kinase 2 is essential for meiosis but not for mitotic cell division in mice. Nat. Genet. *35*, 25–31.

Pandit, S.K., Westendorp, B., and de Bruin, A. (2013). Physiological significance of polyploidization in mammalian cells. Trends Cell Biol. *23*, 556–566.

Papadantonakis, N., Makitalo, M., McCrann, D.J., Liu, K., Nguyen, H.G., Martin, G., Patel-Hett, S., Italiano, J.E., and Ravid, K. (2008). Direct visualization of the endomitotic cell cycle in living megakaryocytes: differential patterns in low and high ploidy cells. Cell Cycle *7*, 2352–2356.

Peters, J.M. (2006). The anaphase promoting complex/cyclosome: a machine designed to destroy. Nat. Rev. Mol. Cell Biol. *7*, 644–656.

Ravid, K., Lu, J., Zimmet, J.M., and Jones, M.R. (2002). Roads to polyploidy: the megakaryocyte example. J. Cell. Physiol. *190*, 7–20.

Sakaue-Sawano, A., Kurokawa, H., Morimura, T., Hanyu, A., Hama, H., Osawa, H., Kashiwagi, S., Fukami, K., Miyata, T., Miyoshi, H., et al. (2008). Visualizing spatiotemporal dynamics of multicellular cell-cycle progression. Cell *132*, 487–498.

Sakaue-Sawano, A., Hoshida, T., Yo, M., Takahashi, R., Ohtawa, K., Arai, T., Takahashi, E., Noda, S., Miyoshi, H., and Miyawaki, A. (2013). Visualizing developmentally programmed endoreplication in mammals using ubiquitin oscillators. Development *140*, 4624–4632.

Santamaría, D., Barrière, C., Cerqueira, A., Hunt, S., Tardy, C., Newton, K., Cáceres, J.F., Dubus, P., Malumbres, M., and Barbacid, M. (2007). Cdk1 is sufficient to drive the mammalian cell cycle. Nature *448*, 811–815.

Sher, N., Von Stetina, J.R., Bell, G.W., Matsuura, S., Ravid, K., and Orr-Weaver, T.L. (2013). Fundamental differences in endoreplication in mammals and Drosophila revealed by analysis of endocycling and endomitotic cells. Proc. Natl. Acad. Sci. USA *110*, 9368–9373.

Thon, J.N., and Italiano, J.E., Jr. (2012). Does size matter in platelet production? Blood *120*, 1552–1561.

Tiedt, R., Schomber, T., Hao-Shen, H., and Skoda, R.C. (2007). Pf4-Cre transgenic mice allow the generation of lineage-restricted gene knockouts for studying megakaryocyte and platelet function in vivo. Blood *109*, 1503–1506.

Trakala, M., Fernández-Miranda, G., Pérez de Castro, I., Heeschen, C., and Malumbres, M. (2013). Aurora B prevents delayed DNA replication and premature mitotic exit by repressing p21(Cip1). Cell Cycle *12*, 1030–1041.

Ullah, Z., Kohn, M.J., Yagi, R., Vassilev, L.T., and DePamphilis, M.L. (2008). Differentiation of trophoblast stem cells into giant cells is triggered by p57/Kip2 inhibition of CDK1 activity. Genes Dev. *22*, 3024–3036.

Vitrat, N., Cohen-Solal, K., Pique, C., Le Couedic, J.P., Norol, F., Larsen, A.K., Katz, A., Vainchenker, W., and Debili, N. (1998). Endomitosis of human megakaryocytes are due to abortive mitosis. Blood *91*, 3711–3723.

Wen, Q., Leung, C., Huang, Z., Small, S., Reddi, A.L., Licht, J.D., and Crispino, J.D. (2009). Survivin is not required for the endomitotic cell cycle of megakaryocytes. Blood *114*, 153–156.

Wen, Q., Goldenson, B., Silver, S.J., Schenone, M., Dancik, V., Huang, Z., Wang, L.Z., Lewis, T.A., An, W.F., Li, X., et al. (2012). Identification of regulators of polyploidization presents therapeutic targets for treatment of AMKL. Cell *150*, 575–589.

Zhang, Y., Wang, Z., and Ravid, K. (1996). The cell cycle in polyploid megakaryocytes is associated with reduced activity of cyclin B1-dependent cdc2 kinase. J. Biol. Chem. *271*, 4266–4272.

Zhu, Y. (2004). A model for CDK2 in maintaining genomic stability. Cell Cycle *3*, 1358–1362.

Zielke, N., Edgar, B.A., and DePamphilis, M.L. (2013). Endoreplication. Cold Spring Harb. Perspect. Biol. *5*, a012948.

Zimmet, J., and Ravid, K. (2000). Polyploidy: occurrence in nature, mechanisms, and significance for the megakaryocyte-platelet system. Exp. Hematol. *28*, 3–16.

Developmental Cell

Supplemental Information

Functional Reprogramming of Polyploidization in Megakaryocytes

Marianna Trakala, Sara Rodríguez-Acebes, María Maroto, Catherine E. Symonds, David Santamaría, Sagrario Ortega, Mariano Barbacid, Juan Méndez, and Marcos Malumbres

Supplementary Figures

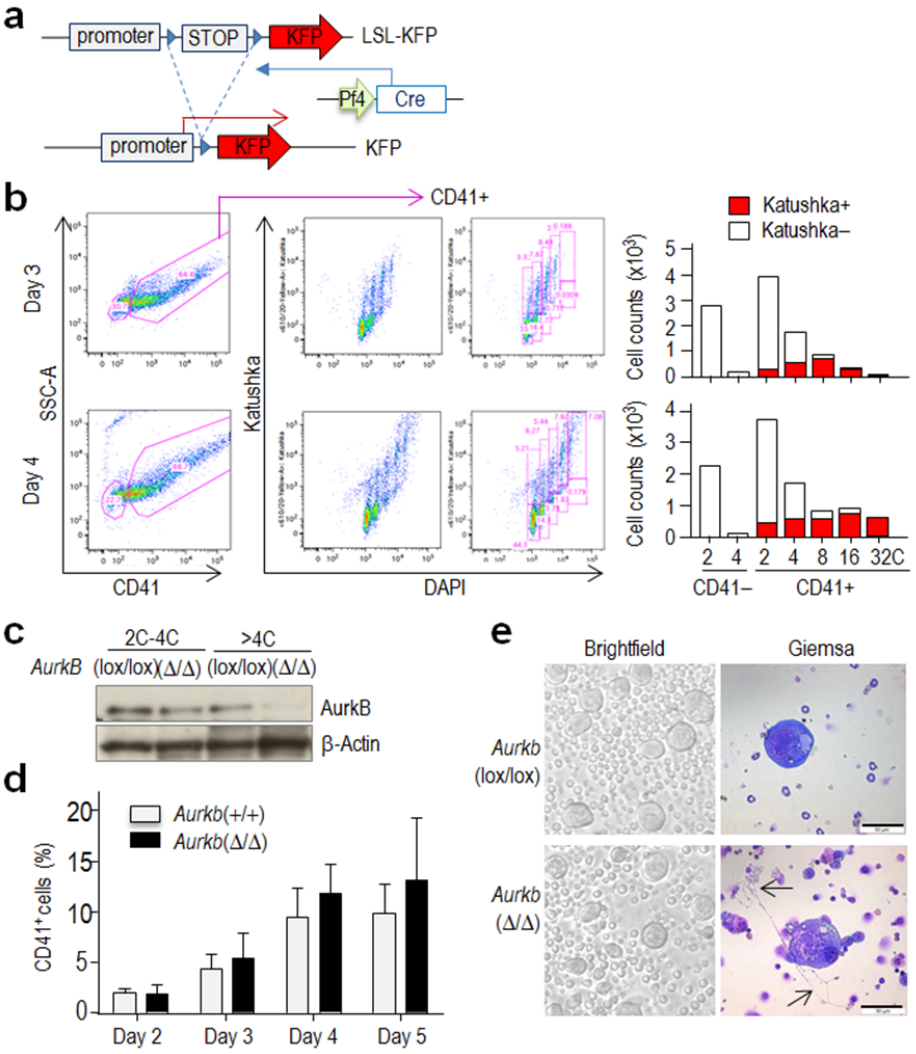

Figure S1. Genetic tools for megakaryocyte-specific ablation of cell cycle regulators (related to Figure 1). a) Schematic representation of the LoxP-STOP-LoxP (LSL)- Katushka-fluorescent protein (KFP) reporter. **b)** Validation of Pf4-Cre activity using the LSL-KFP reporter in polyploid megakaryocytes. Bone marrow progenitors (lin-) carrying the Pf4-Cre and LSL-KFP alleles were stimulated in vitro in the presence of TPO and Cre activity was monitored by analyzing KFP. As shown in the histograms, three or four days after TPO treatment, most polyploid (≥8C) megakaryocytes express KFP as a consequence of the Cre-dependent excision of the STOP cassette, wheras less than half of the 4C cells and a very reduced percentage of 2C cells are positive for this marker. **c)** Immunodetection of Aurora B in low ploidy (2C-4C) or high ploidy (≥4C) megakaryocytes (CD41-positive cells) in the bone marrow from the indicated genotypes. β-actin was used as a loading control**. d)** The cumulative percentage of CD41+ cells (mean ± SEM) is similar in *Aurkb*(Δ/Δ) and *Aurkb*(+/+) cultures (P>0.05; Student's t-test) on days 2-5 after TPO stimulation of E13.5 fetal liver cells. **e**) Representative images of fetal liver-derived megakaryocytes 5 days after stimulation with TPO showing similar number and appearance of large megakaryocytes. Pro-platelet formation occurs in the absence of Aurora B as indicated by arrows in right lower panel. Scale bars, 50 μm.

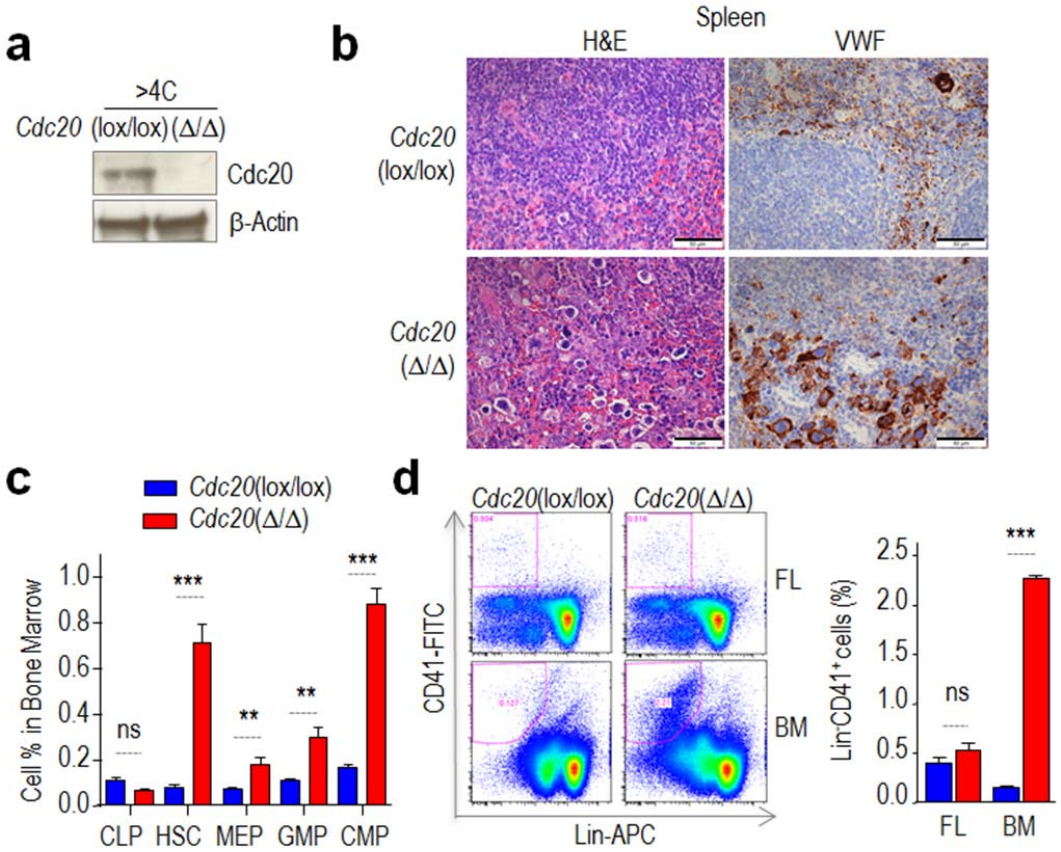

Figure S2. High levels of hematopoietic progenitors as a consequence of severe thrombocytopenia in *Cdc20*(Δ/Δ) mice (related to Figure 2). **a)** Immunodetection of Cdc20 in high ploidy (≥4C) megakaryocytes (CD41-positive cells) in the bone marrow from the indicated genotypes. β-actin was used as a loading control. **b)** Hematoxylin and eosin (H&E) staining and immunohistochemical staining for Von Willebrand Factor (VWF) in spleen sections from in 8-12 week-old animals with the indicated genotypes. Scale bars, 50 μm. **c)** Percentage of hematopoietic progenitors from the bone marrow of *Cdc20*(Δ/Δ) and control in 8-12 week-old mice after FACS analysis with specific markers (see Extended Experimental Protocols). HSCs, Hematopoetic stem cells; CLPs, common lympoid progenitors; CMPs, Common myeloid progenitors; MEPs, megakaryocyte-erythrocyte progenitors; GMPs, granulocyte-macrophage progenitors. n=5 mice per group **d)** Representative data and quantification of the CD41+ population after FACS analysis of total fetal liver (FL) cells from E12.5 embryos or cells from the bone marrow (BM) of 8 week-old mice. n=3 mice per group. All graphs show mean ± SEM. Statistics were performed by Student's t-test; ns, not significant; **, p<0.01; ***, p<0.001.

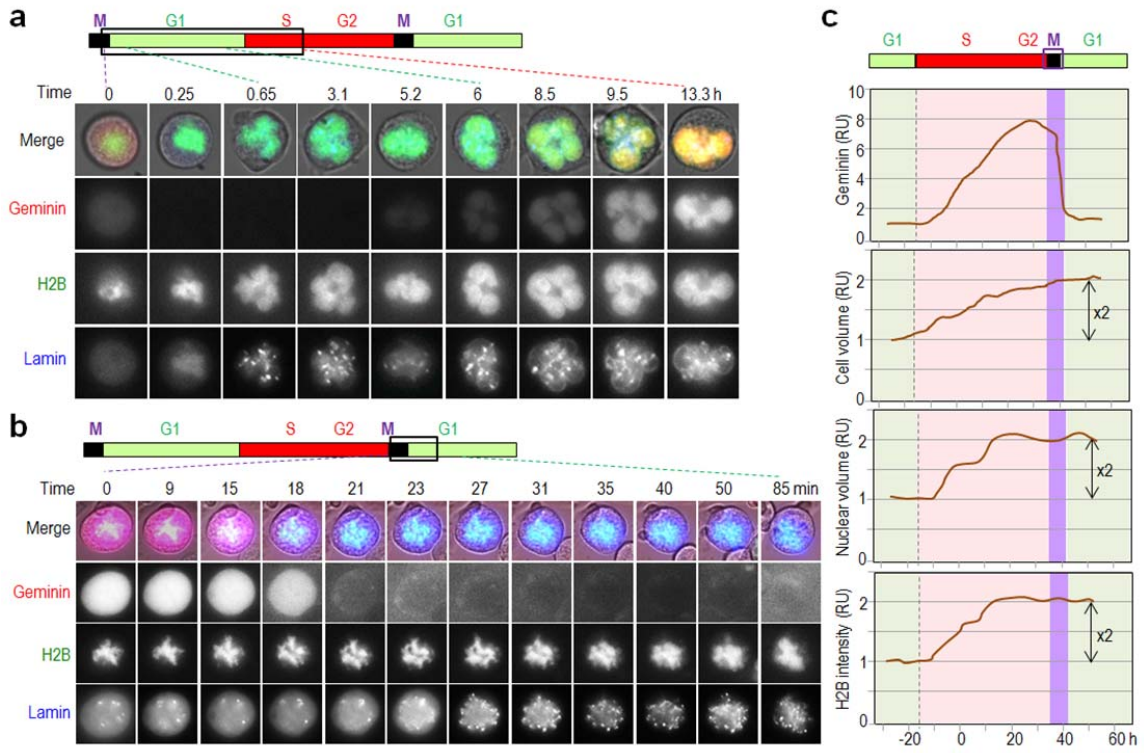

Figure S3. Time-lapse microscopy of endomitotic polyploidization in vitro (related to Figure 4). Time-lapse microscopy of bone marrow derived megakaryocytes stably expressing histone-GFP (H2B-GFP; green), lamin-CFP (blue) and geminin-mCherry (Red). **a**) Representative pictures of an individual cell during the G1-S transition. Time=0 represents the exit from endomitosis characterized by degradation of geminin (red), decondensation of chromatin (green) and nuclear envelope reformation (blue). During G1-phase cells are negative for geminin and start to express it upon G1-S transition. During S-phase the increase in nuclear volume can be appreciated. **b**) Representative images of an individual cell during endomitosis. Endomitosis is characterized by chromatin condensation and the absence of nuclear envelope, resulting in the pancellular distribution of geminin, which is exclusively nuclear during interphase. In late stages of endomitosis, geminin is degraded and nuclear envelope reforms and chromatin decondenses. **c**) Plots showing the relative units of geminin-mCherry mean fluorescent intensity, H2B-GFP mean fluorescent intensity, and nuclear and cellular volume during the endomitotic cell cycle in a representative megakaryocyte. The purple frame depicts endomitosis (M).

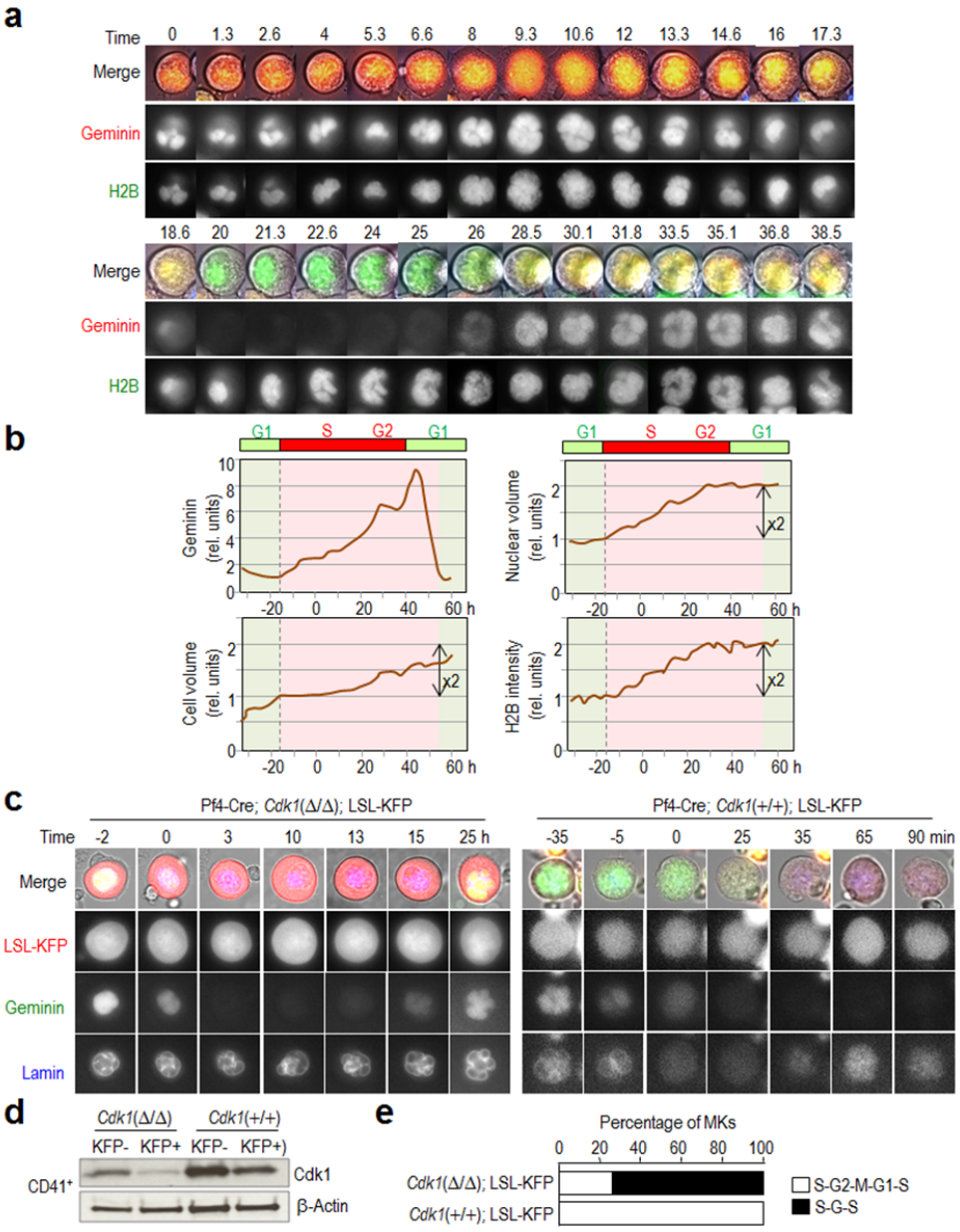

Figure S4. Time-lapse microscopy of endocycling Cdk1-deficient cells in vitro (related to Figure 4). **a**) Time-lapse microscopy of bone marrow derived *Cdk1*(Δ/Δ) megakaryocytes stably expressing histone-GFP (H2B-GFP; green) and geminin-mCherry (Red). Time=0 was arbitrarily set. Geminin is degraded (at ~17-18 h) in the absence of mitosis; i.e. without nuclear envelope breakdown (as detected by the absence of nuclear-to-cytoplasmic redistribution of geminin, and absence of DNA condensation). During G1 cells are negative for geminin and start to express it at the G1-S transition. **b)** Plots showing the relative units of geminin-mCherry mean fluorescent intensity, H2B-GFP mean fluorescent intensity, and nuclear and cellular volume during the endoreplication process in a representative *Cdk1*(Δ/Δ) megakaryocyte. **c)** Time-lapse microscopy of megakaryocytes expressing geminin (green), lamin (blue) and KFP (red). **d)** Immunodetection of Cdk1 in CD41-positive cells isolated from the bone marrow of Pf4-Cre; *Cdk1*(Δ/Δ); LSL-KFP or Pf4-Cre; *Cdk1*(+/+); LSL-KFP animals. KFP-positive (+) or negative (-) cells were isolated by flow cytometry. β-actin was used as a loading control. **e)** Quantification from (c); most KFP-positive Cdk1-null megakaryocytes (n=12) undergo S-G-S (endocycles) whereas all (n=14) KFP-positive control megakaryocytes display typical endomitotic cycles (M, endomitosis).

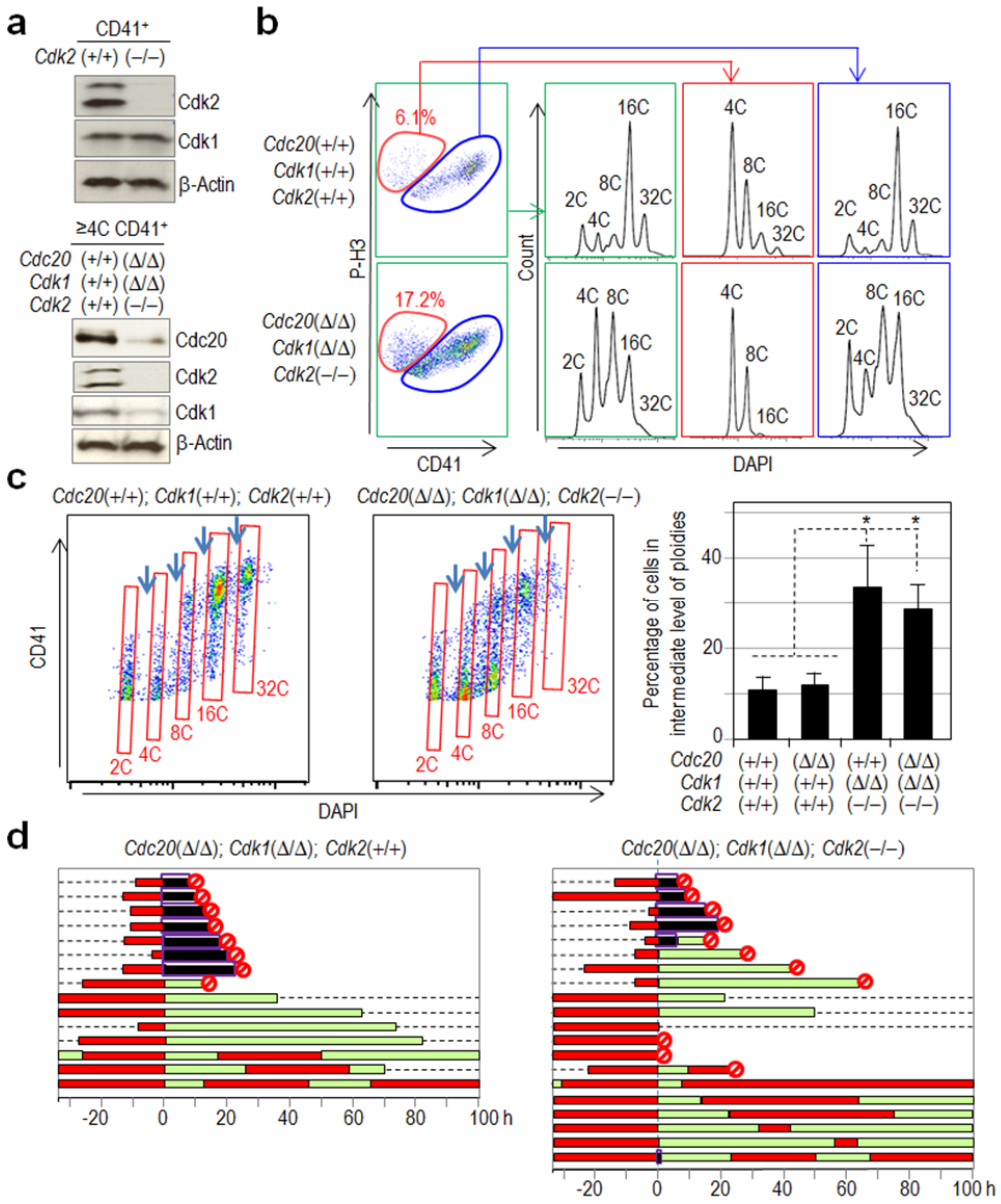

Figure S5. Polyploidization and cell fate of megakaryocytes with Cdk1 and Cdk2-mutant alleles in a Cdc20-null background (related to Figure 6). **a**) Immunodetection of the indicated proteins in total megakaryocytes (CD41-positive cells) or high ploidy (≥4C) CD41-positive cells from the bone marrow. β-actin was used as a loading control. **b)** Analysis of mitosis (phospho-histone H3; P-H3 signal) in CD41+ bone marrow cells from wild-type or *Cdc20*(Δ/Δ); *Cdk1*(Δ/Δ); *Cdk2*(–/–) mice. The ploidy profiles of the whole CD41+ population (green), P-H3-positive (red) or P-H3-negative (blue) cells are shown. **c)** Quantification of cells with intermediate levels of ploidy (arrows). Three animals per genotype were analyzed. Data indicate mean ± SEM; *, p<0.5; Student's t-test. **d)** Cell fate of individual *Cdc20*(Δ/Δ); *Cdk1*(Δ/Δ) [left] or *Cdc20*(Δ/Δ); *Cdk1*(Δ/Δ); *Cdk2*(–/–) [right] bone marrow-derived megakaryocytes recorded by time-lapse microscopy. Cells stably expressed histone H2B-GFP, lamin-CFP and geminin-mCherry. Red and green boxes represent S-G2 (geminin^{high}) or G1 (geminin^{low}) phases, respectively. Endomitosis, prolonged in all cases as a consequence of lack of Cdc20, is illustrated as a black box surrounded by a purple frame and red circles represent cell death.

Supplemental Experimental Procedures

Mouse colony and histological analysis

For genotyping the different alleles from the mouse models tail DNA was isolated from 3-4-week old mice and PCR amplification reactions were performed using the oligonucleotides described in the original manuscripts (Dieguez-Hurtado et al., 2011; Fernandez-Miranda et al., 2011; Manchado et al., 2010; Ortega et al., 2003; Tiedt et al., 2007) Cdk1 mutant mice were genotyped using oligonucleotides Fw: 5'-GAGATGTAGGATGACTCAGTG-3' and Rv: 5'-TAGCTTATCTACCTCAGCCTG-3', which generate amplification bands of 650 bp (wild-type allele) or 800 bp (mutant allele). The following amplification conditions were used: 94ºC during 4 minutes followed by 35 cycles of DNA denaturalization at 94ºC during 30 seconds, primer annealing at 60ºC during 30 seconds and polymerase extension at 72ºC during 60 seconds ending with a single elongation cycle of 7 minutes at 72ºC. For histology sections, sterna and spleens were fixed overnight in 4% formalin. Sterna were then decalcified in Decalcifier I solution (Surgipath) for 2 hours. Samples were dehydrated in 70% ethanol and processed by the Histopathology Facility Unit at CNIO for 3-5 μm longitudinal paraffin sections, hematoxylin and eosin staining, or immunohistochemistry.

Isolation of bone marrow or fetal liver cells and cytometry

For bone marrow derived megakaryocytes, the tibia and femur were isolated from 8-12 week old mice and bone marrow was flushed out by the addition of ice-cold PBS buffer (PBS, 0.5% BSA, 5mM EDTA) through the lumen of the bone. Marrow was mechanically disrupted to achieve single cell suspension followed by filtering through a 40μm nylon strainer to remove bone debris and subsequently subjected to erythrocyte lysis. For red blood cell lysis the bone marrow cell pellet from 1 mouse was resuspended in 1 ml of ACK lysis buffer (150 mM ammonium chloride, 1 mM potassium bicarbonate, 0.1 mM EDTA) and incubated for 1.5 min on ice. The lysis was stopped by the addition of 10 ml PBS buffer and cells were centrifuged at 200*g* for 10 min. Cells were counted and subjected either directly to surface antigen staining for flow cytometry analysis or to lineage depletion with the Miltenyi MACS (magnetic cell shorting) Hematopoietic Progenitor (Stem) Cell Enrichment Set, according to manufacturer's protocol. For fetal liver derived megakaryocytes, cells were obtained from whole livers recovered from mouse fetuses between embryonic days 12.5 and 13.5. Single-cell suspensions were prepared by successive passage through 19-, 22-, and 25-gauge needles.

To determine mouse bone marrow hematopoietic stem cells (HSC; Lin^- $IL7R^-$ $c\text{-}kit^+$ Sca^+), common lymphoid progenitors (CLP; Lin^- $IL7R^+$ $c\text{-}kit^+$ Sca^+), common myeloid progenitors (CMP; Lin^- $IL7R^-$ $c\text{-}kit^+$ Sca^- $CD34^+$, $Fc\gamma R^{low}$), megakaryocyte, erythroid progenitors (MEP; Lin^- $IL7R^-$ $c\text{-}kit^+$ Sca^- $CD34^-$, $Fc\gamma R^{low}$), granulocyte, macrophage progenitors (GMP; Lin^- $IL7R^-$ $c\text{-}kit^+$ Sca^- $CD34^+$, $Fc\gamma R^{high}$), and megakaryocyte progenitors (Lin^- $CD41^+$) cells, freshly obtained BM cells were stained with phycoerythrin (PE) anti-CD34 (BD Biosciences), Alexa Fluor 488 anti- IL7Ra, peridinin chlorophyll Protein Cyanin 5.5 (PerCP-Cy 5.5 anti–Sca-1, allophycocyanin-H7 (APC-H7) anti-cKit (BD

Biosciences), phycoerythrin-cyanin 7 (PE-Cy7) anti-FcγR (BD Biosciences) and allophycocyanin (APC) -labeled lineage cell detection cocktail (BD Biosciences). Flow cytometric analysis was performed with a FACS-Canto flow cytometer or a LSRII flow cytometer (BD Biosciences) and FlowJo Version 8.8.7 software (TreeStar).

Virus preparation

For preparation of viruses, low passage 293T cells were transfected with the vector of interest and the three packaging vectors expressing gag, pol and rev proteins necessary for virion production as well the envelope protein vsvg (Tiscornia et al., 2006). 48 h post transfection supernatants containing viruses were collected and concentrated by centrigufation at 19.400 rpm for 2 hours at 20 ºC. Viral pellets were resuspended in 1x HBSS. This viral preparation is of in vitro grade quality. For retroviruses, 293T cells were transfected with the vector of interest and the packaging vector PCL-Eco. Supernatants were collected and 48 hours post transfection. Packaging vectors are a gift from Dr. Verma´s lab. Transduction of primary megakaryocytes and Lin- bone marrow cells were performed by adding 10 μl of concentrated virus (stock 10^9 viral particles per mL) per million of cells (MOI 10) for 12 h.

Supplemental References

Tiscornia, G., Singer, O., and Verma, I.M. (2006). Production and purification of lentiviral vectors. Nat Protoc 1, 241-245.

MCB
Journals.ASM.org

Genetic Characterization of the Role of the Cip/Kip Family of Proteins as Cyclin-Dependent Kinase Inhibitors and Assembly Factors

Antonio Cerqueira,[a]* Alberto Martín,[a]* Catherine E. Symonds,[a] Junko Odajima,[a]* Pierre Dubus,[b] Mariano Barbacid,[a] David Santamaría[a]

Experimental Oncology, Molecular Oncology Program, Centro Nacional de Investigaciones Oncológicas (CNIO), Madrid, Spain[a]; Université Bordeaux, Bordeaux, France[b]

The Cip/Kip family, namely, $p21^{Cip1}$, $p27^{Kip1}$, and $p57^{Kip2}$, are stoichiometric cyclin-dependent kinase inhibitors (CKIs). Paradoxically, they have been proposed to also act as positive regulators of Cdk4/6-cyclin D by stabilizing these heterodimers. Loss of $p21^{Cip1}$ and $p27^{Kip1}$ reduces Cdk4/6-cyclin D complexes, although with limited phenotypic consequences compared to the embryonic lethality of Cdk4/6 or triple cyclin D deficiency. This milder phenotype was attributed to Cdk2 compensatory mechanisms. To address this controversy using a genetic approach, we generated *Cdk2*$^{-/-}$ *p21*$^{-/-}$ *p27*$^{-/-}$ mice. Triple-knockout mouse embryonic fibroblasts (MEFs) displayed minimal levels of D-type cyclins and Cdk4/6-cyclin D complexes. $p57^{Kip2}$ downregulation in the absence of $p21^{Cip1}$ and $p27^{Kip1}$ aggravated this phenotype, yet MEFs lacking all Cip/Kip proteins exhibited increased retinoblastoma phosphorylation, together with enhanced proliferation and transformation capacity. *In vivo*, *Cdk2* ablation induced partial perinatal lethality in *p21*$^{-/-}$ *p27*$^{-/-}$ mice, suggesting partial Cdk2-dependent compensation. However, *Cdk2*$^{-/-}$ *p21*$^{-/-}$ *p27*$^{-/-}$ survivors displayed all phenotypes described for *p27*$^{-/-}$ mice, including organomegalia and pituitary tumors. Thus, Cip/Kip deficiency does not impair interphasic Cdk activity even in the absence of Cdk2, suggesting that their Cdk-cyclin assembly function is dispensable for homeostatic control in most cell types.

Extracellular signals that promote cell proliferation are transduced via growth factor receptor-associated protein kinases and a plethora of downstream signaling pathways. A significant fraction of these pathways converges on the regulation of the cell cycle by the cyclin-dependent kinases (Cdks) (1). In a simplified scenario, Cdk activity is controlled not only by cyclin binding but also by interaction with Ink4 and the Cip/Kip family of cyclin-dependent kinase inhibitors (CKIs). However, formation of Cdk4-cyclin D functional heterodimers is largely inefficient, suggesting the requirement of assembly factors for stable complex formation (2). Indeed, Cip/Kip inhibitors have been implicated in the assembly of functional Cdk4/6-cyclin D complexes as well as on their import to the nucleus (3–5). Remarkably, some reports suggest that the Cdk4/6-cyclin D-Cip/Kip complexes remain active, since the majority of the Cdk4/6-cyclin D kinase activity in culture cells is found to be associated with Cip/Kip inhibitors (3, 6). Moreover, Cdk4/6-cyclin D complexes are nearly undetectable in extracts from mouse embryonic fibroblasts (MEFs), liver cells, or thymocytes from mice devoid of $p21^{Cip1}$ and $p27^{Kip1}$ (4). In this scenario, the unopposed activity of Cdk2 has been proposed to compensate for the severe reduction in Cdk4/6-cyclin D levels caused by Cip/Kip deficiency (4, 5). Together, these observations led to the hypothesis that Cip/Kip inhibitors are assembly factors for the formation of Cdk4/6-cyclin D complexes and that a substantial fraction of these ternary complexes retains catalytic activity (7).

However, other reports have described that Cdk4/6-cyclin D complexes, albeit reduced and short-lived, readily form in the absence of $p21^{Cip1}$ and $p27^{Kip1}$ either in asynchronous cultures (8, 9) or during cell cycle reentry from quiescence (5). Even though the levels of Cdk4/6-cyclin D complexes were undetectable by Western blot analysis, cells remained sensitive to $p16^{Ink4a}$, suggesting the existence of active Cdk4/6-cyclin D complexes (4). In addition, there are different reports regarding the extent of inhibition caused by Cip/Kip binding on the catalytic activity of Cdk4-cyclin D complexes (3–6, 8, 10, 11). These observations have led to the hypothesis that $p21^{Cip1}$ and $p27^{Kip1}$ are dispensable for the formation of active Cdk4/6-cyclin D complexes and that their binding results in stable but inactive ternary complexes (9).

To evaluate *in vivo* the impact of Cip/Kip deficiency on the formation and stability of Cdk4/6-cyclin D complexes, we set up crosses to eliminate Cdk2 in mice doubly deficient for $p21^{Cip1}$ and $p27^{Kip1}$. We have analyzed the proliferation and transformation properties of *Cdk2*$^{-/-}$ *p21*$^{-/-}$ *p27*$^{-/-}$ MEFs as well as evaluated the impact of Cdk2 elimination in the phenotypes found in $p21^{Cip1}$- and $p27^{Kip1}$-deficient mice. The findings reported here support the notion that the Cip/Kip function as pan-Cdk inhibitors prevails over their role as Cdk4/6-cyclin assembly factors. As a consequence *p21*$^{-/-}$ *p27*$^{-/-}$ cells and mice display various hyperproliferative phenotypes that are all preserved even in the concomitant absence of Cdk2.

MATERIALS AND METHODS

Mouse strains. *Cdk2*$^{-/-}$, *p21*$^{-/-}$, and *p27*$^{-/-}$ mice have been previously described (12). Tissue samples were fixed in 10% buffered formalin for 24 h and embedded in paraffin, and 3-μm sections were analyzed after stain-

Received 3 September 2013 Returned for modification 16 October 2013
Accepted 25 January 2014
Published ahead of print 10 February 2014

Address correspondence to David Santamaría, dsantamaria@cnio.es.

* Present address: Antonio Cerqueira, Progenitor Labs, Stevenage Bioscience Catalyst, Stevenage, United Kingdom; Alberto Martín, Departamento de Bioquímica, Instituto de Investigaciones Biomédicas Alberto Sols, CSIC-UAM, Madrid, Spain; Junko Odajima, Department of Cancer Biology, Dana-Farber Cancer Institute, Boston, Massachusetts, USA.

A.C. and A.M. contributed equally to this work.

doi:10.1128/MCB.01163-13

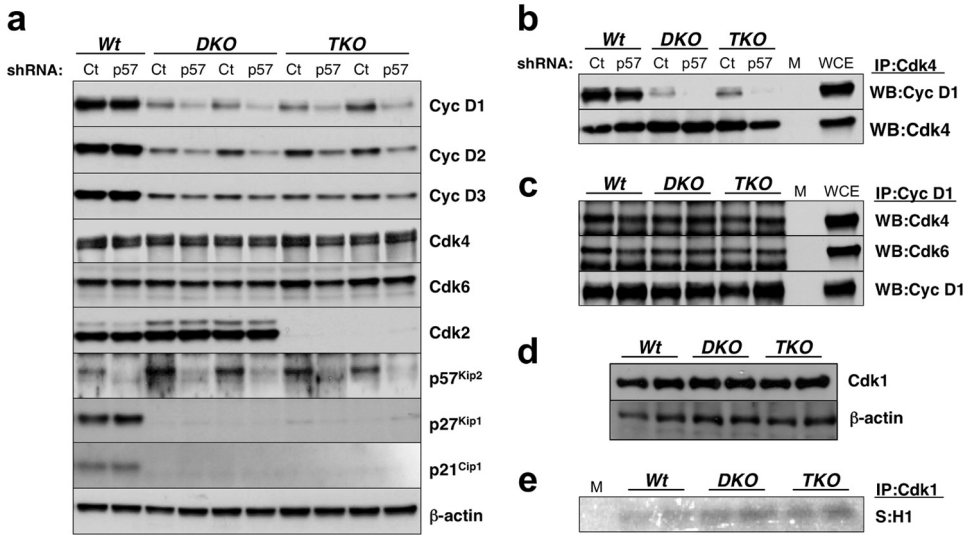

FIG 1 Stability of Cdk-cyclin D complexes in the absence of Cip/Kip inhibitors. (a) Early-passage primary MEFs were infected with lentiviral particles expressing either an shRNA against $p57^{Kip2}$ (p57) or a scramble control (Ct). Protein extracts were prepared, and the levels of a panel of cell cycle regulators were analyzed by immunoblotting with antibodies elicited against the indicated proteins. Expression of β-actin served as a loading control. Results from two independent MEF cultures are shown for $p21^{-/-}$ $p27^{-/-}$ (DKO) and $Cdk2^{-/-}$ $p21^{-/-}$ $p27^{-/-}$ (TKO) mice. Cyc, cyclin. (b) Wild-type, $p21^{-/-}$ $p27^{-/-}$ (DKO), and $Cdk2^{-/-}$ $p21^{-/-}$ $p27^{-/-}$ (TKO) primary MEFs were infected with lentiviral particles expressing either an shRNA against $p57^{Kip2}$ (p57) or a scramble control (Ct). Exponentially growing cells were used to prepare whole-cell extracts, and the amount of Cdk4-cyclin D complexes was estimated by coprecipitation of cyclin D1 with anti-Cdk4 antibodies. The levels of Cdk4, used as a loading control, are shown. WB, Western blotting. (c) The amount of starting whole-cell extract from both $p21^{-/-}$ $p27^{-/-}$ (DKO) and $Cdk2^{-/-}$ $p21^{-/-}$ $p27^{-/-}$ (TKO) MEFs was augmented to equal the cyclin D1 levels in the wild-type controls. The amount of Cdk4 (top) and Cdk6 (middle) that was coimmunoprecipitated with cyclin D1 antibodies was detected by Western blotting. Cyclin D1 levels (bottom) are shown to demonstrate equal estimation of the amount of starting material. Results from two independent MEF cultures are shown. (d) Western blotting of Cdk1 protein levels in whole-cell extracts from wild-type, $p21^{-/-}$ $p27^{-/-}$ (DKO), and $Cdk2^{-/-}$ $p21^{-/-}$ $p27^{-/-}$ (TKO) MEFs. Expression of β-actin, which served as a loading control, is shown. Results from two independent MEF cultures are shown. (e) *In vitro* kinase activity associated with Cdk1 immunoprecipitates obtained from wild-type, $p21^{-/-}$ $p27^{-/-}$ (DKO), and $Cdk2^{-/-}$ $p21^{-/-}$ $p27^{-/-}$ (TKO) MEFs. Histone H1 was used as the substrate (S). Results from two independent MEF cultures are shown. Lanes WCE, whole-cell extract at a 1:10 dilution before immunoprecipitation (IP); lanes M, mock immunoprecipitate.

ing with hematoxylin-eosin (H&E). Histopathological analysis of $p21^{-/-}$ $p27^{-/-}$ $Cdk2^{-/-}$ embryonic day 18.5 (E18.5) embryos and paired controls was performed by thorough inspection of H&E-stained serially sectioned specimens ($n = 7$). The mice used in this study have been maintained in a mixed 129/SvJ × C57BL/6J background according to the *Guide for the Care and Use of Laboratory Animals* (13) and in accordance with the Spanish Animal Protection Law (RD1201/2005) and the European Directive (86/609/CEE) established by the European Union to regulate animal care standards. Animal experiments received approval from the CNIO ethical committee (CEUCA code 032-03).

Cell culture assays. MEFs were isolated from E13.5 embryos and propagated according to standard protocols. No less than 10 independent early-passage primary MEF preparations per genotype were used to perform the experiments. Proliferation assays and S-phase entry analysis were carried out with primary MEFs as previously described (14). Knockdown of $p57^{Kip2}$ was mediated with lentiviral Mission short hairpin RNA (shRNA) plasmids (Sigma no. SHGLY-NM_009876.2) according to the manufacturer's instructions. After infection, cells were selected with 2 μg/ml puromycin for 48 h. Focus formation assays were performed as described previously (12).

Protein analysis. Protein lysates were prepared and used for immunoblotting as previously described (12). Antibodies against the following proteins were used: Cdk2 (M2; Santa Cruz), Cdk4 (C22; Santa Cruz), Cdk6 (our own rabbit polyclonal antibodies), cyclin D1 (DCS6; Neo Markers), cyclin D2 (M-20; Santa Cruz), cyclin D3 (DCS22; Cell Signaling), cyclin A2 (H432; Santa Cruz), $p21^{Kip1}$ (C19; Santa Cruz), $p27^{Kip1}$ (catalog no. 610242; BD Transduction Laboratories), $p57^{Kip2}$ (catalog no. P0357; Sigma), β-actin (clone AC15; Sigma), and phospho-specific antibody to phosphorylated residues S807/811 of the retinoblastoma protein (pRb; catalog no. 9308; Cell Signaling). As secondary antibodies, peroxidase-conjugated IgG (Dako) was used, followed by chemiluminescence detection (ECL kit; Amersham).

RESULTS

Formation of Cdk4/6-cyclin D complexes in the absence of Cip/Kip proteins. As illustrated in Fig. 1a, $p21^{-/-}$ $p27^{-/-}$ MEFs displayed a significant reduction in the overall cellular levels of the three D-type cyclins and retained 5 to 10% of the cyclin D levels present in wild-type cells. To determine whether the third member of the Cip/Kip family of CKIs, $p57^{Kip2}$, may contribute to the stabilization of active Cdk-cyclin D complexes, we generated lentiviral particles expressing an shRNA against $p57^{Kip2}$ and analyzed its impact on cyclin D levels in wild-type and $p21^{-/-}$ $p27^{-/-}$ double mutant MEFs. $p57^{Kip2}$ depletion in $p21^{-/-}$ $p27^{-/-}$ MEFs, irrespective of the presence or absence of Cdk2, caused a further decrease in the levels of expression of cyclins D1 and D2 and a moderate decrease in the case of cyclin D3 (Fig. 1a). Interestingly, we observed a negligible impact in wild-type controls. As expected, the reduction in the overall cellular levels of the D-type cyclins resulted in a similar decrease in the amount of Cdk4-cyclin D complexes, as determined by immunoprecipitation of the kinase subunit (Fig. 1b). These results suggest that $p57^{Kip2}$ contributes to the stabilization of Cdk4/6-cyclin D complexes, at least in the absence of $p21^{Cip1}$ and $p27^{Kip1}$.

In order to determine whether the Cip/Kip proteins are essential for the formation or stabilization of the Cdk4-cyclin D1 complexes, we matched the total levels of cyclin D1 in the immuno-

precipitation assays by scaling up 9-fold the amount of the starting whole-cell extract from *p21*$^{-/-}$ *p27*$^{-/-}$ and *Cdk2*$^{-/-}$ *p21*$^{-/-}$ *p27*$^{-/-}$ MEFs. Technical difficulties owing to the much greater decrease of cyclin D levels upon *p57*^{Kip2} knockdown prevented us from including this condition in the assay. Nevertheless, under these conditions we compensated for the diminution in the overall levels of cyclin D1 caused by the concomitant absence of p21^{Cip1} and p27^{Kip1}, and when immunoprecipitated, it pulled down an equal amount of Cdk4 and Cdk6 in all genotypes (Fig. 1c). This result is in good agreement with those described in a previous report suggesting that free D-type cyclins rapidly associate with their Cdk4/6 cognate catalytic subunits (9), thus suggesting that the kinetics of this association is independent of the Cip/Kip proteins, limiting their role to the stabilization of preformed binary complexes.

Finally, we investigated the expression levels and activity of Cdk1, as it is a likely candidate to compensate for the reduced activity of interphase Cdks. We found that whereas the expression levels of Cdk1 are comparable in MEFs from mice of the three genotypes, its activity is increased in *p21*$^{-/-}$ *p27*$^{-/-}$ and *Cdk2*$^{-/-}$ *p21*$^{-/-}$ *p27*$^{-/-}$ cells compared to its activity in the wild-type controls (Fig. 1d and e).

Proliferation properties of *Cdk2*$^{-/-}$ MEFs devoid of Cip/Kip proteins. To determine the consequences of the reduced levels of Cdk4/6-cyclin D complexes on cell cycle progression in the absence of Cip/Kip proteins, we examined the proliferation properties of primary *p21*$^{-/-}$ *p27*$^{-/-}$ MEFs. In parallel, we also analyzed the proliferation of *Cdk2*$^{-/-}$ *p21*$^{-/-}$ *p27*$^{-/-}$ cells since it has been proposed that in the absence of both Cip/Kip inhibitors Cdk2 could play a compensatory role by functionally replacing Cdk4/6-cyclin D complexes (4, 5). As illustrated in Fig. 2a, *p21*$^{-/-}$ *p27*$^{-/-}$ cells reproducibly displayed a growth advantage compared to the wild-type controls under standard serum conditions. This growth advantage was even more evident when cells were grown in 2% serum, since under these conditions wild-type cells failed to thrive, whereas MEFs devoid of p21^{Cip1} and p27^{Kip1} managed to proliferate (Fig. 2b). Similar results were obtained in primary MEFs also devoid of Cdk2, indicating that Cdk2 activity is not responsible for driving cell proliferation in the absence of these inhibitors. Finally, we assessed the effect of knocking down the third member of the Cip/Kip family of CIKs, p57^{Kip2}. shRNA-mediated depletion of p57^{Kip2} caused a reduction in the proliferative rate compared to that for MEFs infected with control shRNA, particularly under low-serum conditions (Fig. 2). This result, together with the further decrease in the levels of the three D-type cyclins (Fig. 1a), suggests that p57^{Kip2} may function as a Cdk4/6-cyclin D assembly factor in MEFs, at least in the absence of p21^{Cip1} and p27^{Kip1}, yet the proliferation rate observed in the concomitant absence of the three CKIs, even in a Cdk2-null background, was consistently higher than that of wild-type MEFs (Fig. 2). Altogether, these experiments suggest that in terms of cell proliferation, the function of the Cip/Kip proteins as Cdk inhibitors prevails over their putative role as Cdk4/6-cyclin D assembly factors in MEFs. The lack of an effect observed upon ablation of Cdk2 expression suggests that the cell cycle inhibitory activity of the Cip/Kip proteins must be mediated through another Cdk, possibly Cdk1, or by a Cdk-independent mechanism.

Next, we focused our attention on cell cycle reentry, a process particularly reliant on Cdk activity (14). As illustrated in Fig. 3a, serum-starved *p21*$^{-/-}$ *p27*$^{-/-}$ MEFs entered S phase with a higher

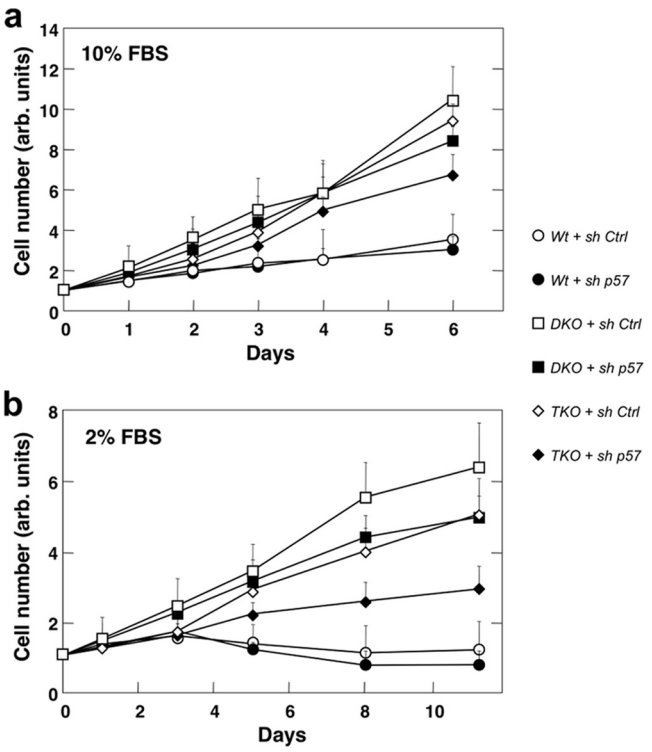

FIG 2 Proliferation of primary MEFs in the absence of Cip/Kip inhibitors. (a) The proliferation of wild-type (Wt), *p21*$^{-/-}$ *p27*$^{-/-}$ (DKO), and *Cdk2*$^{-/-}$ *p21*$^{-/-}$ *p27*$^{-/-}$ (TKO) primary MEFs in 10% fetal bovine serum (FBS) was assessed upon infection with lentiviral particles expressing an shRNA against *p57*^{Kip2} (sh p57) or a scramble control (sh Ctrl). Data are shown as means ± SDs ($n = 3$). (b) Same as for panel a, but MEFs were maintained under limiting serum conditions (2% fetal bovine serum). arb., arbitrary.

efficiency than wild-type control cells. Similar results were obtained with *Cdk2*$^{-/-}$ *p21*$^{-/-}$ *p27*$^{-/-}$ MEFs (Fig. 3a). Accordingly, the phosphorylation of the Ser807/811 residues of the retinoblastoma protein (Rb) and the appearance of cyclin A2 were detected at earlier time points compared to the times of appearance for the wild-type controls (Fig. 3b). Importantly, when the G_0 exit was assessed in p57^{Kip2}-depleted cells, the higher efficiency observed in both *p21*$^{-/-}$ *p27*$^{-/-}$ and *Cdk2*$^{-/-}$ *p21*$^{-/-}$ *p27*$^{-/-}$ MEFs was no longer evident (Fig. 3c), thus adding further evidence that p57^{Kip2} may participate in the assembly of Cdk4/6-cyclin complexes in MEFs. This role of p57^{Kip2}, which appears to be negligible in wild-type cells (Fig. 1a), becomes evident in the absence of p21^{Cip1} and p27^{Kip1}, particularly under conditions that are more dependent on interphase Cdk activity, such as during proliferation under low-serum conditions or during exit from quiescence.

Cellular transformation in the absence of p21^{Cip1} and p27^{Kip1}. To study the role of p21^{Cip1} and p27^{Kip1} in cellular transformation, we infected primary MEFs with retroviral particles expressing combinations of different oncogenes. Transformation was subsequently assessed by focus formation (Fig. 4a). Single H-*Ras*^{G12V} or *E1a* oncogenes did not significantly enhance transformation, irrespective of the genotype (data not shown). The maximal efficiency was achieved using concomitant expression of both oncoproteins. In this context, cells lacking p27^{Kip1} expression displayed a minor (15%) increase in their transformation ability compared to that for the wild-type controls. However, in-

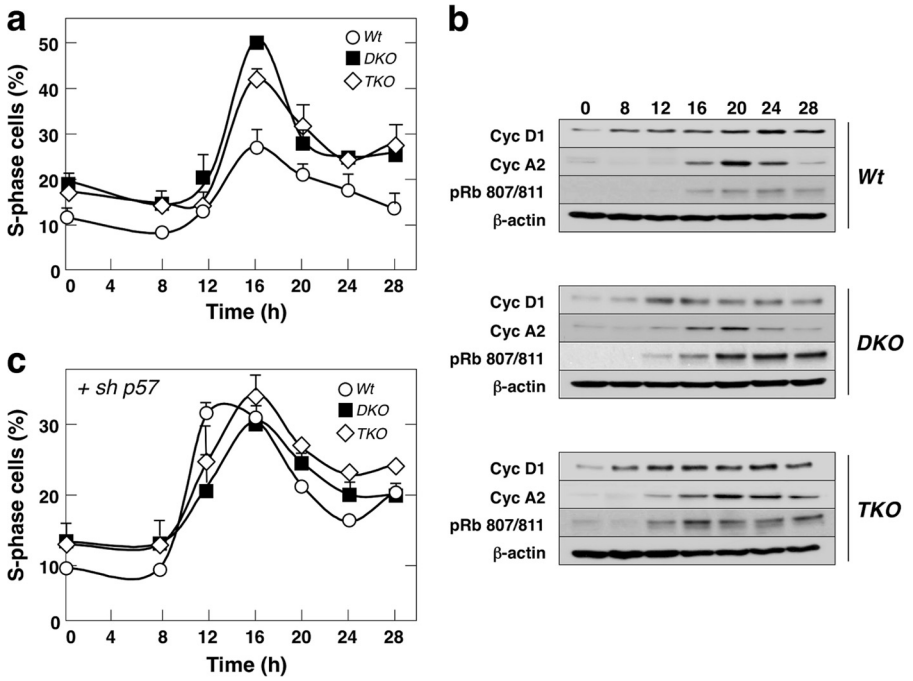

FIG 3 Role of Cip/Kip proteins in cell cycle reentry. (a) Percentage of wild-type (Wt), $p21^{-/-}$ $p27^{-/-}$ (DKO), and $Cdk2^{-/-}$ $p21^{-/-}$ $p27^{-/-}$ (TKO) primary MEFs in S phase at the indicated times following serum stimulation from quiescence. Data are shown as means ± SDs ($n = 3$). (b) Whole-cell extracts from cells for which the results are shown in panel a were prepared at the times (in hours) following serum stimulation from quiescence indicated above each lane. The presence of cyclin D1 and cyclin A2 and the phosphorylation of the Ser807/811 residues of the retinoblastoma protein (pRb) were detected by Western blotting. Expression of β-actin, which served as a loading control, is shown. (c) $p57^{Kip2}$ was depleted in wild-type, $p21^{-/-}$ $p27^{-/-}$ (DKO), and $Cdk2^{-/-}$ $p21^{-/-}$ $p27^{-/-}$ (TKO) primary MEFs by lentivirus-mediated shRNA delivery. Infected MEFs were subsequently made quiescent by serum deprivation. The percentage of S-phase cells at the indicated times (in hours) following serum stimulation from quiescence is shown. Data are shown as means ± SDs ($n = 3$).

fection of $p21^{-/-}$ MEFs or $p21^{-/-}$ $p27^{-/-}$ double mutant MEFs resulted in a 2-fold increase, indicating that $p21^{Cip1}$ and $p27^{Kip1}$ do not cooperate to prevent malignant transformation, at least *in vitro*. Interestingly, loss of Cdk2 expression had no effect on the ability of $p21^{-/-}$ $p27^{-/-}$ MEFs to become transformed by $H\text{-}Ras^{G12V}$ and E1a oncoproteins, indicating that Cdk2 does not compensate for the low levels of Cdk4/6-cyclin D complexes. Moreover, this also illustrates that Cdk2 does not play a role in promoting cell transformation. Finally, we submitted these cells to a standard 3T3 immortalization protocol. As expected, wild-type primary MEFs entered replicative senescence after a few passages, whereas $p21^{-/-}$ $p27^{-/-}$ cells bypassed the crisis period irrespective of their Cdk2 status (Fig. 4b).

Phenotypic characterization of $p21^{-/-}$ $p27^{-/-}$ $Cdk2^{-/-}$ mice. In order to determine whether Cdk2 might compensate for the reduced formation of Cdk4/6-cyclin D complexes *in vivo*, we crossed $p21^{-/-}$, $p27^{+/-}$, and $Cdk2^{+/-}$ mice and scored the resulting genotypes at weaning ($n = 439$). As shown in Table 1, all the possible genotypes matched the expected Mendelian ratio except for those carrying a single *Cdk2* allele (17.3% versus 25%; ratio, 0.69) or no *Cdk2* alleles (5.9% versus 12.5%; ratio, 0.47). Lethality did not appear to occur *in utero*, since all possible genotypes were present at the expected ratios when assayed during late embryogenesis (E18.5) (data not shown). We previously reported that *Cdk2* ablation in $p27^{-/-}$ mice did not result in increased mortality (15). Thus, the cause of death of $p21^{-/-}$ $p27^{-/-}$ $Cdk2^{-/-}$ neonates must be associated with $p21^{Cip1}$ deficiency. This postnatal lethality appears to result from insufficient overall interphase Cdk activity, since neonatal mortality was also observed in $p21^{-/-}$ $p27^{-/-}$ $Cdk2^{+/-}$ mice, albeit to a lesser extent (ratio of surviving mice at weaning, 0.69 versus 0.47). Previous studies using Cdk mutant mice have linked interphase Cdk deficiency with embryonic or neonatal lethality. For instance, mice lacking Cdk4 and Cdk2 died at birth due to cardiac abnormalities, and mice deficient for the three interphase Cdks, Cdk4, Cdk6, and Cdk2, died at midgestation primarily due to hematopoietic defects similar to those observed in Cdk4 and Cdk6 double mutant mice. Careful histopathological analysis in serial sections of E18.5 embryos failed to uncover obvious defects that could account for their postnatal lethality, including in those tissues affected by interphase Cdk deficiency, such as fetal hematopoietic organs and heart. Thus, the cause of death of $Cdk2^{-/-}$ $p21^{-/-}$ $p27^{-/-}$ mice before weaning remains unknown.

We next focused our attention on the characterization of adult mice. Ablation of *p27* alleles results in increased body size, especially in females (12, 16, 17). This and other phenotypic changes associated with $p27^{-/-}$ deficiency were mainly attributed to augmented Cdk activity. Thus, we examined whether the reduced levels of Cdk4/6-cyclin D activity in $p21^{-/-}$ $p27^{-/-}$ mice might revert the phenotypic changes seen in $p27^{-/-}$ animals. Parallel experiments were carried out in $p21^{-/-}$ $p27^{-/-}$ $Cdk2^{-/-}$ mice, which displayed even lower levels of interphase Cdk activity. To this end, we monitored body weight changes from weaning. As represented in Fig. 5, all compound strains devoid of $p27^{Kip1}$ displayed elevated body weights, regardless of their intrinsic Cdk activity. Moreover, all organs with the exception of liver showed

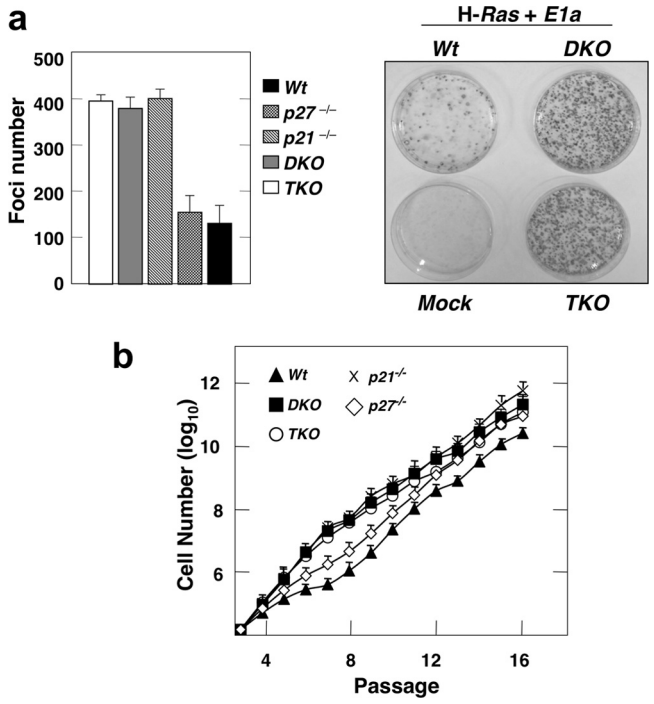

FIG 4 Cip/Kip factors and cellular transformation. (a) Equal amounts of wild-type, $p21^{-/-}$, $p27^{-/-}$, as well as compound mutant $p21^{-/-}$ $p27^{-/-}$ (DKO) and $Cdk2^{-/-}$ $p21^{-/-}$ $p27^{-/-}$ (TKO) MEFs were infected with retroviral particles coexpressing H-*Ras* and *E1a* oncogenes. (Left) At 3 weeks after infection, the number of detectable foci was scored for the different genotypes. Data are shown as means ± SDs ($n = 3$). (Right) A representative image upon crystal violet staining is shown. (b) Immortalization of wild-type, $p21^{-/-}$ and $p27^{-/-}$ single-knockout, $p21^{-/-}$ $p27^{-/-}$ (DKO), and $Cdk2^{-/-}$ $p21^{-/-}$ $p27^{-/-}$ (TKO) primary MEFs following a classical 3T3 protocol. Data are shown as means ± SDs ($n = 3$).

an increased weight (12, 16–18). Pathological examination of livers from $p21^{-/-}$ $p27^{-/-}$ $Cdk2^{-/-}$ mice showed that they did not display detectable architectural or cytological defects, yet we found that the hepatocyte density was consistently reduced compared to that in age-matched $p21^{-/-}$ $p27^{-/-}$ controls (Fig. 5b and c). Since the livers of newborn $p21^{-/-}$ $p27^{-/-}$ $Cdk2^{-/-}$ mice were phenotypically normal (data not shown), the liver hypoplasia may progressively arise during postnatal development. Taken together, these results suggest that the majority of tissues and cell types in adult mice tolerate the combined deficiency of $p21^{Cip1}$ and $p27^{Kip1}$.

Finally, we examined whether these $p21^{-/-}$ $p27^{-/-}$ and/or $p21^{-/-}$ $p27^{-/-}$ $Cdk2^{-/-}$ mutant mice may show defects in the proliferation of insulin-producing pancreatic β-cells, which are exquisitely dependent on the presence of Cdk4 activity for proper proliferation (18–20). All mutant mice were normoglycemic during the course of the study (data not shown). Unlike $Cdk4^{-/-}$ animals, histological analysis of pancreatic sections failed to detect either quantitative or qualitative variations in β-cell islets in any of the tested mice ($n = 21$) (data not shown). These results illustrate that *in vivo*, the decline in Cdk4/6-cyclin D complexes caused by ablation of the $p21^{Cip1}$ and $p27^{Kip1}$ alleles is not sufficient to phenocopy the defects caused by the loss of Cdk4 activity.

Tumorigenesis in $p21^{-/-}$ $p27^{-/-}$ mice. Finally, we analyzed the tumor spectrum of $p21^{-/-}$ $p27^{-/-}$ double-knockout mice. As previously reported, $p21^{Cip1}$-null mice developed a variety of spontaneous tumors at an average age of 16 months (21). $p27^{Kip1}$ deficiency resulted in the appearance of aggressive pituitary tumors, and all mice succumbed by 1 year of age (12, 16, 17). $p21^{Cip1}$ $p27^{Kip1}$-null animals died of pituitary tumors with a timing and pathology indistinguishable from those for the single mutant $p27^{-/-}$ controls, indicating that $p21^{Cip1}$ does not compensate for the absence of $p27^{Kip1}$ (Fig. 6). In contrast, the loss of $p27^{Kip1}$ appears to cooperate with the absence of $p21^{Cip1}$, at least in accelerating tumor development, since about a quarter of the $p21^{-/-}$ $p27^{-/-}$ mice displayed histiocytic sarcomas at a time (10 months) when none of the $p21^{-/-}$ animals had developed such tumors (21–23) (Table 2). We also recorded the appearance of new pathologies in $p21^{-/-}$ $p27^{-/-}$ double mutant mice that were absent in either single-knockout strain. They included a panel of precancerous lesions, such as gastric hyperplasia, pancreatic intraepithelial neoplasia (PanIN), and myeloproliferation (Table 2). The premature death associated with $p27^{Kip1}$ deficiency prevented us from studying the evolution of these lesions.

DISCUSSION

In our hands, primary $p21^{-/-}$ $p27^{-/-}$ MEFs displayed enhanced proliferative properties compared to the wild-type controls (Fig. 2). Interestingly, and in agreement with previous reports, these cells retained only 5% of the cellular Cdk4-cyclin D1 complexes found in the wild-type controls. As a side note, this is equivalent to the fraction of $p27^{Kip1}$ that appears to be tyrosine phosphorylated—and presumably noninhibitory—in asynchronous cells (23), suggesting that a minor proportion of active Cdk4/6-cyclin D complexes suffices to support unperturbed proliferation. Importantly, the enhanced proliferative capacity observed in $p21^{-/-}$ $p27^{-/-}$ MEFs was also present in $Cdk2^{-/-}$ $p21^{-/-}$ $p27^{-/-}$ MEFs (Fig. 2), discarding the possibility that Cdk2 is the putative compensatory mechanism that has been postulated to ameliorate the proliferation of $p21^{-/-}$ $p27^{-/-}$ cells (4, 5). Altogether, these results suggest that in terms of cell proliferation, the Cip/Kip function as pan-Cdk inhibitors is overwhelmingly more relevant than their role as Cdk4/6-cyclin D assembly factors.

It has also been proposed that Cdk4/6-cyclin D complexes perform a relevant noncatalytic role to favor cell proliferation. According to this model, these complexes act as a molecular sink for Cip/Kip proteins, titrating them away from Cdk2 and therefore facilitating its subsequent activation (7). Indeed, no free $p27^{Kip1}$ can be detected *in vivo* (23). Cdk4/6 double-knockout cells have a lower proliferative capacity than wild-type controls (24). Interest-

TABLE 1 Influence of $p21^{Cip1}$, $p27^{Kip1}$, and Cdk2 deficiency on postnatal survival[a]

Genotype			Mendelian ratio[b] (%)	
Cdk2	*p21*	*p27*	Expected	Observed
+/+	−/−	+/−	12.5	18.7
+/+	−/−	−/−	12.5	11.6
+/−	−/−	+/−	25	31
+/−	−/−	−/−	25	17.3
−/−	−/−	+/−	12.5	15.5
−/−	−/−	−/−	12.5	5.9

[a] Data are for 439 mice.
[b] The expected and observed Mendelian ratios of the indicated genotypes were scored at weaning (postnatal day 21).

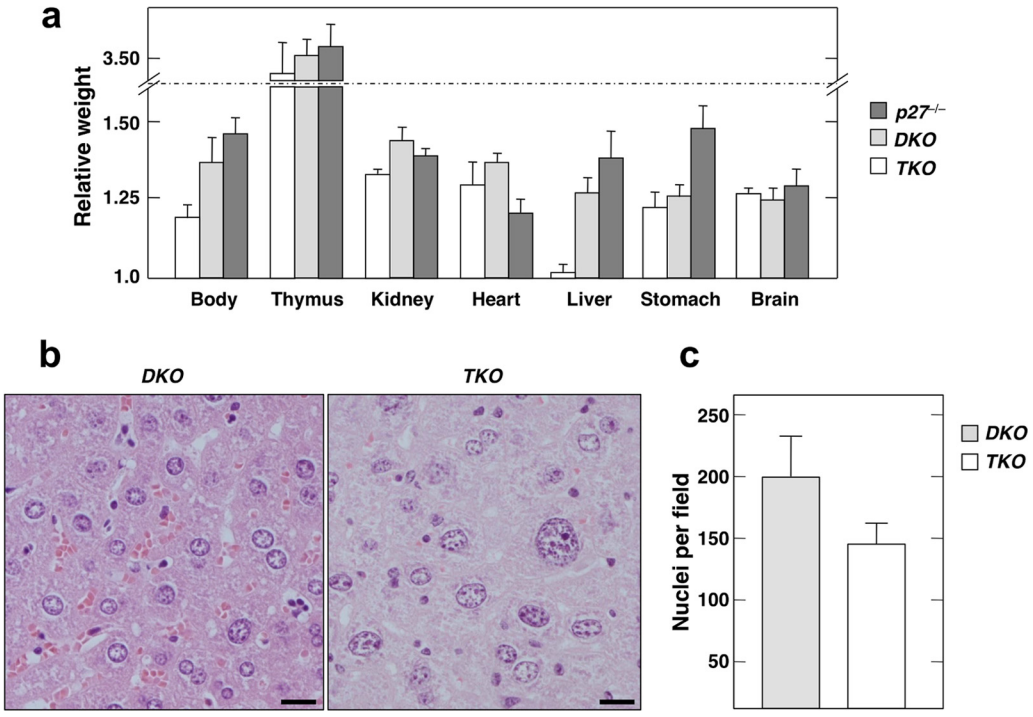

FIG 5 Influence of $p21^{Cip1}$ and $p27^{Kip1}$ deficiency in adult homeostasis. (a) Total body weight and the weight of the indicated individual organs of mice at 11 weeks of age. Values for $p27^{-/-}$, $p21^{-/-}$ $p27^{-/-}$ (DKO), and $Cdk2^{-/-}$ $p21^{-/-}$ $p27^{-/-}$ (TKO) mice normalized to those for wild-type controls of the same age are represented. Data are shown as means ± SDs ($n = 4$). (b) Representative images of hematoxylin-eosin-stained liver sections from 11-week-old $p21^{-/-}$ $p27^{-/-}$ (DKO) and $Cdk2^{-/-}$ $p21^{-/-}$ $p27^{-/-}$ (TKO) mice. Bars, 20 μm. (c) Quantification of the total number of hepatocytes in four randomly selected ×400 microscope fields of liver sections from $p21^{-/-}$ $p27^{-/-}$ (DKO) and $Cdk2^{-/-}$ $p21^{-/-}$ $p27^{-/-}$ (TKO) mice. Data are shown as means ± SDs ($n = 7$).

ingly, $p21^{-/-}$ $p27^{-/-}$ MEFs, which display a severe (20-fold) reduction of Cdk-cyclin D complexes, have the opposite phenotype. This suggests that in wild-type MEFs, the Cip/Kip titration function of Cdk4/6-cyclin D might prevail over their catalytic activity. Indeed, a cyclin D1 mutant that forms kinase-inactive complexes with Cdk4/6 efficiently rescues the developmental defects present in cyclin $D1^{-/-}$ mice (25). Although this could also be attributed to Cdk-independent functions of cyclin D1, we cannot rule out the possibility that in particular cellular contexts the sequestration function of Cdk4/6-cyclin D complexes is dominant over their catalytic activity.

We have also shown that $p57^{Kip2}$, the third component of the Cip/Kip family, participates *in vivo* in the stabilization of Cdk4-

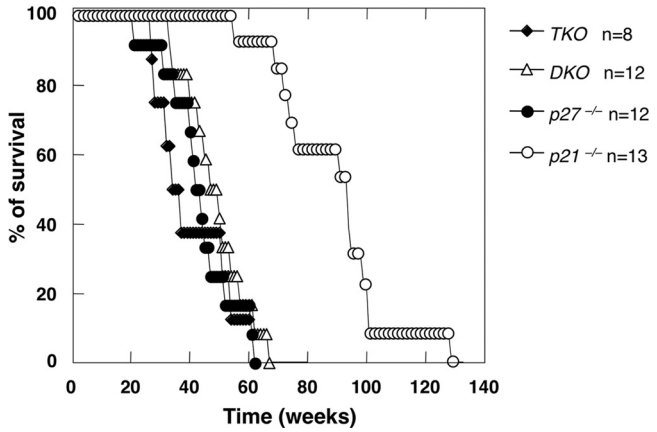

FIG 6 Cooperation between $p21^{Cip1}$ and $p27^{Kip1}$ tumor suppressors. Survival curve of $p21^{-/-}$, $p27^{-/-}$, $p21^{-/-}$ $p27^{-/-}$ (DKO), and $Cdk2^{-/-}$ $p21^{-/-}$ $p27^{-/-}$ (TKO) mice.

TABLE 2 Tumor susceptibility in mice lacking $p21^{Cip1}$ and $p27^{Kip1}$

Lesion type and lesion or pathology	% of mice that developed lesions or pathology[a]		
	$p21^{-/-}$ $p27^{-/-}$ mice ($n = 21$)	$p27^{-/-}$ mice ($n = 11$)	$p21^{-/-}$ mice ($n = 13$)
Hyperplasia/tumor-related lesions			
Gastric neuroendocrine hyperplasia	43	0	0
Gastric mucosa hyperplasia	57	0	0
Histiocytic sarcoma	24	0	0
Myeloproliferation	43	0	0
PanIN	10	0	0
Inflammation/non-tumor-related lesions			
Arteritis	14	0	0
Bone metaplasia	24	0	0
Chronic nephropathy	81	45	23
Chronic pancreatitis	29	0	0
Retinal dysplasia	38	19	0

[a] Animals were sacrificed at 10 months of age. Numbers are rounded up to the nearest digit.

cyclin D complexes, at least in the absence of $p21^{Cip1}$ and $p27^{Kip1}$. shRNA-mediated depletion of $p57^{Kip2}$ in *p21*$^{-/-}$ *p27*$^{-/-}$ MEFs caused a further reduction of Cdk4-cyclin D1 complexes, reaching levels undetectable by Western blotting (Fig. 1b), yet it is significant that upon $p57^{Kip2}$ depletion, *Cdk2*$^{-/-}$ *p21*$^{-/-}$ *p27*$^{-/-}$ MEFs exited G_0 with kinetics comparable to that of the wild-type controls. In this scenario, the Cdk1-cyclin D complexes that become detectable in the absence of Cdk4 (14) may functionally replace Cdk4/6-cyclin D complexes. This would imply that the assembly of Cdk1-cyclin D complexes does not require Cip/Kip proteins or may be facilitated by alternative assembly factors. In this respect, $p34^{Sei1}$ has been described to be an alternative Cdk-cyclin D assembly factor, particularly during quiescence exit (5). We believe that our *Cdk2*$^{-/-}$ *p21*$^{-/-}$ *p27*$^{-/-}$ mouse model may become a useful tool to elucidate whether indeed other assembly factors exist or if Cdk-cyclin D complexes can form *de novo*.

It is also possible that the required levels of Cdk-cyclin D complexes (and, therefore, the importance of their assembly factors) are cell type specific. Whereas *p21*$^{-/-}$ *p27*$^{-/-}$ mice reach adulthood with the expected Mendelian ratio, Cdk4/6 double-knockout (DKO) mice die *in utero* as a consequence of hematopoietic defects (24). This suggests that *in vivo*, redundant mechanisms or the inherent plasticity of the system may bypass the requirement for $p21^{Cip1}$ and $p27^{Kip1}$ proteins as Cdk4/6-cyclin D assembly factors in most cell types. We cannot rule out the possibility that this adaptation was facilitated in part by the use of germ line null alleles. For instance, whereas chronic deficiency of the retinoblastoma protein in MEFs allows adaptation and compensation among other family members, this is largely inefficient upon acute gene ablation (26). In any case, and in support of the functional redundancy model, we show here that $p57^{Kip2}$ stabilizes Cdk4-cyclin D1 in *p21*$^{-/-}$ *p27*$^{-/-}$ MEFs but not in wild-type controls (Fig. 1). In addition, others have demonstrated that a knockin of *p27*^{Kip1} expressed from the *p57*^{Kip2} promoter can rescue most of the developmental defects present in *p57*$^{-/-}$ mice, suggesting that they perform partially redundant roles *in vivo* (27). Interestingly, as described above, $p57^{Kip2}$ knockdown in *p21*$^{-/-}$ *p27*$^{-/-}$ MEFs caused an additional reduction of Cdk-cyclin complexes and affected their proliferation rate, which, nevertheless, remained higher than that of wild-type cells (Fig. 2b). Moreover, unlike single- and double-knockout strains, 53% of *Cdk2*$^{-/-}$ *p21*$^{-/-}$ *p27*$^{-/-}$ mice died perinatally (Table 1). The fact that this was reduced to 31% by introducing a single *Cdk2* allele suggests that the lethality is a dose-dependent phenotype associated with insufficient interphase Cdk activity. Nevertheless, 47% of triple-knockout (TKO) animals reached adulthood and displayed a normal life span, suggesting that the attainment of a Cdk activity threshold compatible with life in the relevant target tissue(s) may rely on several overlapping mechanisms yet to be fully characterized.

This also suggests that the cellular context may dictate which of the seemingly opposed roles of Cip/Kip as Cdk-cyclin D assembly factors versus Cdk inhibitors prevail, to an extent that under some circumstances the Cip/Kip tumor suppressors counterintuitively display oncogenic properties. For instance, oligodendrogliomas with elevated $p21^{Cip1}$ result in more aggressive disease (28). Interestingly, in this tumor type the oncogenic function of $p21^{Cip1}$ is a direct consequence of its role as a Cdk4-cyclin D assembly factor and is directly controlled by tyrosine phosphorylation (29, 30). $p27^{Kip1}$ is equally subject to regulation by tyrosine phosphorylation (23, 31, 32). Unfortunately, the only mouse model in which $p27^{Kip1}$ has been shown to promote tumor development relies on a Cdk-independent function (33), thereby invalidating the option to weigh the importance of the tyrosine phosphorylation control (i.e., its role as an assembly factor) in $p27^{Kip1}$-mediated cancer promotion.

In sum, and in good agreement with previous observations from different laboratories (34), our results emphasize the notion that Cdk-dependent cell cycle control in multicellular organisms is extremely robust and several overlapping mechanisms facilitate not only the proper execution of cell division but also its timely coordination with developmental processes, even in the concomitant absence of allegedly essential factors.

ACKNOWLEDGMENTS

We thank Marcos Malumbres for suggestions and critical reading of the manuscript.

This work was supported by grants from the European Research Council (ERC-AG/250297-RAS AHEAD), EU-Framework Programme (LSHG-CT-2007-037665/CHEMORES, HEALTH-F2-2010-259770/LUNGTARGET, and HEALTH-2010-260791/EUROCANPLAT-FORM), Spanish Ministry of Economy and Competitiveness (SAF2011-30173), and Autonomous Community of Madrid (S2011/BDM-2470/ONCOCYCLE) to M.B. C.E.S. is supported by a grant from the La Caixa/CNIO International Ph.D. Fellowship Program sponsored by the La Caixa Foundation (Spain).

We declare no conflict of interest.

REFERENCES

1. **Morgan DO.** 2007. The cell cycle: principles of control. New Science Press, London, United Kingdom.
2. **Kato JY, Matsuoka M, Strom DK, Sherr CJ.** 1994. Regulation of cyclin D-dependent kinase (cdk4) by cdk4-activating kinase. Mol. Cell. Biol. **14:**2713–2721. http://dx.doi.org/10.1128/MCB.14.4.2713.
3. **LaBaer J, Garrett MD, Stevenson LF, Slingerland JM, Sandhu C, Chou HS, Fattaey A, Harlow E.** 1997. New functional activities for the p21 family of CDK inhibitors. Genes Dev. **11:**847–862. http://dx.doi.org/10.1101/gad.11.7.847.
4. **Cheng M, Olivier P, Diehl JA, Fero M, Roussel MF, Roberts JM, Sherr CJ.** 1999. The p21(Cip1) and p27(Kip1) CDK 'inhibitors' are essential activators of cyclin D-dependent kinases in murine fibroblasts. EMBO J. **15:**1571–1583.
5. **Sugimoto M, Martin N, Wilks DP, Tamai K, Huot TJ, Pantoja C, Okumura K, Serrano M, Hara E.** 2002. Activation of cyclin D1-kinase in murine fibroblasts lacking both $p21^{Cip1}$ and $p27^{Kip1}$. Oncogene **21:**8067–8074. http://dx.doi.org/10.1038/sj.onc.1206019.
6. **Blain SW, Montalvo E, Massagué J.** 1997. Differential interaction of the cyclin-dependent kinase (Cdk) inhibitor $p27^{Kip1}$ with cyclin A-Cdk2 and cyclin D2-Cdk4. J. Biol. Chem. **272:**25863–25872. http://dx.doi.org/10.1074/jbc.272.41.25863.
7. **Sherr CJ, Roberts JM.** 1999. CDK inhibitors: positive and negative regulators of G_1-phase progression. Genes Dev. **13:**1501–1512. http://dx.doi.org/10.1101/gad.13.12.1501.
8. **Bagui TK, Jackson RJ, Agrawal D, Pledger WJ.** 2000. Analysis of cyclin D3-cdk4 complexes in fibroblasts expressing and lacking $p27^{kip1}$ and $p21^{cip1}$. Mol. Cell. Biol. **20:**8748–8757. http://dx.doi.org/10.1128/MCB.20.23.8748-8757.2000.
9. **Bagui TK, Mohapatra S, Haura E, Pledger WJ.** 2003. $p27^{Kip1}$ and $p21^{Cip1}$ are not required for the formation of active D cyclin-cdk4 complexes. Mol. Cell. Biol. **23:**7285–7290. http://dx.doi.org/10.1128/MCB.23.20.7285-7290.2003.
10. **Zhang H, Hannon GJ, Beach D.** 1994. p21-containing cyclin kinases exist in both active and inactive states. Genes Dev. **8:**1750–1758. http://dx.doi.org/10.1101/gad.8.15.1750.
11. **Soos TJ, Kiyokawa H, Yan JS, Rubin MS, Giordano A, DeBlasio A, Bottega S, Wong B, Mendelsohn J, Koff A.** 1996. Formation of p27-CDK complexes during the human mitotic cycle. Cell Growth Differ. **7:**135–146.
12. **Fero ML, Rivkin M, Tasch M, Porter P, Carow CE, Firpo E, Polyak K,**

Tsai LH, Broudy V, Perlmutter RM, Kaushansky K, Roberts JM. 1996. A syndrome of multiorgan hyperplasia with features of gigantism, tumorigenesis and female sterility in $p27^{(Kip1)}$ deficient mice. Cell **85:**733–744. http://dx.doi.org/10.1016/S0092-8674(00)81239-8.

13. **National Research Council.** 2011. Guide for the care and use of laboratory animals, 8th ed. National Academies Press, Washington, DC.
14. **Santamaría D, Barrière C, Cerqueira A, Hunt S, Tardy C, Newton K, Cáceres JF, Dubus P, Malumbres M, Barbacid M.** 2007. Cdk1 is sufficient to drive the mammalian cell cycle. Nature **448:**811–815. http://dx.doi.org/10.1038/nature06046.
15. **Martín A, Odajima J, Hunt SL, Dubus P, Ortega S, Malumbres M, Barbacid M.** 2005. Cdk2 is dispensable for cell cycle inhibition and tumor suppression mediated by $p27^{Kip1}$ and $p21^{Cip1}$. Cancer Cell **7:**591–598. http://dx.doi.org/10.1016/j.ccr.2005.05.006.
16. **Kiyokawa H, Kineman RD, Manova-Todorova KO, Soares VC, Hoffman ES, Hoffman ES, Ono M, Khanam D, Hayday AC, Frohman LA, Koff A.** 1996. Enhanced growth of mice lacking the cyclin-dependent kinase inhibitor function of p27(Kip1). Cell **85:**721–732. http://dx.doi.org/10.1016/S0092-8674(00)81238-6.
17. **Nakayama K, Ishida N, Shirane M, Inomata A, Inoue T, Shishido N, Horii I, Loh DY, Nakayama K.** 1996. Mice lacking $p27^{(Kip1)}$ display increased body size, multiple organ hyperplasia, retinal dysplasia and pituitary tumors. Cell **85:**707–720. http://dx.doi.org/10.1016/S0092-8674(00)81237-4.
18. **Martin J, Hunt SL, Dubus P, Sotillo R, Néhmé-Pélluard F, Magnuson MA, Parlow AF, Malumbres M, Ortega S, Barbacid M.** 2003. Genetic rescue of Cdk4 null mice restores pancreatic β-cell proliferation but not homeostatic cell number. Oncogene **22:**5261–5269. http://dx.doi.org/10.1038/sj.onc.1206506.
19. **Rane SG, Dubus P, Mettus RV, Galbreath EJ, Boden G, Reddy EP, Barbacid M.** 1999. Loss of Cdk4 expression causes insulin-deficient diabetes and Cdk4 activation results in β-cell hyperplasia. Nat. Genet. **22:**44–52. http://dx.doi.org/10.1038/8751.
20. **Tsutsui T, Hesabi B, Moons DS, Pandolfi PP, Hansel KS, Koff A, Kiyokawa H.** 1999. Targeted disruption of Cdk4 delays cell cycle entry with enhanced $p27^{Kip1}$ activity. Mol. Cell. Biol. **19:**7011–7019.
21. **Martin-Caballero J, Flores JM, García-Palencia P, Serrano M.** 2001. Tumor susceptibility of p21(Waf1/Cip1)-deficient mice. Cancer Res. **61:**6234–6238.
22. **García-Fernández RA, García-Palencia P, Sánchez MA, Gil-Gómez G, Sánchez B, Rollán E, Martín-Caballero J, Flores JM.** 2011. Combined loss of p21(waf1/cip1) and p27(kip1) enhances tumorigenesis in mice. Lab. Invest. **91:**1634–1642. http://dx.doi.org/10.1038/labinvest.2011.133.
23. **James M, Ray A, Leznova D, Blain SW.** 2008. Differential modification of $p27^{Kip1}$ controls its cyclin D-cdk4 inhibitory activity. Mol. Cell. Biol. **28:**498–510. http://dx.doi.org/10.1128/MCB.02171-06.
24. **Malumbres M, Sotillo R, Santamaría D, Galán J, Cerezo A, Ortega S, Dubus P, Barbacid M.** 2004. Mammalian cells cycle without the D-type cyclin-dependent kinases Cdk4 and Cdk6. Cell **118:**493–504. http://dx.doi.org/10.1016/j.cell.2004.08.002.
25. **Landis WM, Pawlyk BS, Li T, Sicinski P, Hinds PW.** 2006. Cyclin D1-dependent kinase activity in murine development and mammary tumorigenesis. Cancer Cell **9:**13–22. http://dx.doi.org/10.1016/j.ccr.2005.12.019.
26. **Sage J, Miller AL, Pérez-Mancera PA, Wysocki JM, Jacks T.** 2003. Acute mutation of retinoblastoma gene function is sufficient for cell cycle re-entry. Nature **424:**223–228. http://dx.doi.org/10.1038/nature01764.
27. **Susaki E, Nakayama K, Yamasaki L, Nakayama KI.** 2009. Common and specific roles of the related CDK inhibitors p27 and p57 revealed by a knock-in mouse model. Proc. Natl. Acad. Sci. U. S. A. **106:**5192–5197. http://dx.doi.org/10.1073/pnas.0811712106.
28. **Miettinen HE, Paunu N, Rantala I, Kalimo H, Paljarvi L, Helin H, Haapasalo H.** 2001. Cell cycle regulators (p21, p53, pRb) in oligodendrocytic tumors: a study by novel tumor microarray technique. J. Neurooncol. **55:**29–37. http://dx.doi.org/10.1023/A:1012961918848.
29. **Liu Y, Yeh N, Zhu XH, Leversha M, Cordon-Cardo C, Ghossein R, Singh B, Holland E, Koff A.** 2007. Somatic cell type specific gene transfer reveals a tumor-promoting function for p21(Waf1/Cip1). EMBO J. **26:**4683–4693. http://dx.doi.org/10.1038/sj.emboj.7601886.
30. **Hukkelhoven E, Liu Y, Yeh N, Ciznadija D, Blain SW, Koff A.** 2012. Tyrosine phosphorylation of the p21 cyclin-dependent kinase inhibitor facilitates the development of proneural glioma. J. Biol. Chem. **287:**38523–38530. http://dx.doi.org/10.1074/jbc.M112.366542.
31. **Chu I, Sun J, Arnaout A, Kahn H, Hanna W, Narod S, Sun P, Tan CK, Hengst L, Slingerland J.** 2007. p27 phosphorylation by Src regulates inhibition of cyclin E-Cdk2. Cell **128:**281–294. http://dx.doi.org/10.1016/j.cell.2006.11.049.
32. **Grimmler M, Wang Y, Mund T, Cilensek Z, Keidel EM, Waddell MB, Jäkel H, Kullmann M, Kriwacki RW, Hengst L.** 2007. Cdk inhibitory activity and stability of p27Kip1 are directly regulated by oncogenic tyrosine kinases. Cell **128:**269–280. http://dx.doi.org/10.1016/j.cell.2006.11.047.
33. **Besson A, Hwang HC, Cicero S, Donovan SL, Gurian-West M, Johnson D, Clurman BE, Dyer MA, Roberts JM.** 2007. Discovery of an oncogenic activity in p27Kip1 that causes stem cell expansion and a multiple tumor phenotype. Genes Dev. **21:**1731–1746. http://dx.doi.org/10.1101/gad.1556607.
34. **Malumbres M.** 2011. Physiological relevance of cell cycle kinases. Physiol. Rev. **91:**973–1007. http://dx.doi.org/10.1152/physrev.00025.2010.

MCB
Journals.ASM.org

Genetic Characterization of the Role of the Cip/Kip Family of Proteins as Cyclin-Dependent Kinase Inhibitors and Assembly Factors

Antonio Cerqueira,[a]* Alberto Martín,[a]* Catherine E. Symonds,[a] Junko Odajima,[a]* Pierre Dubus,[b] Mariano Barbacid,[a] David Santamaría[a]

Experimental Oncology, Molecular Oncology Program, Centro Nacional de Investigaciones Oncológicas (CNIO), Madrid, Spain[a]; Université Bordeaux, Bordeaux, France[b]

The Cip/Kip family, namely, $p21^{Cip1}$, $p27^{Kip1}$, and $p57^{Kip2}$, are stoichiometric cyclin-dependent kinase inhibitors (CKIs). Paradoxically, they have been proposed to also act as positive regulators of Cdk4/6-cyclin D by stabilizing these heterodimers. Loss of $p21^{Cip1}$ and $p27^{Kip1}$ reduces Cdk4/6-cyclin D complexes, although with limited phenotypic consequences compared to the embryonic lethality of Cdk4/6 or triple cyclin D deficiency. This milder phenotype was attributed to Cdk2 compensatory mechanisms. To address this controversy using a genetic approach, we generated *Cdk2*$^{-/-}$ *p21*$^{-/-}$ *p27*$^{-/-}$ mice. Triple-knockout mouse embryonic fibroblasts (MEFs) displayed minimal levels of D-type cyclins and Cdk4/6-cyclin D complexes. $p57^{Kip2}$ downregulation in the absence of $p21^{Cip1}$ and $p27^{Kip1}$ aggravated this phenotype, yet MEFs lacking all Cip/Kip proteins exhibited increased retinoblastoma phosphorylation, together with enhanced proliferation and transformation capacity. *In vivo*, *Cdk2* ablation induced partial perinatal lethality in *p21*$^{-/-}$ *p27*$^{-/-}$ mice, suggesting partial Cdk2-dependent compensation. However, *Cdk2*$^{-/-}$ *p21*$^{-/-}$ *p27*$^{-/-}$ survivors displayed all phenotypes described for *p27*$^{-/-}$ mice, including organomegalia and pituitary tumors. Thus, Cip/Kip deficiency does not impair interphasic Cdk activity even in the absence of Cdk2, suggesting that their Cdk-cyclin assembly function is dispensable for homeostatic control in most cell types.

Extracellular signals that promote cell proliferation are transduced via growth factor receptor-associated protein kinases and a plethora of downstream signaling pathways. A significant fraction of these pathways converges on the regulation of the cell cycle by the cyclin-dependent kinases (Cdks) (1). In a simplified scenario, Cdk activity is controlled not only by cyclin binding but also by interaction with Ink4 and the Cip/Kip family of cyclin-dependent kinase inhibitors (CKIs). However, formation of Cdk4-cyclin D functional heterodimers is largely inefficient, suggesting the requirement of assembly factors for stable complex formation (2). Indeed, Cip/Kip inhibitors have been implicated in the assembly of functional Cdk4/6-cyclin D complexes as well as on their import to the nucleus (3–5). Remarkably, some reports suggest that the Cdk4/6-cyclin D-Cip/Kip complexes remain active, since the majority of the Cdk4/6-cyclin D kinase activity in culture cells is found to be associated with Cip/Kip inhibitors (3, 6). Moreover, Cdk4/6-cyclin D complexes are nearly undetectable in extracts from mouse embryonic fibroblasts (MEFs), liver cells, or thymocytes from mice devoid of $p21^{Cip1}$ and $p27^{Kip1}$ (4). In this scenario, the unopposed activity of Cdk2 has been proposed to compensate for the severe reduction in Cdk4/6-cyclin D levels caused by Cip/Kip deficiency (4, 5). Together, these observations led to the hypothesis that Cip/Kip inhibitors are assembly factors for the formation of Cdk4/6-cyclin D complexes and that a substantial fraction of these ternary complexes retains catalytic activity (7).

However, other reports have described that Cdk4/6-cyclin D complexes, albeit reduced and short-lived, readily form in the absence of $p21^{Cip1}$ and $p27^{Kip1}$ either in asynchronous cultures (8, 9) or during cell cycle reentry from quiescence (5). Even though the levels of Cdk4/6-cyclin D complexes were undetectable by Western blot analysis, cells remained sensitive to $p16^{Ink4a}$, suggesting the existence of active Cdk4/6-cyclin D complexes (4). In addition, there are different reports regarding the extent of inhibition caused by Cip/Kip binding on the catalytic activity of Cdk4-cyclin D complexes (3–6, 8, 10, 11). These observations have led to the hypothesis that $p21^{Cip1}$ and $p27^{Kip1}$ are dispensable for the formation of active Cdk4/6-cyclin D complexes and that their binding results in stable but inactive ternary complexes (9).

To evaluate *in vivo* the impact of Cip/Kip deficiency on the formation and stability of Cdk4/6-cyclin D complexes, we set up crosses to eliminate Cdk2 in mice doubly deficient for $p21^{Cip1}$ and $p27^{Kip1}$. We have analyzed the proliferation and transformation properties of *Cdk2*$^{-/-}$ *p21*$^{-/-}$ *p27*$^{-/-}$ MEFs as well as evaluated the impact of Cdk2 elimination in the phenotypes found in $p21^{Cip1}$- and $p27^{Kip1}$-deficient mice. The findings reported here support the notion that the Cip/Kip function as pan-Cdk inhibitors prevails over their role as Cdk4/6-cyclin assembly factors. As a consequence *p21*$^{-/-}$ *p27*$^{-/-}$ cells and mice display various hyperproliferative phenotypes that are all preserved even in the concomitant absence of Cdk2.

MATERIALS AND METHODS

Mouse strains. *Cdk2*$^{-/-}$, *p21*$^{-/-}$, and *p27*$^{-/-}$ mice have been previously described (12). Tissue samples were fixed in 10% buffered formalin for 24 h and embedded in paraffin, and 3-μm sections were analyzed after stain-

Received 3 September 2013 Returned for modification 16 October 2013
Accepted 25 January 2014
Published ahead of print 10 February 2014

Address correspondence to David Santamaría, dsantamaria@cnio.es.

* Present address: Antonio Cerqueira, Progenitor Labs, Stevenage Bioscience Catalyst, Stevenage, United Kingdom; Alberto Martín, Departamento de Bioquímica, Instituto de Investigaciones Biomédicas Alberto Sols, CSIC-UAM, Madrid, Spain; Junko Odajima, Department of Cancer Biology, Dana-Farber Cancer Institute, Boston, Massachusetts, USA.

A.C. and A.M. contributed equally to this work.

doi:10.1128/MCB.01163-13

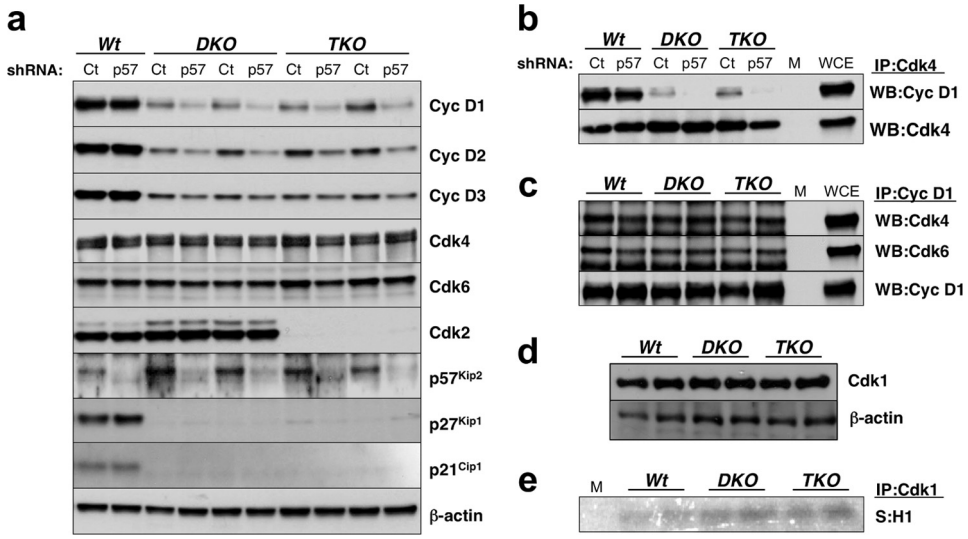

FIG 1 Stability of Cdk-cyclin D complexes in the absence of Cip/Kip inhibitors. (a) Early-passage primary MEFs were infected with lentiviral particles expressing either an shRNA against $p57^{Kip2}$ (p57) or a scramble control (Ct). Protein extracts were prepared, and the levels of a panel of cell cycle regulators were analyzed by immunoblotting with antibodies elicited against the indicated proteins. Expression of β-actin served as a loading control. Results from two independent MEF cultures are shown for $p21^{-/-}$ $p27^{-/-}$ (DKO) and $Cdk2^{-/-}$ $p21^{-/-}$ $p27^{-/-}$ (TKO) mice. Cyc, cyclin. (b) Wild-type, $p21^{-/-}$ $p27^{-/-}$ (DKO), and $Cdk2^{-/-}$ $p21^{-/-}$ $p27^{-/-}$ (TKO) primary MEFs were infected with lentiviral particles expressing either an shRNA against $p57^{Kip2}$ (p57) or a scramble control (Ct). Exponentially growing cells were used to prepare whole-cell extracts, and the amount of Cdk4-cyclin D complexes was estimated by coprecipitation of cyclin D1 with anti-Cdk4 antibodies. The levels of Cdk4, used as a loading control, are shown. WB, Western blotting. (c) The amount of starting whole-cell extract from both $p21^{-/-}$ $p27^{-/-}$ (DKO) and $Cdk2^{-/-}$ $p21^{-/-}$ $p27^{-/-}$ (TKO) MEFs was augmented to equal the cyclin D1 levels in the wild-type controls. The amount of Cdk4 (top) and Cdk6 (middle) that was coimmunoprecipitated with cyclin D1 antibodies was detected by Western blotting. Cyclin D1 levels (bottom) are shown to demonstrate equal estimation of the amount of starting material. Results from two independent MEF cultures are shown. (d) Western blotting of Cdk1 protein levels in whole-cell extracts from wild-type, $p21^{-/-}$ $p27^{-/-}$ (DKO), and $Cdk2^{-/-}$ $p21^{-/-}$ $p27^{-/-}$ (TKO) MEFs. Expression of β-actin, which served as a loading control, is shown. Results from two independent MEF cultures are shown. (e) *In vitro* kinase activity associated with Cdk1 immunoprecipitates obtained from wild-type, $p21^{-/-}$ $p27^{-/-}$ (DKO), and $Cdk2^{-/-}$ $p21^{-/-}$ $p27^{-/-}$ (TKO) MEFs. Histone H1 was used as the substrate (S). Results from two independent MEF cultures are shown. Lanes WCE, whole-cell extract at a 1:10 dilution before immunoprecipitation (IP); lanes M, mock immunoprecipitate.

ing with hematoxylin-eosin (H&E). Histopathological analysis of $p21^{-/-}$ $p27^{-/-}$ $Cdk2^{-/-}$ embryonic day 18.5 (E18.5) embryos and paired controls was performed by thorough inspection of H&E-stained serially sectioned specimens ($n = 7$). The mice used in this study have been maintained in a mixed 129/SvJ × C57BL/6J background according to the *Guide for the Care and Use of Laboratory Animals* (13) and in accordance with the Spanish Animal Protection Law (RD1201/2005) and the European Directive (86/609/CEE) established by the European Union to regulate animal care standards. Animal experiments received approval from the CNIO ethical committee (CEUCA code 032-03).

Cell culture assays. MEFs were isolated from E13.5 embryos and propagated according to standard protocols. No less than 10 independent early-passage primary MEF preparations per genotype were used to perform the experiments. Proliferation assays and S-phase entry analysis were carried out with primary MEFs as previously described (14). Knockdown of $p57^{Kip2}$ was mediated with lentiviral Mission short hairpin RNA (shRNA) plasmids (Sigma no. SHGLY-NM_009876.2) according to the manufacturer's instructions. After infection, cells were selected with 2 μg/ml puromycin for 48 h. Focus formation assays were performed as described previously (12).

Protein analysis. Protein lysates were prepared and used for immunoblotting as previously described (12). Antibodies against the following proteins were used: Cdk2 (M2; Santa Cruz), Cdk4 (C22; Santa Cruz), Cdk6 (our own rabbit polyclonal antibodies), cyclin D1 (DCS6; Neo Markers), cyclin D2 (M-20; Santa Cruz), cyclin D3 (DCS22; Cell Signaling), cyclin A2 (H432; Santa Cruz), $p21^{Kip1}$ (C19; Santa Cruz), $p27^{Kip1}$ (catalog no. 610242; BD Transduction Laboratories), $p57^{Kip2}$ (catalog no. P0357; Sigma), β-actin (clone AC15; Sigma), and phospho-specific antibody to phosphorylated residues S807/811 of the retinoblastoma protein (pRb; catalog no. 9308; Cell Signaling). As secondary antibodies, peroxidase-conjugated IgG (Dako) was used, followed by chemiluminescence detection (ECL kit; Amersham).

RESULTS

Formation of Cdk4/6-cyclin D complexes in the absence of Cip/Kip proteins. As illustrated in Fig. 1a, $p21^{-/-}$ $p27^{-/-}$ MEFs displayed a significant reduction in the overall cellular levels of the three D-type cyclins and retained 5 to 10% of the cyclin D levels present in wild-type cells. To determine whether the third member of the Cip/Kip family of CKIs, $p57^{Kip2}$, may contribute to the stabilization of active Cdk-cyclin D complexes, we generated lentiviral particles expressing an shRNA against $p57^{Kip2}$ and analyzed its impact on cyclin D levels in wild-type and $p21^{-/-}$ $p27^{-/-}$ double mutant MEFs. $p57^{Kip2}$ depletion in $p21^{-/-}$ $p27^{-/-}$ MEFs, irrespective of the presence or absence of Cdk2, caused a further decrease in the levels of expression of cyclins D1 and D2 and a moderate decrease in the case of cyclin D3 (Fig. 1a). Interestingly, we observed a negligible impact in wild-type controls. As expected, the reduction in the overall cellular levels of the D-type cyclins resulted in a similar decrease in the amount of Cdk4-cyclin D complexes, as determined by immunoprecipitation of the kinase subunit (Fig. 1b). These results suggest that $p57^{Kip2}$ contributes to the stabilization of Cdk4/6-cyclin D complexes, at least in the absence of $p21^{Cip1}$ and $p27^{Kip1}$.

In order to determine whether the Cip/Kip proteins are essential for the formation or stabilization of the Cdk4-cyclin D1 complexes, we matched the total levels of cyclin D1 in the immuno-

precipitation assays by scaling up 9-fold the amount of the starting whole-cell extract from *p21*$^{-/-}$ *p27*$^{-/-}$ and *Cdk2*$^{-/-}$ *p21*$^{-/-}$ *p27*$^{-/-}$ MEFs. Technical difficulties owing to the much greater decrease of cyclin D levels upon *p57*^{Kip2} knockdown prevented us from including this condition in the assay. Nevertheless, under these conditions we compensated for the diminution in the overall levels of cyclin D1 caused by the concomitant absence of p21^{Cip1} and p27^{Kip1}, and when immunoprecipitated, it pulled down an equal amount of Cdk4 and Cdk6 in all genotypes (Fig. 1c). This result is in good agreement with those described in a previous report suggesting that free D-type cyclins rapidly associate with their Cdk4/6 cognate catalytic subunits (9), thus suggesting that the kinetics of this association is independent of the Cip/Kip proteins, limiting their role to the stabilization of preformed binary complexes.

Finally, we investigated the expression levels and activity of Cdk1, as it is a likely candidate to compensate for the reduced activity of interphase Cdks. We found that whereas the expression levels of Cdk1 are comparable in MEFs from mice of the three genotypes, its activity is increased in *p21*$^{-/-}$ *p27*$^{-/-}$ and *Cdk2*$^{-/-}$ *p21*$^{-/-}$ *p27*$^{-/-}$ cells compared to its activity in the wild-type controls (Fig. 1d and e).

Proliferation properties of *Cdk2*$^{-/-}$ MEFs devoid of Cip/Kip proteins. To determine the consequences of the reduced levels of Cdk4/6-cyclin D complexes on cell cycle progression in the absence of Cip/Kip proteins, we examined the proliferation properties of primary *p21*$^{-/-}$ *p27*$^{-/-}$ MEFs. In parallel, we also analyzed the proliferation of *Cdk2*$^{-/-}$ *p21*$^{-/-}$ *p27*$^{-/-}$ cells since it has been proposed that in the absence of both Cip/Kip inhibitors Cdk2 could play a compensatory role by functionally replacing Cdk4/6-cyclin D complexes (4, 5). As illustrated in Fig. 2a, *p21*$^{-/-}$ *p27*$^{-/-}$ cells reproducibly displayed a growth advantage compared to the wild-type controls under standard serum conditions. This growth advantage was even more evident when cells were grown in 2% serum, since under these conditions wild-type cells failed to thrive, whereas MEFs devoid of p21^{Cip1} and p27^{Kip1} managed to proliferate (Fig. 2b). Similar results were obtained in primary MEFs also devoid of Cdk2, indicating that Cdk2 activity is not responsible for driving cell proliferation in the absence of these inhibitors. Finally, we assessed the effect of knocking down the third member of the Cip/Kip family of CIKs, p57^{Kip2}. shRNA-mediated depletion of p57^{Kip2} caused a reduction in the proliferative rate compared to that for MEFs infected with control shRNA, particularly under low-serum conditions (Fig. 2). This result, together with the further decrease in the levels of the three D-type cyclins (Fig. 1a), suggests that p57^{Kip2} may function as a Cdk4/6-cyclin D assembly factor in MEFs, at least in the absence of p21^{Cip1} and p27^{Kip1}, yet the proliferation rate observed in the concomitant absence of the three CKIs, even in a Cdk2-null background, was consistently higher than that of wild-type MEFs (Fig. 2). Altogether, these experiments suggest that in terms of cell proliferation, the function of the Cip/Kip proteins as Cdk inhibitors prevails over their putative role as Cdk4/6-cyclin D assembly factors in MEFs. The lack of an effect observed upon ablation of Cdk2 expression suggests that the cell cycle inhibitory activity of the Cip/Kip proteins must be mediated through another Cdk, possibly Cdk1, or by a Cdk-independent mechanism.

Next, we focused our attention on cell cycle reentry, a process particularly reliant on Cdk activity (14). As illustrated in Fig. 3a, serum-starved *p21*$^{-/-}$ *p27*$^{-/-}$ MEFs entered S phase with a higher

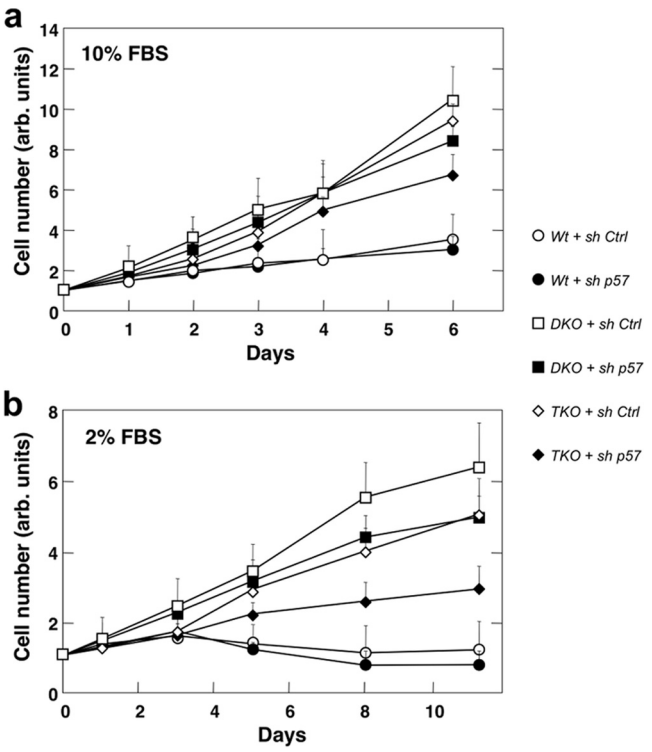

FIG 2 Proliferation of primary MEFs in the absence of Cip/Kip inhibitors. (a) The proliferation of wild-type (Wt), *p21*$^{-/-}$ *p27*$^{-/-}$ (DKO), and *Cdk2*$^{-/-}$ *p21*$^{-/-}$ *p27*$^{-/-}$ (TKO) primary MEFs in 10% fetal bovine serum (FBS) was assessed upon infection with lentiviral particles expressing an shRNA against *p57*^{Kip2} (sh p57) or a scramble control (sh Ctrl). Data are shown as means ± SDs ($n = 3$). (b) Same as for panel a, but MEFs were maintained under limiting serum conditions (2% fetal bovine serum). arb., arbitrary.

efficiency than wild-type control cells. Similar results were obtained with *Cdk2*$^{-/-}$ *p21*$^{-/-}$ *p27*$^{-/-}$ MEFs (Fig. 3a). Accordingly, the phosphorylation of the Ser807/811 residues of the retinoblastoma protein (Rb) and the appearance of cyclin A2 were detected at earlier time points compared to the times of appearance for the wild-type controls (Fig. 3b). Importantly, when the G_0 exit was assessed in p57^{Kip2}-depleted cells, the higher efficiency observed in both *p21*$^{-/-}$ *p27*$^{-/-}$ and *Cdk2*$^{-/-}$ *p21*$^{-/-}$ *p27*$^{-/-}$ MEFs was no longer evident (Fig. 3c), thus adding further evidence that p57^{Kip2} may participate in the assembly of Cdk4/6-cyclin complexes in MEFs. This role of p57^{Kip2}, which appears to be negligible in wild-type cells (Fig. 1a), becomes evident in the absence of p21^{Cip1} and p27^{Kip1}, particularly under conditions that are more dependent on interphase Cdk activity, such as during proliferation under low-serum conditions or during exit from quiescence.

Cellular transformation in the absence of p21^{Cip1} and p27^{Kip1}. To study the role of p21^{Cip1} and p27^{Kip1} in cellular transformation, we infected primary MEFs with retroviral particles expressing combinations of different oncogenes. Transformation was subsequently assessed by focus formation (Fig. 4a). Single H-*Ras*^{G12V} or *E1a* oncogenes did not significantly enhance transformation, irrespective of the genotype (data not shown). The maximal efficiency was achieved using concomitant expression of both oncoproteins. In this context, cells lacking p27^{Kip1} expression displayed a minor (15%) increase in their transformation ability compared to that for the wild-type controls. However, in-

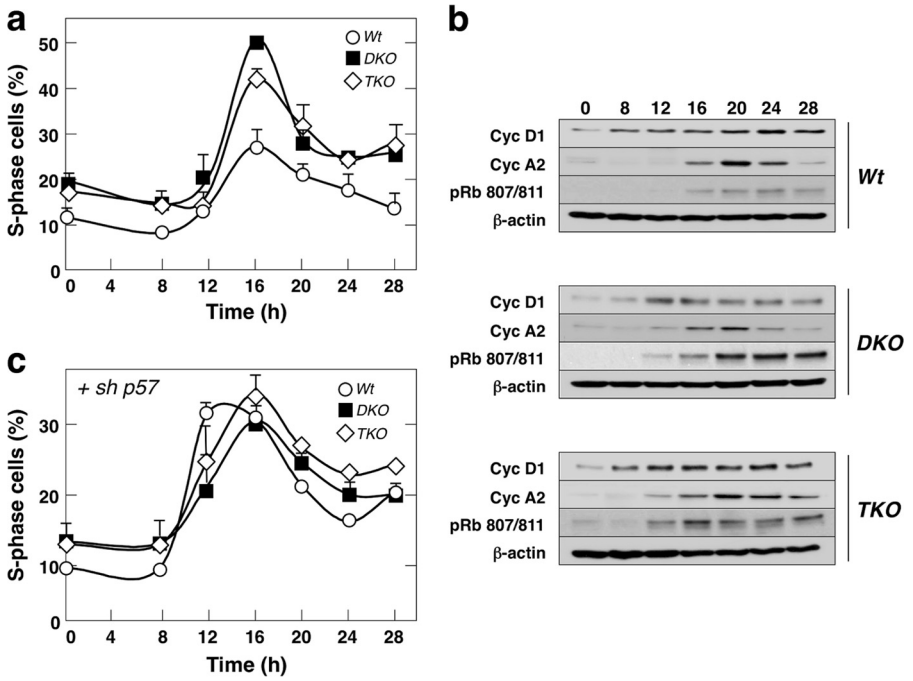

FIG 3 Role of Cip/Kip proteins in cell cycle reentry. (a) Percentage of wild-type (Wt), $p21^{-/-}$ $p27^{-/-}$ (DKO), and $Cdk2^{-/-}$ $p21^{-/-}$ $p27^{-/-}$ (TKO) primary MEFs in S phase at the indicated times following serum stimulation from quiescence. Data are shown as means ± SDs ($n = 3$). (b) Whole-cell extracts from cells for which the results are shown in panel a were prepared at the times (in hours) following serum stimulation from quiescence indicated above each lane. The presence of cyclin D1 and cyclin A2 and the phosphorylation of the Ser807/811 residues of the retinoblastoma protein (pRb) were detected by Western blotting. Expression of β-actin, which served as a loading control, is shown. (c) $p57^{Kip2}$ was depleted in wild-type, $p21^{-/-}$ $p27^{-/-}$ (DKO), and $Cdk2^{-/-}$ $p21^{-/-}$ $p27^{-/-}$ (TKO) primary MEFs by lentivirus-mediated shRNA delivery. Infected MEFs were subsequently made quiescent by serum deprivation. The percentage of S-phase cells at the indicated times (in hours) following serum stimulation from quiescence is shown. Data are shown as means ± SDs ($n = 3$).

fection of $p21^{-/-}$ MEFs or $p21^{-/-}$ $p27^{-/-}$ double mutant MEFs resulted in a 2-fold increase, indicating that $p21^{Cip1}$ and $p27^{Kip1}$ do not cooperate to prevent malignant transformation, at least *in vitro*. Interestingly, loss of Cdk2 expression had no effect on the ability of $p21^{-/-}$ $p27^{-/-}$ MEFs to become transformed by $H\text{-}Ras^{G12V}$ and E1a oncoproteins, indicating that Cdk2 does not compensate for the low levels of Cdk4/6-cyclin D complexes. Moreover, this also illustrates that Cdk2 does not play a role in promoting cell transformation. Finally, we submitted these cells to a standard 3T3 immortalization protocol. As expected, wild-type primary MEFs entered replicative senescence after a few passages, whereas $p21^{-/-}$ $p27^{-/-}$ cells bypassed the crisis period irrespective of their Cdk2 status (Fig. 4b).

Phenotypic characterization of $p21^{-/-}$ $p27^{-/-}$ $Cdk2^{-/-}$ mice. In order to determine whether Cdk2 might compensate for the reduced formation of Cdk4/6-cyclin D complexes *in vivo*, we crossed $p21^{-/-}$, $p27^{+/-}$, and $Cdk2^{+/-}$ mice and scored the resulting genotypes at weaning ($n = 439$). As shown in Table 1, all the possible genotypes matched the expected Mendelian ratio except for those carrying a single *Cdk2* allele (17.3% versus 25%; ratio, 0.69) or no *Cdk2* alleles (5.9% versus 12.5%; ratio, 0.47). Lethality did not appear to occur *in utero*, since all possible genotypes were present at the expected ratios when assayed during late embryogenesis (E18.5) (data not shown). We previously reported that *Cdk2* ablation in $p27^{-/-}$ mice did not result in increased mortality (15). Thus, the cause of death of $p21^{-/-}$ $p27^{-/-}$ $Cdk2^{-/-}$ neonates must be associated with $p21^{Cip1}$ deficiency. This postnatal lethality appears to result from insufficient overall interphase Cdk activity, since neonatal mortality was also observed in $p21^{-/-}$ $p27^{-/-}$ $Cdk2^{+/-}$ mice, albeit to a lesser extent (ratio of surviving mice at weaning, 0.69 versus 0.47). Previous studies using Cdk mutant mice have linked interphase Cdk deficiency with embryonic or neonatal lethality. For instance, mice lacking Cdk4 and Cdk2 died at birth due to cardiac abnormalities, and mice deficient for the three interphase Cdks, Cdk4, Cdk6, and Cdk2, died at midgestation primarily due to hematopoietic defects similar to those observed in Cdk4 and Cdk6 double mutant mice. Careful histopathological analysis in serial sections of E18.5 embryos failed to uncover obvious defects that could account for their postnatal lethality, including in those tissues affected by interphase Cdk deficiency, such as fetal hematopoietic organs and heart. Thus, the cause of death of $Cdk2^{-/-}$ $p21^{-/-}$ $p27^{-/-}$ mice before weaning remains unknown.

We next focused our attention on the characterization of adult mice. Ablation of *p27* alleles results in increased body size, especially in females (12, 16, 17). This and other phenotypic changes associated with $p27^{-/-}$ deficiency were mainly attributed to augmented Cdk activity. Thus, we examined whether the reduced levels of Cdk4/6-cyclin D activity in $p21^{-/-}$ $p27^{-/-}$ mice might revert the phenotypic changes seen in $p27^{-/-}$ animals. Parallel experiments were carried out in $p21^{-/-}$ $p27^{-/-}$ $Cdk2^{-/-}$ mice, which displayed even lower levels of interphase Cdk activity. To this end, we monitored body weight changes from weaning. As represented in Fig. 5, all compound strains devoid of $p27^{Kip1}$ displayed elevated body weights, regardless of their intrinsic Cdk activity. Moreover, all organs with the exception of liver showed

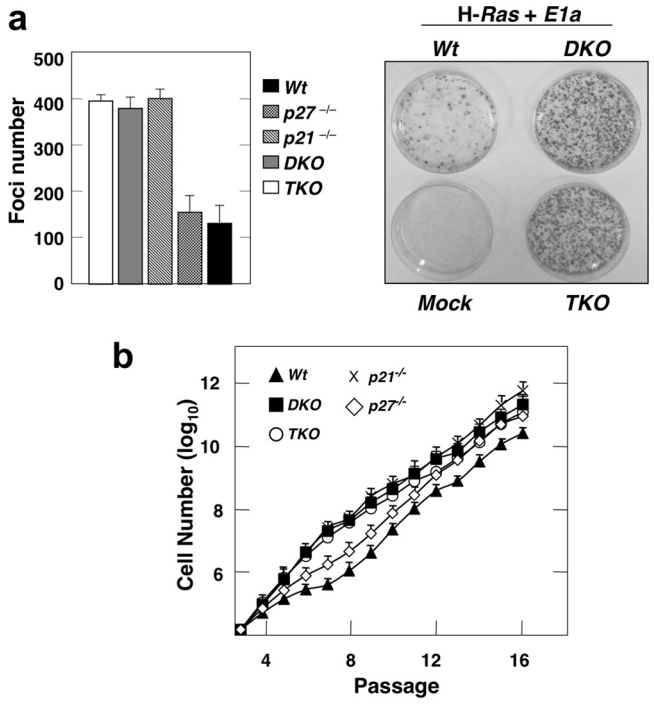

FIG 4 Cip/Kip factors and cellular transformation. (a) Equal amounts of wild-type, $p21^{-/-}$, $p27^{-/-}$, as well as compound mutant $p21^{-/-}$ $p27^{-/-}$ (DKO) and $Cdk2^{-/-}$ $p21^{-/-}$ $p27^{-/-}$ (TKO) MEFs were infected with retroviral particles coexpressing H-*Ras* and *E1a* oncogenes. (Left) At 3 weeks after infection, the number of detectable foci was scored for the different genotypes. Data are shown as means ± SDs ($n = 3$). (Right) A representative image upon crystal violet staining is shown. (b) Immortalization of wild-type, $p21^{-/-}$ and $p27^{-/-}$ single-knockout, $p21^{-/-}$ $p27^{-/-}$ (DKO), and $Cdk2^{-/-}$ $p21^{-/-}$ $p27^{-/-}$ (TKO) primary MEFs following a classical 3T3 protocol. Data are shown as means ± SDs ($n = 3$).

an increased weight (12, 16–18). Pathological examination of livers from $p21^{-/-}$ $p27^{-/-}$ $Cdk2^{-/-}$ mice showed that they did not display detectable architectural or cytological defects, yet we found that the hepatocyte density was consistently reduced compared to that in age-matched $p21^{-/-}$ $p27^{-/-}$ controls (Fig. 5b and c). Since the livers of newborn $p21^{-/-}$ $p27^{-/-}$ $Cdk2^{-/-}$ mice were phenotypically normal (data not shown), the liver hypoplasia may progressively arise during postnatal development. Taken together, these results suggest that the majority of tissues and cell types in adult mice tolerate the combined deficiency of $p21^{Cip1}$ and $p27^{Kip1}$.

Finally, we examined whether these $p21^{-/-}$ $p27^{-/-}$ and/or $p21^{-/-}$ $p27^{-/-}$ $Cdk2^{-/-}$ mutant mice may show defects in the proliferation of insulin-producing pancreatic β-cells, which are exquisitely dependent on the presence of Cdk4 activity for proper proliferation (18–20). All mutant mice were normoglycemic during the course of the study (data not shown). Unlike $Cdk4^{-/-}$ animals, histological analysis of pancreatic sections failed to detect either quantitative or qualitative variations in β-cell islets in any of the tested mice ($n = 21$) (data not shown). These results illustrate that *in vivo*, the decline in Cdk4/6-cyclin D complexes caused by ablation of the $p21^{Cip1}$ and $p27^{Kip1}$ alleles is not sufficient to phenocopy the defects caused by the loss of Cdk4 activity.

Tumorigenesis in $p21^{-/-}$ $p27^{-/-}$ mice. Finally, we analyzed the tumor spectrum of $p21^{-/-}$ $p27^{-/-}$ double-knockout mice. As previously reported, $p21^{Cip1}$-null mice developed a variety of spontaneous tumors at an average age of 16 months (21). $p27^{Kip1}$ deficiency resulted in the appearance of aggressive pituitary tumors, and all mice succumbed by 1 year of age (12, 16, 17). $p21^{Cip1}$ $p27^{Kip1}$-null animals died of pituitary tumors with a timing and pathology indistinguishable from those for the single mutant $p27^{-/-}$ controls, indicating that $p21^{Cip1}$ does not compensate for the absence of $p27^{Kip1}$ (Fig. 6). In contrast, the loss of $p27^{Kip1}$ appears to cooperate with the absence of $p21^{Cip1}$, at least in accelerating tumor development, since about a quarter of the $p21^{-/-}$ $p27^{-/-}$ mice displayed histiocytic sarcomas at a time (10 months) when none of the $p21^{-/-}$ animals had developed such tumors (21–23) (Table 2). We also recorded the appearance of new pathologies in $p21^{-/-}$ $p27^{-/-}$ double mutant mice that were absent in either single-knockout strain. They included a panel of precancerous lesions, such as gastric hyperplasia, pancreatic intraepithelial neoplasia (PanIN), and myeloproliferation (Table 2). The premature death associated with $p27^{Kip1}$ deficiency prevented us from studying the evolution of these lesions.

DISCUSSION

In our hands, primary $p21^{-/-}$ $p27^{-/-}$ MEFs displayed enhanced proliferative properties compared to the wild-type controls (Fig. 2). Interestingly, and in agreement with previous reports, these cells retained only 5% of the cellular Cdk4-cyclin D1 complexes found in the wild-type controls. As a side note, this is equivalent to the fraction of $p27^{Kip1}$ that appears to be tyrosine phosphorylated—and presumably noninhibitory—in asynchronous cells (23), suggesting that a minor proportion of active Cdk4/6-cyclin D complexes suffices to support unperturbed proliferation. Importantly, the enhanced proliferative capacity observed in $p21^{-/-}$ $p27^{-/-}$ MEFs was also present in $Cdk2^{-/-}$ $p21^{-/-}$ $p27^{-/-}$ MEFs (Fig. 2), discarding the possibility that Cdk2 is the putative compensatory mechanism that has been postulated to ameliorate the proliferation of $p21^{-/-}$ $p27^{-/-}$ cells (4, 5). Altogether, these results suggest that in terms of cell proliferation, the Cip/Kip function as pan-Cdk inhibitors is overwhelmingly more relevant than their role as Cdk4/6-cyclin D assembly factors.

It has also been proposed that Cdk4/6-cyclin D complexes perform a relevant noncatalytic role to favor cell proliferation. According to this model, these complexes act as a molecular sink for Cip/Kip proteins, titrating them away from Cdk2 and therefore facilitating its subsequent activation (7). Indeed, no free $p27^{Kip1}$ can be detected *in vivo* (23). Cdk4/6 double-knockout cells have a lower proliferative capacity than wild-type controls (24). Interest-

TABLE 1 Influence of $p21^{Cip1}$, $p27^{Kip1}$, and Cdk2 deficiency on postnatal survival[a]

Genotype			Mendelian ratio[b] (%)	
Cdk2	*p21*	*p27*	Expected	Observed
+/+	−/−	+/−	12.5	18.7
+/+	−/−	−/−	12.5	11.6
+/−	−/−	+/−	25	31
+/−	−/−	−/−	25	17.3
−/−	−/−	+/−	12.5	15.5
−/−	−/−	−/−	12.5	5.9

[a] Data are for 439 mice.
[b] The expected and observed Mendelian ratios of the indicated genotypes were scored at weaning (postnatal day 21).

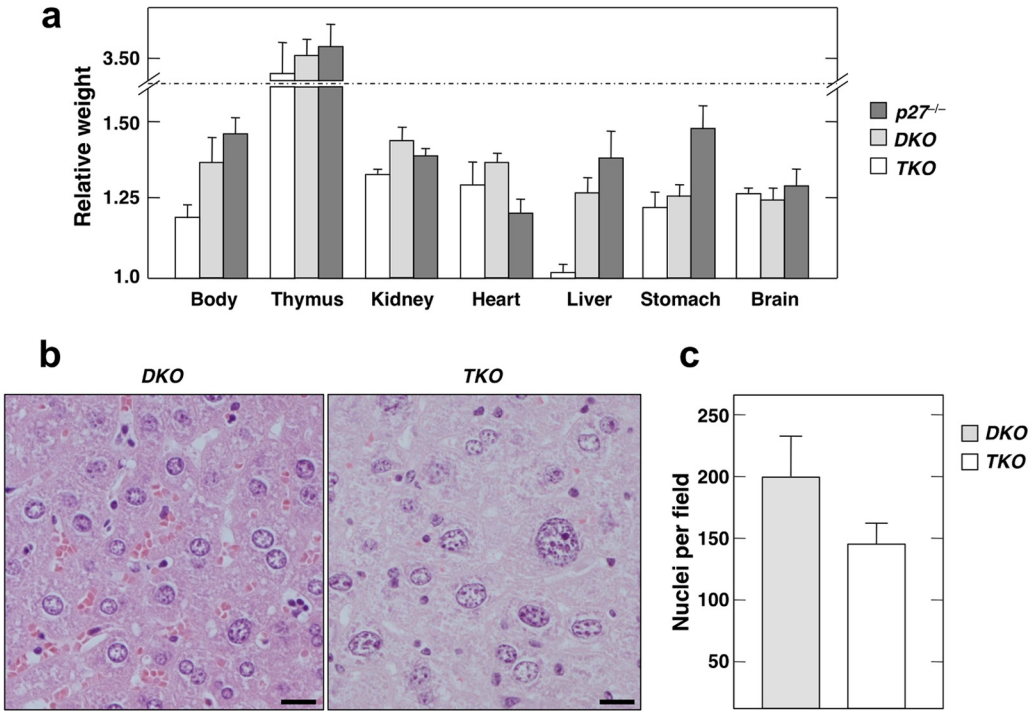

FIG 5 Influence of $p21^{Cip1}$ and $p27^{Kip1}$ deficiency in adult homeostasis. (a) Total body weight and the weight of the indicated individual organs of mice at 11 weeks of age. Values for $p27^{-/-}$, $p21^{-/-}$ $p27^{-/-}$ (DKO), and $Cdk2^{-/-}$ $p21^{-/-}$ $p27^{-/-}$ (TKO) mice normalized to those for wild-type controls of the same age are represented. Data are shown as means ± SDs ($n = 4$). (b) Representative images of hematoxylin-eosin-stained liver sections from 11-week-old $p21^{-/-}$ $p27^{-/-}$ (DKO) and $Cdk2^{-/-}$ $p21^{-/-}$ $p27^{-/-}$ (TKO) mice. Bars, 20 μm. (c) Quantification of the total number of hepatocytes in four randomly selected ×400 microscope fields of liver sections from $p21^{-/-}$ $p27^{-/-}$ (DKO) and $Cdk2^{-/-}$ $p21^{-/-}$ $p27^{-/-}$ (TKO) mice. Data are shown as means ± SDs ($n = 7$).

ingly, $p21^{-/-}$ $p27^{-/-}$ MEFs, which display a severe (20-fold) reduction of Cdk-cyclin D complexes, have the opposite phenotype. This suggests that in wild-type MEFs, the Cip/Kip titration function of Cdk4/6-cyclin D might prevail over their catalytic activity. Indeed, a cyclin D1 mutant that forms kinase-inactive complexes with Cdk4/6 efficiently rescues the developmental defects present in cyclin $D1^{-/-}$ mice (25). Although this could also be attributed to Cdk-independent functions of cyclin D1, we cannot rule out the possibility that in particular cellular contexts the sequestration function of Cdk4/6-cyclin D complexes is dominant over their catalytic activity.

We have also shown that $p57^{Kip2}$, the third component of the Cip/Kip family, participates *in vivo* in the stabilization of Cdk4-

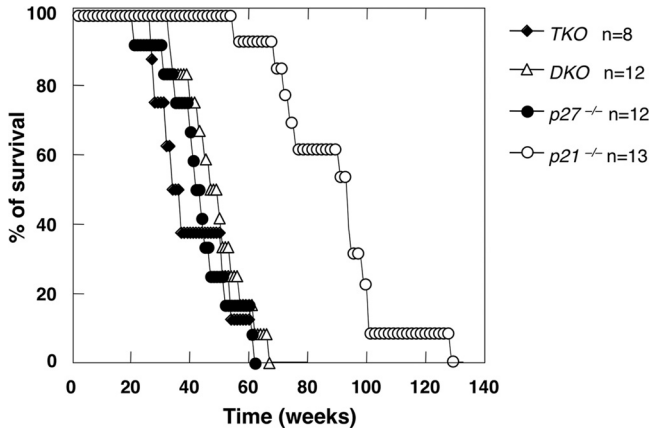

FIG 6 Cooperation between $p21^{Cip1}$ and $p27^{Kip1}$ tumor suppressors. Survival curve of $p21^{-/-}$, $p27^{-/-}$, $p21^{-/-}$ $p27^{-/-}$ (DKO), and $Cdk2^{-/-}$ $p21^{-/-}$ $p27^{-/-}$ (TKO) mice.

TABLE 2 Tumor susceptibility in mice lacking $p21^{Cip1}$ and $p27^{Kip1}$

Lesion type and lesion or pathology	% of mice that developed lesions or pathology[a]		
	$p21^{-/-}$ $p27^{-/-}$ mice ($n = 21$)	$p27^{-/-}$ mice ($n = 11$)	$p21^{-/-}$ mice ($n = 13$)
Hyperplasia/tumor-related lesions			
Gastric neuroendocrine hyperplasia	43	0	0
Gastric mucosa hyperplasia	57	0	0
Histiocytic sarcoma	24	0	0
Myeloproliferation	43	0	0
PanIN	10	0	0
Inflammation/non-tumor-related lesions			
Arteritis	14	0	0
Bone metaplasia	24	0	0
Chronic nephropathy	81	45	23
Chronic pancreatitis	29	0	0
Retinal dysplasia	38	19	0

[a] Animals were sacrificed at 10 months of age. Numbers are rounded up to the nearest digit.

cyclin D complexes, at least in the absence of $p21^{Cip1}$ and $p27^{Kip1}$. shRNA-mediated depletion of $p57^{Kip2}$ in *p21*$^{-/-}$ *p27*$^{-/-}$ MEFs caused a further reduction of Cdk4-cyclin D1 complexes, reaching levels undetectable by Western blotting (Fig. 1b), yet it is significant that upon $p57^{Kip2}$ depletion, *Cdk2*$^{-/-}$ *p21*$^{-/-}$ *p27*$^{-/-}$ MEFs exited G_0 with kinetics comparable to that of the wild-type controls. In this scenario, the Cdk1-cyclin D complexes that become detectable in the absence of Cdk4 (14) may functionally replace Cdk4/6-cyclin D complexes. This would imply that the assembly of Cdk1-cyclin D complexes does not require Cip/Kip proteins or may be facilitated by alternative assembly factors. In this respect, $p34^{Sei1}$ has been described to be an alternative Cdk-cyclin D assembly factor, particularly during quiescence exit (5). We believe that our *Cdk2*$^{-/-}$ *p21*$^{-/-}$ *p27*$^{-/-}$ mouse model may become a useful tool to elucidate whether indeed other assembly factors exist or if Cdk-cyclin D complexes can form *de novo*.

It is also possible that the required levels of Cdk-cyclin D complexes (and, therefore, the importance of their assembly factors) are cell type specific. Whereas *p21*$^{-/-}$ *p27*$^{-/-}$ mice reach adulthood with the expected Mendelian ratio, Cdk4/6 double-knockout (DKO) mice die *in utero* as a consequence of hematopoietic defects (24). This suggests that *in vivo*, redundant mechanisms or the inherent plasticity of the system may bypass the requirement for $p21^{Cip1}$ and $p27^{Kip1}$ proteins as Cdk4/6-cyclin D assembly factors in most cell types. We cannot rule out the possibility that this adaptation was facilitated in part by the use of germ line null alleles. For instance, whereas chronic deficiency of the retinoblastoma protein in MEFs allows adaptation and compensation among other family members, this is largely inefficient upon acute gene ablation (26). In any case, and in support of the functional redundancy model, we show here that $p57^{Kip2}$ stabilizes Cdk4-cyclin D1 in *p21*$^{-/-}$ *p27*$^{-/-}$ MEFs but not in wild-type controls (Fig. 1). In addition, others have demonstrated that a knockin of *p27*^{Kip1} expressed from the *p57*^{Kip2} promoter can rescue most of the developmental defects present in *p57*$^{-/-}$ mice, suggesting that they perform partially redundant roles *in vivo* (27). Interestingly, as described above, $p57^{Kip2}$ knockdown in *p21*$^{-/-}$ *p27*$^{-/-}$ MEFs caused an additional reduction of Cdk-cyclin complexes and affected their proliferation rate, which, nevertheless, remained higher than that of wild-type cells (Fig. 2b). Moreover, unlike single- and double-knockout strains, 53% of *Cdk2*$^{-/-}$ *p21*$^{-/-}$ *p27*$^{-/-}$ mice died perinatally (Table 1). The fact that this was reduced to 31% by introducing a single *Cdk2* allele suggests that the lethality is a dose-dependent phenotype associated with insufficient interphase Cdk activity. Nevertheless, 47% of triple-knockout (TKO) animals reached adulthood and displayed a normal life span, suggesting that the attainment of a Cdk activity threshold compatible with life in the relevant target tissue(s) may rely on several overlapping mechanisms yet to be fully characterized.

This also suggests that the cellular context may dictate which of the seemingly opposed roles of Cip/Kip as Cdk-cyclin D assembly factors versus Cdk inhibitors prevail, to an extent that under some circumstances the Cip/Kip tumor suppressors counterintuitively display oncogenic properties. For instance, oligodendrogliomas with elevated $p21^{Cip1}$ result in more aggressive disease (28). Interestingly, in this tumor type the oncogenic function of $p21^{Cip1}$ is a direct consequence of its role as a Cdk4-cyclin D assembly factor and is directly controlled by tyrosine phosphorylation (29, 30). $p27^{Kip1}$ is equally subject to regulation by tyrosine phosphorylation (23, 31, 32). Unfortunately, the only mouse model in which $p27^{Kip1}$ has been shown to promote tumor development relies on a Cdk-independent function (33), thereby invalidating the option to weigh the importance of the tyrosine phosphorylation control (i.e., its role as an assembly factor) in $p27^{Kip1}$-mediated cancer promotion.

In sum, and in good agreement with previous observations from different laboratories (34), our results emphasize the notion that Cdk-dependent cell cycle control in multicellular organisms is extremely robust and several overlapping mechanisms facilitate not only the proper execution of cell division but also its timely coordination with developmental processes, even in the concomitant absence of allegedly essential factors.

ACKNOWLEDGMENTS

We thank Marcos Malumbres for suggestions and critical reading of the manuscript.

This work was supported by grants from the European Research Council (ERC-AG/250297-RAS AHEAD), EU-Framework Programme (LSHG-CT-2007-037665/CHEMORES, HEALTH-F2-2010-259770/LUNGTARGET, and HEALTH-2010-260791/EUROCANPLAT-FORM), Spanish Ministry of Economy and Competitiveness (SAF2011-30173), and Autonomous Community of Madrid (S2011/BDM-2470/ONCOCYCLE) to M.B. C.E.S. is supported by a grant from the La Caixa/CNIO International Ph.D. Fellowship Program sponsored by the La Caixa Foundation (Spain).

We declare no conflict of interest.

REFERENCES

1. **Morgan DO.** 2007. The cell cycle: principles of control. New Science Press, London, United Kingdom.
2. **Kato JY, Matsuoka M, Strom DK, Sherr CJ.** 1994. Regulation of cyclin D-dependent kinase (cdk4) by cdk4-activating kinase. Mol. Cell. Biol. **14:**2713–2721. http://dx.doi.org/10.1128/MCB.14.4.2713.
3. **LaBaer J, Garrett MD, Stevenson LF, Slingerland JM, Sandhu C, Chou HS, Fattaey A, Harlow E.** 1997. New functional activities for the p21 family of CDK inhibitors. Genes Dev. **11:**847–862. http://dx.doi.org/10.1101/gad.11.7.847.
4. **Cheng M, Olivier P, Diehl JA, Fero M, Roussel MF, Roberts JM, Sherr CJ.** 1999. The p21(Cip1) and p27(Kip1) CDK 'inhibitors' are essential activators of cyclin D-dependent kinases in murine fibroblasts. EMBO J. **15:**1571–1583.
5. **Sugimoto M, Martin N, Wilks DP, Tamai K, Huot TJ, Pantoja C, Okumura K, Serrano M, Hara E.** 2002. Activation of cyclin D1-kinase in murine fibroblasts lacking both $p21^{Cip1}$ and $p27^{Kip1}$. Oncogene **21:**8067–8074. http://dx.doi.org/10.1038/sj.onc.1206019.
6. **Blain SW, Montalvo E, Massagué J.** 1997. Differential interaction of the cyclin-dependent kinase (Cdk) inhibitor $p27^{Kip1}$ with cyclin A-Cdk2 and cyclin D2-Cdk4. J. Biol. Chem. **272:**25863–25872. http://dx.doi.org/10.1074/jbc.272.41.25863.
7. **Sherr CJ, Roberts JM.** 1999. CDK inhibitors: positive and negative regulators of G_1-phase progression. Genes Dev. **13:**1501–1512. http://dx.doi.org/10.1101/gad.13.12.1501.
8. **Bagui TK, Jackson RJ, Agrawal D, Pledger WJ.** 2000. Analysis of cyclin D3-cdk4 complexes in fibroblasts expressing and lacking $p27^{kip1}$ and $p21^{cip1}$. Mol. Cell. Biol. **20:**8748–8757. http://dx.doi.org/10.1128/MCB.20.23.8748-8757.2000.
9. **Bagui TK, Mohapatra S, Haura E, Pledger WJ.** 2003. $p27^{Kip1}$ and $p21^{Cip1}$ are not required for the formation of active D cyclin-cdk4 complexes. Mol. Cell. Biol. **23:**7285–7290. http://dx.doi.org/10.1128/MCB.23.20.7285-7290.2003.
10. **Zhang H, Hannon GJ, Beach D.** 1994. p21-containing cyclin kinases exist in both active and inactive states. Genes Dev. **8:**1750–1758. http://dx.doi.org/10.1101/gad.8.15.1750.
11. **Soos TJ, Kiyokawa H, Yan JS, Rubin MS, Giordano A, DeBlasio A, Bottega S, Wong B, Mendelsohn J, Koff A.** 1996. Formation of p27-CDK complexes during the human mitotic cycle. Cell Growth Differ. **7:**135–146.
12. **Fero ML, Rivkin M, Tasch M, Porter P, Carow CE, Firpo E, Polyak K,**

Tsai LH, Broudy V, Perlmutter RM, Kaushansky K, Roberts JM. 1996. A syndrome of multiorgan hyperplasia with features of gigantism, tumorigenesis and female sterility in $p27^{(Kip1)}$ deficient mice. Cell **85:**733–744. http://dx.doi.org/10.1016/S0092-8674(00)81239-8.

13. **National Research Council.** 2011. Guide for the care and use of laboratory animals, 8th ed. National Academies Press, Washington, DC.
14. **Santamaría D, Barrière C, Cerqueira A, Hunt S, Tardy C, Newton K, Cáceres JF, Dubus P, Malumbres M, Barbacid M.** 2007. Cdk1 is sufficient to drive the mammalian cell cycle. Nature **448:**811–815. http://dx.doi.org/10.1038/nature06046.
15. **Martín A, Odajima J, Hunt SL, Dubus P, Ortega S, Malumbres M, Barbacid M.** 2005. Cdk2 is dispensable for cell cycle inhibition and tumor suppression mediated by $p27^{Kip1}$ and $p21^{Cip1}$. Cancer Cell **7:**591–598. http://dx.doi.org/10.1016/j.ccr.2005.05.006.
16. **Kiyokawa H, Kineman RD, Manova-Todorova KO, Soares VC, Hoffman ES, Hoffman ES, Ono M, Khanam D, Hayday AC, Frohman LA, Koff A.** 1996. Enhanced growth of mice lacking the cyclin-dependent kinase inhibitor function of p27(Kip1). Cell **85:**721–732. http://dx.doi.org/10.1016/S0092-8674(00)81238-6.
17. **Nakayama K, Ishida N, Shirane M, Inomata A, Inoue T, Shishido N, Horii I, Loh DY, Nakayama K.** 1996. Mice lacking $p27^{(Kip1)}$ display increased body size, multiple organ hyperplasia, retinal dysplasia and pituitary tumors. Cell **85:**707–720. http://dx.doi.org/10.1016/S0092-8674(00)81237-4.
18. **Martin J, Hunt SL, Dubus P, Sotillo R, Néhmé-Pélluard F, Magnuson MA, Parlow AF, Malumbres M, Ortega S, Barbacid M.** 2003. Genetic rescue of Cdk4 null mice restores pancreatic β-cell proliferation but not homeostatic cell number. Oncogene **22:**5261–5269. http://dx.doi.org/10.1038/sj.onc.1206506.
19. **Rane SG, Dubus P, Mettus RV, Galbreath EJ, Boden G, Reddy EP, Barbacid M.** 1999. Loss of Cdk4 expression causes insulin-deficient diabetes and Cdk4 activation results in β-cell hyperplasia. Nat. Genet. **22:**44–52. http://dx.doi.org/10.1038/8751.
20. **Tsutsui T, Hesabi B, Moons DS, Pandolfi PP, Hansel KS, Koff A, Kiyokawa H.** 1999. Targeted disruption of Cdk4 delays cell cycle entry with enhanced $p27^{Kip1}$ activity. Mol. Cell. Biol. **19:**7011–7019.
21. **Martin-Caballero J, Flores JM, García-Palencia P, Serrano M.** 2001. Tumor susceptibility of p21(Waf1/Cip1)-deficient mice. Cancer Res. **61:**6234–6238.
22. **García-Fernández RA, García-Palencia P, Sánchez MA, Gil-Gómez G, Sánchez B, Rollán E, Martín-Caballero J, Flores JM.** 2011. Combined loss of p21(waf1/cip1) and p27(kip1) enhances tumorigenesis in mice. Lab. Invest. **91:**1634–1642. http://dx.doi.org/10.1038/labinvest.2011.133.
23. **James M, Ray A, Leznova D, Blain SW.** 2008. Differential modification of $p27^{Kip1}$ controls its cyclin D-cdk4 inhibitory activity. Mol. Cell. Biol. **28:**498–510. http://dx.doi.org/10.1128/MCB.02171-06.
24. **Malumbres M, Sotillo R, Santamaría D, Galán J, Cerezo A, Ortega S, Dubus P, Barbacid M.** 2004. Mammalian cells cycle without the D-type cyclin-dependent kinases Cdk4 and Cdk6. Cell **118:**493–504. http://dx.doi.org/10.1016/j.cell.2004.08.002.
25. **Landis WM, Pawlyk BS, Li T, Sicinski P, Hinds PW.** 2006. Cyclin D1-dependent kinase activity in murine development and mammary tumorigenesis. Cancer Cell **9:**13–22. http://dx.doi.org/10.1016/j.ccr.2005.12.019.
26. **Sage J, Miller AL, Pérez-Mancera PA, Wysocki JM, Jacks T.** 2003. Acute mutation of retinoblastoma gene function is sufficient for cell cycle re-entry. Nature **424:**223–228. http://dx.doi.org/10.1038/nature01764.
27. **Susaki E, Nakayama K, Yamasaki L, Nakayama KI.** 2009. Common and specific roles of the related CDK inhibitors p27 and p57 revealed by a knock-in mouse model. Proc. Natl. Acad. Sci. U. S. A. **106:**5192–5197. http://dx.doi.org/10.1073/pnas.0811712106.
28. **Miettinen HE, Paunu N, Rantala I, Kalimo H, Paljarvi L, Helin H, Haapasalo H.** 2001. Cell cycle regulators (p21, p53, pRb) in oligodendrocytic tumors: a study by novel tumor microarray technique. J. Neurooncol. **55:**29–37. http://dx.doi.org/10.1023/A:1012961918848.
29. **Liu Y, Yeh N, Zhu XH, Leversha M, Cordon-Cardo C, Ghossein R, Singh B, Holland E, Koff A.** 2007. Somatic cell type specific gene transfer reveals a tumor-promoting function for p21(Waf1/Cip1). EMBO J. **26:**4683–4693. http://dx.doi.org/10.1038/sj.emboj.7601886.
30. **Hukkelhoven E, Liu Y, Yeh N, Ciznadija D, Blain SW, Koff A.** 2012. Tyrosine phosphorylation of the p21 cyclin-dependent kinase inhibitor facilitates the development of proneural glioma. J. Biol. Chem. **287:**38523–38530. http://dx.doi.org/10.1074/jbc.M112.366542.
31. **Chu I, Sun J, Arnaout A, Kahn H, Hanna W, Narod S, Sun P, Tan CK, Hengst L, Slingerland J.** 2007. p27 phosphorylation by Src regulates inhibition of cyclin E-Cdk2. Cell **128:**281–294. http://dx.doi.org/10.1016/j.cell.2006.11.049.
32. **Grimmler M, Wang Y, Mund T, Cilensek Z, Keidel EM, Waddell MB, Jäkel H, Kullmann M, Kriwacki RW, Hengst L.** 2007. Cdk inhibitory activity and stability of p27Kip1 are directly regulated by oncogenic tyrosine kinases. Cell **128:**269–280. http://dx.doi.org/10.1016/j.cell.2006.11.047.
33. **Besson A, Hwang HC, Cicero S, Donovan SL, Gurian-West M, Johnson D, Clurman BE, Dyer MA, Roberts JM.** 2007. Discovery of an oncogenic activity in p27Kip1 that causes stem cell expansion and a multiple tumor phenotype. Genes Dev. **21:**1731–1746. http://dx.doi.org/10.1101/gad.1556607.
34. **Malumbres M.** 2011. Physiological relevance of cell cycle kinases. Physiol. Rev. **91:**973–1007. http://dx.doi.org/10.1152/physrev.00025.2010.